Faculty of Science and Engineering
School of Earth and Planetary Sciences
Discipline of Spatial Sciences

Assessing Extreme Rainfall Variation and its Relation to Flood Hazard in Sri Lanka

Kodithuwakku Arachchige Saseeka Sumudu Wijesekera

This thesis is presented for the Degree of Doctor of Philosophy
of
Curtin University

February 2024

DECLARATION

To the best of my knowledge and belief, this thesis contains no material previously published by any other person except where due acknowledgement has been made.

This thesis contains no material which has been accepted for the award of any other degree or diploma in any university.

Signature:

Date: 14/02/2023

ABSTRACT

Due to climate change, increase in extreme rainfall has become a common feature in most tropical regions. Consequently, in recent years Sri Lanka has seen several extreme weather events whose subsequent hazards have caused significant damage to human lives, the economy, and the environment. This has a detrimental impact on a developing country like Sri Lanka. Hence, a detailed investigation of extreme rainfall in Sri Lanka is useful for understanding climate change dynamics and improving preparedness and early warning systems for natural disasters. Due to the complex interaction between climate change and geographical conditions, river flow variables vary significantly across the island, frequently resulting in extreme weather and associated hazards like floods. There is a recurring pattern of ongoing flood hazards in Sri Lankan River basins which have resulted in significant economic losses and interruptions to human life. Given these considerations, three main objectives are to be addressed in this research.

i. Analysis of spatial and temporal extreme rainfall variations over Sri Lanka.
ii. Identification of rainfall and water-level fluctuations and their relationships in the Kelani River Basin.
iii. Assessment of flood risk due to extreme rainfall in the Lower Kelani River Basin.

To achieve the first objective, the study calculated nine distinct extreme rainfall indices (R10mm, R20mm, R995p, R99p, RX5day, RX1day, PRCPTOT, CWD, and SDII) using daily rainfall data obtained from 19 meteorological stations spread across Sri Lanka from 1991 to 2020. Mann-Kendall (MK), sequential Mann-Kendall (SqMK), Sen's slope estimator, and Innovative Trend Analysis (ITA) were used to determine temporal variations of extreme rainfall, while the inverse distance weighted (IDW) interpolation method was used to identify the spatial variations of these extreme rainfall indices.

According to the analysis, most meteorological stations (68%) showed discernibly increasing trends (95% confidence level) in extreme rainfall. These increasing trends were largely centred in the dry and intermediate zones of the northern and eastern parts

of the island. Conversely, a notably decreasing trend was observed at some of the stations in the wet zone in the southwest part of Sri Lanka (95% confidence level). Moreover, the PRCPTOT index has shown considerably less annual total precipitation in the northern and eastern regions than in the southern region. The SDII index, on the other hand, had its largest accumulation in the east coast region. The same region has lower values for PRCPTOT and CWD indices, revealing low rainfall but with high intensity. Furthermore, the study found an increase in the intensity and frequency of very heavy rainfall events across the island. As a whole, the results indicated that the wet zone was getting drier and the intermediate and dry zones were getting wetter in the period considered. The consequential increase in extreme rainfall events increases the likelihood of the floods and landslides that adversely affect agricultural and transportation activities throughout the country.

The Kelani River Basin (KRB), situated in the wet zone of the country, experiences regular flooding. The basin is highly populated and urbanized than other basins in Sri Lanka, and it flows through the commercial capital of the country, the city of Colombo. Thus, changes in the KRB directly affects many people. To fulfil the second objective, daily rainfall data from 10 meteorological stations were obtained from the Department of Meteorology, while water-level data were obtained from the Irrigation Department for Hanwella and Nagalagam Street hydrology stations. The mean-based adjustment technique was used to homogenise hydro-meteorological data. The modified Mann-Kendall (MMK) test, Sen’s slope, Pearson's correlation coefficient tests, and lag correlation were used to examine the data. To identify extreme rainfall over the basin, the extreme rainfall indices PRCPTOT, SDII, R99p, R95p, CWD, RX5day, and RX1day were calculated. The results showed that, during the study period, there was a significant increasing trend in the annual total rainfall over the KRB. At the same time, a significant decreasing trend in water level was observed at Hanwella Hydrology Station, while a significant increasing trend appeared at N’Street Station.

The results indicate that over the study period a decreasing trend in rainfall was observed at approximately 40% of the meteorological stations analysed, including at all meteorological stations in the upper KRB (except for Maliboda). In particular, 70% of the stations showed the highest decreasing trend in rainfall during the Southwest Monsoon (SWM) period, the highest of the four seasons. Contrary to this, the

Northeast Monsoon (NEM) produced the highest increasing trend in stations (70%). When considering extreme rainfall over the basin, it is evident that the intensity has reduced, but the frequency and duration have increased. There is a moderately positive correlation between water level and rainfall in the basin, which indicates that there are some other factors that affect the water level. When considering the monthly correlation of rainfall and water level, the months of May, June, July, and November have the highest correlations. The lag correlation for 10 lags shows an increase in lags in the first zero to four lags and then a gradual decrease. This can be used to describe the synchronicity of rainfall and water level in flood events, and the results are essential for establishing a sustainable water use plan for the KRB.

The increase in extreme rainfall events over the Kelani River Basin (KRB) has led to an increasing number of severe flooding threats in the lower part of the basin. Thus, in the third objective, this study aimed to analyse flood risk in the Lower Kelani River Basin (LKRB). This objective consists of two parts.

The first part of this objective is a detailed analysis of flood risk with the help of the Analytical Hierarchy Process (AHP)-based Multi-Criteria Decision Method (MCDM) method. As the risk is a combination of hazards and vulnerabilities, the study set hazards and vulnerabilities as criteria for the AHP process. Under these two criteria, thirteen factors were analysed and flood hazard and flood vulnerability maps for the LKRB were prepared prior to prepare the flood risk map. The eastern side of the LKRB is identified on the risk map as a low-risk area due to its high elevation and slope, drainage density, and vegetation. The urbanised, highly populated areas with poor drainage density on the western side are considered high-risk areas for flood susceptibility. Most of the land area (40.26%) is categorised as having a moderate risk of flooding and 16.43% is at high to very high risk for flood susceptibility. The spatial extents and levels of risks were systematically identified based on the maps produced. Applying risk information will assist the authorities in developing prompt flood management strategies and detecting highly affected areas in which to implement appropriate mitigation strategies. This model can also be applied to any other geographical area to detect flood risk by inputting the necessary data and information. In the second part, this study proposed a new integrated model for flood hazard assessment. The study used nine flood hazard criteria for this proposed model. This

model integrates the Analytical Hierarchy Process (a decision-making model), Frequency Ratio Analysis (a statistical model), and Height Above Nearest Drainage Model (HAND - a flood inundation model). The model has been validated with the help of the Area Under Curve (AUC) method. The AUC value for the model is 0.807, denoting this as a very good model for flood hazard assessment. This proposed methodology can be used to assess flood hazards in any part of the world with different criteria, as it provides a detailed flood risk zonation map for users. According to this new methodology-based flood zonation map for the LKR, 16.4% of the total land is under the risk and high-risk category for flood hazard.

Finally, the findings of this study give valuable insights into the shifting trends of extreme rainfall, water levels, and flood threats in Sri Lanka, particularly in the Kelani River Basin. The conclusions extend to disaster preparedness and mitigation activities, assisting scientists and policymakers to understand and effectively handle the current situation.

ACKNOWLEDGEMENTS

I would like to express my sincere appreciation to my supervisors, Dr. Ashraf Dewan and Dr. Michael Kuhn, for their continuous guidance, support, and encouragement throughout the research, enabling me to complete this research successfully.

I also extend a thank you to the thesis committee chairperson, Dr. Ivana Ivánová, for her valuable advice during the stages of my research.

Special thanks go to the Department of Geography, University of Kelaniya, Sri Lanka, for continuous support and dedicated extra time to bear the workload during my study leave.

I am grateful to my beloved mother, Rohini Shanthilatha, who dedicated her whole life with many difficulties to giving me the best education and all the opportunities to pursue my dreams. Her immense support during my PhD journey is invaluable.

A very special thanks to my husband, Suranga, and my children, Sanuki and Kian, for their tremendous support and patience, especially when I was heavily preoccupied with my research.

I am very thankful for my grandmother and my aunt, Savithri, who have dedicated their lives beyond the borders to raising me and my sister for the best education.

My sincere remembrance goes to my sister, Kanchana Wijesekera, and her family.

I would like to thank my fellow graduate students and staff members at Curtin University in Perth, Australia, who helped me directly and indirectly with their suggestions and encouragement.

A very special acknowledgment goes to my PhD colleagues Khlood Ghalib, Bazarzagd Lkhagvasuren, Ali Hassan Ghandurah, Ratovoson Robert Andriambololonaharisoamalala, and Philemon Eddie Akao, for their valuable time and advice during this PhD Journey.

A special thanks goes to Professor Nishan Sakalasooriya, who approved my study leave request as the Head of the Department in 2019, even with a very limited number of staff members.

I highly appreciate the valuable support of Mr. A.L.K. Wijemannage in obtaining climate data from the Department of Meteorology, Sri Lanka.

I greatly appreciate the support of the Irrigation Department of Sri Lanka for providing me with water level data for the Kelani River Basin that I used in my research.

My heartiest thanks to Ms. Chandra Lekamarachchi and Ms. Sujani Rathnasekara for giving me emotional support during this journey.

I acknowledge the AHEAD scholarship provided by the government of Sri Lanka and the University of Kelaniya higher education financial support that opened up the opportunity for this PhD.

I would also like to acknowledge the Curtin HDR and completion scholarships, which helped me continue my research without difficulties.

A very special thanks goes to Peter Krockenberger, who did my PhD proofreading.

LIST OF ACRONYMS

AFH	AHP, FR, and HAND integrated model
AHP	Analytical Hierarchy Process
ENSO	El Niño-Southern Oscillation
FR	Frequency Ratio
GIS	Geographical Information Systems
HAND	Height Above Nearest Drainage
IM1	First Inter Monsoon
IM2	Second Inter Monsoon
IOD	Indian Ocean Dipole
ITA	Innovative Trend Analysis
ITCZ	Inter-Tropical Convergence Zone
MK	Mann-Kendall trend test
MMK	Modified Mann-Kendall test
KRB	Kelani River Basin
LKRB	Lower Kelani River Basin
LULC	Land Use Land Cover
MCDM	Multi-Criteria Decision Making
MJO	Madden Julian Oscillation
NEM	Northeast Monsoon
SAM	South Asian Monsoon
SF	Sendai Framework
SWM	Southwest Monsoon
UKRB	Upper Kelani River Basin
WMO	World Meteorological Organization

TABLE OF CONTENT

LIST OF FIGURES

LIST OF TABLES

1. INTRODUCTION

1.1 Background

Precipitation is one of nature's most precious resources, with many implications for the sustainability of humans and the environment. Over time and space, the response of human activities to changes in rainfall distribution and other climatic factors is not consistent (Department of Meteorology, 2019). Accordingly, rainfall significantly influences economic, ritual, and cultural activities, especially in developing countries in the tropics, where nearly half the global population lives (NASA, 1999). However, it is unfortunately possible that severe and prolonged rainfall may lead to negative consequences like flooding, with adverse impacts on society and the environment.

Folland et al. (2001) found that rainfall fluctuations around the globe have occurred over different time scales than other significant long-term trends. Hence, a comprehensive understanding of precipitation patterns is essential to determine the dynamic nature of interactions between humans and the environment. Investigations of rainfall patterns thus have an extensive history. As articulated by Turkes (1996), there are many studies of the spatiotemporal complexities of rainfall patterns at both micro- and macro-levels worldwide. These studies have been devoted to determining the many factors involved in changes in rainfall (Adler et al., 2018; Kumar et al., 2010; Nisansala et al., 2020; Pinault, 2012). For instance, a study conducted by Sun et al. (2018) analysed global precipitation trends and found that regions at lower altitudes demonstrated slightly more pronounced variations of extreme precipitation events than those at higher altitudes. In addition, an extensive study conducted by Guagliardi et al. (2016) examined the patterns of seasonal and annual rainfall across Europe and the Mediterranean region, and found that there is a negative trend of annual rainfall in the Mediterranean basin. Conversely, a positive trend of precipitation has been observed in northern Europe. Nevertheless, as rainfall patterns change with climate change, continuing studies of precipitation are still necessary to unravel the complicated variations of global patterns of precipitation.

Precipitation is a vital component of the hydrological cycle and the primary way that atmospheric water returns to the Earth's surface. The hydrological cycle has been

significantly altered by global climate change, leading to increased flooding potential in different regions of the world (Arnell & Gosling, 2013). As temperatures rise to unprecedented levels (IPCC, 2021), the hydrological cycle is being distinctly affected, leading to increasing rainfall and evaporation levels (WMO, 2013). Accordingly, changes in spatiotemporal rainfall patterns affecting overall magnitudes and seasonal distributions have already been observed due to this hydro-cycle change (Feng et al., 2013). Moreover, Nouaceur and Murărescu (2016) predicted that many areas would become wetter due to the recurrence of extreme events and the intensification of overall rainfall caused by climate change. South Asia, including Sri Lanka, has become a global hotspot for climate change (Dissanayaka & Rajapakse, 2019). Hence, above-average extreme rainfall events have increased in recent decades (Sheikh et al., 2015). Shahid (2011) observed evidence of a significant increase in annual and pre-monsoonal rainfall in Bangladesh. Nanditha et al. (2023) discussed extreme rainfall-related flood hazards, which badly hit Pakistan's southern province in 2022. As Samantaray and Gouda (2023) show, India is also experiencing an increased trend of heavy rainfall events.

South Asia is home to more than 2 billion people (Worldometer, 2023). Any changes in climate can severely affect the roughly 1 billion of them who depend on agriculture (ACIAR, 2023). This underlines the vital role that rainfall plays in the South Asian climate. The South Asian Monsoon system (SAM) brings most precipitation from May to September (Indian summer monsoon) to the region. Spatiotemporal distribution of rainfall in the South Asian region depends on a number of factors, such as climate, topography, and orography. In winter, occasional precipitation is produced by westerly systems originating in the Arabian Sea and Mediterranean region (Krishnan et al., 2019; Lang & Barros, 2004). Atmospheric teleconnection systems – such as El Niño-Southern Oscillation (ENSO), the Indian Ocean Dipole (IOD), and the Madden Julian Oscillation (MJO) – may also influence the SAM (Halpert & Ropelewski, 1992; Saji et al., 1999).

Sri Lanka, a small tropical island in the Indian Ocean, has a distinctive climate with unique orography. Amidst many climatic variables, rainfall measurements and patterns are crucial for informing the social and economic decisions of the nation (Suppiah & Yoshino, 1984). For instance, Zubair et al. (2007) indicated that changes in

precipitation patterns have a significant influence on agricultural productivity and food security, as well as substantial implications for the subsistence livelihoods of communities in Sri Lanka. The inter-annual variation of rainfall across the island is governed by the SAM, and analysis of rainfall patterns gives insights into the complex behaviour of the SAM. Accordingly, much research is carried out to analyse rainfall behaviour (Madduma Bandara & Wickramagamage, 2004; Nisansala et al., 2020; Thevakaran et al., 2019). Extreme rainfall and drought events have recently been reported in Sri Lanka due to the overall effects of climate change. The impact of these rainfall changes across the country is substantial, significantly affecting the environment and many aspects of human life. However, only a few studies have considered extreme rainfall events (Abeysekera et al., 2015; Jayawardena et al., 2018; Sheikh et al., 2015; Stolbova et al., 2014). These studies considered a few rainfall stations or specific rainfall seasons to identify the extreme rainfall pattern. For example, the study by Abeysekera et al. (2015) analysed extreme rainfall anomalies, but only for the Dry zone of Sri Lanka. Therefore, this study aims to fill this void.

Studying river flow variability provides valuable background to understanding the interaction between a region's hydrological processes, climate patterns, and environmental systems (Döll & Schmied, 2012; Jain & Singh, 2018). There is significant spatial variation in the discharges of local and regional rivers, due to their complex interaction with climate and other geographical variables (Arnell & Gosling, 2013; Frans et al., 2013). However, the results of modelling indicate that changes in discharges into the world's rivers will continue to be driven by climate change and land use and land cover (LULC) (Tao et al., 2014). The average annual flows in nearly half of the world's major river basins are projected to decline, while flows are expected to increase in over 35% of these basins by the mid-21st century (Arnell & Gosling, 2013). Furthermore, Santini and di Paola (2015) have explained that extreme water discharge will decrease in 60% of the major river basins in the northern hemisphere by the end of the 21st century. Accordingly, Jain and Singh (2018) argue that studying river flow variability is paramount for assessing freshwater climate change risks (Jain & Singh, 2018). Hence, many studies have been conducted to assess how climate change impacts river flow variability across the globe. For instance, the study by Hariadi et al. (2023) analysed extreme rainfall and river flow variability in Myanmar, revealing that northern Myanmar will experience longer dry spells in future. In contrast, its east coast

will experience more extreme rainfall conditions, which will lead to lower river flows across Myanmar. The study by Rameshwaran et al. (2021) demonstrated that river flow variability across West Africa, particularly in the Sahelian region, will increase due to climate change. Martins et al. (2016) studied the impact of rainfall and land cover on river flow changes in the Ivai River Basin of Brazil. They found that river flows change mainly due to land cover changes. Furthermore, the paper of Manawadu and Wijeratne (2021) showed that human activities are major contributors to the complex patterns of river flow variability.

In the Sri Lankan context, the scholarly work of Imbulana et al. (2018), Ampitiyawatta and Guo (2009), Khaniya et al. (2019), Panditharathne et al. (2022), and Alahacoon and Edirisinghe (2021) assessed the complex interactions between rainfall and river flow variability in the nation's different watersheds. As the fourth largest watershed on the island, the Kelani River Basin (KRB) covers a significant portion of the country's western and central hill regions (Jayasekara et al., 2020). Socioeconomically, the basin is much more important than other basins on the island, as it surrounds critical urban and industrial centres like Colombo, Sri Lanka's commercial centre and capital city (Manawadu & Wijeratne, 2021). The KRB is home to more than 20% of the Sri Lankan population (Mahagamage & Manage, 2018). High population density exerts enormous pressure on the basin's water resources, sanitation processes, and infrastructure development (Manawadu & Wijeratne, 2021; Samarasinghe et al., 2022). Randil et al. (2022) stressed that the basin is vulnerable to annual flooding. Therefore, plenty of studies have been carried out in the KRB to analyse floods (De Silva et al., 2012; Samarasinghe et al., 2022; Wijetunge & Neluwala, 2023), human activities (Manawadu & Wijeratne, 2021; Wijeratne & Li, 2022), rainfall (Dissanayaka & Rajapakse, 2019; Perera et al., 2022), and so on. However, given the changing climatic conditions, it is clear that there is a compelling need to examine the link between rainfall and water level dynamics in the KRB. Jayasekara et al. (2020) discussed in depth the relationship between rainfall and stream flow variability in the KRB between 1983 and 2013. They found that rainfall variation is significantly attributable to catchment streamflow. Further, most studies (Dissanayaka & Rajapakse, 2018; Jayasekara et al., 2020; Samarasinghe et al., 2022) revealed that, the average rainfall over the basin is decreasing in past decades. However, the climate and the environment are changing day by day. The study by Samarasinghe et al. (2022)

explained that increased flood intensities and land use changes in the KRB had significantly contributed to the severity of flooding. Hence, it should be confirmed that the rainfall over the KRB has changed over the past decades.

Flooding is one of the most severe, widespread, and destructive types of natural disaster, affecting about 250 million people worldwide annually, with estimated annual economic losses of more than USD 40 billion (OECD, 2016). According to the Emergency Event Database (EM-DAT) 2023 report, flood was the most common natural disaster in 2022 (176 events worldwide). For instance, flooding in Pakistan has caused an estimated USD 15 billion in direct damage, killed more than 1,700 people, and displaced 8 million, which will cause economic hardship for a long time (United Nations Office for Disaster Risk Reduction and World Meteorological Organizatio, 2023). In August 2018, the southern Indian state of Kerala faced catastrophic floods caused by heavy rainfall, resulting in economic losses exceeding USD 3 billion and the deaths of more than 440 people (Mishra et al., 2018). In August 2019, Kerala again faced a similar situation, which left more than 1.5 million people homeless and 244 dead (The Guardian, 2019). Similarly, in 2013 in India and Nepal, 6,648 people died in floods caused by heavy rains. Kundzewicz et al. (2014) pointed out that in 2012, Madagascar, Niger, and Nigeria on the African continent, China, India, North and South Korea, Bangladesh, and the Philippines on the Asian continent, and Argentina and the United States in the Americas encountered killer flood events due to heavy rainfall. The evidence indicates that extreme rainfall-related flood is one of the most costly and dangerous natural hazards.

The intensity and duration of rainfall events have caused a number of recent major floods across Sri Lanka. For example, in May 2016 flooding in the Lower Kelani River Basin (LKRB) had an adverse impact on livelihoods, property, and the surrounding environment. During that event, the Kelani River catchment area was subject to 350 mm of rain on three consecutive days (15 – 17 May 2016). Over 4,000 houses were damaged, with 340,000 people injured and 104 fatalities. The economic damage to homes was estimated at around USD 310 million (Ministry of National Policies and Economic Affairs, 2016). Again in 2017, the southern part of the island received 600 mm of rainfall within two days, resulting in significant floods and landslides (Disaster Information Management System in Sri Lanka, 2017). These floods spread over 15

districts, affecting almost 717,622 people (Disaster Information Management System in Sri Lanka, 2017). Severe rainfall again caused flooding in the northern and eastern parts on the island in December 2019, affecting more than 65,316 people (International Federation of Red Cross and Red Crescent Societies, 2020).

Managing human well-being and the surrounding environment in flood-prone areas is essential for authorities relate with disaster management. Managing human wellbeing and the surrounding environment in flood-prone areas is essential for authorities like disaster management. Consequently, assessment of flood hazards and vulnerability is one of the most important aspects of flood management and mitigation (Nasiri et al., 2016). Numerous studies worldwide (Brouwer et al., 2007; Gordon Tami & Moses, 2015; Kelly & Kuleshov, 2022) have reinforced the importance of hazard and vulnerability assessment for flood-risk management. When assessing flood risk, many studies combine decision-making models and statistical models. The most prominent integration method uses the Analytical Hierarchy Process (AHP)-based Multi-Criteria Decision Making (MCDM) tool and a bivariate statistical technique called FR for flood susceptibility mapping (Tariq et al., 2022; Waqas et al., 2021; Yilmaz, 2022). For instance, the study by Ali et al. (2019) applied integrated AHP and FR method to map flood-vulnerable and at-risk areas in the Sundarbans region, India. This integrated model was 81.42% accurate in predicting flood hazards in the region. The study revealed that this combined method was very useful and accurate for flood mitigation strategies, rather than depending on a one assessment method. Also, flood inundation mapping is one of the essential components of flood risk mapping. Among the flood inundation mapping methods, Height Above Nearest Drainage (HAND) model is often used one of the best methods (Godbout et al., 2019; Speckhann et al., 2018). This model is used to generate the inundation map, which shows the variance in elevation between a pixel and the pixel in the drainage network to which it drains (Nobre et al., 2011). At present many studies use the HAND model for flood inundation mapping coupled with other models (Aristizabal et al., 2023; Chaudhuri et al., 2021; Fang et al., 2023). For instance, the study by Komolafe et al. (2020) for the first time combined the AHP and HAND models for flood susceptibility mapping in the Ogun River Basin, Nigeria. The study revealed that this integrated model provided a more accurate background for flood zoning maps. Hence, the integration of AHP, FR and HAND

(AFH) method would provide a more accurate and detailed path for flood hazard mapping, but still, no research has been conducted to combine these three methods.

In the Sri Lankan context, flood risk and vulnerability have been analysed by various researchers (Dissanayake et al., 2018; Samarasinghe et al., 2010; Sivakumar, 2015). Nevertheless, only a few studies have used AHP-based MCDM for flood risk assessment in Sri Lanka (Perera, 2021; Wijesinghe et al., 2023). Also, there are no FR-based flood risk assessments have been carried out for the country yet. As mentioned earlier, floods in the LKRB cause severe damage to humans and the surrounding environment. The government of Sri Lanka then has to spend massive sums of money on rehabilitation. However, only one study (Perera, 2021) was found that used AHP-based flood risk assessment for the LKRB. Perera's study used six physical factors to assess flood risk in the basin. Nevertheless, both physical and social factors should be considered for better flood risk assessment. Also, there should be a method to generate a detailed map of flood risk in the basin. Therefore, the use of the integrated AFH method would be beneficial for flood hazard assessment in the LKRB. Accordingly, this study attempted to assess the flood risk of LKRB in two ways. These two methods are the detailed AHP-based flood risk assessment and the proposed integrated AFH method for flood susceptibility mapping.

The specific research questions covered in this thesis are:

1. What were the spatial and temporal patterns of extreme rainfall in Sri Lanka from 1991 to 2020?
2. Are current fluctuations in rainfall in the KRB continuing to affect streamflow patterns, or are there significant changes in this relationship?
3. Which areas in the LKRB can be classified as being at risk of flooding, as a result of extreme rainfall?

1.2 Objective of the study

This research aims to assess extreme rainfall variation and its relation to flood hazards in Sri Lanka. Based on this aim and the research questions formulated above, this study addressed the objectives below.

1. Analysis of spatial and temporal extreme rainfall variations over Sri Lanka

This objective was achieved by analysing *in situ* daily rainfall data from 1991 to 2020. Using the extreme rainfall indices, it was possible to identify extreme rainfall events throughout the country. This objective discussed the monotonic extreme rainfall variation according to extreme rainfall indices. Such studies provide background to address the social, economic, and environmental challenges associated with extreme rainfall events.

2. Identification of rainfall and water level fluctuations and their relationships in the Kelani River Basin

In situ daily rainfall and water-level data in the KRB were used for this objective for the same period from 1991 to 2020. This is expected to improve the understanding of how these two variables vary over time. It is essential to determine the relationship between rainfall and water levels in rivers as this is linked with complex impacts on different sectors and aspects of society and water resource management in a river basin.

3. Assessing flood risk due to extreme rainfall in the Lower Kelani River basin

This objective has explained how the MCDM method can be applied to flood risk assessment in the LKRB. Further, this study has introduced, a new integrated AFH method for flood risk assessment in the LKRB. In order to ensure environmental protection and the safety of lives and property, flood-risk assessments are essential tools. These assessments can reveal possible impacts and vulnerabilities in order to develop preventive measures that will better protect living conditions in communities faced with flood hazard risks, as well as informing good policy choices.

1.3 Significance of the Study

This research significantly deviates from other studies in the following ways.

- Investigations of precipitation patterns in Sri Lanka have provided valuable information for understanding the behavioural complexity of the SAM and its atmospheric teleconnections. As the country is one of the tropical hotspots of climate change, it is necessary to investigate extreme climate events on the island. However, the existing research relating to extreme rainfall events on the island has had a limited scope. More comprehensive spatiotemporal studies are needed to address this gap.

- This study is the first attempt to distinguish monotonic trends of extreme rainfall and subsequently map them across the entire island of Sri Lanka. It represents the first step in using such methodologies to analyse extreme rainfall patterns in Sri Lanka. A thorough understanding of extreme rainfall patterns is essential because of the inherent risk of hazards like flooding and landslides in the Sri Lankan context. Hence, the findings of this research are beneficial for future researchers and policymakers to understand extreme rainfall in Sri Lanka.

- Sri Lanka is an agriculture-dominated country, so water is essential for sustainable development. However, streamflows are influenced by changes caused by climate change. Therefore, there should be more studies of river flow changes in the river basins of the country. The KRB is the most highly populated river basin in the country and any changes in river flow and rainfall variability greatly affect its population. Limited studies have been carried out to identify the relationship between rainfall and water levels in the KRB, and most focus on periods more than a decade ago. Therefore, this study has identified variations in the relationship between rainfall and water levels in the KRB in recent years in detail.

- This study is the first to combine, a decision-making tool, a statistical model, and a flood inundation model (AFH method) for flood susceptibility mapping

in a river basin. This novel method provides potential background for generating detailed flood susceptibility map.

- When considering the LKRB, AHP-based MCDM flood risk assessments have been minimal and considered only a few physical factors. Accordingly, this study is the first to consider both physical and social criteria, with many factors. Hence, this study significantly deviates from previous studies and has illustrated a much more detailed flood-risk map.

- In order to identify areas vulnerable to flood hazards, Sri Lanka has not carried out any extensive mapping of the country, and relocations have been on a reactive and *ad hoc* basis. Accordingly, this study will prepare flood-risk maps based on ARH method and AHP method in the LKRB, which will serve as baseline maps for flood management in the LKRB basin.

1. 4 Thesis outline

This thesis has six chapters.
Chapter 1: The Introduction chapter describes some background information on extreme rainfall due to climate change and the consequent flood hazards, and then outlines the aims and objectives of the study, and its significance.

Chapter 2: The Literature Review summarises and analyses the theories related to the objectives and previous research. Further, it highlights any gaps in the research to date.

Chapter 3: The Methodology chapter briefly introduces the geographical setting of the three study areas (Sri Lanka, the KRB, and the LKRB) and the data and methods used.

Chapter 4: The Results chapter presents the results according to each objective. The Objective 1 results have illustrated the spatial and temporal patterns of extreme rainfall indices. Trends of extreme rainfall indices are also presented in this chapter. For Objective 2, the relationship between rainfall and water levels in the KRB is presented.

Objective 3 results have informed the preparation of maps defining flood hazards, flood vulnerability, and flood risks.

Chapter 5: The Discussion chapter discusses the results comprehensively in preparation for the conclusions and recommendations of the study.

Chapter 6: This chapter provides conclusions and recommendations for future works.

2 LITERATURE REVIEW

2.1 The influence of climate change on extreme rainfall

In the context of global warming, there will likely be changes in the water cycle which have a profound impact on humans and ecosystems worldwide (Padrón et al., 2020). Trenberth (2005) reported that atmospheric water-holding capacity increases by 6-7% with every 1 °C of warming. The WMO (2013) has reported increased extreme rainfall events in many parts of the world. The Intergovernmental Panel on Climate Change (IPCC, 2012) has also stated that the frequency, intensity, and duration of extreme rainfall have increased both spatially and temporally due to anthropogenic climate change. However, these changes in extreme precipitation are not geographically uniform and they vary from region to region due to the interaction of different drivers (Figure 2.1) (Tabari et al., 2019). The rate at which extreme precipitation increases with land surface temperature is not linear (Tabari, 2020). Furthermore, the effect of extreme precipitation in existing wet regions can be intensified by increased atmospheric moisture convergence. In dry areas, evaporation may counteract the increased precipitation (Held & Soden, 2006).

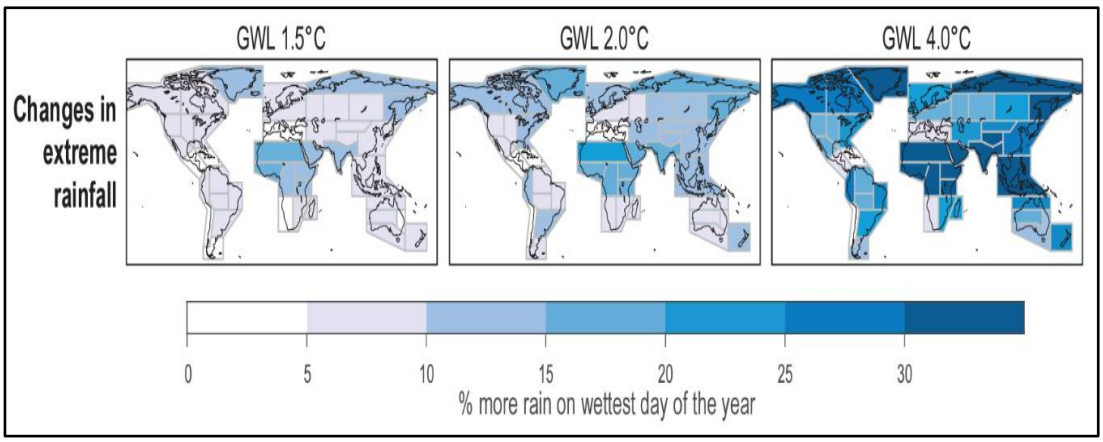

Figure 2.1 *Projections of regional changes of extreme rainfall for different levels of global warming (GWL). The maps of extreme rainfall changes show the percentage change in the amount of rain falling on the wettest day of a year (Rx1day, relative to 1995–2014), averaged across each region when the respective GWL is reached. (Source:* IPCC, 2021).

Goswami and Ramesh (2008) show that extreme rainfall events have become a severe threat to many populated and urbanised areas in recent times. According to IPCC's Fifth Assessment Report (2014), during the second half of the twentieth century many regions of the world showed an increasing number of heavy precipitation events concurrently with decreasing total precipitation amounts. As a result, extreme rainfall events were accompanied by floods and droughts, posing significant health, social, economic, and environmental consequences for millions of people and ecosystems worldwide (Bhatti et al., 2020). This demonstrates how climate change and the associated increases in heavy rainfall events cause serious adverse impacts, including on crucial sectors like water, energy, and food worldwide. Hence, comprehensive knowledge of the spatiotemporal patterns of extreme rainfall events has become essential in understanding the relationship between human activities and environmental change.

Many studies (Asadieh & Krakauer, 2015; Fu et al., 2013; Khadgarai et al., 2021), based on various precipitation data, have found a relationship between climate change and extreme rainfall patterns at global, regional, and local scales. For example, Asadieh and Krakauer (2015) used precipitation data from the Hadley Centre global land-based gridded climate extremes dataset (HadEX2) for 11,600 stations across the world, covering the period from 1901 to 2010. Their revealed that extreme rainfall has increased since 1901, with significant changes in tropical equatorial areas, and that annual maximum daily precipitation has increased globally by an average of 5.73 mm during the period.

Significantly, Southern and Southeastern Asia (Dissanayaka & Rajapakse, 2019), where agriculture dominates economies, have become climate change hotspots. As a result, the intensity and frequency of extreme climate events have increased in South Asia, including Sri Lanka (Sivakumar & Stefanski, 2011). In general, a rise in the frequency and magnitude of rainfall causes severe flooding, landslides, and debris flows across most parts of Asia (IPCC, 2007). These increases in temperature and extreme rainfall caused by climate change will speed up in the future. They have already reduced water availability and reduced high-quality groundwater, and subsequently increased water demand (Pachauri et al., 2014). Therefore, many studies have been conducted to identify extreme rainfall patterns in the Asian region. For instance, the study by Khadgarai et al. (2021) identifies extreme rainfall across

monsoonal Asia. They used the Asian Precipitation Highly Resolved Observation Data Integration Towards Evaluation of Extreme Events (APHRODITE-2) gridded rainfall program to calculate extreme rainfall indices. They found positive trends in heavy rainfall days in central India, the monsoonal region of China, the equatorial nations, and some parts of Japan and the Philippines (Figure 2.2). Fu et al. (2013) studied the temporal variation of extreme rainfall events over China for the period 1961–2009. They used daily precipitation data for 599 meteorological stations distributed across the country. Using the Extreme Precipitation Index (EPI), they found a decreasing trend in extreme rainfall in northeast China, north China, and the Yellow River Basin. On the other hand, the Yangtze River Basin, southeast Coast, south China, Inner Mongolia, northwest China, and Tibetan plateau experienced an increasing trend.

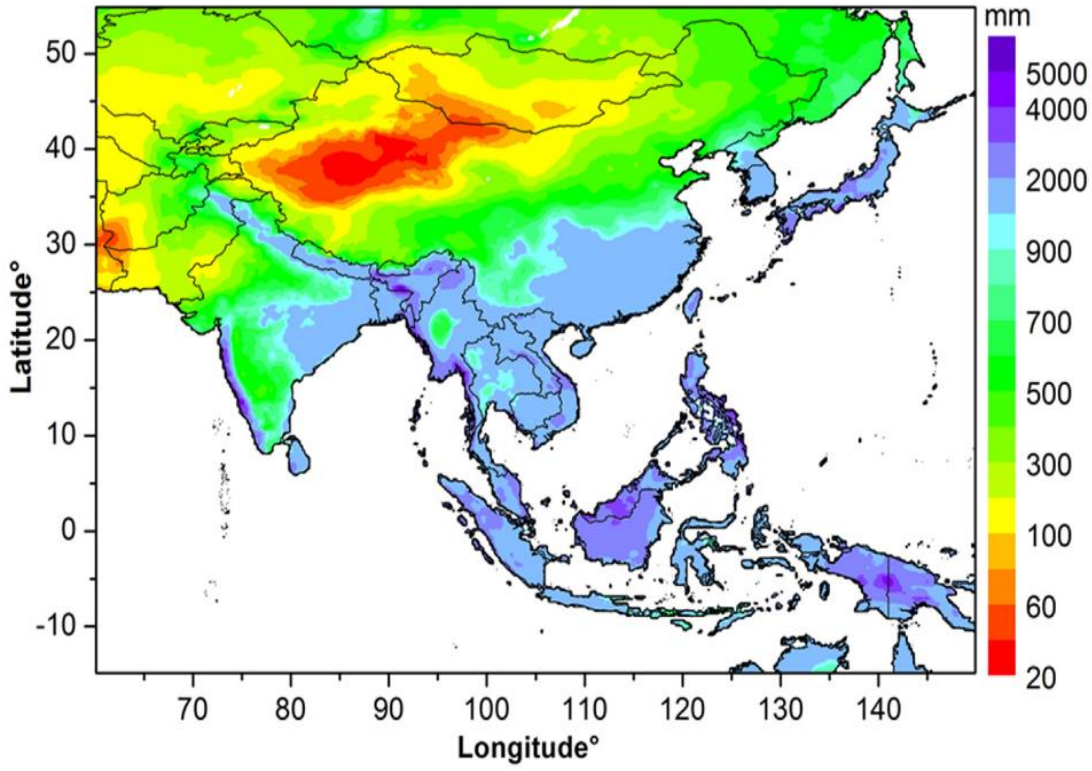

Figure 2.2 Spatial distribution of mean annual rainfall (1998–2015) over monsoonal Asia (Source: Khadgarai et al., 2021)

Extreme climate indices are widely used to analyse extreme rainfall events. The study by Alexander et al. (2006) of temperature and rainfall reveals a general increase in precipitation indices (Annual precipitation total (PRCPTOT), simple daily intensity index (SDII), very wet days (R95p), and consecutive wet days (CWD)) worldwide. However, rainfall patterns show less spatial coherence and minimal statistical significance compared with temperature changes. Sheikh et al. (2015) studied trends in extreme daily rainfall and temperature in the South Asian region using extreme climate indices. The study revealed that spatially coherent changes in extreme precipitation are visible only on a relatively small scale. However, most extreme precipitation indices they used for the study showed an increase in the region. The study by Basher et al. (2018) used extreme climate indices to analyse extreme rainfall in northeast Bangladesh. They revealed a decreasing trend in extreme rainfall between 1984 and 2016 during both pre-monsoon and monsoon periods. Similarly, there are several studies (Brown et al., 2010; Sun et al., 2017) that have used extreme climate indices to analyze trends in precipitation across the world.

The above chapters summarise a fraction of the knowledge that has been gained in massive climate change researches. In addition, the progressive evolution of climate models and projections has emerged as a key element in scientific research on climate dynamics, which highlights their crucial role in enhancing our understanding of meteorological phenomena.

2.2 Advancements in climate modelling and projections

Climate models are essential tools for understanding and projecting future climate scenarios, guiding policy decisions, and developing climate adaptation and mitigation strategies. Over the past few years, significant improvements in climate modelling techniques have enhanced our ability to replicate Earth's complex climate system with greater accuracy and precision. Given that this study focuses on the examination of extreme rainfall patterns, special attention has been paid to identifying advancements in climate modelling and projections.

a) High-resolution modelling

Through high-resolution climate models with improved spatial and temporal resolution, scientists now have the opportunity to obtain more detailed information on climate systems. These models incorporate detailed representations of atmospheric circulation, ocean currents, land surface processes, and biogeochemical cycles, allowing for more accurate simulations of regional climate variability and extreme weather events (Giorgi et al., 2021), such as changes in precipitation patterns, temperature extremes, and sea level rise.

b) Improved representation of feedback mechanisms

Feedback mechanisms in the Earth's climate system are processes that either amplify or mitigate the consequences of climate change. Recent advancements in climate modelling have contributed to the identification of improved representations of feedback mechanisms within the Earth system. For instance, climate models now integrate sophisticated parameterizations of cloud processes, aerosol interactions, and carbon cycle dynamics, which have enhanced our understanding of how feedback influences or dampens climate change (Collins et al., 2013). The improved representation of feedback mechanisms facilitates the refinement of climate sensitivity projections, thereby enabling a more thorough analysis of the likelihood of rapid climate changes.

(c) Integration of Earth system components

The latest generation of climate models integrates various components of the Earth system, including the atmosphere, hydrosphere, land surface, and biosphere. By simulating interactions between these components, scientists can explore the complex dynamics of climate change, including responses within the physical climate system and ecosystems (Flato et al., 2013). The integration of Earth's system components makes it possible to assess the impacts of climate change on ecosystems, agriculture, water resources, and human societies in a holistic manner.

(d) Ensemble modelling techniques

Ensemble modelling techniques are increasingly being used for the quantification of uncertainties in climate forecasts. By running multiple simulations with variations in model parameters or initial conditions, researchers can generate probabilistic forecasts

that account for the inherent uncertainty in climate modelling (Taylor et al., 2012). By providing estimates of future climate scenarios through probabilistic models, these approaches make it easier for policymakers to understand the potential risks and uncertainties associated with climate change.

Accordingly, these advancements in climate modelling and projections have profound implications for our understanding of future climate scenarios and associated risks.

2.3 Rainfall over Sri Lanka

As an agriculture-based South Asian country, rainfall is an essential factor in human activities in Sri Lanka (Sirinanda, 1983). Although the country is a relatively small (65,610 km^2) island, its weather patterns deviate significantly from place to place due to the orography. Therefore, comprehensive knowledge of spatiotemporal rainfall patterns provides valuable insights into the unique climate of the country. Hence, many studies have discussed Sri Lanka's distinctive rainfall variations from different perspectives and provided more up-to-date information Madduma Bandara & Wickramagamage, 2004; Nisansala et al., 2019; Sirinanda, 1983; Thambyahpillay, 1965. For instance, the study by Nisansala et al. (2019) revealed that the western, central, and northwestern parts of the country showed a decreasing trend in rainfall, while the north, east, and northeastern parts showed an increasing trend.

In its unique location, atmospheric circulation over the country is governed by the Inter-Tropical Convergence Zone (ITCZ) and the trade winds (Peries, 2004). The South Asian region has two monsoonal showers due to the annual movement of ITCZ from boreal summer (20^0 N) to boreal winter (20^0 S) De Silva & Hornberger, 2019 (Figure 2.3). Accordingly, the climate of Sri Lanka can be divided into four main seasons, depending upon the influence of causative factors: First Inter Monsoon (IM 1 – from March to April); South West Monsoon (SWM – from May to September); Second Inter Monsoon (IM2 – from October to November); and North East Monsoon (NEM – from December to February) (Sirinanda, 1983). When SWM and NEM are acting, there is a trend of increased flood and landslide incidences associated with heavy rainfall. Thus, Zubair et al. (2007) argued that analysing rainfall patterns over Sri Lanka would give valuable insight into the vast Asian monsoon system. However, changes in monsoonal strength are the main reason for changes in precipitation

intensity in Sri Lanka. Likewise, Shelton and Pushpawela (2022) revealed a weakening of the SWM and a strengthening of the NEM over the island, leading to changes in rainfall.

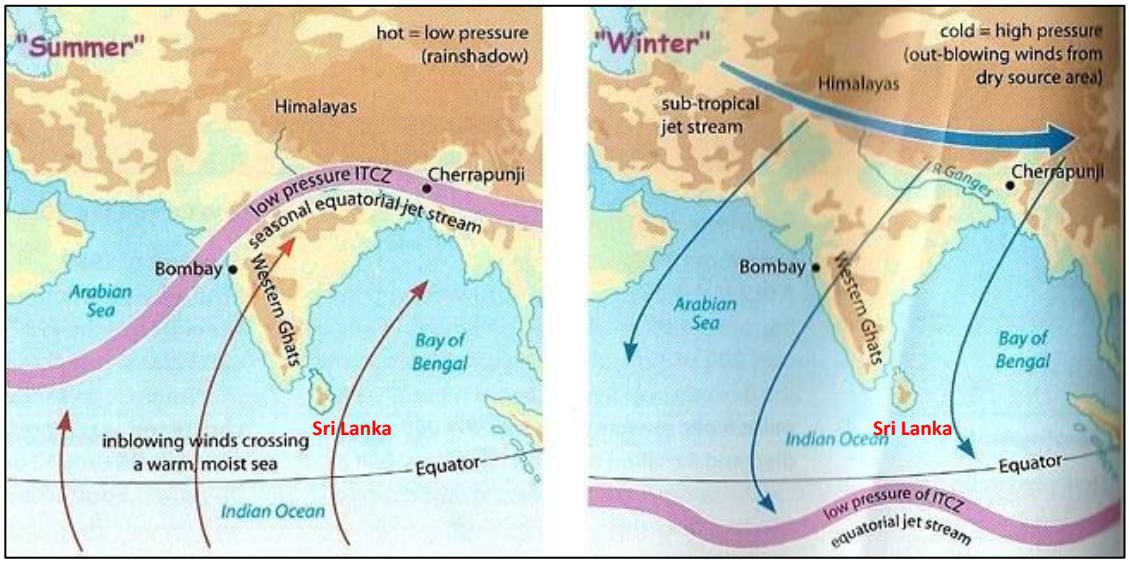

Figure 2.3 Annual movement of ITCZ (SAM). Sri Lanka is situated in the middle of the ITCZ movement path. (Source: Brewer et al., 2015)

Apart from ITCZ, rainfall anomalies across South Asia are intensely influenced by atmospheric teleconnections, which have a noticeable impact on the intensity of precipitation events and the initiation of drought conditions. Accordingly, the study by Halpert and Ropelewski (1992) noted that the El-Niño Southern Oscillation (ENSO) strongly affects the rainfall and temperature patterns of the surrounding Indian Ocean countries. Further, Ashok et al. (2001) showed that the Indian Ocean Dipole (IOD) plays a significant role as a modulator between Indian summer monsoon rainfall and ENSO. For instance, when IOD is positive, it produces extreme rainfall and flooding in East Africa as well as drought conditions in Indonesia (Saji et al., 1999). As explained by Jones et al. (2004), Madden-Julian Oscillation (MJO) significantly influences extreme rainfall in tropical regions. Along with that, in the Sri Lankan context, Suppiah (1996), Zubair et al. (2007), Burt and Weerasinghe (2014), Jayawardena et al. (2017), and De Silva and Hornberger (2019) explained the influence of the ENSO, IOD, and MJO on rainfall over the country. For example, Jayawardena et al. (2017) revealed that there is a significant impact of the MJO, causing heavy

rainfalls during SWM and IM2. The studies of Zubair et al. (2003) and Malmgren et al. (2003) found that in El-Niño years IM2, and in La-Niña years SWM, cause heavy rainfall over Sri Lanka.

However, climate change is influencing the SAM. The SAM greatly impacts global atmospheric circulation and its future behavioural patterns will significantly affect the world (Yadav, 2022). Ayantika et al. (2021) discovered that absorption of shortwave radiation above the atmospheric boundary over the Asian area causes a shortfall in surface radiation and stabilises the lower troposphere, leading to weaker monsoonal winds, reduced evaporation over the Indian Ocean, as well as decreased moisture convergence across South and Southeast Asia, due to climate change. Ashfaq et al. (2009) explained suppression of the South Asian Summer Monsoon due to climate change, which may decrease summer rainfall in South Asian countries. However, Yadav (2022) noted that ENSO and IOD, combined with the SAM, bring extreme rainfall over the South Asian region during active and breaks spells of monsoon (months with high rainfall and low rainfall during the SAM), which have been prominent in recent years. Figure 2.4 depicts the average annual rainfall of Sri Lanka, whose orography affects the spatial distribution of rainfall, as explained in section 3.1.

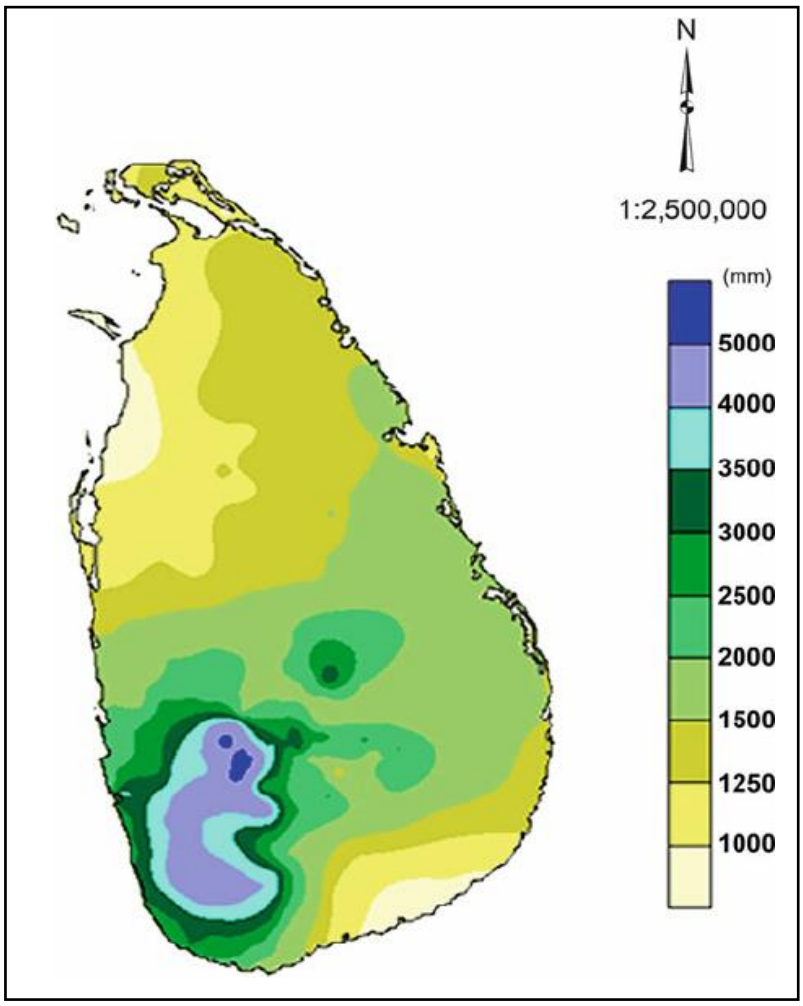

Figure 2.4 Average annual rainfall of Sri Lanka
(Source: Department of Meteorology, Sri Lanka)

When considering recent rainfall trends in Sri Lanka, Alahacoon and Edirisinghe (2021) and Amarasinghe (2020) reported the overall increasing trend, which might be related to climate-change-related extreme rainfall events. Even though there is plenty of work on Sri Lankan rainfall patterns, in recent years only a few studies have analysed extreme rainfall events over the country. Jayawardena et al. (2018) used extreme precipitation indices derived from daily rainfall data and showed an overall increase in extreme rainfall across the island. Hapuarachchi and Premalal (2021) studied extreme rainfall events from 1970 to 2019 in Sri Lanka, using percentile-based analysis (90^{th} and 95^{th} percentiles) to project emission scenarios until 2100 and their Representative Concentration Pathways (RCP). They found a significantly increasing trend in heavy and very heavy rainfall across the country. However, these two studies

did not investigate monotonic trends and the magnitudes of extreme rainfall events. The study by Abeysekera et al. (2015) examined rainfall anomalies, but was limited to Sri Lanka's Dry Zone. Thevakaran et al. (2019) studied trends in extreme rainfall data for the 1961–2010 period. They mainly calculate numbers of dry days, numbers of dry spells, and 95^{th} percentile indices from daily rainfall data for 13 meteorological stations. The Mann Kendall (MK) test was used to determine the trends of those climate indices. This study revealed a decreasing number of wet days during the SWM period, the summer half of the year, caused by climate change. Due to the limited number of recent studies of extreme rainfall over Sri Lanka, it is necessary to conduct more comprehensive studies analysing location and time aspects in order to address the existing research gap. These studies will serve as a foundation for tackling the social, economic, and environmental obstacles linked to extreme rainfall occurrences.

2.4 Rainfall and river flow variability

Water plays a fundamental role in human existence, occupying a distinct position as one of the primary elements of life. Consequently, civilisations emerged around rivers in ancient times, influenced by this crucial resource. Despite the availability of diverse technical approaches to securing water for consumption, major urban centres and densely populated regions worldwide continue to be predominantly situated alongside rivers. The global climate is changing and the impact of this on river flow changes is unavoidable (Palmer et al., 2008). At present, most of the major rivers in the world do not show the same magnitudes of fluctuation in their water flows as they did in the past (Palmer et al., 2008). Climate change connects extreme rainfall events and sea level rise and influences the flow variability of rivers, while some river basins are also under water stress due to increasing population. Due to many parameters, including precipitation, temperature, and solar radiation, the relationship between climate and water is complicated and varies greatly from region to region (Oti et al., 2020). Changing any of these variables can increase or decrease runoff, precipitation, and evaporation rates, thus altering the water cycle.

In general, studies have found that changing patterns of streamflows were influenced by changes in rainfall caused by climate change (Azari et al., 2016; Chauluka et al.,

2021; Xu et al., 2022). The study by Azari et al. (2016) showed how climate change impacted streamflow and sediment yield in the Gorganroud River Basin in the north of Iran. They used the Soil and Water Assessment Tool (SWAT) hydrological model to simulate streamflow and sediment yield, and the SUFI-2 algorithm from the SWAT-CUP program was used for parameter optimisation. This study projected increases in annual streamflows of 5.8%, 2.8%, and 9.5%, and in sediment yields of 47.7% and 44.5%, in the 2040–2069 period compared with now. Chauluka et al. (2021) assessed the long-term variability of rainfall and streamflow in the Thuchila River, southern Malawi, from 1985 to 2016. They used Mann Kendall (MK), Sen's slope, and Person's correlation coefficient tests to analyse rainfall and streamflow data. This study revealed that extreme weather events influence streamflow. Another study by Xu et al. (2022), on the Caojiang River Basin in China, discussed climate change and human influences on streamflow variation.

There are some studies of rainfall over river basins in Sri Lanka. Rainfall analysis for the Mahaweli River Basin in the Dry Zone of Sri Lanka shows an increase in annual rainfall (Imbulana et al., 2018). There is a decreasing trend in annual rainfall over the Kalu Ganga Basin in the Wet Zone (Ampitiyawatta & Guo, 2009). A study of the Uma Oya Basin found that there is no significant negative rainfall trend over the catchment (Khaniya et al., 2019). With changing rainfall variations, river flow variations keep changing. However, only a few studies have been conducted to identify the relationship between rainfall and streamflows across the island. The study by Panditharathne et al. (2022) confirmed a strong positive correlation between rainfall and the streamflows of the Nilwala River Basin. By analysing Climate Hazards Group Infra-Red Precipitation (CHIRPS) data, Alahacoon and Edirisinghe (2021) predicted that during the NEM season there would be flood risks in the southern and western provinces of Sri Lanka, but drought conditions on the eastern side. However, as an agriculture-based developing country, any change in rainfall and river flow variability greatly affects development. Therefore, there should be more comprehensive studies examining the relationship between rainfall and river flow variability on the island.

The KRB is the fourth-largest river basin in Sri Lanka (Jayasekara et al., 2020). The Kelani River rises in the central hills, flows through highly populated and urbanised areas, and drains into the Indian Ocean near the commercial capital of Colombo.

Hence, the KRB is highly influenced by anthropogenic factors like unplanned construction on riverbanks, destruction of natural drainage systems, pollution of water, and so on (Manawadu & Wijeratne, 2021; Samarasinghe et al., 2022). The basin is vulnerable to annual flooding (Randil et al., 2022). The study by Manawadu and Wijeratne (2021) outlined the impact of anthropogenic drivers on urban flooding in the LKRB, finding that human activities cause major flooding every two to three years, affecting around 200,000 people. Their study revealed that a significant decline in green cover and the conversion of paddies and marshlands into home gardens had worsened the effects of flooding. However, only the study by Jayasekara et al. (2020) has thoroughly discussed the relationship between rainfall and streamflow in the KRB from 1983 to 2013. Their study discussed trends in streamflows of the Kelani River and their association with rainfall. They used the Innovative Trend Analysis (ITA) method, the MK test with Sen's slope estimator, and Spearman's rho correlation coefficient to assess the rainfall and river flow data. They found that variation in streamflow is significantly attributable to catchment rainfall. They also reported that annual, NEM, and IM1 data show increasing trends in rainfall at most rain gauge stations. After that period, no such detailed study has been carried out to identify the relationship between rainfall and water levels at decadal, annual, seasonal, and monthly scales. Further, the study of Dissanayaka and Rajapakse (2018), examined about extreme rainfall impacts on streamflow variability in the KRB. During the study, the researchers collected daily rainfall data from seven rainfall gauging stations from 1970 to 2015. Also, daily streamflow data from the Hanwella gauging station have been collected between 1985 and 2010. To detect instances of extreme rainfall in the basin, series of extreme rainfall indices, like PRC PTOT, CWD, R95p, were employed. The findings of this study exposed a decreasing trend in the annual average rainfall throughout the KRB, with an increasing trend of extreme weather events. Furthermore, the flow data from the Hanwella station showed a decreasing trend during that period of time. However, climate and the environment are changing day by day. As mentioned earlier, land use changes, population growth, extreme rainfall over the basin and frequent flood hazards are evident in the KRB. Hence, it should be confirmed whether or not these findings have continued over the most recent decade.

2.5 Flood hazards

2.5.1 Overview of flood hazards

Floods are the most prevalent form of natural calamity globally and they present significant hazards to human life, property, the environment, and agricultural production. According to Jarvis (1936), a flood is a waterflow event that significantly inundates dry areas or where a stream overflows channel banks. Nevertheless, the public perception of flooding is of catastrophic events resulting in severe losses of life and disturbance or damage to their property (Birkholz et al., 2014). Floods can be classified according to their generative mechanisms (Mishra et al., 2022). There are three main types of flood – inland flood, coastal flood, and compound flood, as seen in Figure 2.5.

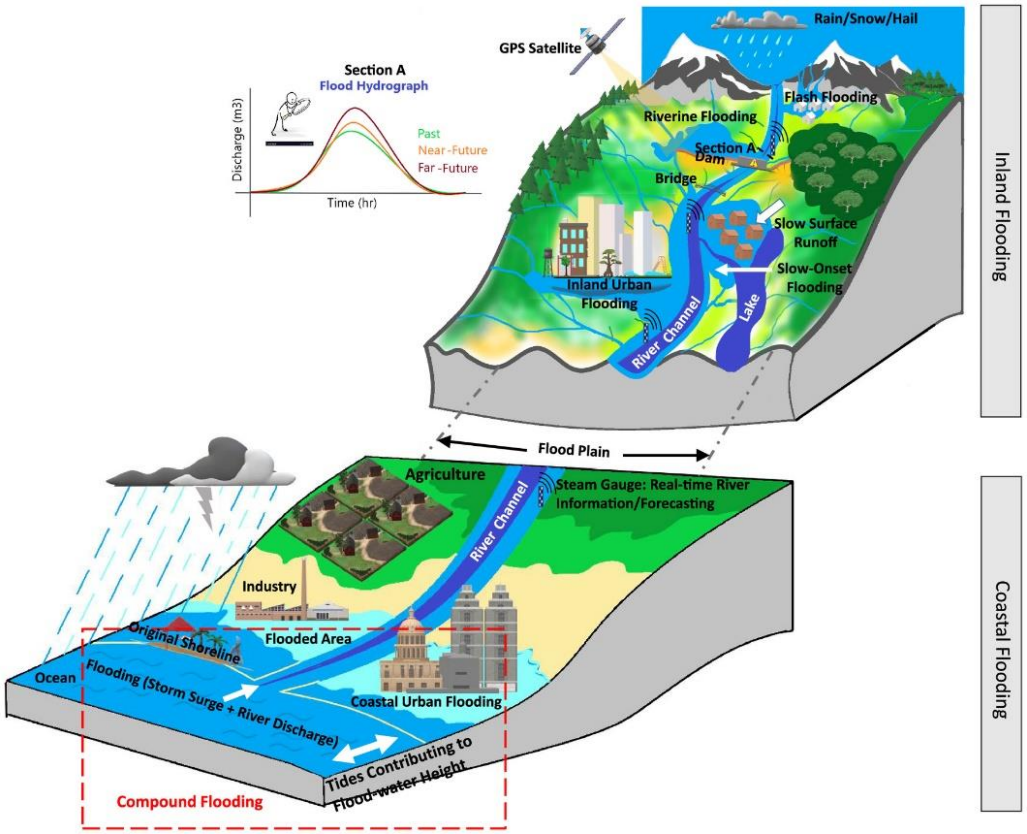

Figure 2.5 Schematic diagram of the different flood types (Source: Mishra et al., 2022)

2.5.1.1 Inland flooding

Inland flooding can be broadly classified into three categories – riverine flood, flash flood, and urban flood (Mishra et al., 2022).

- Riverine flood: Extreme rainfall, tropical cyclone, or atmospheric rivers (large, narrow sections of the Earth's atmosphere that carry moisture from the Earth's tropics near the equator to the poles) making landfall (Aryal et al., 2018; Mishra et al., 2022), persistent thunderstorms over a specified area (Smith et al., 2001), and snowmelt (Bell et al., 2016).

- Flash flood: Heavy or extreme rainfall over a short time, rapid water level rises in creeks, rivers, and urban areas (Ávila et al., 2016; Khajehei et al., 2020; Ozturk et al., 2018).

- Urban flood: Rainfall over an urban area, where impervious surfaces prevent the infiltration of water into the soil, leading to high surface runoff (Mishra et al., 2022).

2.5.1.2 Coastal flooding

Coastal flooding is caused by tidal waves, storm surges, heavy rainfall, and strong onshore winds (Mishra et al., 2022). This type of flooding is prominent in South Asia (Douglas, 2009; Mirza, 2011), northwestern Europe (Ganguli et al., 2020), and the southeastern United State (Gornitz et al., 1994; Mishra et al., 2022). Storm surges happen when water levels increase beyond the usual tidal levels, strengthened by the forces of powerful winds blowing onto the shore, waves, and decreased atmospheric pressure (Mishra et al., 2022).

2.5.1.3 Compound flooding

This type of flood is caused by the interaction among various physical drivers, such as landforms at coastal boundaries, and hydro-meteorological-related mechanisms (Couasnon et al., 2020). Anthropogenic climate change, sea level rises, and augmented impermeable surface accompanying urban development have resulted in notable inundation by compound floods in prominent coastal urban areas over the past century (Mishra et al., 2022).

2.5.2 Global flood hazard

As a consequence of climate change, the world is becoming more and more vulnerable to unforeseen events. Therefore, there is a shift in the magnitude, frequency, intensity, spatial extent, duration, and timing of various natural disasters caused by these extreme weather or climate events (Perera, 2021). However, global natural disasters are increasing. According to the Emergency Event Database (EM-DAT, 2023) report, there were more natural disasters in 2022 than in 2021.

Focusing on 2022, the EM-DAT report found that 387 natural hazards and worldwide disasters affected 85 million people and resulted in the loss of 30,704 lives. The same EM-DAT report indicated that flood was the most common type of disaster across the globe in 2022 (176 events worldwide), and floods are some of the most devastating natural disasters, causing severe damage and significant socioeconomic impacts on different sectors (Sun et al., 2020). For instance, a United Nations Office for the Coordination of Humanitarian Affairs (OCHA, 2023) report indicates that in 2023, 7.7 million people were affected by flood events in Pakistan. The EM-DAT (2023) report indicated that floods in Brazil in February 2022 killed 272 people and floods in Eastern Australia in February and March 2022 cost USD 6.6 billion. Furthermore, Nigeria lost 603 lives in that year to flood. In 2021, 3 million people in Zhengzhou and Henan Provinces of China were affected by flood hazards (Flood-List, 2021). In August 2020, in Madya Pradesh, India, 24 died and 11,000 were evacuated due to severe flood hazards (Flood-List, 2020). Also in 2022, 7.2 million people were affected by flood in Bangladesh (EM-DAT, 2023). Mirza (2011) has outlined that South Asia is considered one of the most vulnerable regions in the world due to the increases there in severe

flood frequency, magnitude, and extent. Figure 2.6, depicts Global flood risk under climate change.

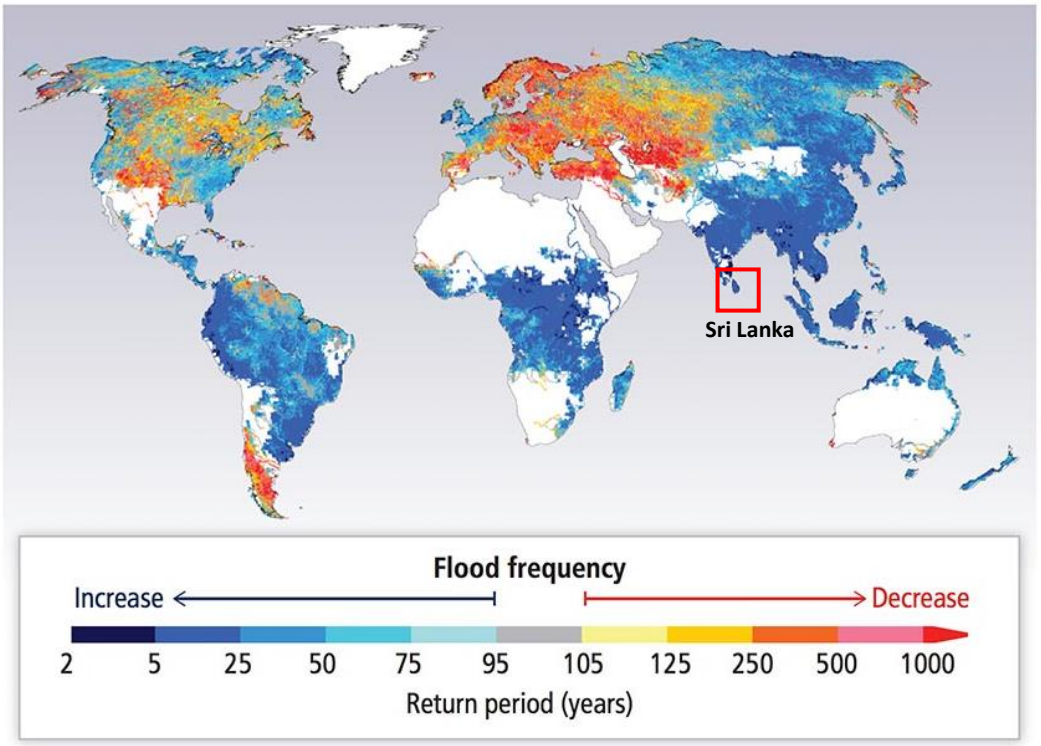

Figure 2.6 Global flood risk under climate change. Sri Lanka as a small island belongs to the increase in flood frequency category. (Source: Polka, 2018)

2.5.3 Flood hazards in Sri Lanka

Sri Lanka is a disaster-prone area, particularly floods and landslides, due to its geographic conditions and geomorphology (UNDP, 2009). Floods are said to be the most common natural disasters affecting the economy and society (Manawadu & Wijeratne, 2021). Almost 75% of annual average rainfall is recorded during the SWM and the NEM, and 60% of annual average rainfall accompanies a few intense storms (Alahacoon et al., 2018). Severe floods have occurred in some years because of tropical depressions and cyclones accompanying the southwest monsoon (Wijesinghe et al., 2023). For instance, on 25-26 May 2017, the island received 600 mm of rainfall, causing floods and landslides in the country's southwest region. Total deaths were 212

and 683,831 people were affected (Disaster Managment Center, 2018). The same IM2 and NEM periods also witness serious flood hazards. The country is receiving massive rainfall over and above its normal monsoonal rain because of the frequent development of low-pressure and tropical cyclones in the Bay of Bengal (Perera, 2021). Furthermore, most cyclonic floods occur (Basnayake et al., 2019) between October and December in the island's east, north, and north-central areas. However, the history of Sri Lankan floods provides further evidence suggesting that there has been an increase in the frequency of floods since 1925, with a substantial further acceleration since 1989 (Manawadu & Wijeratne, 2021). According to recent data, every two to three years on average Sri Lanka has experienced large-scale flooding affecting around 200,000 people (Ministry of National Policies and Economic Affairs and Ministry of Disaster Management, 2017). Further, the Kelani, Kalu, Nilwala, and Gin River Basins of Sri Lanka have the highest susceptibility to annual flooding among 103 river basins. For example, the Disaster Management Centre of Sri Lanka reported significant levels of flooding in low-lying areas of the Gin River basin in May 2023 (OCHA, 2023). In the Wet Zone, the Kelani and Kalu Rivers have been identified as having the highest frequency of flooding and accompanying damage (UNDP, 2011).

2.6 Flood risk assessment

According to the UN (1992), “Risk is the expected loss (of lives, persons injured, property damaged, and economic activity disrupted) due to a particular hazard for a given area and reference period.” This is the broadly acknowledged definition articulating the multidimensionality of risk, which also applies to flood risk assessment. Accordingly, flood risk assessment considers the potential negative effects of floods on human health, economic activity, the environment, and cultural heritage, in addition to the probability of flooding events. As shown by UNDP (2004) and UN (1992) flood risk is a combination of flood hazard and flood vulnerability.

a) Flood hazard (natural phenomena): Flood characteristics determine the degree to which objects in an economy, society, or environmental system are exposed to flooding (Solin & Skubincan, 2013).

b) Flood vulnerability: Analysis of economic, social, and environmental systems regarding their susceptibility to damage, resilience, and capacity for recovery which already existed before a flood event (Solin & Skubincan, 2013).

Flood risk assessment can be done using two methods – **a)** *absolute assessment* and **b)** *relative assessment* (Solin & Skubincan, 2013). In the absolute approach to flood risk assessment, the anticipated loss from any level of hazard severity combined with its probability is considered (Coburn et al., 1994). That means the area under the damage probability curve represents the risk of flooding (Solin & Skubincan, 2013) (Figure 2.7).

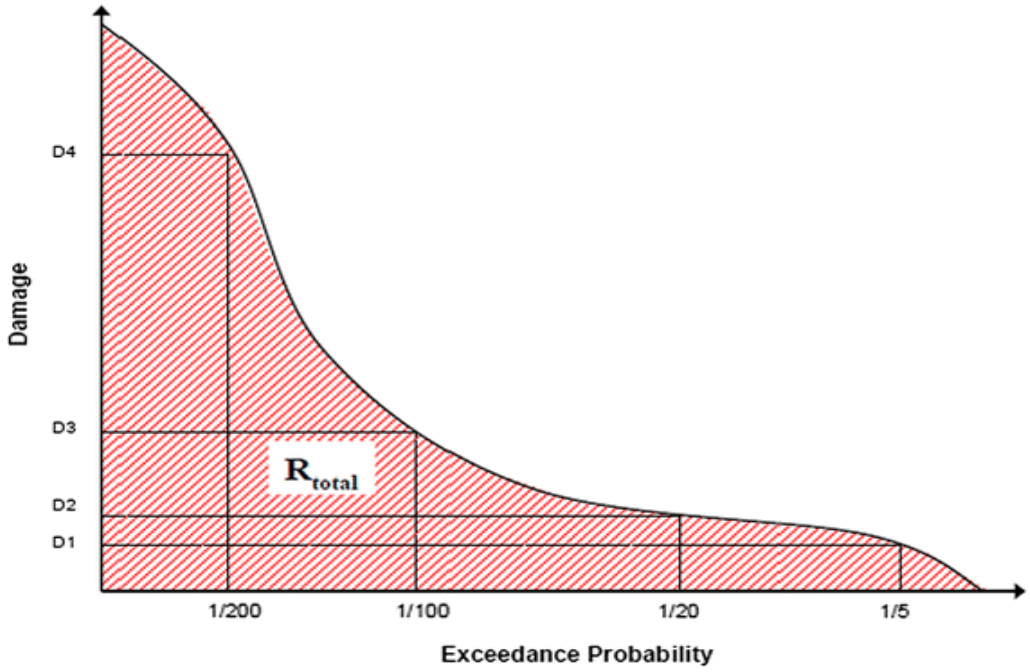

Figure 2.7 Damage probability curve (Source: Floodsite, 2006)

The size of the area under the damage probability curve (Figure 2.7) represents the average annual damage. Nevertheless, Haimes (2009) and Merz et al., 2009 emphasise that it is very difficult to assess the effectiveness of flood defence measures using the average yearly damage as an indicator of flood risk. Haimes (2009, cited in Solin and Skubincan, 2013) shows that the use of average yearly damage as the sole measure in risk estimation is the primary cause of chaotic projections of flood risk and incorrect management conclusions and decisions. Further, Solin and Skubincan (2013) argued that, according to the probability curve, as the expected average annual flood risk value

bears the same weight, one side can express a negative effect with a small probability while the other side expresses a small negative effect with a greater probability. Therefore, using the average annual damage by floods does not lead to judicious decisions in flood-risk management. The study by Merz et al. (2009) also indicated that the use of average annual damage may provide a misleading picture for flood-risk management. They showed that the low probability of high-damage floods contributes only a small part to average annual damage and should therefore have little impact on flood-risk management decisions. On the other hand, they point out that mitigation measures are often initiated in reaction to the high damage caused by severe floods, despite their low likelihood. Further, according to the average annual damage concept, decision-makers and individuals are risk-neutral, but this assumption is wrong due to the human tendency to be safety-conscious. To avoid these problems, flood-risk analysis via relative assessment is now prevalent.

Cochrane (2004, cited in Rose 2004) explained that there are problems regarding the financial assessment of social and environmental effects. Therefore, risk analysis using relative assessment can provide meaningful background to flood-risk management. In the relative method, the dimensionless values are aggregated and ranked in classes expressing a high, moderate, or low level of risk regarding vulnerabilities and potential negative consequences for economic, social, and environmental systems (Solin & Skubincan, 2013). This process is the core of spatial multi-criteria analysis and decision-making (MCDA/MCDM) (Solin & Skubincan, 2013; Taherdoost & Madanchian, 2023). The MCDM process weights the alternatives and ranks them from best to worst (Taherdoost & Madanchian, 2023) and is shown in Figure 2.8.

Figure 2.8 Steps of MCDM (Source: Taherdoost & Madanchian, 2023)

With the development of Geographic Information Systems (GIS), MCDM is rapidly advancing. The MCDM consists of two main components (Hwang & Yoon, 1981). They are multi-attribute decision-making (MADM) and multi-objective decision-making (MODM) (Hwang & Yoon, 1981; Solin & Skubincan, 2013). To address a problem, MADM selects the best alternative from a set of available alternatives. Further, the MADM uses raster-based GIS operations for evaluating the alternatives. In MODM, the number of alternatives is not specifically defined, which makes it indefinite. In the GIS environment, MODM uses vector-based operations for decision-making (Malczewski, 1999).

Considering the above information, when dealing with complex decision constellations, the MCDM method can be considered as a Decision Support Tool because it links with technological, economic, ecological, and social aspects (Ogato et al., 2020). In the MCDM environment, weighting individual variables indicates how far those variables influence the overall level of flood risk. This is a very delicate step for MCDM, since even small changes in overall weights can transform into more significant changes that will influence the analysis (Solin & Skubincan, 2013). In order to get a better understanding of the selected variables and criteria of the study on a hierarchical basis, Saaty (1977) proposed the Analytical Hierarchy Process (AHP) methodology. Thus, the use of MCDA with AHP in research has been a widespread and accepted method for several decades (Wijesinghe et al., 2023). The ability of users to define the weight of variables and provide a solution is one of the main features of the AHP method (Dissanayake et al., 2020). Hence, AHP will be one of the most valuable methods for flood vulnerability assessment (Ouma & Tateishi, 2014). There are many studies of flood vulnerability and risk assessment which use the AHP-based MCDA method (Cai et al., 2021; Danumah et al., 2016; Gacu et al., 2022; Ghosh & Kar, 2018; Ogato et al., 2020).

Nevertheless, the use of a geographical information systems (GIS) with the AHP-based MCDM method for flood modelling has become popular in recent years. Geospatial technology offers the most efficient way of analysing and delivering the results needed to make prompt and effective decisions regarding floods (Dewan & Yamaguchi, 2009; Ogato et al., 2020). For instance, Ghosh and Kar (2018) used a composite flood hazard and vulnerability index to establish policy measures to reduce the risk of flooding in

the Malda district in West Bengal, India. In their study, the AHP was applied with the help of GIS to develop flood hazard and vulnerability indicators. Previous flood risk and vulnerability maps had been prepared based on morphological and hydro-geomorphological elements. In contrast, demographic, socioeconomic, or infrastructure factors were also used to draw up their maps. The study by Hu et al. (2017) employed the AHP-based MCDM approach to map flood-risk zones in Fangshan District, China. They used six factors for flood hazard assessment, while three were considered for vulnerability assessment. The study demonstrated the effectiveness and reliability of assessing and mapping flood risks, comparing the risk map they developed with a real flood event. Further, Rahmati et al. (2016) evaluated the AHP's effectiveness in identifying flood hazard zones compared to that of hydrographical models. Their comparison results indicate that it is possible to accurately and reliably predict the extent of flood risk with an AHP. Their results suggest that a combination of GIS and AHP for flood hazard assessment is appropriate in an area with relatively little or no data.

2.6.1 AHP-based flood risk assessment in Sri Lanka

Few studies have used the AHP-based MCDM method for flood vulnerability assessment in Sri Lanka. Wijesinghe et al. (2023) used the AHP method for flood vulnerability assessment in the Neluwa Divisional Secretariat (DS) division of Sri Lanka. The study used elevation, slope, stream density, water bodies, Normalised Difference Vegetation Index (NDVI), land use, population, road networks, and buildings as parameters to create a flood vulnerability map. The feedback from 50 people in the Neluwa DS division validated the flood vulnerability map. More than 50% of them were highly satisfied with the flood vulnerability assessment. The study provides valuable insights for decision-makers to mitigate flood effects in Neluwa DS. Weerasinghe et al. (2018) conducted a qualitative flood risk assessment for the western province of Sri Lanka using the AHP method. The statistical assessment of risks, exposures, and vulnerabilities is the essence of this method which determines the overall level of flood risk. The risks considered were social, economic, and physical (housing). The results indicated that economic vulnerability is more important than social vulnerability for the population. The study recommended taking necessary

action to reduce the population's vulnerability and allocating sufficient relief and rehabilitation funds. The study by Perera (2021) of flood hazard assessment in the LKRB also used the AHP method, but only considering the physical factors that affect flood hazards. These factors include slope, elevation, land use, drainage density, rainfall, and soil type (six criteria) in the analysis. The study revealed that land use is the main contributor to flood hazards in the LKRB. Although socioeconomic factors not being considered is one of the shortcomings of this study, the flood vulnerability map generated is a good outcome of AHP-based assessment. However, it seems that there is relatively less research on the use of the AHP methodology for evaluating the risk of flooding in Sri Lanka. The findings from comprehensive studies employing the AHP approach to assess the flood risk of river basins in Sri Lanka would be extremely beneficial to inform flood-risk control.

2.6.2 FR analysis as a hazard assessment method

The FR is a bivariate statistical technique for assessing hazard susceptibility based on observed connections between hazard distributions and causative factors. This method is highly recommended by various scholars to establish a spatial correlation regarding various hazard aspects between the hazard area and the causative factors (Khan et al., 2019; Tiwari et al., 2021; de Santana et al., 2021; Ullah & Zhang, 2020; Santana et al., 2021). Some examples of FR-based hazard assessment are discussed below.

The study by Silalahi et al. (2019) shows how the FR method can serve as an advanced method of landslide susceptibility assessment. The FR model was implemented with the help of GIS to assess landslide contribution factors in Bogor, Indonesia. Soil, rainfall, land cover, geology, and DEM maps were prepared to examine landslide factors. The landslide inventory map includes 173 points. The results showed that lithology, soil, and land cover are the most prominent generators of landslides in the study area, from the middle to the southern part of the Bogor area, which is categorised as a moderate-to-high landslide susceptibility zone. The results were validated with the Area Under Curve (AUC) test, which defines the accuracy of the prediction rate curve as 87.30%. Megahed et al. (2023) used the FR method to develop a flood prediction map for New Cairo City, Egypt. They used elevation, slope, aspect, LULC,

lithology, stream distance, stream density, topographic wetness index (TWI), surface runoff, and terrain ruggedness index (TRI) as primary factors driving and defining flash floods in the city. 143 spatial points were included in their flood inventory map. They found that 19.32% of the total area of New Cairo City is highly susceptible to flooding. The AUC result was 90.11%, showing that the FR model was extremely effective for mapping flood hazards in New Cairo City.

Some researchers coupled the FR model with other statistical methods and decision-making models for hazard assessment (Biswas et al., 2023; Rehman et al., 2022; Wubalem et al., 2020). The study by Tiwari et al. (2021) is one example of such studies. This study discusses forest fires in Pauri Garhwal, India. As it was a comparative study, it used FR, AHP, and Fuzzy AHP (FAHP) modelling techniques for forest fire mapping in the study area. They used fourteen different topographic, biological, climatic, and human-induced criteria for forest fire assessment. The validated AUC revealed the maximum prediction accuracy of FAHP as 83.47%, with AHP at 81.75% and FR at 77.21%.

As this study mainly considers island's flood risk assessment, prior use of the FR model for risk assessment in the Sri Lankan context should be considered. Hence the study discusses some studies in which the FR model has already been used to assess and analyse risks in Sri Lanka.

Senanayake et al. (2020) investigated soil erosion hazards in Sabaragamuwa Province, Sri Lanka. For the mapping and classification of soil erosion hazards, input data on rainfall, soil type, terrain characteristics, and land coverage were used. They mainly used Landslide FR for hazard zoning. Further, they used a revised universal soil loss equation (RUSLE) model and informatics techniques to analyse soil erosion hazards associated with land uses. They found that soil erosion increased from 14.56 to 15.53 t/ha/year between 2000 and 2019, that the highest landslide frequency ratios were seen in less dense forest areas, and that cropping areas are very vulnerable to future landslides. Parts of Athtanagalu Oya, Kalani River-south, and Kalani River-north basins, which are in Sabaragamuwa Province, were identified as immediate priority soil conservation areas. Liyanage et al. (2019) undertook a comprehensive study on predicting landslide susceptibility in Kalutara District, Sri Lanka. 84 landslide areas

were considered for this study, with 12 conditioning factors (slope, aspect, geology, hydrology, soil type, soil thickness, land use, landform, Sediment Transport Index (STI), TWI, Stream Power Index (SPI), and rainfall). The landslide susceptibility prediction model used the Random Forest algorithm, FR, and Information Gain Ratio (IGR) models. The study found that soil thickness is the most crucial factor affecting flood hazard in the district.

However, this study found very limited studies, those used the FR method for hazard assessment in Sri Lanka. However, no any study has carried out for flood hazard assessment using FR in the islands. Our study will be able to fill the gap.

2.6.3 HAND Model for Flood Inundation Mapping

Simplified conceptual models for flood inundation mapping have developed rapidly in recent decades. The digital elevation model (DEM) and digital terrain model (DTM) are the basis of these models and can be used as primary input with only a couple of parameters needing adjustments because they do not normally solve hydraulic equations or they require an initial and boundary condition for the calculation (Li et al., 2023). In future, these models may be able to use DEM products for hyper-resolution algorithms (Demiray et al., 2021).

The HAND model is one of the simplified models derived from a DEM, which is often used for flood inundation mapping (Godbout et al., 2019; Speckhann et al., 2018). A pixel by pixel comparison of a certain water depth with the HAND value is used to generate the inundation map, which shows the variance in elevation between a pixel and the pixel in the drainage network to which it drains (Nobre et al., 2011).

At present many studies use the HAND model for flood inundation mapping coupled with other models (Aristizabal et al., 2023; Chaudhuri et al., 2021; Fang et al., 2023). For instance, the study by Speckhann et al. (2018) developed methodology for flood hazard mapping for the Itajaí River Basin, Santa Catarina State, Southern Brazil, combining flow frequency analysis with the HAND model. The map derived from this combined method showed a 92% match with the 2011 flood event in the basin. Another study by Tewari et al. (2021) proposed a hybrid flood prediction model using Long Short Term Memory (LSTM) and the HAND model for flood mapping of Cedar

Rapids City in Linn County, Iowa, USA. Their study proved that this hybrid model is more efficient and easy to use for real-time flood mapping than traditional forecasting models. Further, the study by Komolafe et al. (2020) for the first time combined the AHP and HAND models for flood susceptibility mapping in the Ogun River Basin, Nigeria. In order to identify areas where vulnerable populations and assets are located, the flood hazard map was overlayed over the demographic data. The study revealed that this integrated model provided a more accurate background for flood zoning maps.

When assessing flood risk, many studies combine decision-making models and statistical models. The most prominent integration method uses AHP and FR for flood susceptibility mapping (Tariq et al., 2022; Waqas et al., 2021; Yilmaz, 2022). For instance, the study by Ali et al. (2019) applied both AHP and FR to map flood-vulnerable and at-risk areas in the Sundarban region, India. This integrated model was 81.42% accurate in predicting flood hazards in the region. The study revealed that this combined method was very useful for flood mitigation strategies. However, there is no research combining the decision-making model, statistical model, and flood inundation model. Therefore, for the first time, this research proposed an integrated model for flood susceptibility, using AHP, FR, and HAND models. This proposed methodology is discussed in section 3.2.11.

2.7 Disaster risk reduction processes

As flood risk assessment is a component of flood risk reduction strategy, this section briefly mentioned international agreements and frameworks used to reduce flood risk globally. When considering flood risk reduction, mitigation and adaptation are crucial factors to be taken into account. Flood mitigation involves actions aimed at reducing the severity or the impact of floods, such as implementing land-use planning regulations, constructing flood barriers, and improving drainage systems (Abbas et al., 2016; Ahmad & Afzal, 2020; Qi et al., 2021). Additionally, flood adaptation strategies, timely and accurate warning systems, forecasts, rainwater harvesting, and impact mitigation measures (such as relocating vulnerable infrastructure or communities to safer areas, enhancing community preparedness and resilience, and so on.) can decrease vulnerability to flooding in any region (Tamagnone et al., 2020; Zainudini & Sardarzaei, 2022).

In order to reduce the risk of disasters, there are several international frameworks and agreements reflecting the collective efforts of countries to address the challenges posed by disasters. In view of the focus of the study on natural hazards, it is important to highlight the two main processes of disaster risk reduction implemented by the United Nations (UN), as described below.

a. Sendai Framework (SF)

The Sendai Framework is an international document adopted by UN member countries to achieve a substantial reduction in disaster risk and losses in terms of lives, livelihoods, health, and the economic, physical, social, cultural, and environmental assets of individuals, businesses, communities, and countries during the period from 2015 to 2030 (United Nations Office for Disaster Risk Reduction – UNDRR, 2024). The framework is widely followed by countries to reduce risks arising from hazards. The Sedai Framework outlines seven global targets to be achieved by 2030.

i. Reduce global disaster mortality
ii. Reduce the number of affected people globally
iii. Reduce direct economic loss in relation to GDP
iv. Reduce disaster damage to critical infrastructure and disruption of basic services
v. Increase the number of countries with national and local disaster risk reduction strategies
vi. Substantially enhance international cooperation to developing countries
vii. Increse the availability of and access to multi-hazard early warning system

(UNDRR, 2024)

SF is the main process most of countries follow to reduces risk from hazard.

b. The Paris Agreement on climate change

The Paris Agreement is an international accord on climate change that was initiated in 2015 and entered into force on 4 November 2016. This treaty covers climate change adaptation, mitigation, and finance. It is followed by 196 member countries of the

United Nations Framework Convention on Climate Change (UNFCCC). The Agreement sets long-term goals for all member countries to follow.

- substantially reduce global greenhouse gas emissions to hold global temperature increase to well below 2°C above pre-industrial level and pursue efforts to limit it to 1.5°C above pre-industrial levels, recognizing that this would significantly reduce risks and the impacts of climate change
- periodically assess collective progress towards achieving the purpose of this agreement and its long-term goals
- provide financing to developing countries to mitigate climate change, strengthen resilience, and enhance abilities to adapt to climate impacts.

(UNDRR, 2019)

As a member state of the United Nations, Sri Lanka has undertaken essential measures to reduce risks associated with hazards. The Disaster Management Centre of Sri Lanka, together with the UN and others involved in disaster management institutions such as the Irrigation Department, Meteorology Department, Central Environment Authority, and so on, has set up initiatives to ensure livelihood protection for citizens (UNDRR, 2019). These organizations show an acute concern for hazards linked to extreme rainfall events and continue to tackle every aspect that is threatening the welfare of citizens in a proactive manner. Early warning systems for a wide range of natural disasters have been implemented by the Disaster Management Centre and it has taken appropriate mitigation measures in order to reduce risks (UNDRR, 2019). In addition, to increase the effectiveness of risk reduction strategies and ensure their compatibility with international frameworks such as the Sendai Framework or the Paris Agreement, a concerted effort is being made to work together with researchers.

2.8 Chapter summary

This chapter began by examining the impact of climate change on extreme weather events, particularly in South Asia, which is emerging as a key region for global warming. The ramifications of an increase in extreme rainfall are far-reaching and will severely impact the delicate balance between human wellbeing and ecosystems, especially in regions where agriculture is the main economic activity. Moreover, this

chapter notes that extreme precipitation events are linked to a number of consequential hazards, particularly floods and landslides. However, analysis of extreme rainfall in the Sri Lankan context is limited. There should be more comprehensive studies conducted of Sri Lankan extreme rainfall patterns.

Floods have become the most common hazard associated with extreme rainfall in the recent past. This chapter covers key concepts and definitions relating to flood, as well as analyses of current flooding situations around the world, with particular attention to floods in Sri Lanka. The chapter delves into the concepts related to flood-risk assessment, which is a critical part of flood management and mitigation. There are two distinct methods of flood-risk assessment: a) absolute assessment and b) relative assessment. Risk assessment studies recommend relative assessment as the preferred method because it incorporates MCDM techniques and provides a more comprehensive and nuanced assessment of flood risks. Furthermore, this chapter explained the integration of GIS and AHP-based MCDM as a promising method for flood-risk assessment.

Flooding is a recurrent natural disaster in Sri Lanka, causing significant damage to human life, property, and the environment. The country's geographic location, SAM, and climate change all contribute to the vulnerability of different regions to flooding. Despite the fact that Sri Lanka has already carried out some AHP-based flood risk assessments, it is necessary to carry out more extensive studies to address current research gaps and present a clear basis for policies and measures dealing with floods.

It is significant that no studies have been carried out to predict flood hazards based on FR technique. Existing research, as described in sections 2.4.2 and 2.4.3, emphasise the need of integrated models in providing comprehensive flood risk maps required for effective flood management strategies. In light of previous mentioned matter, the present study introduces a novel approach to flood risk mapping by integrating AHP, FR and HAND models.

Governments, communities, and relevant stakeholders must work together at a high level to address the increasing threat of extreme precipitation events and their associated hazards, in particular flooding. To reduce the adverse effects of climate

change on vulnerable regions and to strengthen overall resilience, a comprehensive understanding of the spatiotemporal patterns of extreme rainfall events is needed in combination with effective flood risk assessment and management strategies. To this end, a coherent and structured framework to reduce risks arising from different hazards is provided for by the Sendai Framework and the Paris Agreement.

3. METHODOLOGY

This study examines the relationship between extreme rainfall and flood hazards in Sri Lanka. Three main objectives were set as instrumental benchmarks to achieve the identified research objectives within the research framework. This chapter presents the methodological framework used to achieve these objectives in two main sections. The first section will define the study area and explain the dataset according to the main objectives. The methodologies used to systematically analyse explained in the next section. This chapter is an introductory exposition of the parameters and processes needed to objectively examine the relationship between extreme rainfall events and subsequent flooding hazards.

3.1 Description of the study area and data

3.1.1. Spatial and temporal variations of extreme rainfall events over Sri Lanka

Sri Lanka is situated close to the southernmost point of the Indian subcontinent, extending from latitude 5°55′ N to 9°51′ N and from longitude 79°42′ E to 81°53′ E. The country has a total land area of around 65,610 km^2 Malmgren et al., 2003, and experiencing relatively low mean annual temperature variation, between 26.5 °C and 28.5 °C (Department of Meteorology, 2019). The island has significant spatiotemporal variations in mean annual rainfall, between 880 mm and 5500 mm (De Silva M & Hornberger, 2019). The inter-annual variation of rainfall is governed by the ITCZ and SAM. Cyclones and low-pressure systems are frequent during the inter-monsoon period (IMP). Based on the amount of annual rainfall it receives, the island can be divided into three climatic zones (Figure 3.1) – the Wet Zone (> 2500 mm), the Intermediate Zone (2500 mm - 1750 mm), and the Dry Zone (< 1750 mm) (De Silva M & Hornberger, 2019). The Wet Zone is located in the southwestern area, which is dominated by heavy rainfall during the SWM. The elevation of the country varies between 0 and 2524 metres (Survey Department, 2019), with the highest point in the central highlands of the southern central area.

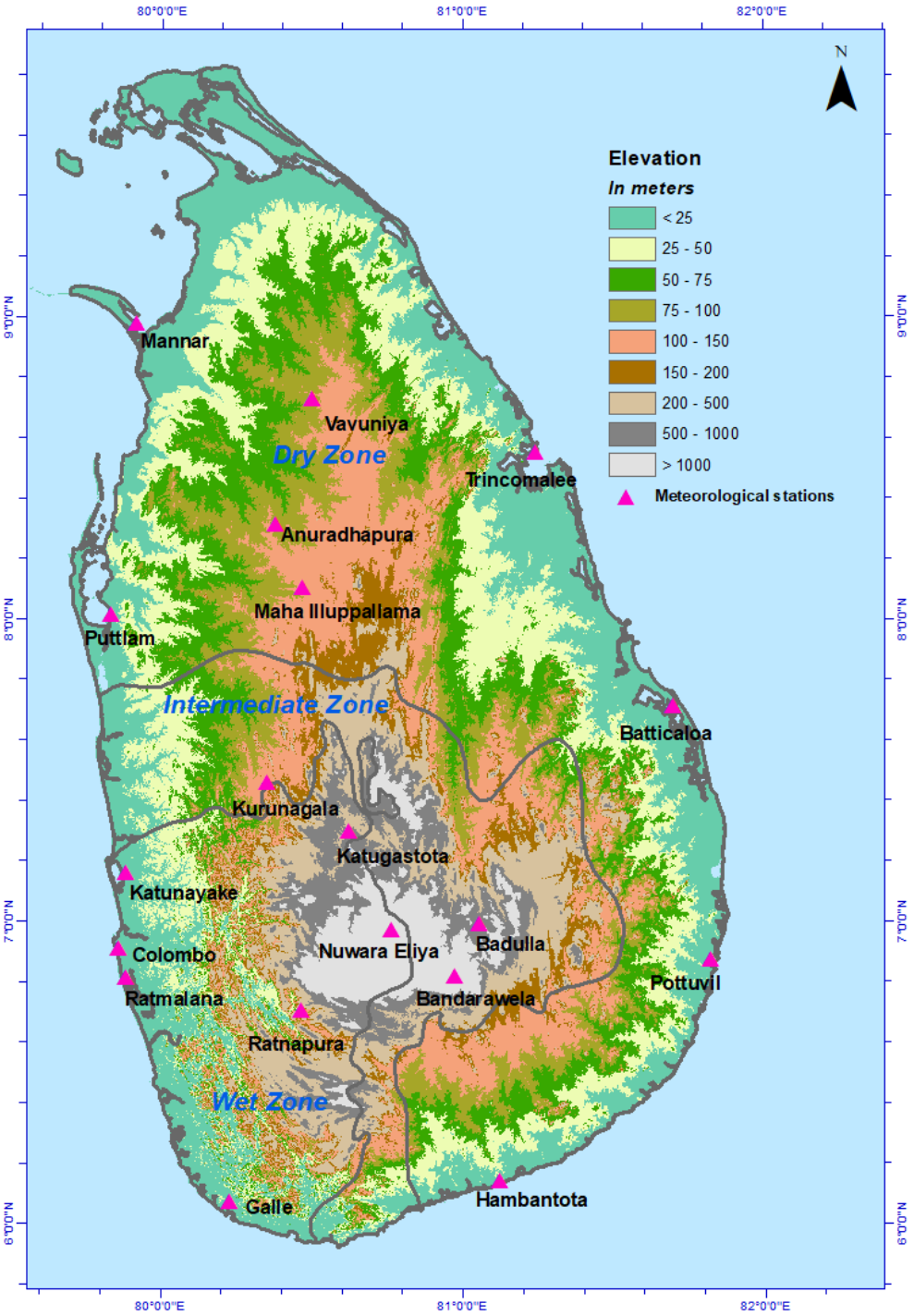

Figure 3.1 Elevation of Sri Lanka with climate zones and the distribution of meteorological stations

When considering the spatial distribution of rainfall over the country, the importance of the central highland should be considered (Figure 3.1). As the island is situated in the path of the ITCZ oscillation, the central highland acts as a climate barrier to monsoon air masses, causing considerable orographic effects. As a result of monsoonal wind and air masses in the SWM and NEM and their directions, the central highland divides into windward and leeward flanks to form a *föhn* or *foehn*[1] (Domroes, 1998). When the SWM (May – September) hits the central highland, the southwestern lowlands and the windward flanks of the southwestern highland area receive copious rainfall. After that, rain-desiccating monsoonal winds blow across the north, north-central, and southeastern regions (Domroes, 1998). The circulation of the atmosphere during the SWM provides prime conditions for thunderstorms which lead to extreme rainfall over the Wet Zone and heavy rainfall over the western slopes of the central highland region (Thevakaran et al., 2019).

For this task, daily rainfall data (1991–2020) from 19 meteorological stations (main stations covering the whole island) were obtained from the Department of Meteorology (see Figure 3.1). Table 3.1 lists the geographical locations and elevations of each station. The rationale for using these 19 stations is that they have minimal missing data for the period being considered, less than 2%. Azman et al. (2021) have suggested that Inverse Distance Weighted (IDW) is the best method to estimate missing rainfall values because it has minimum Root Mean Square Error (RMSE) and Mean Absolute Error (MAE) values. Hence, this study used the IDW method to estimate the missing rainfall values.

After filling in the missing data, the quality of the dataset was checked with the help of RClimDex in the R package (Yang, 2004). It is important to mention that the Department of Meteorology follows standard procedures, as used by WMO, to collect and convert its data into the metric system and carry out quality control. The data can thus be regarded as homogeneous (Malmgren et al., 2006).

[1] Foehn winds are warm, dry, and strong winds that form in the lee of mountains or major hills (Sharples, 2018).

Table 3.1 Location and elevation of the 19 meteorological stations across Sri Lanka used in this study. The climate zone for each station is listed as well.

No	Station	Latitude (^{0})	Longitude (^{0})	Elevation (m)	Climate zone
01	Anuradhapura	8.35	80.38	92	Dry
02	Batticaloa	7.72	81.70	8	Dry
03	Hambantota	6.12	81.13	16	Dry
04	Maha-Illuppallama	8.12	80.47	117	Dry
05	Mannar	8.98	79.92	4	Dry
06	Pottuvil	6.88	81.83	4	Dry
07	Puttalam	8.03	79.83	2	Dry
08	Trincomalee	8.58	81.25	24	Dry
09	Vavuniya	8.75	80.50	98	Dry
10	Badulla	6.98	81.05	670	Intermediate
11	Bandarawela	6.84	80.98	1225	Intermediate
12	Kurunegala	7.47	80.37	116	Intermediate
13	Colombo	6.90	79.87	7	Wet
14	Galle	6.03	80.22	12	Wet
15	Katugastota	7.33	80.63	417	Wet
16	Katunayake	7.17	79.88	8	Wet
17	Nuwara Eliya	6.97	80.77	1894	Wet
18	Ratmalana	6.82	79.88	5	Wet
19	Rathnapura	6.68	80.40	86	Wet

(Compiled by researcher, 2023)

3.1.2 Identification of rainfall and water level fluctuations and their relationships in the Kelani River Basin

The Kelani River Basin (KRB) is a region of great ecological and socioeconomic significance. The basin covers a vast area of about 2230 km^2 and stretches from the central highland to the coastal plains (Figure 3.2). The KRB lies between northern latitudes 6^0 47' and 7^0 05' and between eastern longitudes of 79^0 52' to 80^0 13', with a mean altitude of between 1.8 m and 2300 m above sea level (Samarasinghe et al., 2022). The Kelani River originates in the peak wilderness sanctuary of the central hills. It provides vital freshwater to a large population through its tributaries, which make it the primary local source of drinking water, irrigation, and hydropower. It meanders through lush forests, picturesque landscapes, and urban areas, before finally discharging into the Indian Ocean close to the commercial city of Colombo.

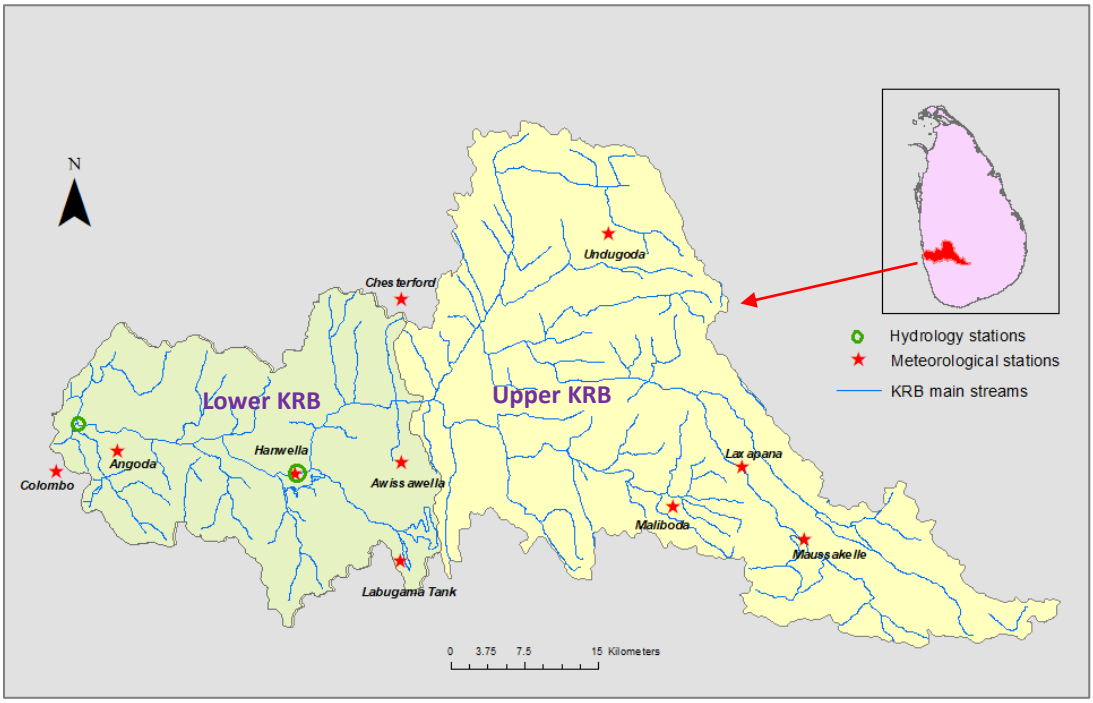

Figure 3.2 The KRB with meteorology and hydrological stations

The whole KRB is situated in the Wet Zone of the country. Centred on the Hanwella hydrology station, the KRB is divided into two main parts, the lower KRB (LKRB) and upper KRB (UKRB) (Samarasinghe et al., 2022). The lower KRB is highly urbanised, while the upper areas have dense vegetation. The rainfall distribution across the catchment varies, with the upper catchment receiving an average annual rainfall of around 5700 mm, while the lower basin receives approximately 2300 mm (Hettiarachchi, 2016). This rainfall corresponds to an approximately 7860 10^6 water volume, of which 43% is discharged into the Indian Ocean. The basin receives its highest rainfall during the SWM. During the monsoon season, streamflow varies between 600 and 1800 m^3/s along the river's length (Dissanayaka & Rajapakse, 2019).

Under this objective, the study obtained rainfall data and river flow data for the KRB.

Rainfall data

The study used rainfall data from 1991 to 2020 from the Department of Meteorology of Sri Lanka for ten stations spread over the KRB (Table 3.2). These stations had less than 2% missing data, which was essential for this study. The missing values were estimated with the IDW method, as outlined in section 3.1.1. The mean-based adjustment technique (available in the RHtestsV4 package) was used to homogenise hydro-meteorological data.

Table 3.2 Rainfall stations and hydrology stations in the KRB

No	Station name	Latitude (0)	Longitude (0)	Elevation (m)
Meteorology stations				
1	Awissawella Estate	6.92	80.18	229
2	Chesterford	7.07	80.18	198
3	Hanwella Group	6.88	80.12	82
4	Labugama Tank	6.83	80.18	172
5	Laxapana	6.90	80.52	1105
6	Maliboda	6.88	80.43	274
7	Maussakelle	6.85	80.55	1195
8	Undugoda	7.13	80.37	332
9	Angoda Hospital	6.93	79.92	15
10	Colombo	6.90	79.87	7
Hydrology stations				
1	Hanwella Station	6.91	80.08	17
2	Nagalagam Street	6.98	79.88	7

Discharge and water level data

The study used water level data from 1991 to 2020 from Hanwella and Nagalagam Street (N'Street) hydrological stations (Table 3.2), provided by the Irrigation Department of Sri Lanka. The reason for choosing these two stations was that they are located in the lower river basin area, which has a high population density and is most vulnerable to flood hazards. Dushyantha and Ptuhina (2020) found that these two stations are at high risk of being inundated due to heavy rainfall. The Hanwella hydrology station is located approximately 25 km from the sea, whereas the N'Street station is situated nearly 2 km from the coast.

3.1.3 Assessing flood risk due to extreme rainfall in the LKRB

This objective considers the LKRB (Figure 3.3) as the study area. The LKRB lies below Hanwella River Gauging Station, on generally flat terrain covering nearly 808 km^2. The lower catchment is a highly urbanised and highly populated area. However, the river gauge station located at Nagalagam Street records that the lower part of the basin is frequently flooded during the SWM season, for example, the floods of 1989, 2016, and 2018. Rapid urbanisation, reduction in drainage density, and unplanned development activities are the leading causes of floods in the LKRB (Samarasinghe et al., 2022).

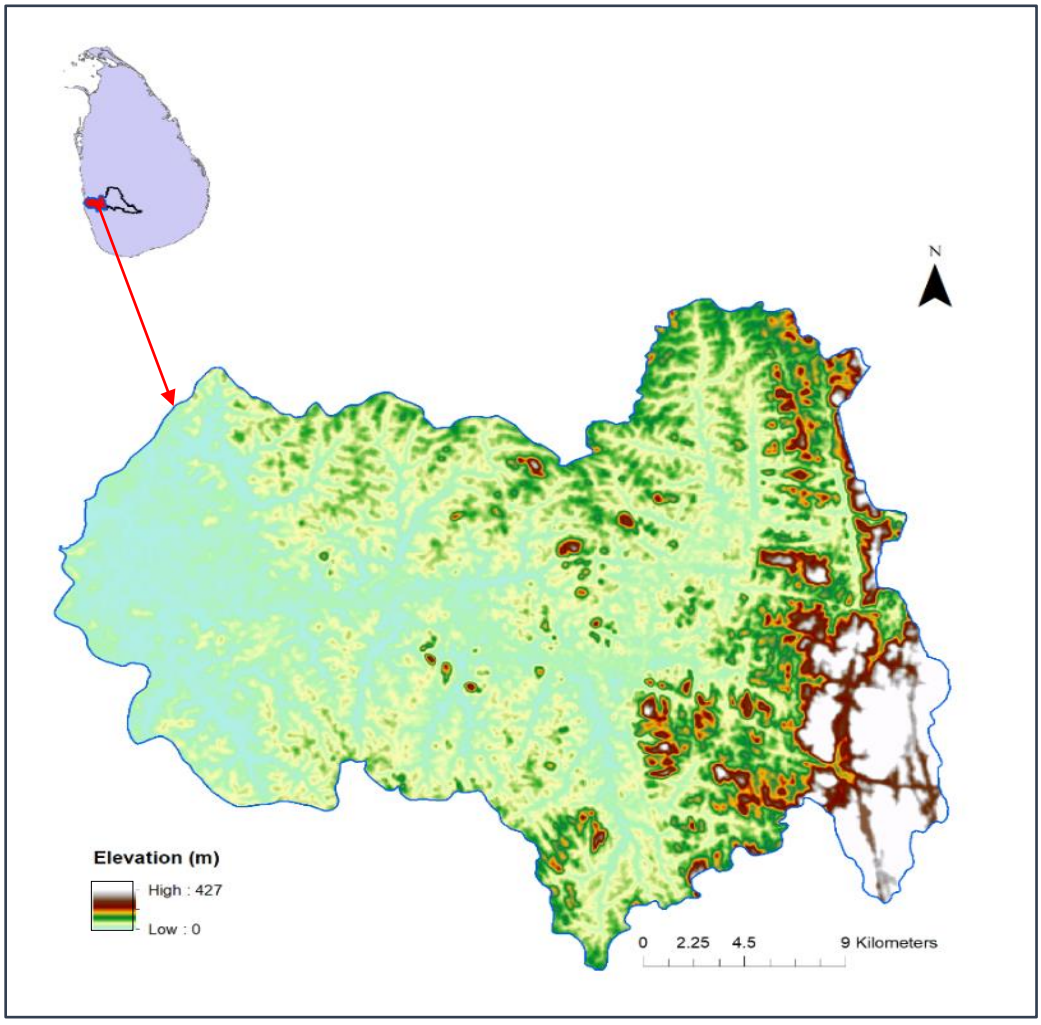

Figure 3.3 The Lower Kelani River Basin (LKRB)

As this study used AHP-based MCDM, FR, and HAND models in a GIS environment for flood risk assessment, the data mentioned below were obtained from various different sources (Table 3.3) according to hazard and vulnerability factors. The relevance of the factors used in flood-risk assessment is discussed in section 3.2.3. Two main criteria have been selected, with thirteen factors for the mapping of flood risk set out along with a comprehensive literature review and expert opinion survey.

Table 3.3 Hazard and vulnerability factors and their data sources

Criteria	Factors	Data source
Hazard	Daily rainfall data (1991 – 2020)	Department of Meteorology of Sri Lanka
	Topological Wetness Index (TWI)	Survey Department of Sri Lanka, Digital Elevation Model (DEM) layer, accuracy 1 m
	Slope	Survey Department of Sri Lanka, Digital Elevation Model (DEM) layer
	Drainage density	Survey Department of Sri Lanka, Digital Elevation Model (DEM) layer
	Soil permeability	Survey Department Digital data layers
	Proximity to the river	Irrigation Department of Sri Lanka, stream of the LKRB layer
	Elevation	Survey Department of Sri Lanka, Digital Elevation Model (DEM) layer
	Normalised difference vegetation index (NDVI)	United States Geological Survey (USGS), Landsat 8 OLI/TIRS (30 m resolution) https://earthexplorer.usgs.gov/
	Land use / Land Cover (LULC)	United States Geological Survey (USGS), Landsat 8 OLI/TIRS (30 m resolution) https://earthexplorer.usgs.gov/

	Population Density	Oak Ridge National Laboratory, LandScan Data (Gridded data - Approximate 1 km spatial resolution - Reclassified to 30m) https://landscan.ornl.gov/
Vulnerability	Road Network	Survey Department of Sri Lanka, road network layer
	Distance to flood shelter	Survey Department of Sri Lanka, buildings and places layer
	Normalised difference built-up index (NDBI)	United States Geological Survey (USGS), Landsat 8 OLI/TIRS (30 m resolution) https://earthexplorer.usgs.gov/

(Compiled by researcher, 2023)

The criteria and alternatives for the current study were chosen based on the literature, the available data, and their applicability and impact on flood risk. Using spatial thematic layers were created for each factor as raster layers. The spatial resolution was set as a cell size of 30 m x 30 m using the 'Reclassify' tool.

Further, this study created NDVI, NDBI, and land use / land cover thematic layers based on the Landsat OLI/TIRS 8 image.

Normalised Difference Vegetation Index (NDVI)

NDVI was calculated using Landsat 8 OLI/TIRS images. The NDVI values range from -1 to +1. Values close to +1 indicate high vegetation in an area. Values varied between -0.13 and 0.58 in the LKRB. The NDVI was calculated using equation 2 (Tucker, 1979).

$$\boldsymbol{NDVI} = \frac{(NIR - RED)}{(NIR + RED)} \qquad \textit{Equation 4.1}$$

Where, NIR refers to near-infrared and RED refers to red reflectance bands in the Landsat image.

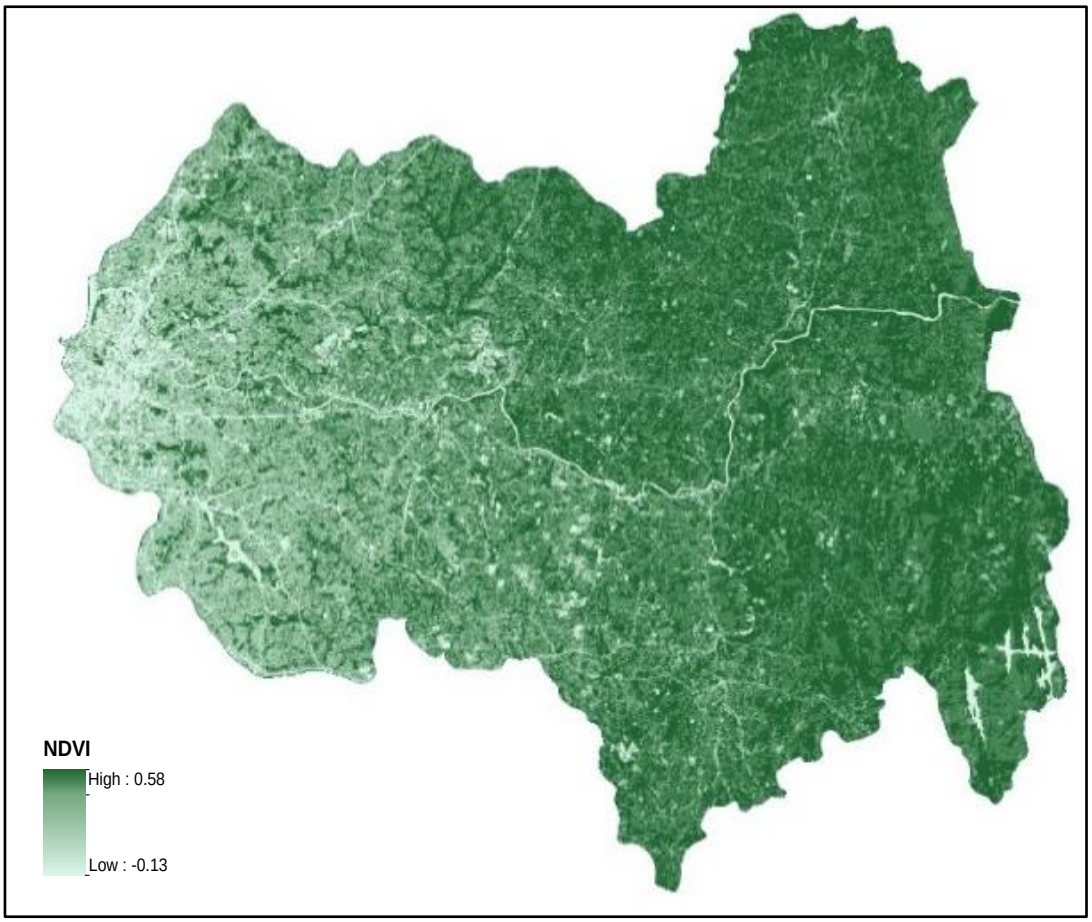

Figure 3.4 NDVI in the LKRB

Normalised Difference Built-up Index

NDBI was calculated with the help of Landsat 8 OLI/TIRS data using Equation 2 (Zha et al., 2003). The values lie between -1 and +1. If values are positive and close to +1, this denotes built-up areas. NDBI values for vegetation are low. NDBI values vary between -0.4 and 0.3 in the LKRB.

Equation 4.2

$$\boldsymbol{NDBI} = \frac{(SWIR - NIR)}{(SWIR + NIR)}$$

Where, SWIR refers to shortwave infrared and NIR refers to near-infrared reflectance in the Landsat image.

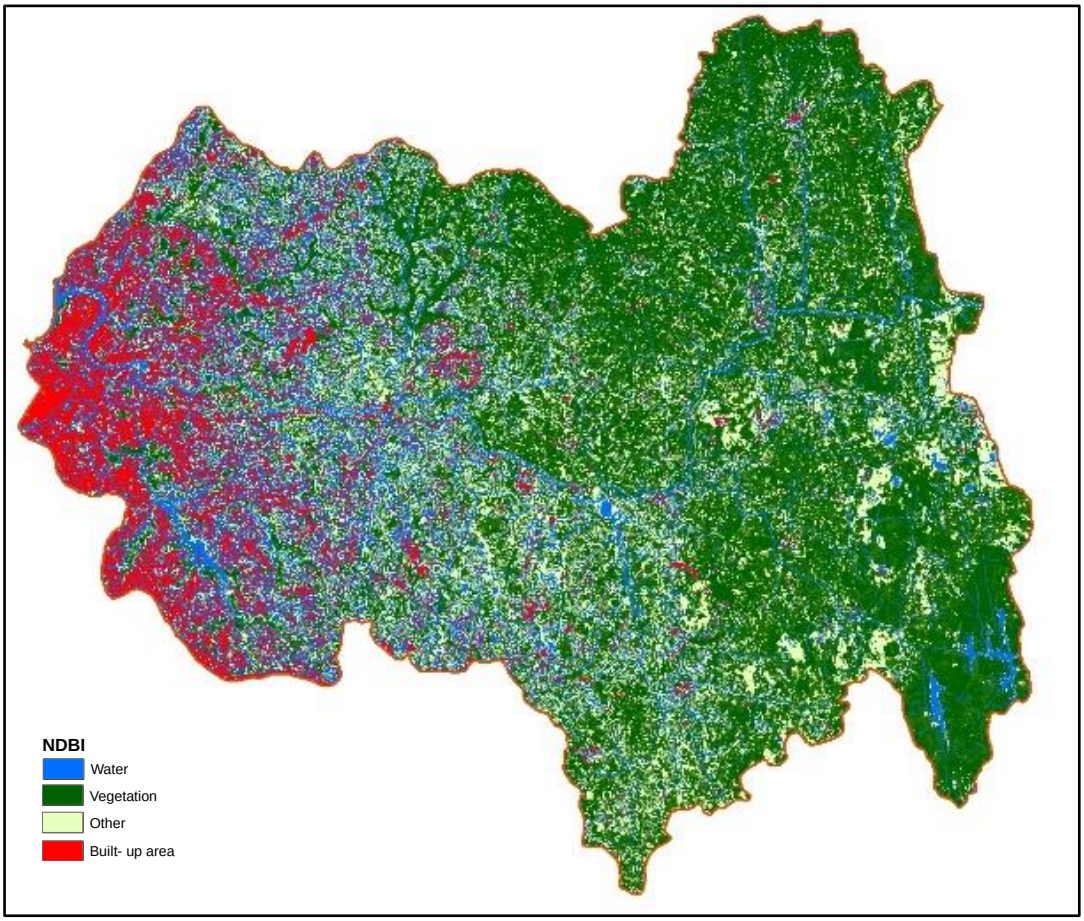

Figure 3.5 NDBI in the LKRB

Land Use / Land Cover Classification

A pixel-based supervised classification was performed on the Landsat 8 OLI/TIRS. Five classes (vegetation, built-up, agricultural land, water bodies, and other) were extracted. By using majority filters and hybrid classification methods, issues of misclassification error or 'salt and pepper effect' caused by spectral confusion were solved (Zhou & Zhang, 1999).

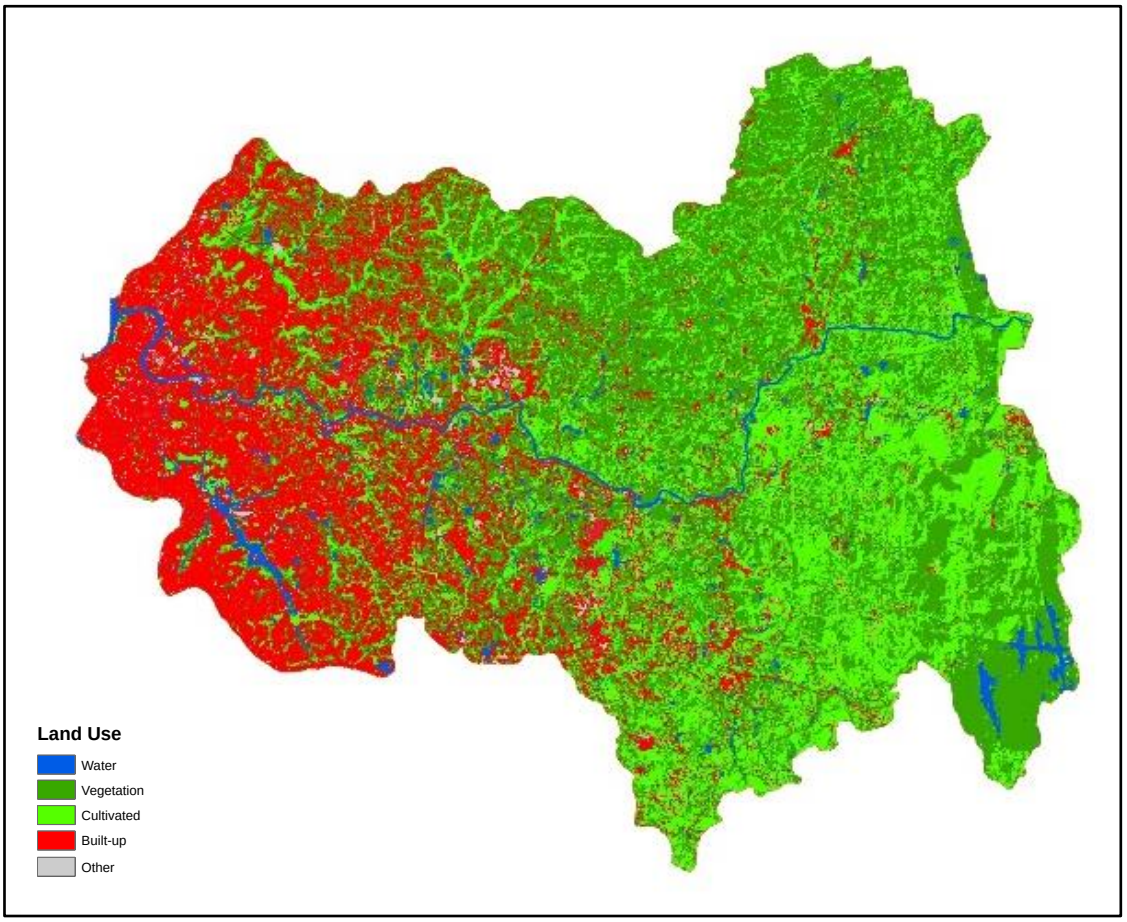

Figure 3.6 Land uses of the LKRB

Further, this study prepared a TWI map layer based on the DEM layer obtained from the Survey Department of Sri Lanka.

Topological Wetness Index (TWI)

Beven and Kirkby (1979) first proposed TWI as a Water Transport Initiative by integrating the stream accumulation areas upstream and the catchment slopes. This index is widely used to evaluate the impact of terrain on flood occurrence, soil saturation, and environmental and hydrological processes (Fatah et al., 2022; Koriche & Rientjes, 2016). Figure 3.7 depicts, TWI of the LKRB.

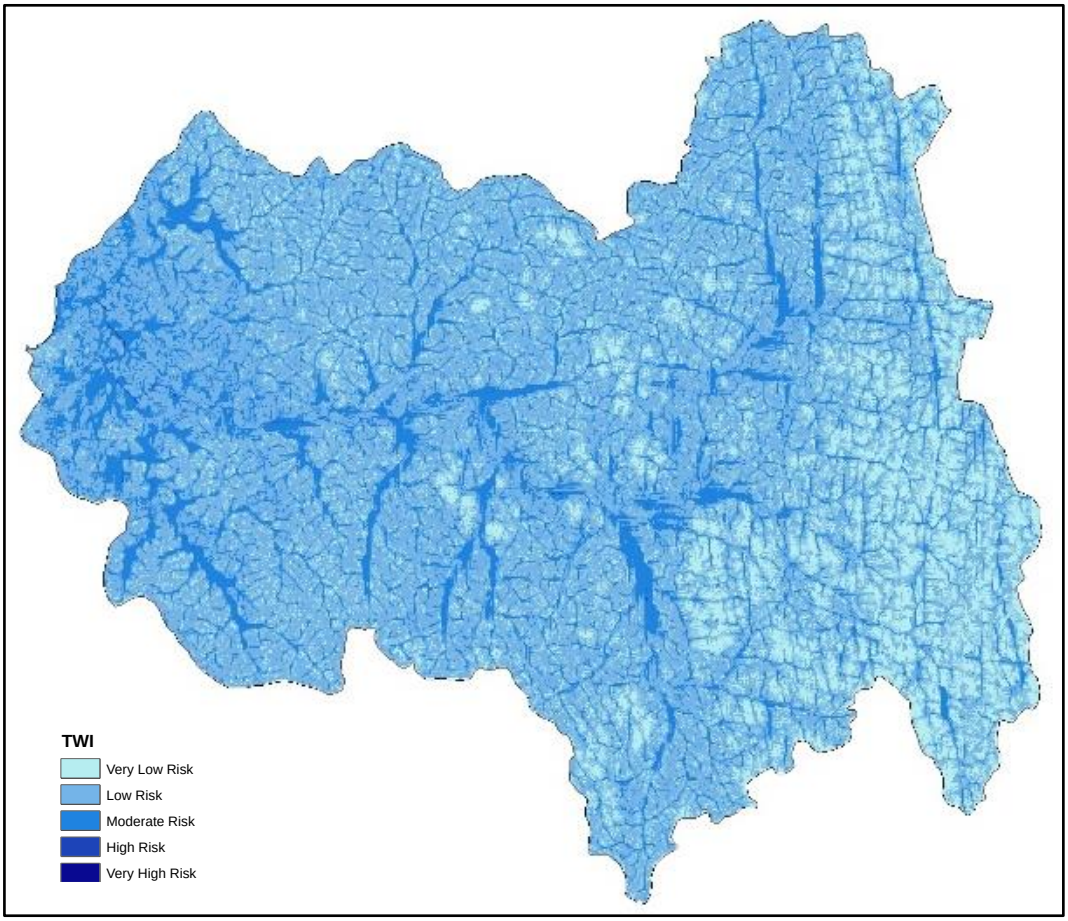

Figure 3.7 TWI in the LKRB

The TWI is calculated using below equation.

$$TWI = In\left(\frac{Acc}{tan\beta}\right) \qquad \textit{Equation 4.3}$$

Where Acc and β are the contributing areas of upslope and slope gradient, respectively. In this study, the TWI ranged from 5.13 to 22. Highest TWI values represent higher susceptibility for flooding. The values were classified using natural breaks classification method into five classes of flood influence.

3.2 Methods

3.2.1 Processing rainfall and water level data

Gradual or abrupt changes in the various components of the hydro-climate data collection, its transformation methods, and the locations of the measuring stations may result in non-natural changes to climatic time-series data (Costa & Soares, 2009). Hence, the RHtestsV4 package in R software (R-Core-Team, 2013) was used to test the homogeneity of the daily water level time-series data, while the RHtests_dlyPrcp package was used to process the daily rainfall time-series. The software also provides for the inclusion of a data-adaptive Box-Cox transformation procedure with a penalised maximal F test and, secondly, it considers non-normal distributions of daily rainfall data series (Wang et al., 2010). Subsequently, non-homogeneous daily time-series data were homogenised by applying mean-based adjustments, as available in the RHtests_dlyPrcp package.

3.2.2 Extreme precipitation indices

This study examined extreme rainfall over Sri Lanka. For this purpose, this research used nine extreme precipitation indices (Table 3.4) to identify extreme precipitation over the island, defined by the Expert Team on Climate Change Detection Indices (ETCCDI) of the WMO (2020).

Table 3.4 List of indices used in this study (after ETCCDI, 2012)

Index	Name	Description	Unit
RX5day	*Wettest 5-day period*	Monthly maximum consecutive 5-day precipitation.	mm/year
RX1day	*Wettest Day*	Monthly maximum 1-day precipitation.	mm/year
R99p	*Rainfall on Extremely Wet Days*	Annual total precipitation when daily rainfall amount on a wet day > 99 percentile.	mm/year
R95p	*Rainfall on Very Wet Days*	Annual total precipitation when daily rainfall amount on a wet day > 95 percentile.	mm/year
SDII	*Average Daily Rainfall Intensity*	Annual total precipitation divided by the number of wet days (mm/day) in the year. Wet days are defined as precipitation ≥ 1.0 mm.	mm/days/year
PRCPTOT	*Total Precipitation*	Annual total precipitation in wet days (precipitation ≥ 1 mm).	mm/year
R20-mm	*Days with ≥ 20mm Rain*	The R20mm index is the annual count of the number of days when daily precipitation exceeds 20 mm (R ≥ 20mm) during the study period.	days/year
R10-mm	*(Days with ≥ 10mm Rain)*	The R10mm index is the annual count of the number of days when daily precipitation exceeds 10 mm (R ≥ 10mm) during the study period.	days/year
CWD	*Consecutive Wet Days*	The CWD index is annual count of maximum number of consecutive days when daily precipitation exceeds at least 1 mm (R ≥ 1 mm).	days/year

SDII and PRCPTOT indices provide average and total values, respectively, while the other seven indices identify extreme events.

3.2.3 Interpolation techniques

This study tries to identify the spatial pattern of extreme rainfall as part of first objective. Accordingly, the RMSE and MAE were calculated for the IDW, Kriging, and Spline interpolation techniques, regarding extreme rainfall indices. In particular, the IDW interpolation method has shown to be the lowest RMSE and MAE values for extreme rainfall indices compared with other techniques evaluated. For instance, for the RX5day index, the IDW technique showed an RMSE value of 0.12, whereas the Kriging technique showed an RMSE value of 19.66. Subsequently, the IDW interpolation technique was used to map the spatial pattern of extremely rainfall over the island. IDW assumes that the local influence and weight of each measured point

decreases parallel to the distance from the observed and sample points (Li & Revesz, 2004).

3.2.4 Statistical techniques

For the first two objectives, this study attempted to analyse trends in rainfall and water level data. For the trend analysis, the Mann Kendall test, Modified Mann Kendall test, and Sen's slope were used.

3.2.4.1 Mann-Kendall (MK) test and Modified Mann-Kendall (MMK) test

This study used MK and MMK test to identify the trends in rainfall and water level data.

The non-parametric MK test is widely applied to the analysis of trends in precipitation indices (Alahacoon & Edirisinghe, 2021; Jiang et al., 2019). The MK test (Kendall, 1962; Mann, 1945) is based on a nonparametric approach that searches for monotonic changes over time without necessarily assuming their statistical distribution. Assuming that the rainfall time series was independent, then Mann-Kendall statistic S was computed as,

$$S = \sum_{i=1}^{n-1} \sum_{j=i+1}^{n} sgn\,(x_j - x_i), \qquad \textit{Equation 4.4}$$

where n is the sample size and $x_j - x_i$ are sequential data for the i^{th} and j^{th} terms. Assuming $(x_j - x_i) = \theta$, the value of $sgn\,(\theta)$ is calculated as:

$$\text{sgn}(\theta) = \begin{cases} 1 & if\ \theta > 0 \\ 0 & if\ \theta = 0 \\ -1 & if\ \theta < 0 \end{cases} \qquad \textit{Equation 4.5}$$

The statistic S is approximately Gaussian when n = 18 with the mean $E[S]$ and variance $Var\ (S)$of the statistic S given by

$$E[S] = 0, \qquad Var\ (S) = \frac{n(n-1)(2n+5)}{18} \qquad \textit{Equation 4.6}$$

However, if ties (zero difference between compared values) exist in the dataset, then the expression for $Var\ (S)$ has to be adjusted and becomes

$$Var[S] = \frac{n(n-1)(2n+5) - \sum_{k=1}^{n} t_k\ (t_k - 1)(2t_k + 5)}{18} \qquad \textit{Equation 4.7}$$

The variables n and t_k in equation 4.7 area a number of tied groups and a number of data values in the p^{th} group, respectively. The standardized statistic Z for the one-tailed test of the statistic S is given as follows.

$$Z_{mk} = \begin{cases} \dfrac{s-1}{\sqrt{Var(s)}} & if\ S > 0 \\ 0 & if\ S = 0 \\ \dfrac{s+1}{\sqrt{Var(s)}} & if\ S < 0 \end{cases} \qquad \textit{Equation 4.8}$$

If Z_{mk} is positive, then the trend is increasing, and if Z_{mk} is negative, then the trend is decreasing.

However, serial correlation, very often found in hydro-climatic time-series, is not considered by the MK test (Hamed & Rao, 1998). When there is a serial correlation in a dataset, it increases the probability of finding significant trends even if they don't exist, which may lead to a misleading interpretation of results. Hamed and Rao (1998) propose the MMK method to avoid serial correlation in hydro-climatic datasets. In the presence of autocorrelation, this methodology is strong and relies on modified variations of the MK test (Hamed & Rao, 1998). To compensate for the effects of serial correlation on variance, the modified variance should be calculated using an effective sample size (Hamed & Rao, 1998).

MMK is calculated as,

$$Var\ (S)^* = V(S)\frac{n}{n^*} \qquad \textit{Equation 4.9}$$

where $Var\ (S)^*$ is the modified variance and n^* is the effective sample size. The n/n^* ratio was computed with equation 4.9, as proposed by Hamed & Rao (1998).

$$\frac{n}{n^*} = 1 + \frac{2}{n(n-1)(n-2)}\sum_{i=1}^{n-1}(n-i)(n-i-1)(n-i-2)r_i \qquad \textit{Equation 4.10}$$

where n = actual number of observations and r_i = lag-i significant autocorrelation coefficient of rank i of time series. Once $Var\ (S)^*$ was computed with equation 4.9, it was then substituted for $Var(s)$ in equation 4.10. Finally, the Mann-Kendall Z was tested for significance of trend, comparing it with the threshold level of 1.96 for a 5 % level of significance.

3.2.4.2 Sen's slope estimator

The MK test shows only the direction of a trend but does not quantify its magnitude. Therefore, the nonparametric Sen's slope (Sen, 1968) is used to determine the magnitude of an underlying trend. This test is recommended by WMO (2018) for detecting trends in hydro-meteorological data. In this study, Sen's slope value were calculated to detecting the magnitude of the rainfall and water level trend. Sen's slope for a monotonically increasing or decreasing time (t) series $f(t)$ is computed as

$$f(t) = Qt + B, \qquad \textit{Equation 4.12}$$

where Q is slope of the trend $f(t)$, and B is the intercept. To determine Q in equation 4.12, slopes between each data pair are calculated using:

$$Q_i = \left[\frac{X_j - X_k}{(j-k)}\right] where\ j > k \qquad \textit{Equation 4.13}$$

If there are n values of X_j in the time series, then there will be N = n (n − 1)/2 slope estimates of Q_i. Sen's estimator of the slope is the median of these N values of Q_i.

3.2.4.3 Sequential Mann Kendall (SqMK) Test

In 1990, Sneyers, developed a sequential version of Mann-Kendall (SqMK) test statistics for time-series to detect recognised events or change-points in long-term time-series. This method is widely applied for detecting change points in a time series by various scholars (Tiwari & Pandey, 2019; Zarenistanak et al., 2023). The SqMK test requires calculating two series, one progressive and the other regressive. A statistically significant turning-point occurs when the two series cross and deviate above the 95 % confidence limit. SqMK calculation depends on ranked values, y_i of the original values in analysis (x_1, x_2, x_3, … x_n). The magnitudes of y_i (i = 1,2,3, ……, n) are compared with y_j (j = 1,2,3, ……., i - 1). For each comparison, the cases where $y_i > y_j$ are counted and denoted by n_i (Sneyers, 1990). Hence, t_i can be defined as,

$$t_i = \sum_{j=1}^{i} n_i \qquad \textit{Equation 4.14}$$

The mean and variance of t are calculated by equations 4.15 and 4.16, respectively.

$$E(t_i) = \frac{i(i-1)}{4} \qquad \textit{Equation 4.15}$$

$$Var\ (t_i) = \frac{i(i-1)(2i+5)}{72} \qquad \textit{Equation 4.16}$$

The sequential values of the statistic $u(t)$ are then calculated as,

$$u(t) = \frac{t_j - E(t)}{\sqrt{Var\ (t_j)}} \qquad \textit{Equation 4.17}$$

The values of the $u(t)$ regressive series are calculated as for progressive calculations, but starting from the end of the data series.

3.2.4.4 Pearson's correlation coefficient

The Pearson's correlation coefficient is used to determine the relationship that exists between two variables and it is used when both variables being studied are normally distributed (Mukaka, 2012). Hence, this study applied Pearson's correlation coefficient to identify the relationship between water level and rainfall across the KRB for the second objective.

$$r = \frac{\sum(x_i - \bar{x})(y_i - \bar{y})}{\sqrt{\sum(x_i - \bar{x})^2 \sum(y_i - \bar{y})^2}} \qquad \textit{Equation 4.18}$$

where r is the correlation coefficient, x_i is value of the x-variable in a sample, $\bar{x}$ is the mean of the values of the x-variable, y_i is the value of the y-variable in a sample, and $\bar{y}$ is the mean of the values of the *y*-variable.

3.2.4.5 Lag correlation

If we use X-values from earlier periods to explain present Y-values, then a lag correlation should be used for the two different time-series (Good data, 2023). The following equation is used for calculating lag correlation between rainfall and water levels in the KRB.

$$CCF(k) = \frac{\sum[(\mathrm{R_t} - \bar{\mathrm{R}})(\mathrm{W_{t-k}} - \bar{\mathrm{W}})]}{[\sqrt{(\Sigma(\mathrm{R_t} - \bar{\mathrm{R}})^2 * \Sigma(\mathrm{W_{t-k}} - \bar{\mathrm{W}})^2)}]} \qquad \textit{Equation 4.19}$$

Where, CCF (k) represents the cross-correlation at lag k, R denotes rainfall, and W is water level. $\mathrm{R_t}$ and $\mathrm{W_{t-k}}$ are the values of the rainfall and water level time-series at time t and time t-k, respectively. $\bar{\mathrm{R}}$ and $\bar{\mathrm{W}}$ are the mean values of the rainfall and water level time-series, correspondingly. Σ is the summation of the specified range of data-points, which is derived from the beginning of the time series to the end.

3.2.5 Innovative Trend Analysis (ITA)

The ITA method introduced by Şen (2012), as a new non-parametric basis methodology for detecting trends in a time series. Because of its advantages over other nonparametric methods, the ITA approach has been used in most studies to analyse and detect trends in climatological, meteorological, and hydrological data time-series around the world (Gujree et al., 2022; Wang et al., 2020). The first stage of this strategy will be to split the hydro-meteorological time-series data into two equal parts, with each one progressively placed in a different order. In the second phase, the first half of the sub-series (Xi; I = 1, 2… n/2) is positioned at the X-axis, while the second (1/2 (Xj; j = n/2 + 1, n/2 + 2… n) is positioned at the Y-axis of a Cartesian coordinate system, as depicted in Figure 3.8. In order to describe the domain differences of individual subgroups (low, medium, and high), a number of clusters can be applied. If the data-points in the scatterplot are placed on the 1:1 (45°) line, it is revealed that they are trendless. The ± 10% lines are used to get a better understanding of the distance from the 1.1 line.

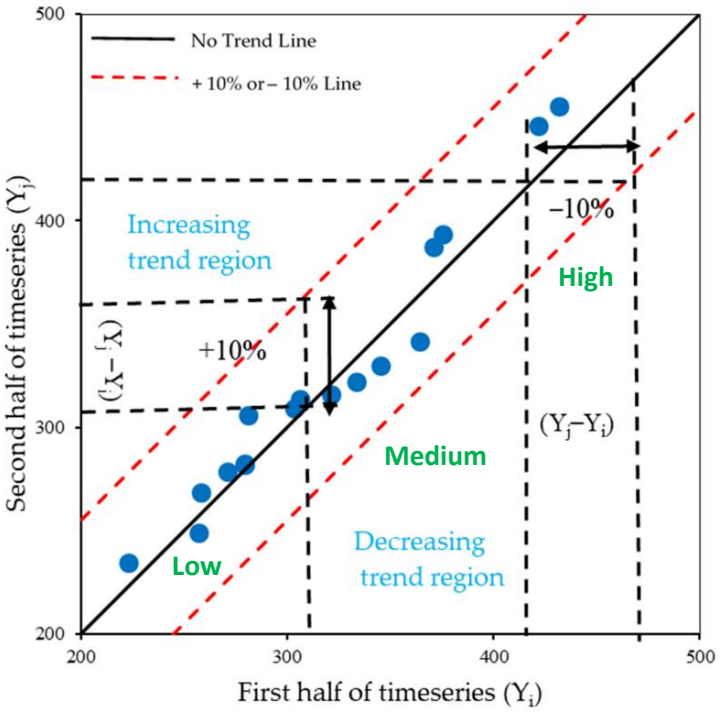

Figure 3.8 Illustration of ITA (Source: Sen, 2012)

For the third objective, this study proposes new integrated method (ARH method) for flood susceptibility mapping. Accordingly, the following topics described process of AHP, FR, and HAND models.

3.2.6 AHP-based flood risk assessment

This study has performed detailed analysis of how AHP-based MCDM can be used to analyse the flood risk in the LKRB. This method was developed by Saaty (1977). The AHP is an easy way of designing prototypes, and it is one of the most popular techniques for combining decision-making processes with geospatial analysis (Wijesinghe et al., 2023). This method is widely applied as an MCDM method for flood-risk estimation in various regions (de Brito & Evers, 2016). A common approach with the AHP is gathering expert information (Chandio et al., 2013; Laura & Deswal, 2018). Accordingly, this study also used ten expert opinions (from a hydrologist, two geomorphologists, two climatologists, and five researchers) and a literature review to define the criteria and factors for flood-risk assessment in the LKRB. The relevance of the data for flood-risk assessment is explained below.

Rainfall is the most important factor in creating floods (Costache et al., 2019). Especially when heavy rainfall occurs, the intensity of occurring floods arises. Hapuarachchi et al. (2011) explained the capacity of extreme rainfall to create flash floods within a few hours. The KRB has witnessed severe flood hazards due to extreme rainfall events in recent years, especially in 2016. The study used daily rainfall data from six meteorological stations (at Awissawella Estate, Chesterford, Hanwella Group, Labugama Tank, Angoda Mental Hospital, and Colombo) for the study.

TWI is used to quantify topographic controls on hydrological processes (Sørensen et al., 2006) and greater TWI values are usually found in flooded areas (Shafapour et al., 2019). The usefulness of TWI for flood susceptibility mapping using the AHP method has been shown in many studies (Mehravar et al., 2023; Ullah & Zhang, 2020; Vilasan & Kapse, 2022). This study generated the TWI map layer with the help of the DEM layer obtained from the Survey Department of Sri Lanka.

Slope is an important factor that contributes to the destructive strength of floods (Gacu et al., 2022). Most of the LKRB is generally flat terrain with a low slope profile. Hence,

the LKRB is one of the river basins in Sri Lanka most exposed to floods (Randil et al., 2022). Every 2 to 3 years the basin experiences large-scale flood events, affecting approximately 200,000 people (Manawadu & Wijeratne, 2021). Accordingly, the slope map for the LKRB was generated with the help of the DEM layer.

Elevation is one of the most crucial factors in flood susceptibility. Also, flood and elevation are inversely proportional to food security risk (Sarkar & Mondal, 2019). As mentioned regarding slope above, most of the LKRB is low-lying areas which are highly vulnerable to flood hazards. Using the DEM layer, an elevation map was created for the LKRB.

Drainage density is one of the crucial factors in determining flood events in a river basin (Yang et al., 2022). In general, a decrease in soil infiltration capacity or permeability increases drainage density (Radwan et al., 2018). Radwan et al. (2018), show how high drainage density values indicate the presence of impervious subsurface materials or geomorphology, or of sparse vegetation. Drainage density for the LKRB was mapped using the DEM layer.

NDVI is a widely used remote sensing index used as a flood control factor (Tang et al., 2020). The index is frequently used as an appropriate factor in flood-zone mapping (Chowdhuri et al., 2020; Saha et al., 2021). The study prepared a NDVI map for the LKRB with the help of Landsat OLI/TIRS 8.

Soil permeability is primarily an indicator of soil's ability to store water. Permeability changes can be used as early warning signs of flood risk and soil degradation (Desertification Indicator System for Mediterranean Europe, 2004). Soil type and texture are also very important factors in determining infiltration and water-holding capacity, which affect an area's susceptibility to flooding (Seejata et al., 2018). The Kelani River Basin includes different types of soil. The lower basin has alluvial soils with variable drainage and texture on its flat terrain (Goonatilake et al., 2016), but the area has more construction than the UKRB.

Proximity to the river is a crucial factor in flood vulnerability. Areas close to main canals and stream accumulation are more prone to flooding. Human proximity to rivers especially determines the magnitude of flood risks (Mård et al., 2018). Due to the urbanisation and high human settlement density of the LKRB, people close to the Kelani River suffer from extreme hydrological events (Wijeratne & Li, 2022). This

study applied Multiple Buffer Rings analysis (ArcGIS 10.8 software) to the stream layer to detect distances from streams.

LULC is one of the most crucial factors in flood susceptibility. Areas with sparse vegetation are more prone to flood (Rahman et al., 2021) and urbanised areas with impervious surfaces and barren land increase surface runoff (Mojaddadi et al., 2017). The study prepared a LULC map, using the Landsat OLI/TIRS data. Supervised classification was carried out to identify the five LULC classes – vegetation, agricultural land, built-up areas, water bodies, and other.

Population is a very important factor in flood vulnerability assessment. Highly populated areas are often more susceptible to floods. The risk of flood increases with population increase (Li et al., 2019). Because the LKRB includes two highly populated districts, Colombo and Gampaha, high population density and industrial density are evident in the area (Amarasinghe, 2016). Using LandScan satellite imagery, population density for the LKRB was extracted. This imagery has a nearly 1 km spatial resolution and reclassifies into 30 m x 30 m raster cell size. LandScan satellite imagery provides researchers with data on population density, especially in countries that do not conduct a regular census.

Building density is another factor increasing flood risk. Floodwater is assumed to be impeded and flow more slowly when in contact with buildings (Kelman & Spence, 2004). This study used satellite-derived NDBI to identify built-up areas in the LKRB, using Landsat OLI/TIRS 8 data. This index is used by researchers for flood susceptibility mapping (Bui et al., 2020; Vilasan & Kapse, 2022).

Road networks play an important part during flood relief work (Ghosh & Kar, 2018). On the other hand, impermeable surfaces like roads also increase the rainfall surface runoff (Mukherjee & Mishra, 2021). Therefore, road networks are another factor affecting flood risk.

Distance to flood shelter is an important factor in flood risk management. Due to submergence by flood, people leave their homes for safety, hygiene, and sanitisation reasons (Ghosh & Kar, 2018). In Sri Lanka, government schools and religious buildings act as flood shelters during flooding events. Therefore, this study extracted government schools and Buddhist temples from a buildings and places digital layer.

Afterwards, distances were calculated in the ArcGIS 10.8 software environment using Multiple Buffer Rings analysis.

3.2.6.1 Establishment of criteria and factors for the AHP

After collecting the necessary data, this study prepared the AHP-based flood risk assessment. In the AHP, a hierarchical structure is established from the highest to the lowest levels, interrelating and connecting all the decision sections, and the study's objectives were set on the upper part of the hierarchical structure. Figure 3.9 illustrates this composite flood risk assessment model.

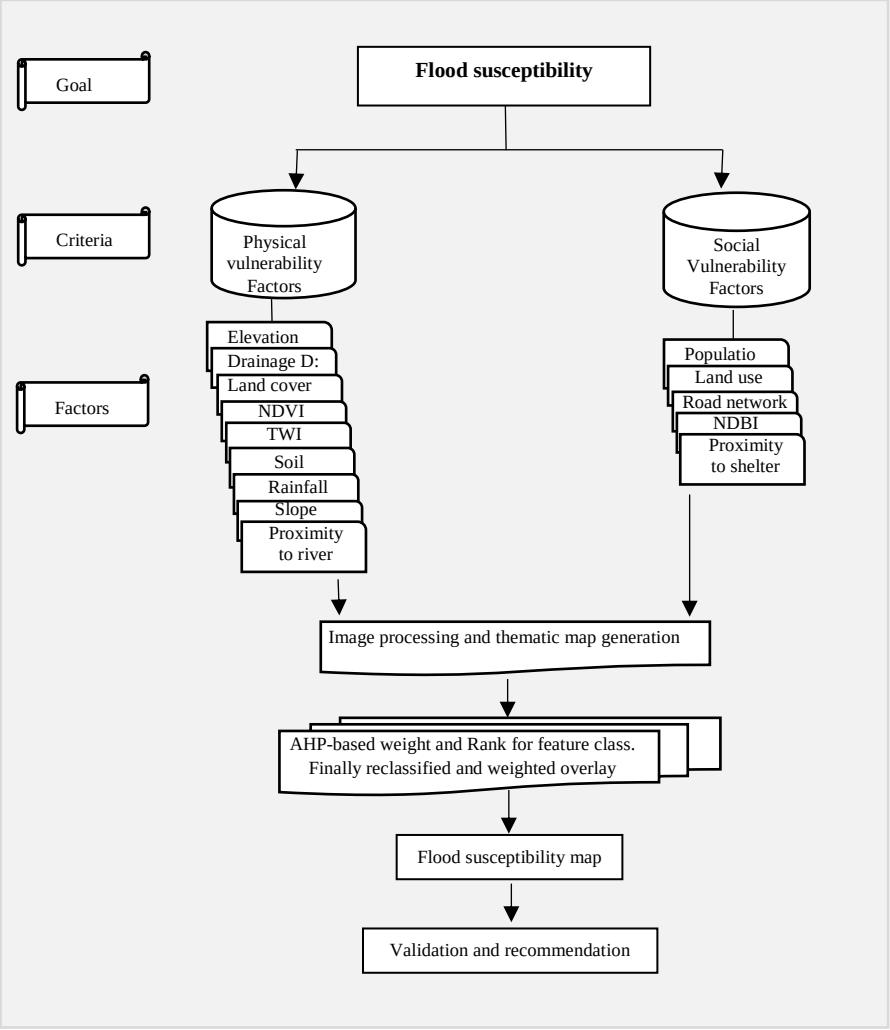

Figure 3.9 AHP process for creating flood susceptibility map

All the factors have been divided into five separate risk classes, which are assigned as per the functional relationships to risk level, followed by ranking values (Table 3.5). Very high to very low flood risk was valued from 5 to 1. Reclassification was performed on these risk classes to produce the final risk map.

Table 3.5 Ranking of flood factors

No	Factors	Very high risk 5	High risk 4	Moderate risk 3	Low risk 2	Very low risk 1
			Physical vulnerability			
1	TWI*	17 – 20.5	13.5 - 17	10 – 13.5	6.5 - 10	3.7 – 6.5
2	LULC (Perera, 2021; Weerasinghe et al., 2018)	Water bodies and marsh	Built-up area	Agricultural land	Barren lands	Forest/ Forest Plantation/ Scrubland
3	Elevation (m) (Weerasinghe et al., 2018)	0 – 2	2 - 5	5 - 10	10 - 20	> 20
4	Slope (Perera, 2021)	$0\text{-}3^0$	$3\text{-}6^0$	$6\text{-}9^0$	$9\text{-}12^0$	$> 12^0$
5	Rainfall (Average annual rainfall)	> 3500 mm	3200 - 3500 mm	2900-3200 mm	2600-2900 mm	< 2600 mm
6	NDVI*	-0.13 – 0.14	0.14 – 0.25	0.25 – 0.34	0.34 – 0.41	0.41 – 0.58
7	Drainage density (sq. km) (Hagos et al., 2022; Perera, 2021)	0 – 0.5	0.5 – 1	1 – 1.7	1.7 – 2.5	2.5 – 4.4
8	Soil permeability (Perera, 2021)	Alluvial soil, bog and half-bog soil, sandstone and claystone	Red-yellow podzolic soils with soft or hard laterite, rolling and undulating terrain	Red-yellow podzolic soils with strongly mottled subsoil & low humic clay soils	Red-yellow podzolic soils steeply dissected	Bog and half-hog soils, high terrain
9	Proximity to the river (m) (Weerasinghe et al., 2018)	< 100	100 - 200	200 - 300	300 - 500	> 500

		Social Vulnerability				
10	Population density* (km^2)	>5000	3000 - 5000	2000 - 3000	2000 - 1000	< 1000
11	NDBI*	0 to 0.27	-0.11 to 0	-0.17 to -0.11	-0.23 to -0.17	-0.44 to -0.23
12	Distance to flood shelter*	< 500 m	500 – 1000 m	1000 – 1500 m	1500 – 2000 m	> 2000 m
13	Distance to road (Wijesinghe et al., 2023)	< 100 m	100 -200 m	200 – 300 m	300 – 600 m	> 600 m

Note: * Factors classified into five classes according to the generated maps of the LKRB

3.2.6.2 Assigning normalised weights to AHP factors

Logical decisions are based on a complete analysis of criteria and alternatives, and many factors may influence one decision. The AHP method is a semi-quantitative decision-making value-judgment approach for decision-makers to achieve various objectives (Razandi et al., 2015; Saaty, 1977). This method enables planning to make group decisions by splitting problems into hierarchical structures and solving them with AHP (Dissanayake et al., 2020; Razandi et al., 2015). The AHP process was developed by Saaty (1977). In the present study, hazard and vulnerability factors were assigned weights according to the AHP.

This study used four steps for the AHP: construct the decision hierarchy; determine the relative importance of attributes and sub-attributes; evaluate each alternative and calculate its overall weight regarding each attribute; and check the consistency of the subjective evaluations (Ogato et al., 2020; Ouma & Tateishi, 2014). A pairwise comparison was performed for hazard and vulnerability factors as the first step of the AHP. This pairwise comparison was done according to the experts' preferences, on a scale from 1 to 9 (Ammarapala et al., 2018), and the existing literature. Table 3.6 shows the pairwise comparison scales.

Table 3.6 AHP pairwise comparison scales

Scale	Definition	Explanation
1	Equal importance	Two elements contribute equally to the objective.
3	Moderate importance	Experience and judgment slightly favour one parameter over another.
5	Strong importance	Experience and judgment strongly favour one parameter over another.
7	Very strong importance	One parameter is favoured very strongly and is considered superior to another; its dominance is demonstrated in practice.
9	Extreme importance	The evidence favouring one parameter as superior to another is of the highest possible order of affirmation.
2,4,6,8	Intermediate values	The importance lies in-between two degrees.

(Sources: Ogato et al., 2020; Saaty, 1977)

In the second step, a pairwise comparison matrix was constructed. For example, Table 3.7 shows this study's pairwise comparison matrix of hazard factors. The matrix was

completed by rating each factor against every other factor by assigning scores between 1 and 9 depending on relative importance (Ogato et al., 2020; Saaty, 1977). Accordingly, the pairwise comparison matrix (Table 3.7) was normalised using equation 4.20 (Saaty, 1977).

$$a_{ij} = \frac{1}{\sum_{i=1}^{n} a_{itj}} \quad For\ all\ j = 1, 2, 3, \ldots . n \qquad \textit{Equation 4.20}$$

Then the vector of weights for the normalised pairwise comparison matrix was computed, with W= [w1, w, w3, ….] based on Saaty's eigenvector procedure, using the following equation:

$$a_{ji} = \frac{\sum_{j=1}^{n} a_{ji}}{n} \quad For\ all\ i = 1, 2, 3, \ldots . n \qquad \textit{Equation 4.21}$$

Table 3.7 Comparison matrix for physical vulnerability factors

Matrix	*TWI*	*Land Cover*	*Elevation*	*Slope*	*Rainfall*	*NDVI*	*Drainage density*	*Soil*	*Proximity to river*
TWI	1	1	1	1	1	3	3	3	1
Land cover	1	1	1	2	3	1	2	3	3
Elevation	1	1	1	0.5	0.5	2	0.5	2	1
Slope	1	0.5	2	1	1	2	0.5	2	0.5
Rainfall	1	0.33	2	1	1	2	2	2	2
NDVI	0.33	1	0.5	0.5	0.5	1	1	1	0.5
Drainage density	0.33	0.5	2	2	0.5	1	11	2	1
Soil	0.33	0.33	0.5	0.5	0.5	1	0.5	1	0.33
Proximity to river	1	0.33	1	2	0.5	2	1	3	1
Column Total	**7**	**6**	**11**	**10.5**	**8.5**	**15**	**11.5**	**19**	**10.33**

After calculating the pairwise matrix, a weighted, normalised pairwise matrix was computed. Let $[A]_{9X9}$ be the normalised pairwise matrix, then $[A]_{9X9}$ is given in Tables 3.8 and 3.9.

Table 3.8 Normalised pairwise matrix for physical vulnerability factors

Matrix	TWI	L. cover	Ele.	Slope	Rainf.	NDVI	Dra.D	Soil	Pro. River	Weight	Priority (%)
TWI	0.14	0.17	0.09	0.10	0.12	0.20	0.26	0.16	0.10	0.15	14.85
L. cover	0.14	0.17	0.09	0.19	0.35	0.07	0.17	0.16	0.29	0.18	18.19
Ele.	0.14	0.17	0.09	0.05	0.06	0.13	0.04	0.11	0.10	0.10	9.89
Slope	0.14	0.08	0.18	0.10	0.12	0.13	0.04	0.11	0.05	0.11	10.63
Rainfall	0.14	0.06	0.18	0.10	0.12	0.13	0.17	0.11	0.19	0.13	13.35
NDVI	0.05	0.17	0.05	0.05	0.06	0.07	0.09	0.05	0.05	0.07	7.00
Dra.D	0.05	0.08	0.18	0.19	0.06	0.07	0.09	0.11	0.10	0.10	10.00
Soil	0.05	0.06	0.05	0.05	0.06	0.07	0.04	0.05	0.03	0.05	5.20
Pro.River	0.14	0.06	0.09	0.19	0.06	0.13	0.09	0.16	0.10	0.11	10.73
	1	1	1	1	1	1	1	1	1	1	100

Table 3.9 Normalised pairwise matrix for social vulnerability factors

Matrix	Pop. Den.	Land Use	NDBI	Road dis.	Pro. Shelter	Weight	Priority (%)
Pop. Den.	0.35	0.46	0.40	0.20	0.31	0.34	34.44
Land Use	0.18	0.23	0.27	0.30	0.31	0.26	25.63
NDBI	0.12	0.12	0.13	0.20	0.15	0.14	14.40
Road dis	0.18	0.08	0.07	0.10	0.08	0.10	9.94
Pro. Shelter	0.18	0.12	0.13	0.20	0.15	0.16	15.58
	1	1	1	1	1	1	100

A relationship exists between the vector weights, W, and the judgment matrix $[A]_{9X9}$ as shown in equation 4.22, developed by Saaty (1977).

$$A_w = \lambda_{max} w \qquad \textit{Equation 4.22}$$

The λmax value is an important validating parameter in AHP (Saaty, 1977). After that, this study calculated the estimated vector consistency ratio (CR). To calculate CR, the consistency index (CI) for each matrix of order n was obtained from equation 4.23.

$$CI = {}^{\lambda_{max} - n}/_{(n-1)} \qquad \textit{Equation 4.23}$$

The final step is calculating *CR*. This ratio calculates *CI* and random index (*RI*). It can be derived from equation 4.24 below. The maximum threshold value for *CI* is < 0.1 and *CR* < 10% (Saaty, 1977).

$$CR = {}^{CI}/_{RI} \qquad \textit{Equation 4.24}$$

Saaty (1980) has suggested *RI* values relating to the number of factors we consider in a study. The *RI* values are shown in Table 3.10. Accordingly, the *RI* value for the nine hazard factors is 1.45 and the *RI* for the five vulnerability factors is 1.12.

Table 3.10 Random Index (RI)

N	**1**	**2**	**3**	**4**	**5**	**6**	**7**	**8**	**9**	**10**
RI	0	0	0.58	0.90	1.12	1.24	1.32	1.41	1.45	1.49

Further, the *CI* and *CR* values for hazard factors are 0.096 and 0.066, respectively. *CI* and *CR* values for vulnerability factors are 0.092 and 0.082, respectively. Hence the pairwise matrix ranking for both criteria, hazard and vulnerability, is accepted.

The flood-risk map for the LKRB was created with the help of ArcGIS weighted overlay tools. Depending on the weighted overlay tool, this study created two separate maps for hazard and vulnerability. After that, using Equation 4.25, the final risk map was prepared.

$$Risk = Hazard \ \mathbf{x} \ Vulnerability \qquad \textit{Equation 4.25}$$

3.2.7 Frequency Ratio (FR) Analysis

The FR model can be used as a basic geospatial assessment tool to compute the probabilistic connection between dependent and independent variables, such as found in multi-classification maps (Oh et al., 2017). Bonham-Carter (1994) introduced the FR approach, which represents the likelihood of a specific characteristic occurring. It is important to note that a sub-class with a higher value indicates higher potential for a particular event in the FR model. In this model, the physical vulnerability factors

utilised in the AHP process, were used to generate the FR values. For this study of flood susceptibility mapping, the FR model has been calculated based on equations presented by Bonham-Carter (1994):

$$FR = (N_{ij}/P_{ij}) \ / \ (N/P) \qquad \textit{Equation 4.26}$$

Where, FR indicates the frequency ratio of the sub-classes, N_{ij} is the number of flood locations, P_{ij} is the total number of flood locations in the study area, N is the total number of pixels for each class of factors, and P is the total number of pixels in the study area.

To examine the association between flood locations and factor classes, the flood relative frequency (FRF) index was used. The FRF is the normalised value of the previous frequency ratios for the variables and can be calculated with the following equation, presented by Bonham-Carter (1994).

$$FRF = \frac{FR_{fc}}{\sum FR_{fc}} \qquad \textit{Equation 4.27}$$

Where, FRF is the flood relative frequency, FR is the frequency ratio, FR_{fc} is the factor class of FR, and $\sum FR_{fc}$ is the summation of factor classes of FR. Appendix A shows FRF values for each physical factor class with prediction rate.

The predicted rate was estimated with Equation 4.28 below to identify the relational interdependencies between independents Bonham-Carter (1994).

$$PR = \frac{(Max_{RF} - Min_{RF})}{Min_{(Max_{RF} - Min_{RF})}} \qquad \textit{Equation 4.28}$$

Where PR is the predicted rate, Max_{RF} and Min_{RF} are the maximum and minimum values of the relative frequency, and $Min_{(Max_{RF} - Min_{RF})}$ is the minimum value of all

selected variables ($Max_{RF} - Min_{RF}$). Appendix A presents the table of PR values for each factor.

3.2.8 Height Above Nearest Drainage (HAND) Model

Rennó et al. (2008) first proposed the HAND model as a quantitative terrain descriptor and the model characterises the hydrological behaviour of the catchment and hillslope (Komolafe et al., 2020) in a watershed. Through two sets of procedures, the HAND terrain model normalises the altitude of the basin based on the relative height of the drainage network and determines the gravitational and relative drainage potential of the area (Nobre et al., 2010). For the calculation of the HAND index, the DEM of the study area and the drainage contributing area should be used (Komolafe et al., 2020). The ultimate goal of this model is to produce flood inundation maps. Figure 3.10 indicates the steps in creating the HAND model.

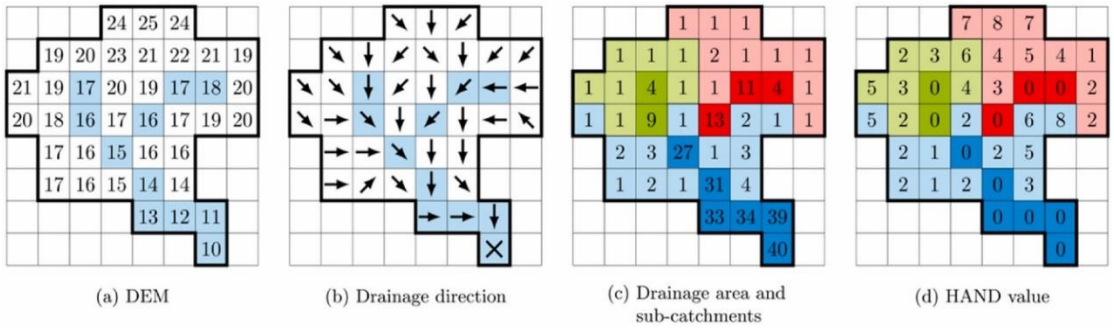

Figure 3.10 Process for preparing the HAND model (Source: Rebolho et al., 2018)

The first step of creating the HAND model is defining flow direction based on DEM. To compute the drainage direction map, this study used the D8 method with flow direction functions available in ArcGIS 10.8 software. To compute the drainage direction, the D8 method calculates the steepest slope from the eight possible directions for a given cell. After computing the drainage direction, the flow accumulation should be computed to identify the drainage cell. The drainage cell is a part of a number of flow chains exceeding an accumulated area threshold. The nearest drainage cell is then the drainage cell for a first cell in the flow chain. Finally, the

HAND model can be calculated by subtracting the height of the cell in the original DEM from the height of the nearest drainage cell in the original DEM.

3.2.9 Model Validation

To verify the efficiency and applicability of a model, validation is an essential element of natural hazard susceptibility mapping. The Area Under the Curve (AUC) approach was used to validate the results generated by the flood hazard map. AUC is a simple, widely applicable method based on science that allows us to make accurate evaluations of the tests (Sarkar & Mondal, 2019). In the AUC curve, the false positive rate is shown on the x-axis while the true positive rate is on the y-axis. AUC is used to validate a model's predictions, and AUC values can be categorised as follows: 0.5–0.6 (poor); 0.6–0.7 (average); 0.7–0.8 (good); 0.8–0.9 (very good); and 0.9–1.0 (excellent) (Al-Abadi, 2017; Sarkar & Mondal, 2019)

3.2.10 Flood Inventory Mapping

Flood inventory mapping is a systematic assessment of existing floods across a region using different techniques, including field survey, Google Earth imagery interpretation or aerial photographs, satellite information interpretation, and literature searches for historical flood records, government reports, technical and scientific reports, and interviews with experts (Wubalem et al., 2020). In this study, 140 points were identified based on the flood event of May 2018. For this purpose, Google Earth images for the time-period considered, filed observations, satellite images, and 2018 flood maps from the Survey Department, Sri Lanka were considered. Usually, 70% of flood occurrences are used in training datasets for developing flood susceptibility models, with the remaining 30% used for validation of the output model (Sarkar & Mondal, 2019; Wubalem et al., 2020). In this study, 98 (70%) of the flood locations were used to train flood susceptibility models, while the remaining 42 (30%) were used to validate the models. Figure 3.11 illustrates flood inventory map for the LKRB.

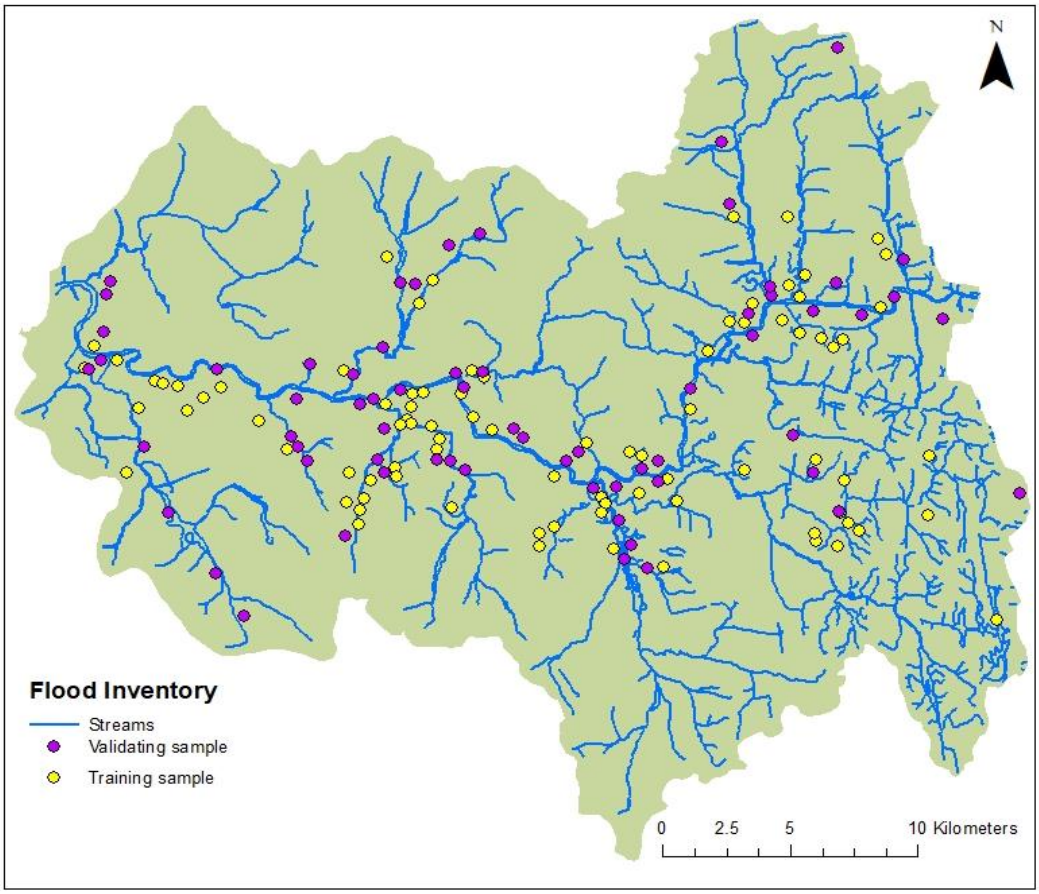

Figure 3.11 Flood inventory map of the LKRB

3.2.11 Proposed integrated flood risk assessment method (AFH-Method)

This task, introduces an innovative approach, integrating AHP, FR, and HAND method (geo-spatial model) for flood risk assessment in the LKRB. For the new technique, only physical vulnerability factors were considered. Figure 3.12 shows a methodological flowchart for the suggested flood hazard mapping process. This new combination provides extensive insights into the physical factors that influence hazard zonation, improving the accuracy and efficacy of flood risk assessments. This method was developed in ArcGIS 10.8.2 package.

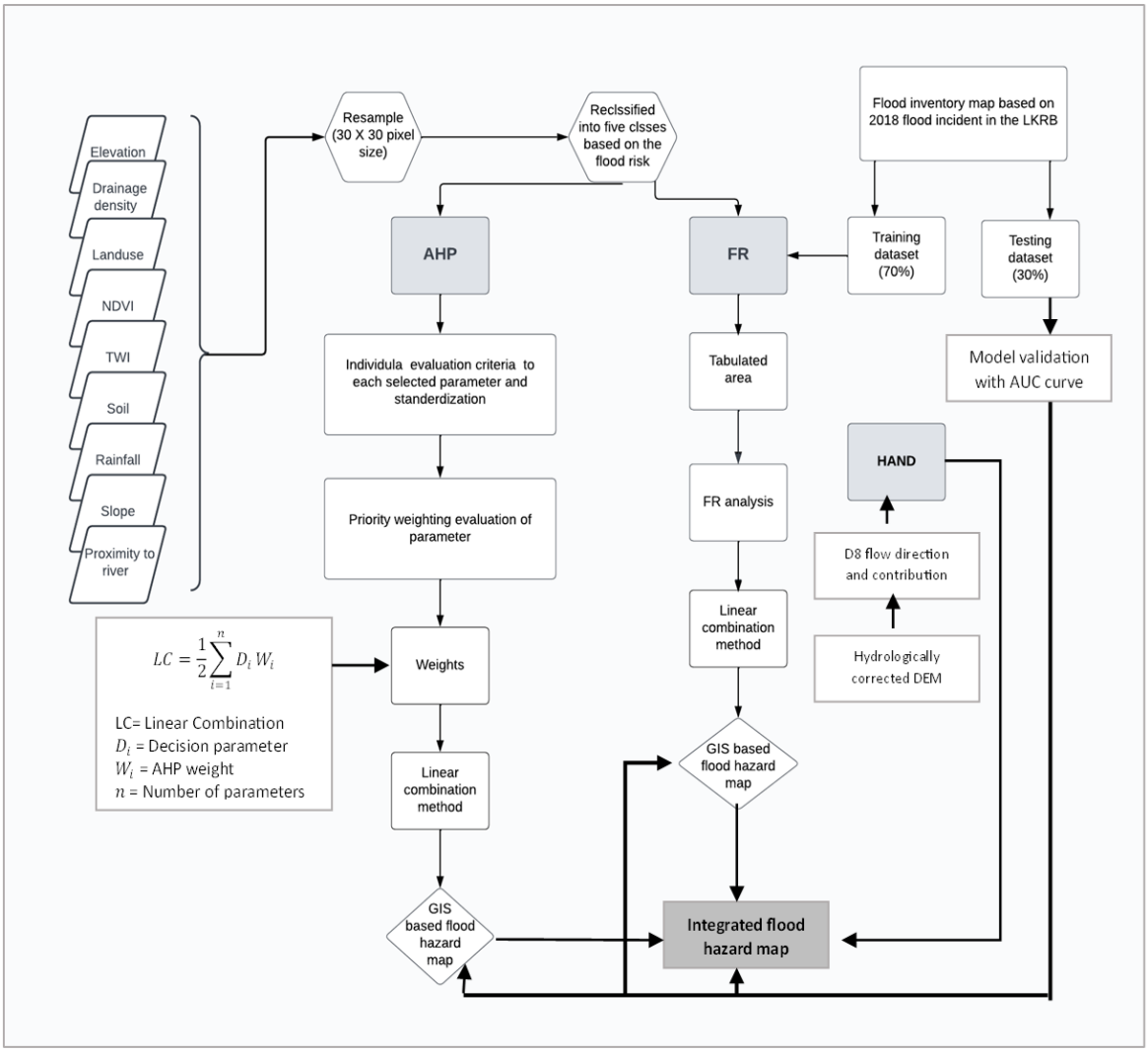

Figure 3.12 Proposed integrated AFH method for flood risk assessment

4. RESULTS

Climate change has a wider impact on rainfall pattern of Sri Lanka, with various consequences such as an increase in the incidence of extremely high rainfall events and associated hazards. Over the past three decades (1991-2020), the island has witnessed a noticeable increase in extreme rainfall events and flood occurrences. This chapter describes the findings derived from analysis of data in accordance with three specified objectives. In particular, this chapter includes identifying extreme rainfall events throughout the island and within the KRB following an analysis of flood susceptibility using AHP, FR, and AFH methods.

4.1 Rainfall variations over Sri Lanka

4.1.1 Spatial patterns of extreme rainfall events

This research is a significant advance in this field of research, as it has for the first time identified and illustrated the spatial distribution of extreme rainfall over Sri Lanka. Nine distinct indices of extreme rainfall were analysed and their results presented in this section. In pursuit of that aim, the study has calculated mean values of those extreme rainfall indices for each meteorological station. Following that, the study employed the Inverse Distance Weighted (IDW) interpolation technique to map the spatial patterns of extreme rainfall (Figure 4.1) and the results indicate that all nine indices covered by the abovementioned methodology display complex topographical patterns across the island.

It can be seen at a glance that the island's orography significantly impacts the spatial distribution of its extreme rainfall indices, shown in Figure 4.1. Nonetheless, it has generated a somewhat different pattern for the annual mean rainfall over the island. (See Figure 2.4 for an average annual rainfall pattern for Sri Lanka). Accordingly, all indices show their highest values in the southwest part of the country (Wet Zone), except for the SDII index. Thereafter, indices' values gradually decrease towards the country's northern and eastern sides (Dry and Intermediate Zones).

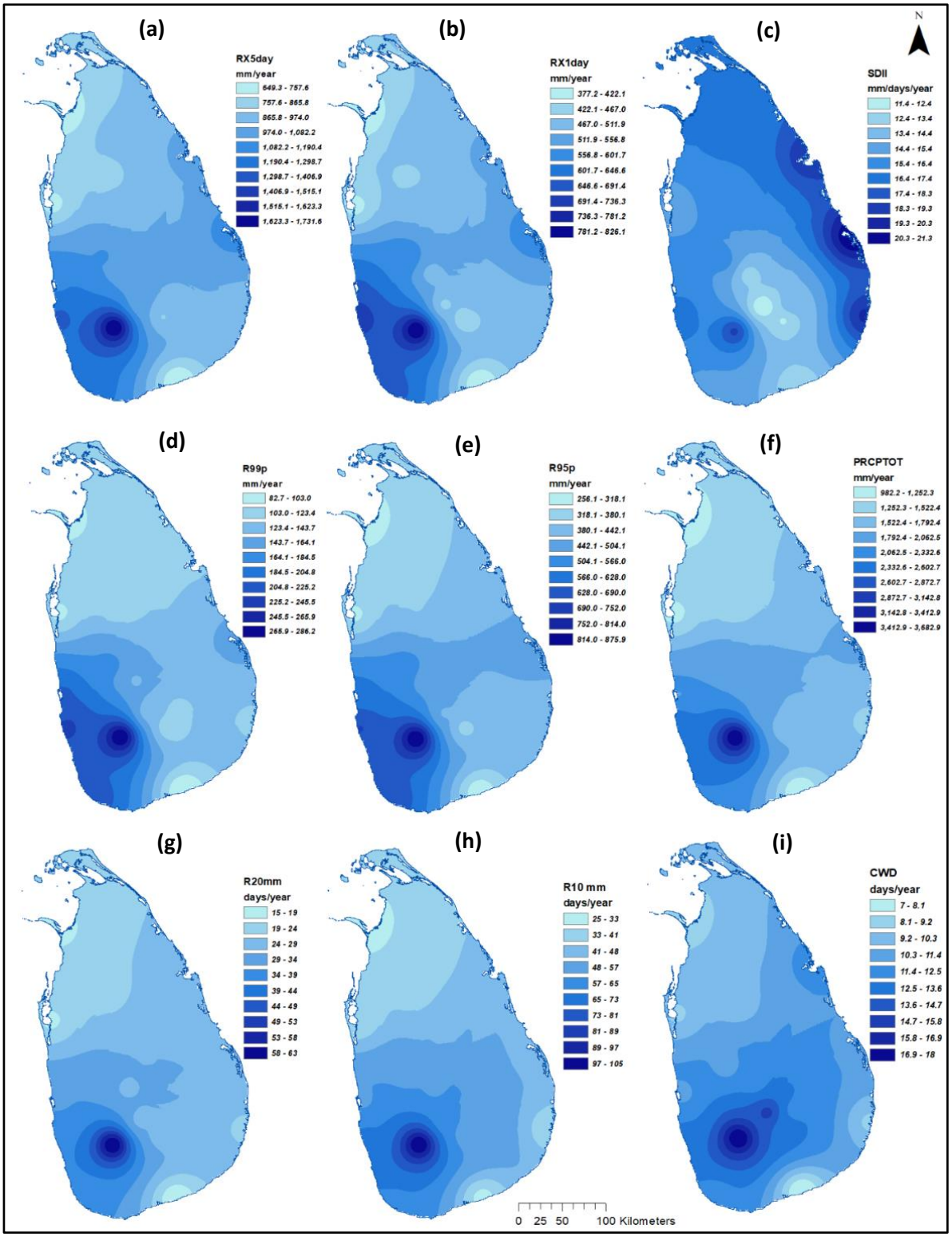

Figure 4.1 Spatial pattern of extreme rainfall indices based on the IDW interpolation method. Note: All indices show similar spatial pattern having highest accumulation in the southwest part of the island but SDII index: (a) RX5day (b) RX1day (c) SDII (d) R99p (e) R95p (f) PRCPTOT (g) R20mm (h) R10mm (i) CWD

To ascertain the effect of orography, the study considered the R99p index values at Badulla Meteorological Station on the eastern side of the central highlands (in the Intermediate Zone), and Rathnapura Meteorological Station, which is closed to the SWM windward flanks of the central highlands (in the Wet Zone) (Figure 4.2). It is visible that Rathnapura station received more than twice the extreme rainfall of Badulla station. It is clear from the data shown in Figure 4.2 that, over approximately ten years, Rathnapura station consistently produced nearly 700 mm of rainfall, and this distinctive pattern does not appear to be found on any other indices throughout the study period.

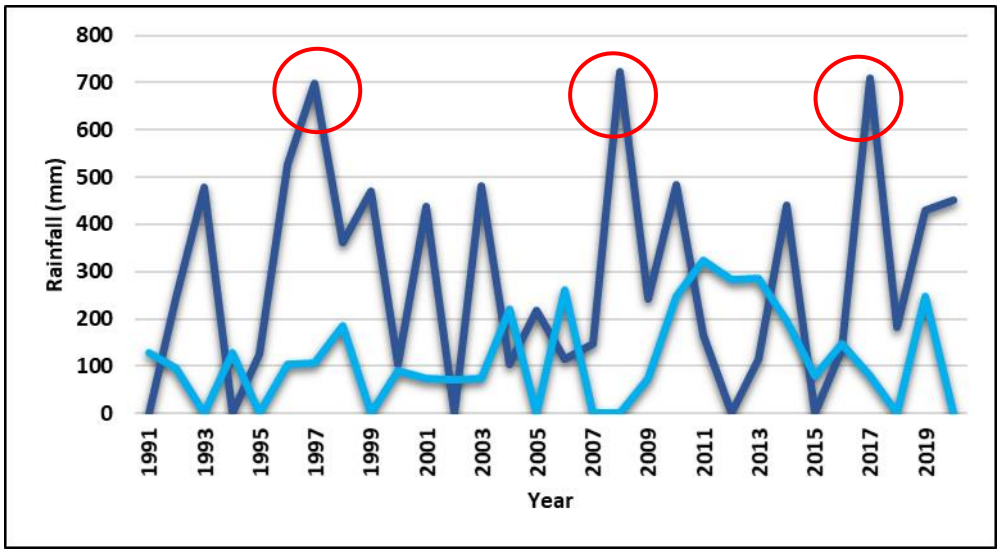

Figure 4.2 R99p indices values. Note: Dark blue line represents Ratnapura station and light blue line represents Badulla station. Red circles indicate peak points in every 10-year cycle.

Conversely, as seen with the indices SDII, RX1day, and R99p, there are areas of markedly reduced extreme rainfall, particularly in the central hills. Nuwara Eliya meteorological station is the most elevated station in the study, situated in the middle of the central highlands. This station shows comparatively low values for all extreme rainfall indices, which could lead to show low spatial distribution of extreme rainfall in these indices for the central highland in Figure 4.1.

The spatial pattern of extreme rainfall indices according to climate zones, is presented in Table 4.1.

Table 4.1 Ranges of annual average extreme rainfall indices arranged according to the climate zones

Indices	Wet Zone	Intermediate Zone	Dry Zone
RX5day	974.0 – 1731.6 mm	865.8 – 1190.4 mm	649.3 – 1190.4 mm
RX1day	422.1 – 826.1 mm	511.9 – 646.6 mm	377.2 – 601.7 mm
R99p	164.1 – 286.2 mm	103.0 – 184.5 mm	82.7 – 164.1 mm
R95p	442.1 – 875.9 mm	318.1 – 628.0 mm	256.1 – 504.1 mm
R20 mm	24 – 63 days	34 – 44 days	15 – 34 days
R10 mm	48 – 105 days	48 – 73 days	25 – 65 days
PRCPTOT	1792.4– 3682.9 mm	1522.4 – 2602.7 mm	982.2 – 2062.5 mm
SDII	11.4 – 19.3 days	12.4 – 17.4 days	12.4 – 21.3 days
CWD	10.3 – 18 days	10.3 – 14.7 days	7 – 13.6 days

Table 4.1 indicates that the Wet Zone is typically characterised by a wide range of rainfall extremes, signifying a higher degree of variability in extreme rainfall events. Compared with the Intermediate and Dry Zones, these extreme rainfall indices are characterised by a narrower range, indicating more consistent but generally lower values. These findings are of decisive importance in understanding local differences between extreme rainfall patterns across different climate zones. Table 4.1 also indicates the SDII index difference, showing the highest values in the Dry Zone.

However, when focusing on the spatial pattern of extreme rainfall, the most surprising finding was that the SDII index is highest along the east coast part of the Dry Zone. At the same time, the lowest values are recorded in the Intermediate Zone. Moreover, this same coastal region exhibits reduced values for the annual total precipitation index (PRCPTOT), and a parallel decrease is apparent in the consecutive wet days (CWD) values. It is visible that this area has less rain, but its intensity is high. The highest SDII values, for the east coast area, are a novel illustration of the extreme rainfall pattern in Sri Lanka, contributing to advancing knowledge in this field.

4.1.2 Temporal pattern of extreme rainfall events

Upon identifying the spatial pattern of extreme rainfall events, the study attempted to identify the temporal pattern of extreme rainfall indices. The calculations in this analysis were based on the average Z-values for each station derived from the MK and Sen's slope tests (Appendix B). A visual representation of how these trends are distributed in different spatial orders is provided in Figure 4.3, which specifically focuses on the differences between meteorological stations located in Wet, Intermediate, and Dry Zones.

In particular, it was noted that the intensities of extreme rainfall increased substantially in the Dry Zone. As illustrated in Figure 4.3 (a) and (b), the trend in RX5day and RX1day indices are already increasing at almost all stations in the Dry Zone. The Anuradhapura station has shown an upward trend for both indices. Similarly, the Batticaloa station showed a significant increase in the RX5day index, with a Z-value of 2.68 mm per year and a P-value of 0.01. In contrast, the Pottuvil station shows a significant increase in the RX5day index, with a Z-value of 2.34 mm per year and a P-value of 0.01. SDII showed an overall increasing trend in the intensity of rainfall >0.14 days in all stations apart from Katunayaka, Pottuvil, and Rathnapura (Figure 4.3 (c)). Mannar (Z-value 2.39 mm/days/year and p-value 0.02) and Anuradhapura (Z-value 2.52 mm/days/year and p-value 0.01) showed the highest significant increasing trend in the SDII index. All these stations are situated in the northern part of the country. A significant increasing trend in the SDII index in the northern part of the country is one of the exciting findings of this study.

Figure 4.3 (d) represents the R99p index. Anuradhapura meteorological station, situated in the Dry Zone, is the only station that showed a significant increasing trend in rainfall on extremely wet days (p-value = 0.009). Apart from that, Maha Illuppallama, Puttalam, Trincomalee, Hambantota, Gall, and Ratmalana stations showed annual precipitation ≤ 99 percentile daily rainfall (mm). Nevertheless, they were not significant data. Other stations showed a slight increase in extreme rainfall events. Figure 4.3 (e) shows heavy rainfall distribution over the country. Overall, the stations showed an increasing trend. The most significant point is that the Mannar

station showed the highest annual precipitation ≥ 95th percentile daily rainfall (mm) in the Dry Zone. It has MK trend test Z-value = 3.287 mm/year (p-value 0.001; Sen's slope 10.49). Significantly, the PRCPTOT (Figure 4.3 (f)) in the Dry Zone has an increasing trend, apart from in Puttalam. When considering stations in the Wet Zone, most of them showed a decreasing trend.

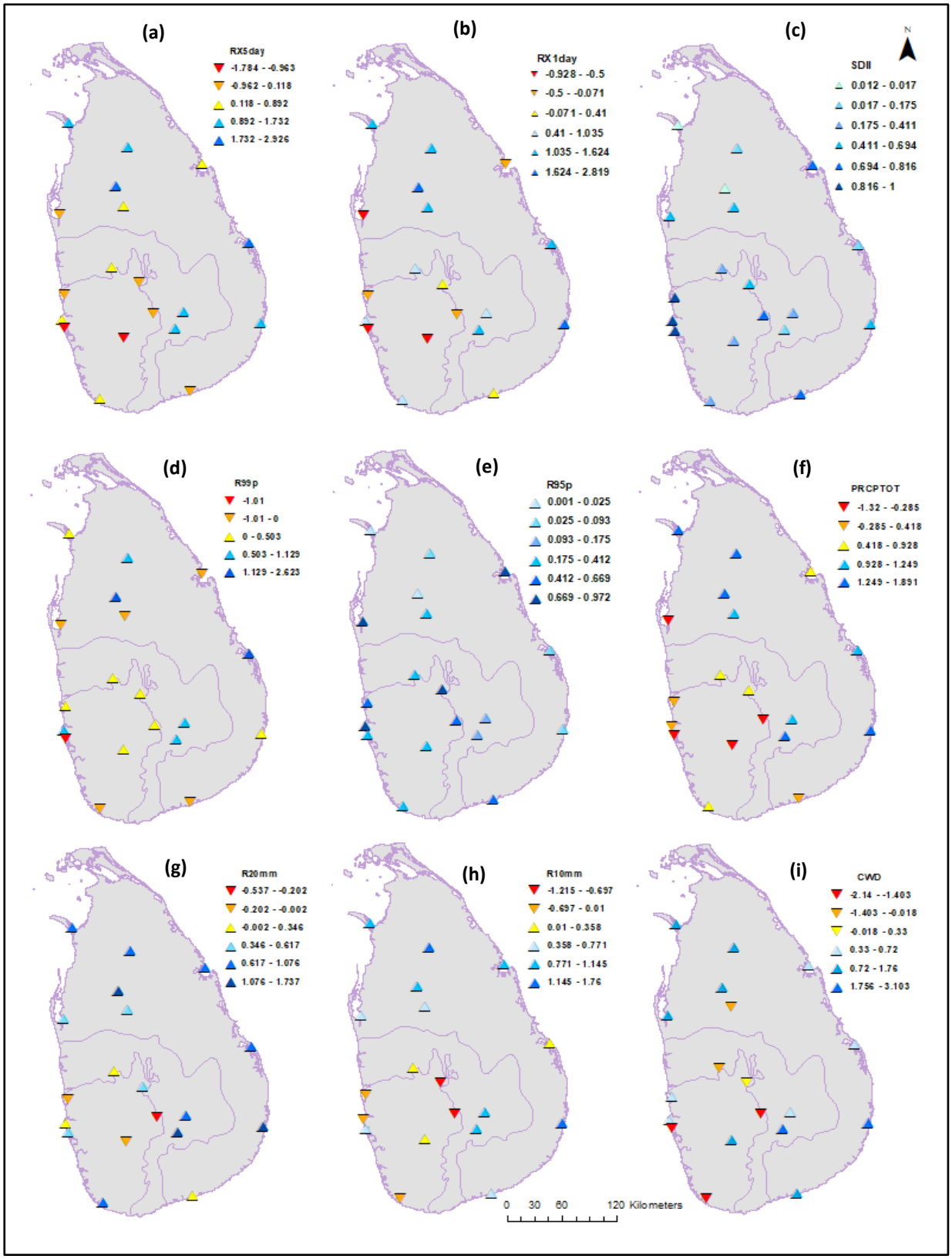

Figure 4.3 Spatial pattern of rainfall trend. Note: (a) RX5day (b) RX1day (c) SDII (d) R99p (e) R95p (f) PRCPTOT (g) R20mm (h) R10mm (i) CWD

When considering heavy precipitation days with a magnitude ≥ R10 mm (Figure 4.3 (h)), almost every meteorological station in the Dry Zone had an increasing trend. The index had a decreasing trend, except for Rathnapura and Ratmalana stations in the Wet Zone. Interestingly, all stations in the Intermediate Zone show a growing trend in heavy precipitation days (average 0.197 days/year). Very heavy precipitation days with a magnitude of R20 mm are shown in Figure 4.3 (g). Only three stations in the Wet Zone show a decreasing trend, while others offer an increasing trend. Anuradhapura (1.737 days) and Bandarawela (1.612 days) have the highest number of heavy precipitation days. Nuwara Eliya meteorological station shows a remarkable decrease in heavy precipitation days, a characteristic that is also compatible with the annual total precipitation (PRCPTOT) trend.

The CWD (Figure 4.3 (i)) index also showed the highest decreasing trend in Nuwara Eliya, Galle, and Ratmalana stations in the Wet Zone. Galle station was the only station with a significant decreasing trend (Z-value -2.14 days/year and p-value 0.03). Pottuvil in the Dry Zone shows the highest significant increasing trend (Z-value 3.1 days/year and p-value 0.002). However, in the Wet Zone, Rathnapura station is the only station that shows a positive magnitude increasing trend in CWD (Sen's Slope = 0.11).

The most notable observation from this temporal pattern analysis is that the Wet Zone is getting drier while the Intermediate and Dry zones are getting wetter regarding extreme rainfall events. This observation is a new contribution to the knowledge base in the field of climate studies in the region. For further investigation, the non-monotonic ITA approach was used to identify further trends in extreme rainfall in each climate zone.

4.1.3 Identifying non-monotonic trends in extreme rainfall indices

The Innovative Trend Analysis (ITA) method was used to identify the non-monotonic trends (also hidden trends) in each extreme rainfall index based upon different climate zones. Extreme climatic index values observed at different meteorological stations have been used to calculate the average value for each climate zone. Figures 4.4 and 4.5 show the results of ITA for each individual extreme rainfall index within a given climate zone.

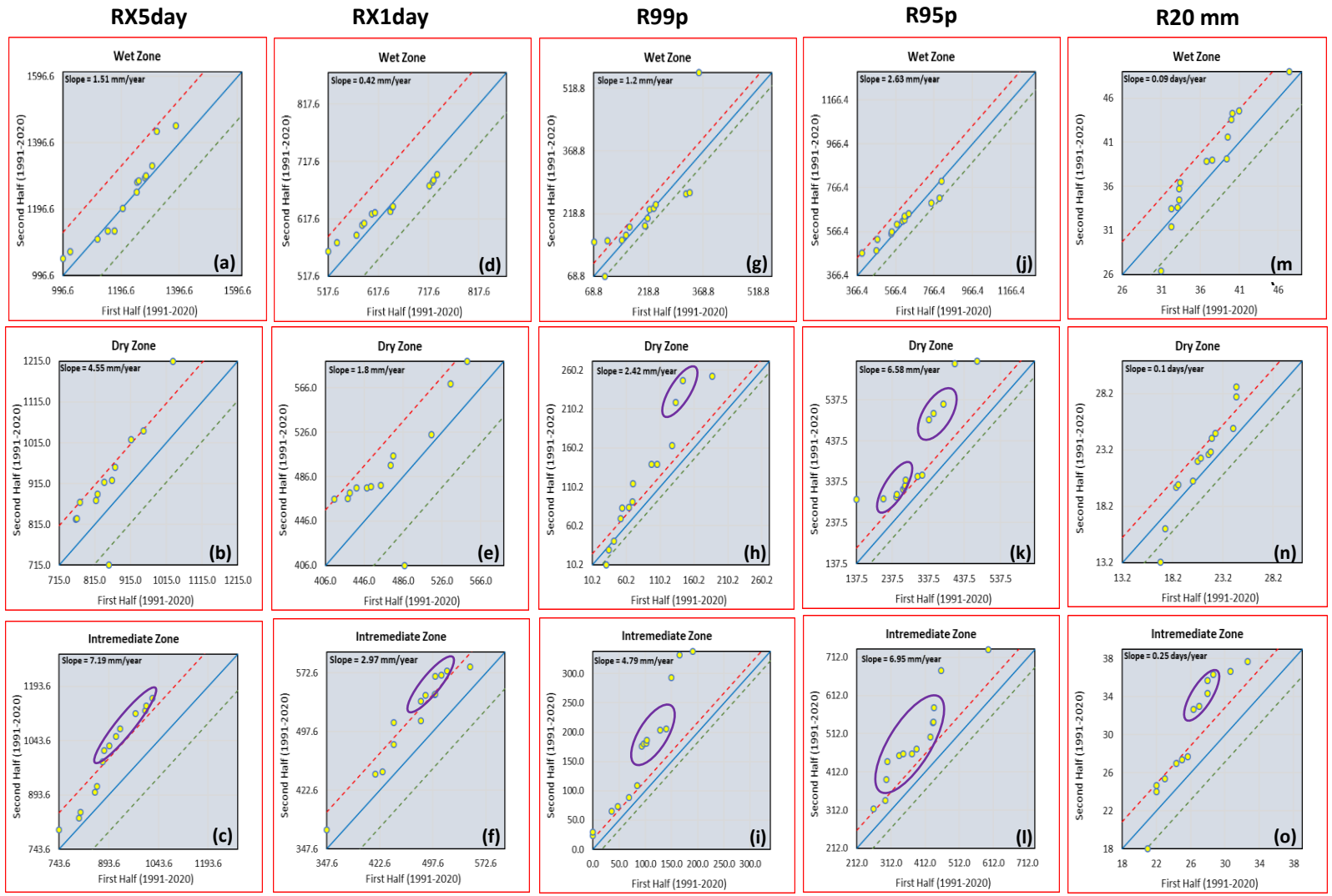

Figure 4.4 ITA results for extreme rainfall indices in climate zones.

Note: The blue diagonal line indicates the 1.1 line or no-trend line.

Data in the upper triangle denote increased trend and lower triangular denote decreased trend. The other two dashed lines (red and green) indicate ± 10% from 1.1 line (distance of the points from the no-trend line).

Purple circles indicate data clusters with significant trends. Also, trend slope (magnitude) of ITA for each index is shown in the upper left part of each scatterplot.

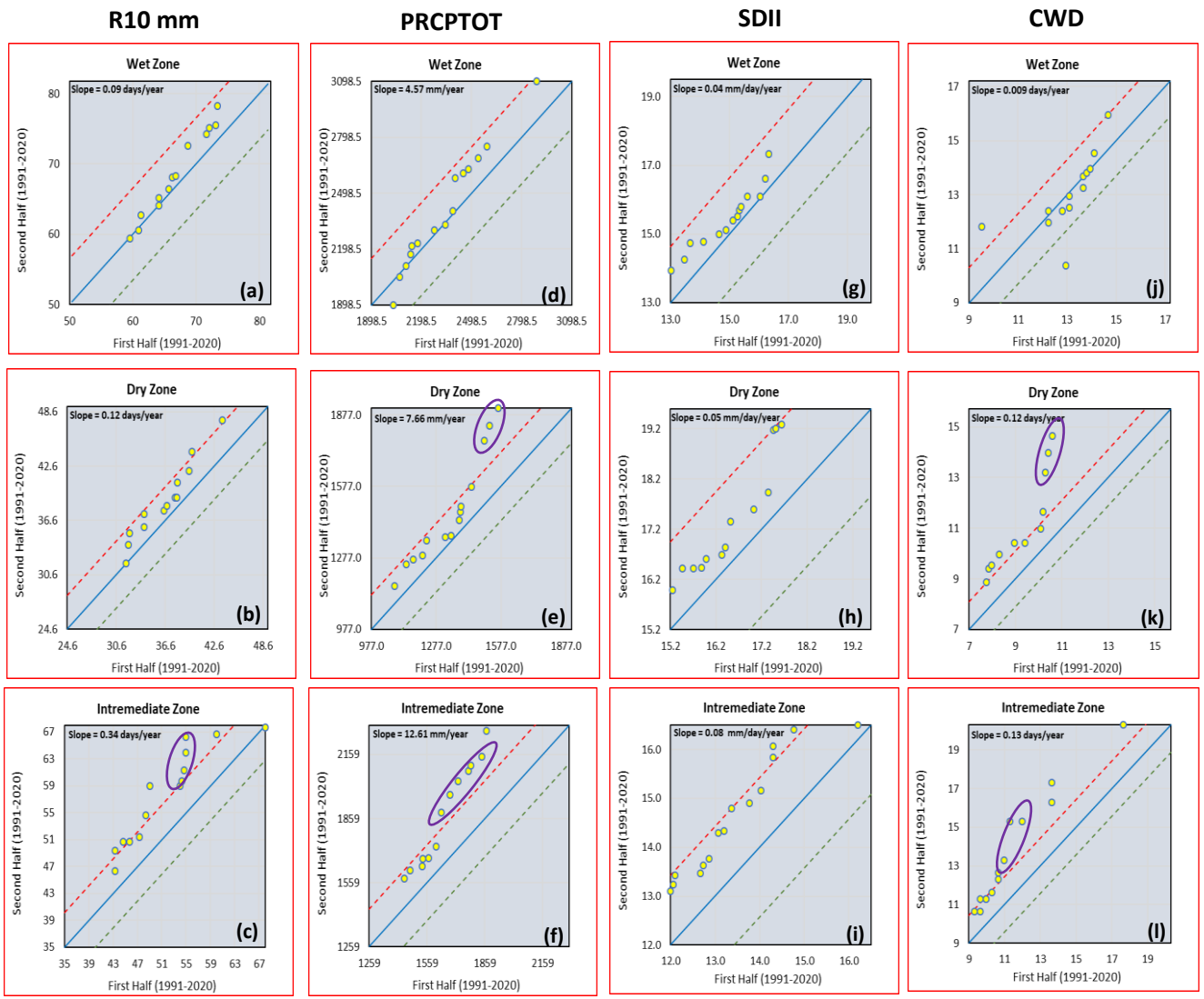

Figure 4.5 ITA results for extreme rainfall indices in climate zones.

Note: The blue diagonal line indicates the 1.1 line or trend-free line.

Data in the upper triangle denote increased trend and in the lower triangle denote decrease trend. The other two dashed lines (red and green) indicate ± 10% from the 1.1 line (distance of the points from the no-trend line).

Purple circles indicate data clusters with significant trends. Also, trend slope (magnitude) of ITA for each index is shown in the upper left part of each scatterplot.

Focusing on the RX5day index, the Intermediate Zone shows a significant trend compared to the other two zones (Figure 4.4 (c)). It is discernible that the majority of scatter points appear in the medium value region (see Figure 3.8 for identifying medium value region) in the RX5day plot, indicating a high and increasing trend. Compared with the other two zones, the Wet Zone shows the minimum ITA results in monthly maximum consecutive 5-day precipitation. Most of the scatter points lie within the dashed lines or close to that, showing that the RX5day trend is to monotonic trends in the region. The Dry Zone also shows an increasing trend in RX5day indices, but it is less significant than in the Intermediate Zone. For the RX1day index, the Dry Zone and Intermediate Zone show an increasing trend. The magnitude of these upward trends was estimated to be 1.8 to 2.97 mm/year, respectively. There is a high-value point cluster in the Intermediate Zone scatterplot (Figure 4.4 (f)). Along with the RX5day index, the Dry Zone shows the lowest trend in the RX1day index.

The indices for extremely wet days (R99p) and very wet days (R95p) show an interesting pattern of ITA results. In the Wet Zone, scatter points for both the indices located in lower values lie within ± 10% from the region, closer to the 1.1 line (no-trend). In the Dry Zone, R99p and R95p (Figure 4.4 (g) and (j)) indices show a significant non-monotonic trend. Most of the points are above the 10+ line. The scatter points in the Intermediate Zone for both indices show an increasing trend. All the scatter points are above the 10+ line. Nevertheless, all these points scatter in the medium x and y value regions above the 1.1 line. Thus, a medium increase non-monotonic trend in both indices can be predicted.

The magnitude of the trend values for the R10 mm index varies between 0.09 days/year to 0.34 days/year in all the climate zones. Most of the scatter points in the Wet Zone spread between the ±10% line (very close to the 1.1 line, showing a trend-free pattern). In the Dry Zone, 10 mm shows a monotonic trend, as seen in Figure 4.5 (b). Most of the points scatter between ±10% areas. Only the Intermediate Zone shows a cluster beyond the +10% line. This cluster appears in the upper part of the medium value region above the +10% line. Concerning R20 mm, the magnitude of trend values varies by 0.09-0.25 days/year for all climate zones. Among the three climate zones, the Intermediate Zone has a significant increasing non-monotonic trend (Figure 4.4 (o)), with scatter points clustered in the upper area of the medium-value region. The other two zones have their points scattered between the ±10% lines. These results

generally indicate that very heavy rainfall days (R20 mm) have occurred more frequently in this Zone during the period considered.

The annual total precipitation of wet days (PRCPTOT) for Dry Zone and Intermediate Zone scatter points (Figure 4.5 (e) and (f)) shows an increasing trend. Even though Wet Zone scatter points show an increasing trend, located between the +10 line and 1.1 line (closer to 1.1 line). Focusing on the simple daily intensity index (SDII), all the climates exhibit an increasing trend. All the scatter points in Wet Zone and Dry Zone lay between the +10 and 1.1 lines. Compared with the other two climate zones, there is a tendency to increasing scatter points beyond the 10+ line in the Intermediate Zone. According to Figure 4.5 (k) and (l), an increasing non-monotonic trend appears in the CWD index for the Dry and Intermediate zones.

4.1.4 Detecting possible turning point (year) for extreme rainfall

The study attempted to detect possible turning points (trend change years) of extreme rainfall trends in the island. For this purpose, the study used the SqMK test statistic, which allows the detection of the approximate beginning of a developing trend in a time-series. As explained in section 3.2.4.3, when U(t) and U'(t) exceed a specific confidence limit before and after the crossing points, this turning point is considered significant at the corresponding level of 1.96. Consequently, the results of SqMK test statistics for yearly mean values of extreme rainfall indices are shown in Figure 4.6.

Concerning the R99p index (Figure 4.6 (a)), there is a decreasing trend from 1994 to 1997. Though the curves intersect the 1992, 1993, 1994, and 1995 years, they cannot be recognised as significant turning points. There is a slight increase from 1997 to 2001 and a drastic drop in visible ageing in both U(t) and U'(t) lines after the 2001 to 2005 period. From 2007 onward, there was a gradual increase in extreme precipitation. There are five intersections of U(t) and U'(t) in the R99p index. Among them, the 2009 intersection point lies in an increasing trend. After 2015, there was a decrease up to 2017 and again a slight increase until now. Also, the R95p indices (Figure 4.6 (b)) illustrate a similar pattern to the R99p indices. When considering R95p indices, the prograde and retrograde cross in 1992, 1995, and 2010. A drastic drop can be seen after the 1995 intersection until 2005. After 2010, there is a significant increasing trend in the R95p. RX5day and RX1day indices (Figure 4.6 (c) and (d)) have some similar

patterns. Both the indices show a decreasing trend from the 2001 to 2005 period. PRCPTOT (Figure 4.6 (e)) shows a slight decreasing trend until 2005 and a significant increasing trend beginning in 2009.

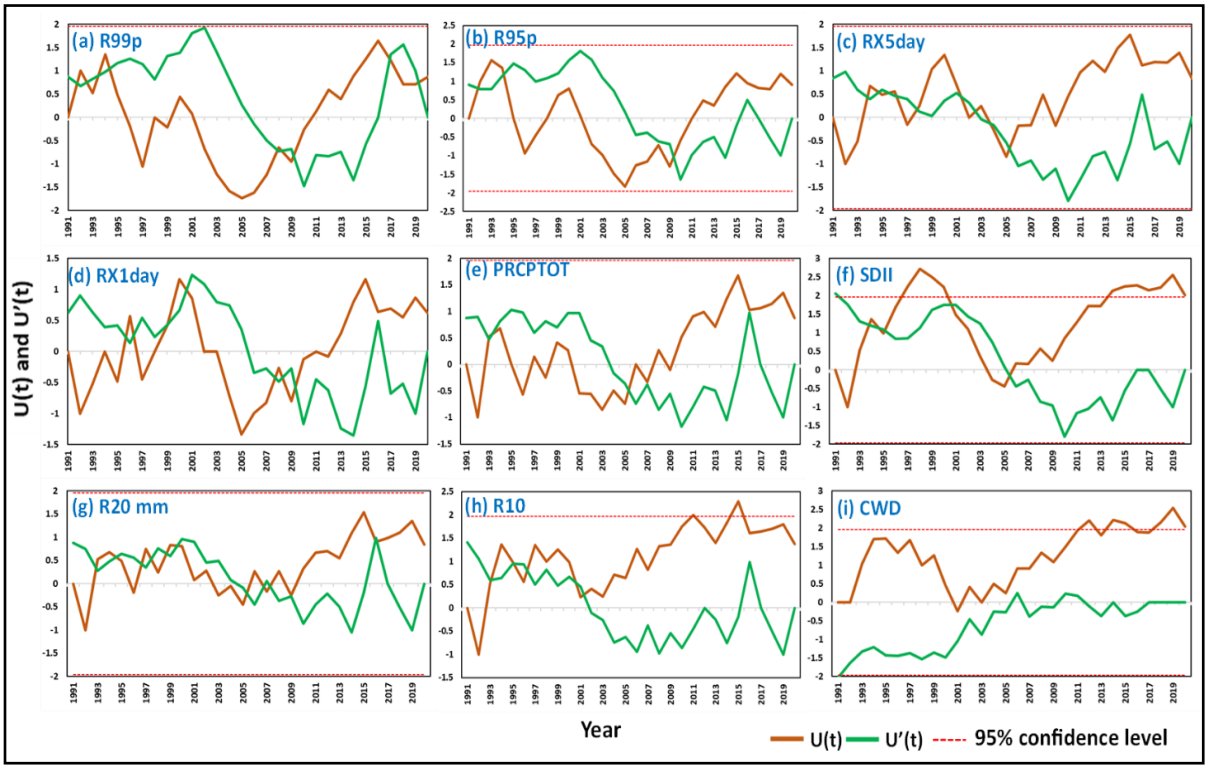

Figure 4.6 SqMK statistics for extreme precipitation indices: Note: None of the indices have possible turning year of extreme rainfall. (a) R99p; (b) R95p; (c) RX5day; (d) RX1day; (e) PRCPTOT; (f) SDII; (g) R20mm; (h) R10 mm; and (i) CWD.

For the SDII index (Figure 4.6 (f)), U(t) shows an increasing trend from 1992 to 1994/1995, while a decreasing trend can be seen in the U'(t) trend line. The curves intersect each other in 1994, 1995, and 1996 respectively. Again, there is an increase after 2005 in the U(t) trend line while there is fluctuation in the U'(t) line. 2001 and 2007 show intersections again. However, none of these five intersections have significant probability values much higher than the accepted significance level ($p \leq 0.05$). 20 mm index (Figure 4.6 (g)) shows a decreasing trend for the 2000 to 2006 period. After 2006, the U(t) line shows an increasing trend while the U'(t) line shows a fluctuating trend. The 10 mm index (Figure 4.6 (h)) shows a similar pattern to the 20 mm index. After 2001, the U(t) curve shows an increasing trend while the U'(t) curve shows fluctuation. CWD index (Figure 4.6 (i)) illustrates an interesting pattern

showing no intersection of U(t) and U'(t) lines. Nevertheless, when focusing on all these indices, there are no significant turning points in the period considered.

4.2 Identification of rainfall and water level fluctuations and their relationships in the Kelani River Basin

After identifying the spatial and temporal patterns of extreme rainfall, the study focused on examining the relationship between rainfall and water levels in the KRB.

4.2.1 Detecting long-term trends in rainfall and water level in the KRB during the period 1991 to 2020

The current study carried out an important analysis of overall trends for rainfall distribution and water level fluctuations in the KRB as a preliminary phase. In this first effort, a calculation of the total annual and seasonal rainfall was carried out for the ten meteorological stations. Subsequently, as illustrated in Figure 4.7 and Figure 4.8, the resulting total values have been used to calculate the annual average and seasonal average rainfall in the KRB.

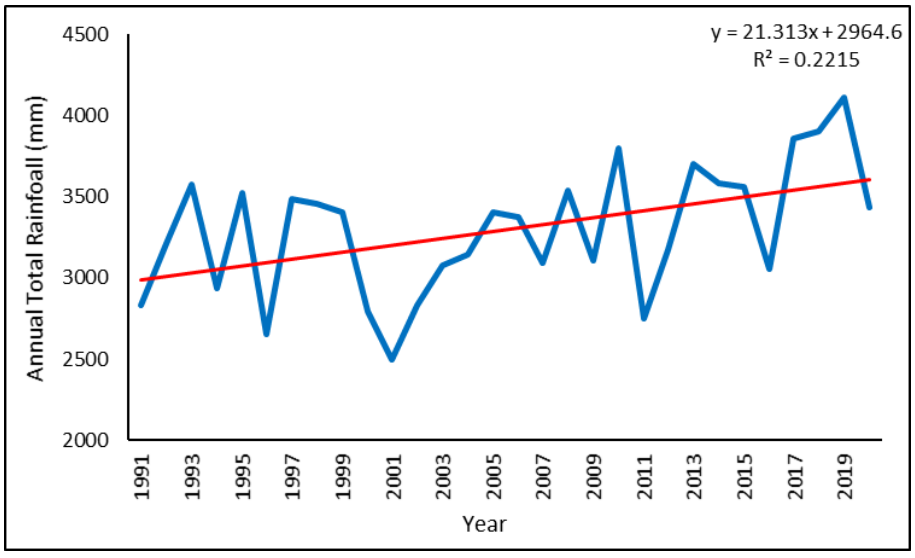

Figure 4.7 Annual total rainfall of the KRB (at 95% confidence level)

Figure 4.7 clearly displays that annual total rainfall had a gradual increase from 1991 to 2020. Upon initial examination, it was apparent that annual precipitation patterns vary from year to year. The lowest annual total rainfall occurred in the year 2001 with

a value of 2494.2 mm, while the highest value was reported in 2019, reaching 4108.9 mm. The inherent dynamism of the rainfall levels is underlined by this very wide range in annual variability. The variability indicates that the region has experienced both dry and wet years, which is typical of many climate systems. As for the overall temporal trend, it appears that, from the early 1990s to the early 2000s, there was a period of decreasing precipitation, followed by increases in the period from the late 2000s to the early 2020s. There was a very high annual total precipitation of 4108.9 mm in 2019, which is considered to be an extreme year. It's possible this was due to a particularly wet year. On the other hand, 2001 is a year with significantly lower precipitation, 2494.2 mm, suggesting a dry year. The last few years, such as 2017 to 2020, appear to have had more precipitation than is typical.

The seasonal behaviour of rainfall also showed interesting patterns between 1991 and 2020 (Figure 4.8).

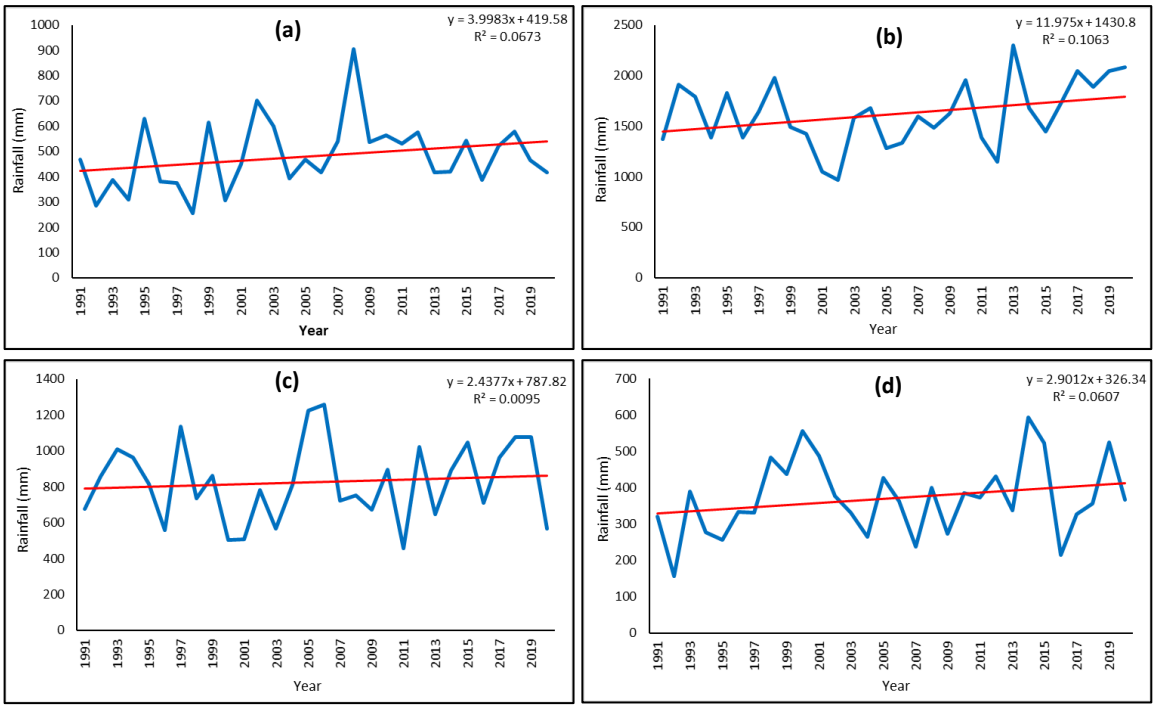

Figure 4.8 Seasonal rainfall in the KRB. Note:(a) IM1; (b) SWM; (c) IM2; (d) NEM (at 95% confidence level).

Upon initial examination, a clear upward trend can be observed in the amount of precipitation across all seasons. Focusing on Figure 4.8 (a) as characteristic of the IM1 season, year-to-year variability is noted in common rainfall amounts. Examining temporal trends, the study observed several fluctuations over time. For instance, in the years 1991 to 2002, there was a significant increase in IM1 rainfall, with notable fluctuations between 1995, 1999, and 2002. Overall, rainfall during IM1 has been decreasing steadily since 2002, with occasional peaks and troughs. This shows that rainfall patterns in the IM1 have changed during this period. The year 2008 is an outlier, with exceptionally high IM1 precipitation of 903.66 mm, whilst the lowest rainfall was 254.23 mm, in 1998. Figure 4.8 (b) illustrates the SWM rainfall pattern during the study period. Looking at temporal trends, SWM rainfall has been fluctuating over time. A strong linear trend is not apparent, but there are periods in which more or less rainfall can be observed. For instance, the incidence of high rainfalls in 1992, 1998, and 2010 is noted, while 2001 and 2012 were characterised by low precipitation. Exceptionally high SWM rainfalls of 2298.41 mm in 2013 and 2082.49 mm in 2020 are noted as extremes. Conversely, 2002 recorded the lowest SWM rainfall (967.01 mm). Figure 4.8 (c) depicts the total rainfall amount in the IM2. The fluctuations in IM2 rainfall can be observed by examining time patterns. The exceptional rainfall of 1225.30 mm in 2005 and 1260.25 mm in 2006 represent some remarkable extremes. On the other hand, the lowest IM2 rainfalls of 455.59 mm were observed in 2011. Figure 4.8 (d) shows the total rainfall pattern for the NEM season for the 1991 to 2020 period considered. Due to the transitional and variable nature of NEM seasons, there is a significant difference in annual rainfall totals between years. In the catchment area of the KRB, this season is linked to the lowest rainfall amounts. However, high total rainfalls in 2014 (593.14 mm) and 2015 (523.04 mm) were among the most significant extremes. By contrast, NEM rainfall was at an all-time low of 214.55 mm in 2016. As this study is about the relationship between rainfall and water level in the KRB, the general pattern of water levels at the Hanwella and N'Street hydrology stations was also studied.

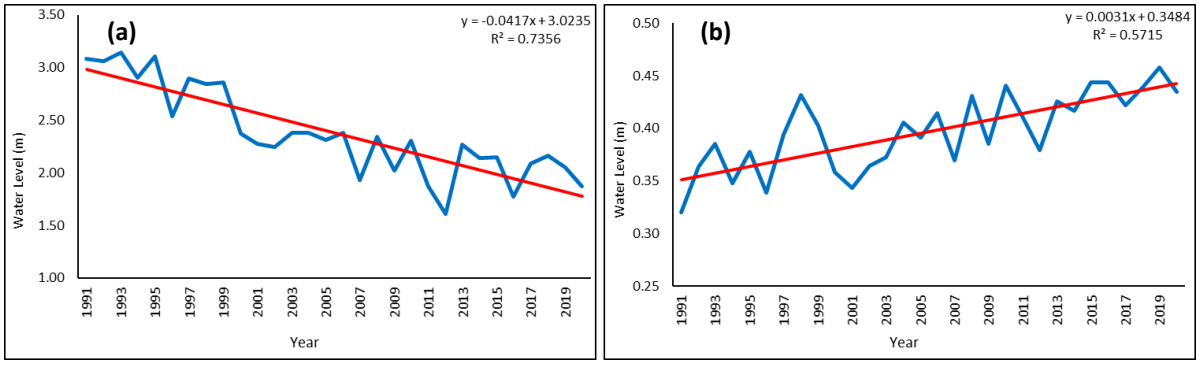

Figure 4.9 Water level at hydrology station. Note:(a) Hanwella and (b) N'Street stations respectively.

An interesting observation can be made about the levels of water recorded at Hanwella and N'Street hydrology stations. During the period between 1991 and 2020, there has been a decline in water levels at the Hanwella hydrographic station (Figure 4.9 (a)), whereas N'Street hydrographic station shows an increasing trend Figure 4.9 (b). The seasonal pattern also provides a clear picture of water level changes in the KRB (Figure 4.10).

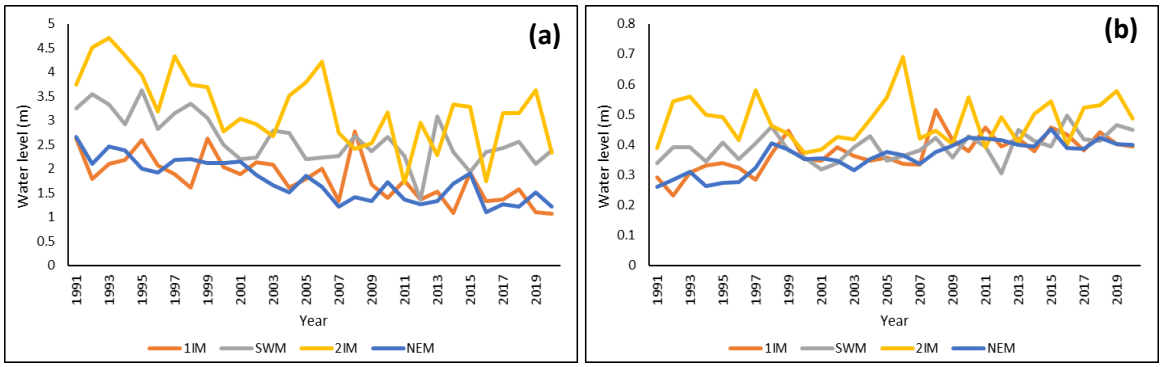

Figure 4.10 Seasonal water level. Note: (a) Hanwell (b) N'Street stations

In all seasons, Hanwella station shows a decreasing trend while N'Street has an increasing trend. For Hanwella station, the highest water levels are observed in the IM2 season, from October to November, which is associated with heavy rainfall convection currents. The second highest water levels are observed in the SWM season,

from May to September. This corresponds to a period of heavy rainfall in Sri Lanka associated with the SWM. Even though during the SWM season the general pattern of water levels shows a decreasing trend, after 2015 there is an increasing trend towards 2020. Conversely, the lowest water levels have been recorded during the NEM season, which is consistent with the drier weather conditions which are characteristic of NEM due to the orography of the island. The IM1 season displays intermediate water levels, which are characterised by the development of transitional weather patterns between major monsoon seasons. The water level variation is comparatively high among the seasons. The N'Street station also has its highest water levels in the IM2 and second-highest during the SWM season. The lowest levels were recorded in the NEM and IM1 periods. However, variations between the water levels in climate seasons were minimal during the study period.

After identifying the general pattern of rainfall and water level in the KRB, the MMK test and Sen's slope (Appendix C) were used to identify trends trend in these two variables. The MMK results indicate that the basin had a significant increasing (Z-value 5.36) trend over the study period. Figure 4.11 depicts the MMK Z-values for rainfall at meteorological stations.

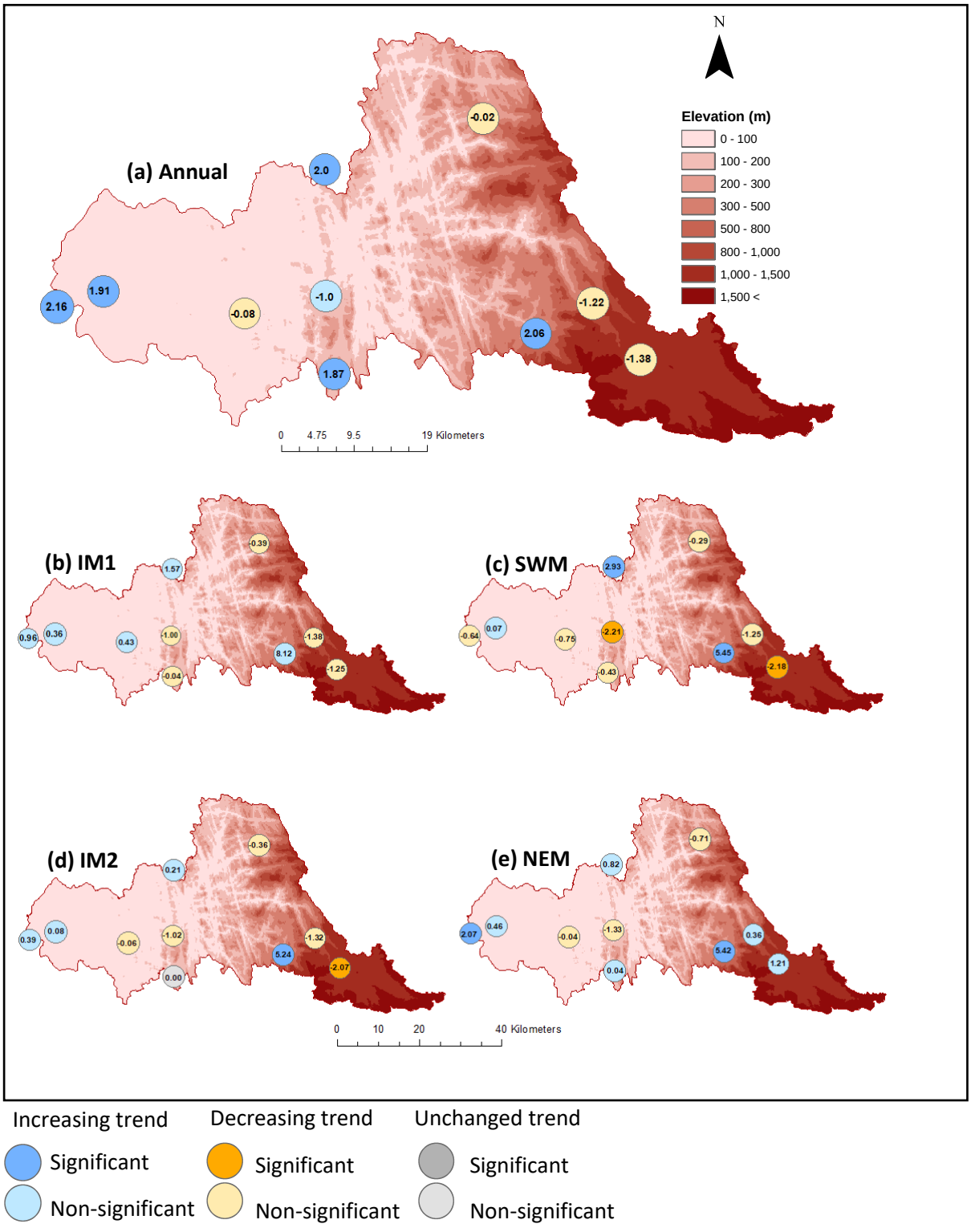

Figure 4.11 Rainfall trends in the KRB. Note: The values generated at 95% confidence level.

According to the MMK results, 60% of the meteorological stations show an increasing trend in the 1991 to 2020 period (Figure 4.11 (a)). Colombo, Angoda, Chesterford, Labugama Tank, and Maliboda stations show a significant increasing trend. Out of the four stations, three stations (Undugoda, Laxapana, and Maussakelle) in the more elevated areas show a decreasing trend.

During the IM1 period (Figure 4.11 (b)), Colombo, Angoda, Maliboda, Chesterford, and Hanwella meteorological stations show an increasing but not significant trend. Further, stations in more elevated areas (except Maliboda) show a decreasing trend. During the SWM season (Figure 4.11 (c)), 70% of the meteorological stations showed a decreasing trend. Among the stations with decreasing trends, Awissawella, and Maussakelle show a significant decrease trend (P-values of 0.0269 and 0.0295 respectively). The highest increasing trend belongs to the Maliboda meteorological station, with a P-value of 0.00. Chesterford Meteorological Station also has a significant increasing trend in rainfall (P-value of 0.0034). During the IM2 season (Figure 4.11 (d)), 50% of the meteorological stations showed a decreasing trend, with Maussakelle having a significant P-value (0.04). During this season, the Maliboda meteorological station showed the highest significant increasing trend (P-value of 0). It is notable that the Labugama Tank station had an unchanged trend during this season, from 1991 to 2020. During the NEM season (Figure 4.11 (e)), 70% of the meteorological stations had an increasing trend. Colombo and Maliboda meteorological stations had a prominent increasing trend, with P-values of 0.0385 and 0, respectively. Hanwella, Awissawella, and Udugoda stations showed a decreasing trend. Even though Colombo, Labugama Tank, Maussakelle, and Laxapana meteorological stations showed an increasing trend during NEM, the picture was different during the SWM season. Accordingly, trends in water levels at Hanwella and N'Street stations are shown in Table 4.2.

Table 4.2 Trends in water level in the KRB. Note: Values generated at 95% confidence level. *Denotes significant trends.

	Annual		1IM		SWM		2IM		NEM	
1991-2020 period	*Z-value*	*Sen's Slope*	*Z-value*	Sen's Slope	*Z-value*	*Sen's Slope*	*Z-value*	*Sen's Slope*	*Z-value*	*Sen's Slope*
Hanwella Station	-7.52*	-0.04	-15.65	-0.04	-5.67*	-0.04	-6.5*	-0.05	-9.03*	-0.04
N'Street Station	13.27*	0.00	9*	0.00	5.26*	0.00	1.58	0.00	8.21*	0.00

The annual trend in both these hydrological stations shows a completely different direction during the study period. The water level at Hanwella station shows a significant decrease, while N'Street station shows a significant increase. During all four seasons, Hanwella hydrology station has a decreasing trend. Among all four seasons, only the IM1 shows a non-significant decreasing trend, at Hanwella. For N'Street hydrology station, all four seasons show an increasing trend. Remarkably, during the IM2 season the station had a non-significant increasing trend while other three seasons significant increase trend.

4.2.2 Extreme rainfall in the KRB

In order to identify the extreme rainfall over the basin, extremes precipitation indices, including R99p, R95p, RX5day, PRCPTOT, CWD and SDII were calculated based on daily rainfall data of the ten meteorological stations. To evaluate the intensity and variability of extreme rainfall events within an area, the calculation of these extreme rainfall indices has served as a comprehensive measure. The general pattern of extreme rainfall events in the KRB is illustrated in Figure 4.12.

Figure 4.12 General pattern of extreme rainfall in the KRB (95% confidence level). Note: (a) R99p, (b) R95p, (c) RX5day, (d) PRCPTOT, (e) CWD, and (f) SDII. Blue line indicates average extreme values and yellow line indicates five year moving average values

The general pattern of extreme rainfall over the basin shows that, contrasting with other indices, there is a reduction in the intensity of extreme rainfall. This observation aligns with the findings in sections 4.1.1 and 4.1.2. Also, from 1993 to 2001 a general decline in extreme rainfall is observed in all the indices. Except for the SDII, all indices have shown an increasing trend since 2001. It revealed that, although with lower intensity, an increased incidents of extreme rainfall events are expected in the basin.

After calculating extreme rainfall indices, the MK and Sen's Slope tests were employed to identify the trends in extreme rainfall indices (Table 4.3).

Table 4.3 Trends in extreme rainfall over the KRB. Note: These MK Z values generated at 95% confidence level and * presents significant trends.

Met Stations	RX5day	R95p	R99p	PRCPTOT	CWD	SDII
Angoda	-0.57	-0.75	1.69	0.71	0.90	-3.57*
Awissawella	-3.89*	-2.82*	-3.14*	-2.85*	-0.32	-3.32*
Chesterford	1.21	0.78	0.34	2.66*	3.13*	-0.09
Colombo	0.14	-0.07	0.62	0.14	0.47	0.14
Hanwella	-1.39	-1.50	-0.84	-0.43	0.43	0.54
Labugama	-0.71	-0.64	-0.47	-0.43	-0.23	-1.37
Laxapana	-1.71	-0.64	-0.36	-1.82	-1.50	-1.04
Maliboda	5.82*	4.69*	3.42*	6.60*	6.00*	3.53*
Maussakelle	-2.36*	-1.64	-0.81	-2.78*	-1.15	-2.79*
Undugoda	-1.00	0.57	1.23	-0.54	-0.45	-1.64
Average of indices	0.68	0.01	0.89	2.39*	1.52	-0.75

In the analysis of extreme rainfall patterns in the KRB, a discernible trend of overall increase is evident across all averages of indices except SDII. Notably, the Maliboda station shows a significant increase in extreme rainfall. Contrarily, the Avissawella station portrays a significant decreasing trend.

When focusing on the monthly maximum 5-day precipitation (RX5day) index, 70% of stations exhibit a decreasing trend. The Avissawella and Maussakelle stations have a significant decreasing trend with Sen's slope values of -2.05 and -1.24, respectively. Chesterford, Colombo, and Maliboda stations show an increasing trend. Among these three stations, Maliboda exhibits a significant trend (Sen's slope value is 8.13). The average values of RX5day indicate an increasing trend.

The heavy rainfall (R95p) in the basin also shows an increasing trend (with the lowest increasing trend found in the average value) during the study period. However, only three stations (Undugoda, Maliboda, and Chesterford) have an increasing trend. The

Maliboda station has a significant trend with Sen's slope value of 0.15. Further, all other 70% of other stations show a decreasing trend in R95p. The extreme rainfall in the basin (R99p) is also on the rise. Fifty percent of stations (Angoda, Chesterford, Colombo, Maliboda, and Undugoda) indicate an increasing trend. Regarding the decreasing trend, the Avissawella station stands out with a significant trend having Sen's slope value of -11.4. It is ascertained that the increasing trend of R99p leads to more extreme rainfall-related hazards in the basin.

The Annual total precipitation on wet days (PRCPTOT) presents a significantly increasing trend in the basin for the average value (Z-value of 2.39, Sen's slope value of 21.02). This marks the highest increasing value among any average index value in the basin. However, 60% of stations indicate an increasing trend, with Avissawella and Maussakelle trends being significant (Sen's slope value of -44.76 and -29.69, respectively). On the other hand, Chesterford and Maliboda stations exhibit a significant increasing trend (Sen's slope value of 35.22 and 286.71). The average CWD index value also increases in the KRB. Fifty percent of stations show an increasing trend from the CWD index. Among them, Chesterford and Maliboda stations display a significant increasing trend (Sen's slope value of 0.71 and 1, respectively). The other five stations with decreasing trends do not have any significant value. Nevertheless, an increasing trend in the CWD index signals flood hazards in the KRB. When focusing on the SDII index, the basin exhibits a decreasing trend, though it is not significant (Sen's slope value of -0.26). The Maliboda station is the only station having a significant increasing trend (Sen's slope value of 0.53). Angoda, Avissawella, and Mausskelle stations have a significant decreasing trend (Sen's slope value of -0.25, -0.21, and -0.14, respectively). In general, 70% of the stations show a decreasing pattern.

4.2.3 Relationship between rainfall and water levels in the KRB

When considering the relationship between rainfall and water levels in the basin, as its first step this study calculated correlation coefficients for these two variables on a daily basis. The correlation coefficient value for daily rainfall and water level at Hanwella station is 0.42, a moderately positive relationship. On the other hand, the coefficient value for N'Street is 0.36, a weakly positive correlation (with 95%

confidence interval). Subsequently, the monthly relations between rainfall and water level in the KRB were considered. According to Figure 4.13, it is apparent that the increase in rainfall has led to increased water levels, a positive correlation between water levels in the KRB and precipitation.

During the Southwest Monsoon (IM2) season, where strong winds with widespread rain affect the whole island, the peak of water level and precipitation is discernible in the months of October and November. The correlation between seasonal average water level and rainfall during the IM2 is 0.63 (Hanwella station) and 0.88 (N'Street station) is the highest among all four seasons, with a 95% confidence level.

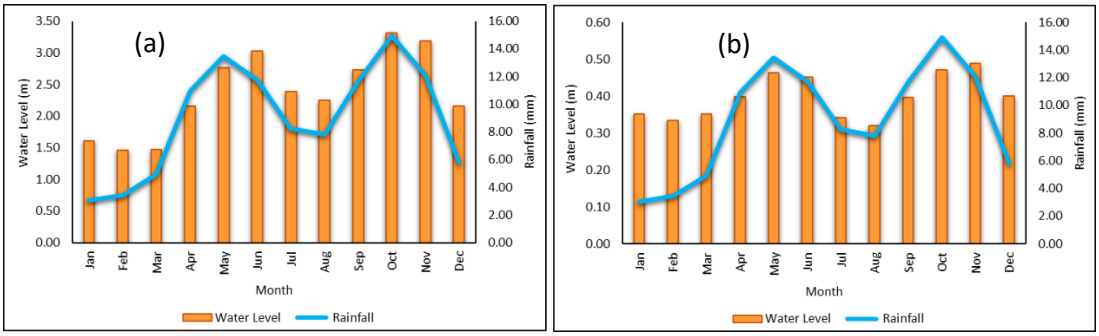

Figure 4.13 Monthly water levels and rainfall in the KRB from 1991 to 2020.

After the IM2, the first phase of SWM (May and June) shows the second-highest peaks in rainfall and water discharge/water level. In the SWM period, there is a 0.41 and 0.81 correlation between rainfall and water discharge in Hanwella and N'Street stations respectively. This correlation value is 0.16 (Hanwella) and 0.48 (N'Street) during NEM, the lowest of the four seasons. During the IM1, 0.34 and 0.6 correlation is seen at Hanwella and N'Street stations respectively, with a 95% confidence level. Even though the correlation shows a moderate to high positive correlation between water levels and rainfall, season-wise, it shows a strong positive correlation. Further, the study examined the relationship between monthly rainfall and water levels. See Appendix D for the monthly average correlation coefficients.

As mentioned above, an analysis of daily rainfall and water levels in the KRB shows a moderately positive correlation. Nevertheless, the monthly relationship between these two variables shown in Figure 4.14 and 4.15 demonstrate a fascinating pattern. It is generally a positive relationship throughout the year, except for January. During

the month of January, the N'Street station showed a negative correlation of 0.03 (Figure 4.14 (b)), with a 95% confidence level, while the Hanwella station showed a moderately positive correlation (0.49). Nevertheless, the monthly correlation coefficient varies between moderately positive (0.4) and highly positive (0.9) for the remaining months at N'Street station. On the other hand, correlation coefficients ranged from 0.3 to 0.83 at Hanwella station, indicating a variation between low and high positive correlations throughout the year. The month of May has a nearly perfect relationship at both stations (Figure 4.14 (i) and (j)). Also, the highest positive coefficient values belong to the month of May, 0.83 and 0.9 for Hanwella and N'Street stations, respectively. In particular, the strong relationship observed in Figure 4.14 for the relevant months is apparent between the SWM and IM2 seasons. Both stations indicate that the relationship of water level to rainfall approaches a near-perfect relationship (Figure 4.14 (k), (l), and Figure 4.15 (a), (b), (f), (h), (i), (j)) in the months of June, July, September, and November. During these months, the correlation coefficients for Hanwella station were 0.63, 0.76, 0.75, and 0.64, respectively. Correlation coefficients of 0.71, 0.76, 0.87, and 0.81 were observed at N'Street station in the same months. This detailed analysis shows the complex monthly and seasonal dynamic of the correlation between rainfall and water levels in the KRB, which is essential for information management and planning regarding water resources.

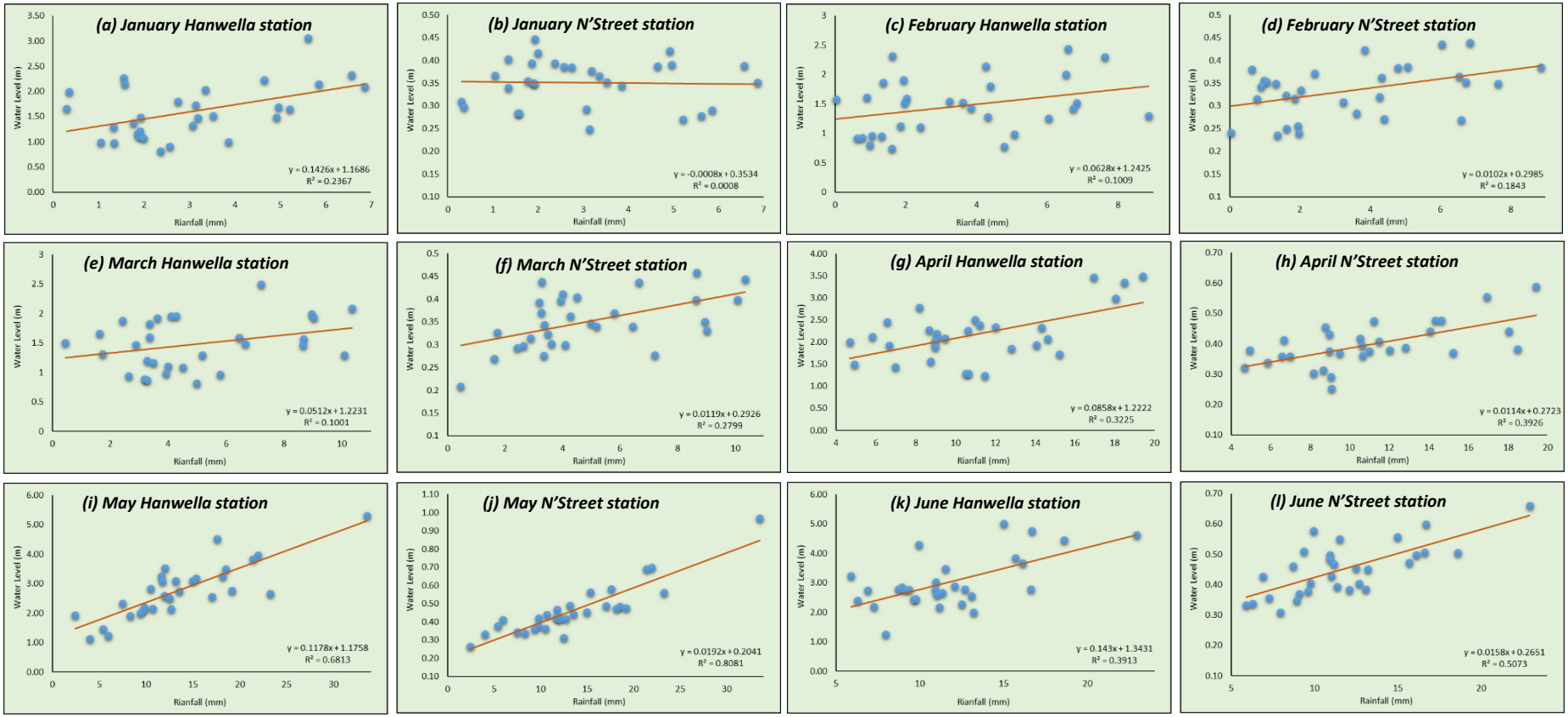

Figure 4.14 Relationship between rainfall and water level in the KRB at monthly scale.

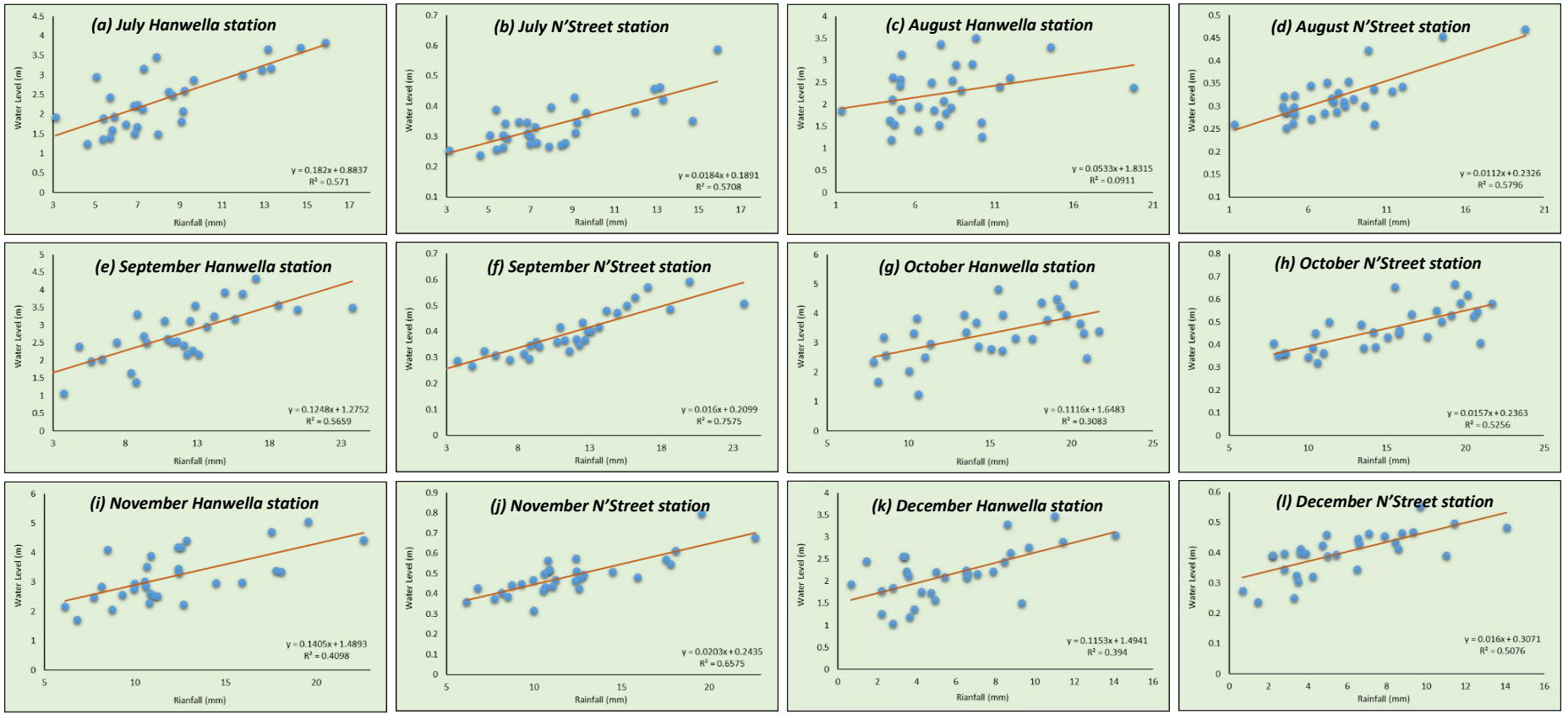

Figure 4.15 Relationship between rainfall and water level in the KRB at monthly scale.

As its next step, this study tried to identify when rainfall increases will be in sync with water levels at different time lags. The study used lag correlation for this task. Figures 4.16 and 4.17 illustrate a scatter plot for the lag correlation over 10 days. The study used a 10-day period for lag correlation because when floods occur in the basin their effects remain for at least 7-10 days.

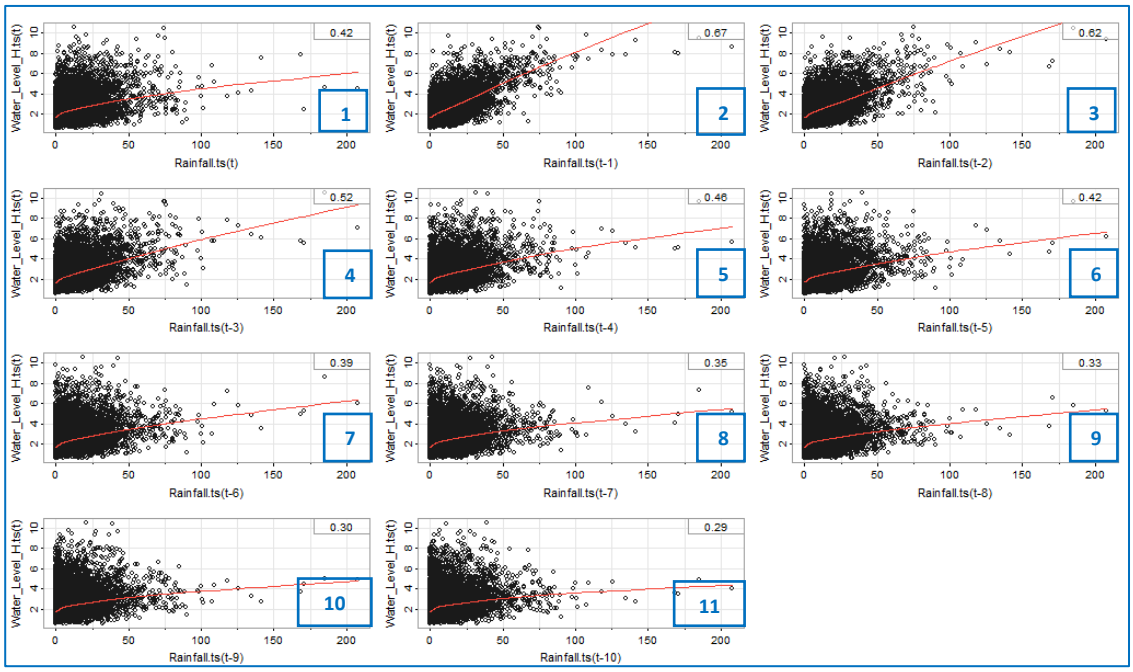

Figure 4.16 Lag effect between rainfall and water levels at Hanwella hydrology station (at 95% confidence level)

The lag correlation analysis shows that the station at Hanwella (Figure 4.16) exhibits a moderate positive correlation of 0.42 during the initial interval. Subsequently, the correlation increases in the second lag interval and gradually decreases from the second to the eleventh lag. In particular, there were notably high positive correlation coefficients of 0.65, 0.62, and 0.52 for the second, third, and fourth lags. This positive correlation indicates that, after a certain period of time, an increase in rainfall in the Kelani River Basin is accompanied by an increase in water levels. Such correlation patterns can be observed in the lag analysis for N'Street station shown in Figure 4.17. A moderately positive correlation is shown for the first lag of the N Street station, though with a slightly lower coefficient of 0.36 than for the first lag correlation of the Hanwella station. N'Street, on the other hand, shows a strong positive correlation, with

coefficients of 0.61, 0.62, and 0.51 in the second, third, and fourth lags, similarly to Hanwella. It should be noted that there are certain differences between these two stations' lag correlation patterns, mainly regarding the lags where a higher correlation coefficient was recorded. In particular, the Hanwella station has the highest lag correlation in the second lag, while the N'Street station has the highest lag correlation in the third lag. These findings provide insight into the temporal dynamics of rainfall and water levels at these two hydrological stations in the KRB. The lag correlation clearly illustrated that, when rainfall is high, it is linked with water level increases in the basin which is useful for understating extreme rainfall related flooding.

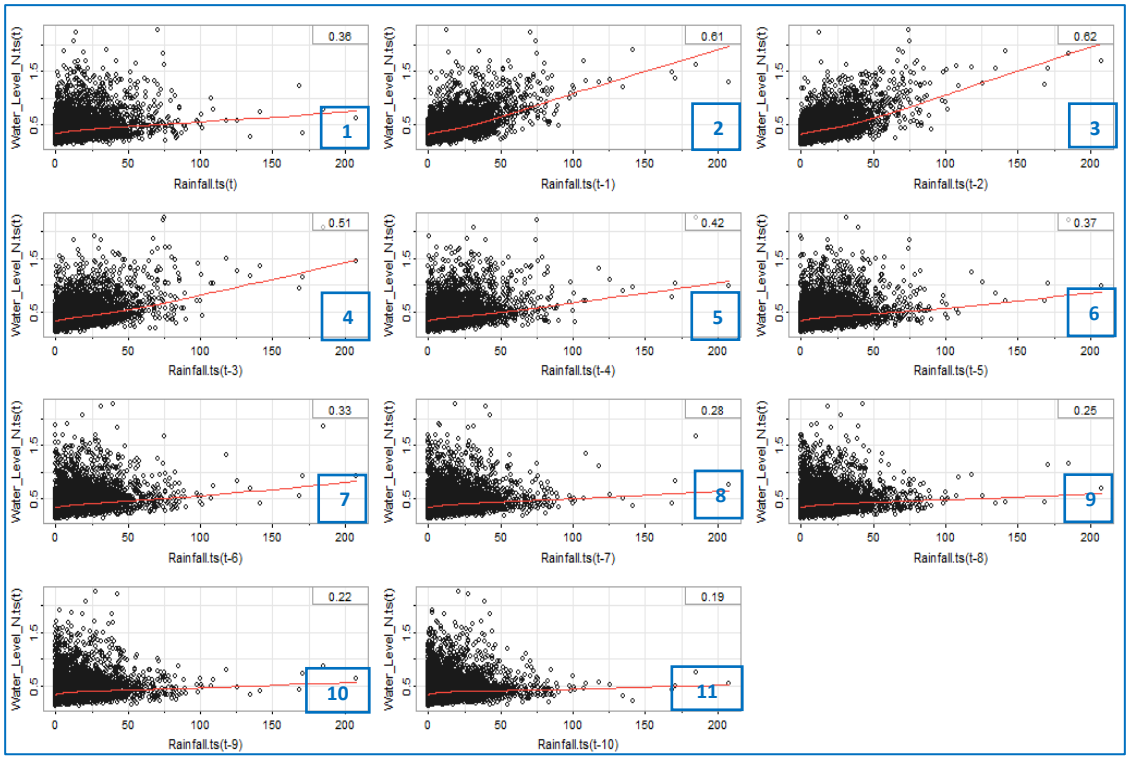

Figure 4.17 Lag effect between rainfall and water level at N'Street hydrology station (at 95% confidence level)

According to the results, it is clearly visible that there is a positive relationship between rainfall and water levels in the KRB. There is thus a high tendency toward flood hazards with extreme rainfall over the basin. Therefore, the next objective requires presenting the AHP-based flood-risk assessment results of this study.

4.3 Examining flood risks caused by extreme rainfall in the Lower Kelani River Basin

The third objective has two main parts:

1. Detailed flood risk assessment based on the AHP method.
2. The proposed Integrated AFH method for flood risk assessment.

4.3.1 AHP based flood risk assessment

4.3.1.1 Determining weight and weight prioritisation for hazard and vulnerability factors

Weights were calculated for factors based on expert opinions and the literature with the help of a pairwise matrix. The descriptive statistics of weight assigned factors for each criterion are shown in Table 4.4.

Table 4.4 Weights assigned for factors of each criterion. Note: AHP weights are based on expert opinion and literature

Criteria	Factors	Weight	Relative weight (%)	Rank
Physical Vulnerability	TWI	0.14	14.85	2
	Land cover	0.18	18.19	1
	Elevation	0.10	9.89	7
	Slope	0.11	10.63	4
	rainfall	0.13	13.35	3
	NDVI	0.07	7.00	8
	Drainage Density	0.10	10.00	6
	Soil	0.05	5.20	9
	Proximity to river	0.11	10.73	5
Social Vulnerability	Population Density	0.34	34.44	1
	Land Use	0.26	25.63	2
	NDBI	0.14	14.40	4
	Distance from Road	0.10	9.94	5
	Distance to shelter	0.16	15.58	3

When considering Table 4.3, higher weight values indicate higher causativity of flood hazard and vulnerability. The weights vary between zero and one, equalling the sum of weights marked as one (weighted linear combination). In flood hazards, land cover (18.19%), TWI (14.85%), and heavy rainfall (13.35%) play prominent roles in causing flood hazards in the LKRB. Focusing on flood vulnerability, population density (34.44%) and land use (25.63%) have the highest weighted values. It is evident that during a flood event people face many difficulties and their property may be lost or damaged.

4.3.1.2 Composite maps for physical vulnerability and social vulnerability

The study has prepared composite maps for each factor according to the flood risk levels. In the first phase, composite maps for physical vulnerability are illustrated in Figure 4.18.

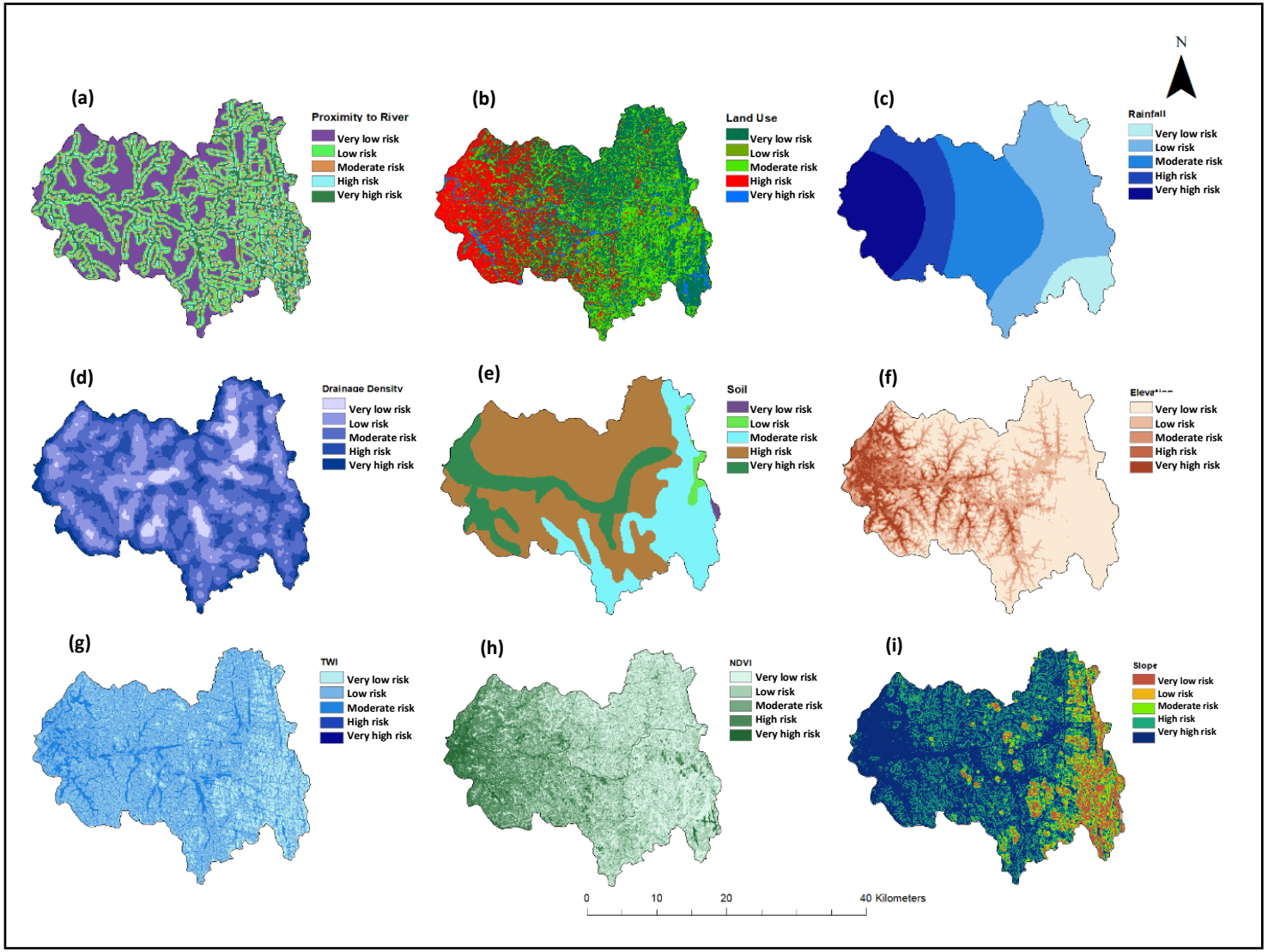

Figure 4.18 Thematic maps for physical vulnerability of floods in the LKRB.

Note: All maps were reclassified according to the flood risk level. The legends indicate very low risk to very high risk for flood hazards.

(a) Proximity to river,

(b) Land use

(c) Rainfall

(d) Drainage density

(e) Soil

(f) Elevation

(g) TWI

(h) NDVI

(i) Slope

As mentioned in 2.1, the eastern part of the LKRB is elevated at nearly 450 m and the western seaward part is almost a flat terrain. Figure 4.18 (a) shows the proximity to the river. The eastern hilly part of the study area has more streams than the western side. The closer to the river or stream, the greater the probability of susceptibility to flood. In Figure 4.18 (b) depicts the reclassified land cover of the LKRB. More built-up areas can be seen towards the sea and the hillsides are covered with forests and plantations. Built-up areas are highly susceptible to flooding, while forest and plantation areas have very low susceptibility to flooding. Out of the total land area (808 km2) of the LKRB, 41.47% (335.13 km2) is at very low risk, 2.31% (18.64 km2) is at low risk, 26.20% (211.78 km2) is at moderate risk, 25.52% (206.29 km2) is at high risk, and 4.50% (36.38 km2) is at very high risk of flood. Figure 4.18 (c) depicts the reclassified map of rainfall effects on flood risk. As we know, the higher altitudes of the KRB receive more rainfall than the lower altitudes.

Nevertheless, when it comes to flood hazards, the rainfall layers have been reclassified. Figure 4.18 (d) shows the drainage density of the LKRB. Nearly 25% (193.06 km^2) of the total land area of the LKRB has rich drainage density. Especially in the eastern side of the study area is at low risk for flood susceptibility. Accordingly, due to poor drainage systems, nearly 49% (392.2 km^2) of the total land area is highly affected by flood hazards. Nearly 27% of the total land area has a moderate flood risk due to moderate drainage density. According to Figure 4.18 (e), nearly 58% of the study area is covered by rolling and undulating terrain red-yellow podzolic soils with soft or hard laterite. The surface runoff process is more prominent in hard laterite soils than water is infiltration. Thus, according to the soil type, the area has high susceptibility to flood hazards. The elevation of the LKRB is one of the main factors influencing flood hazards (Figure 4.18 (f)). Most of the land area (53.95% or 435.37 km^2) in the LKRB is 20 m or more above mean sea level and is thus marked as very low risk of flood susceptibility.

11.59 % (93.55 km^2) of the total study area is < 5 m elevation and is thus at high and very high risk of flood susceptibility. Figure 4.18 (g) illustrates the TWI of the LKRB. The highest values were concentrated in the study area's western side, which is flat terrain with very high flood susceptibility. The highest areas in the eastern part of the LKRB have the lowest TWI values, representing the lowest susceptibility to flood hazards. Values obtained for NDVI reclassification (Figure 4.18 (h)) reveal that most

of the study area is covered by vegetation. Due to the urbanisation process and increased population density, most dense vegetation can be observed on the eastern side of the study area. At the same time, low concentrations are visible in the west. According to the reclassification, nearly 511 km^2 (63.20%) of the LKRB total area is marked as low and very low for flood risk. Only 137.81 km^2 (17.04%) of the land area is high or very high for flood susceptibility, according to the NDVI values. Flood susceptibility by slope is seen in Figure 4.18 (i), showing that more than half of the study area (53.73%) is under a 30-degree slope angle, which causes a very high risk of flood. 17% (141.34 km^2) of the total land area is above a 60-degree slope angle, causing moderate to very low risk of flood. The remaining 28.69 % (230.57 km^2) of the area is at high risk of flood.

After the thematic reclassified maps were prepared, a weighted overlay was performed to prepare a flood hazard map of the LKRB (Figure 4.19).

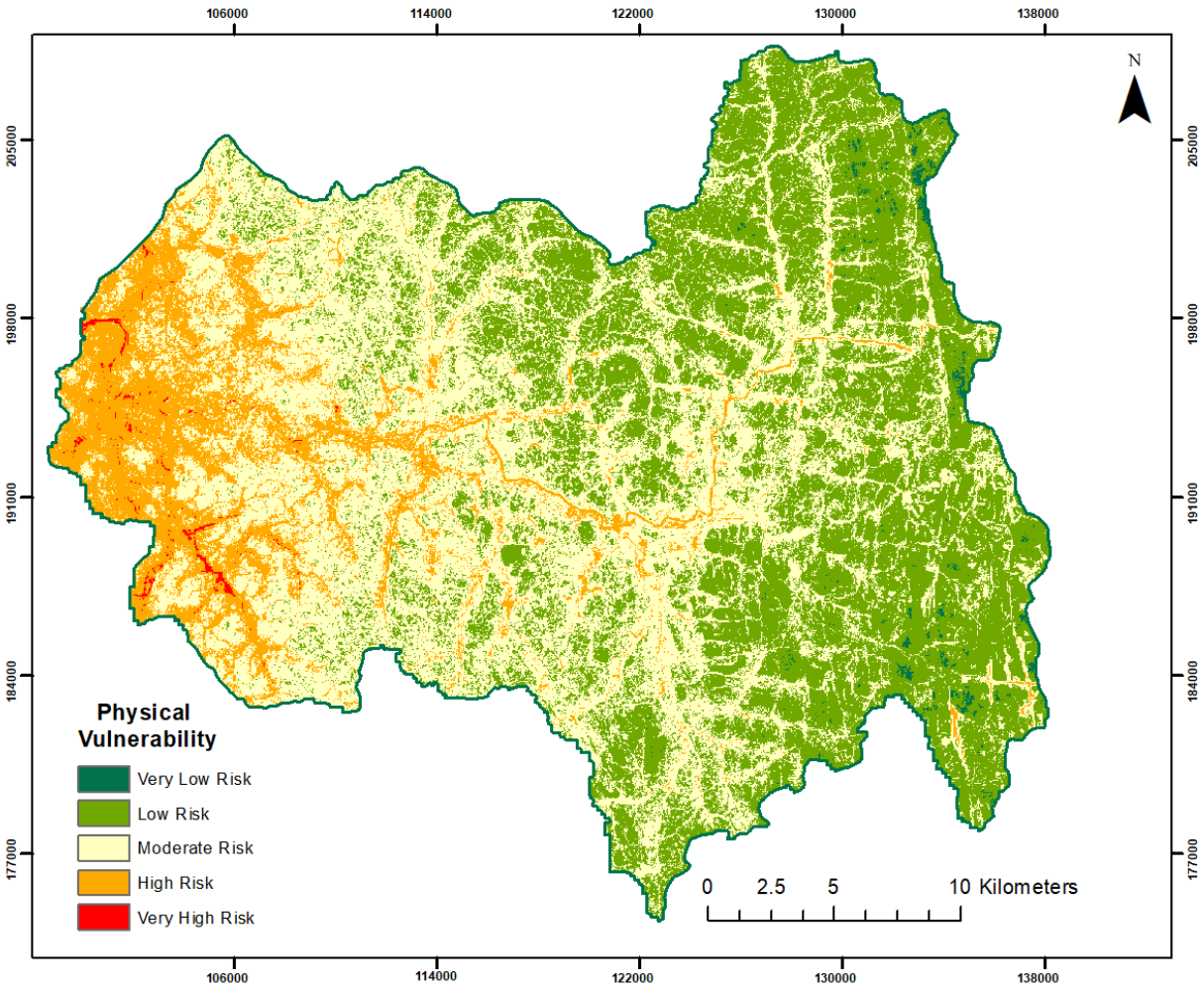

Figure 4.19 Physical vulnerability for flood hazard in the LKRB

According to the physical vulnerability map (Figure 4.19), nearly 0.43% of the area is marked at very low risk of flood susceptibility. 39.11% (315.7 km^2) of the area of the LKRB, primarily spread over the eastern side of the study area, is at low risk of flood. Nearly half of the total land area (47.34%) belongs the moderate risk of flood category. The high risk and very high risk areas are observable on the western side of the LKRB (10.5.88 km^2), especially along the main river and in very low-lying regions. After prepared physical vulnerability map, the study focusses on preparing social vulnerability map for the LKRB. As the first step study prepared thematic maps for flood vulnerability factors (Figure 4.20).

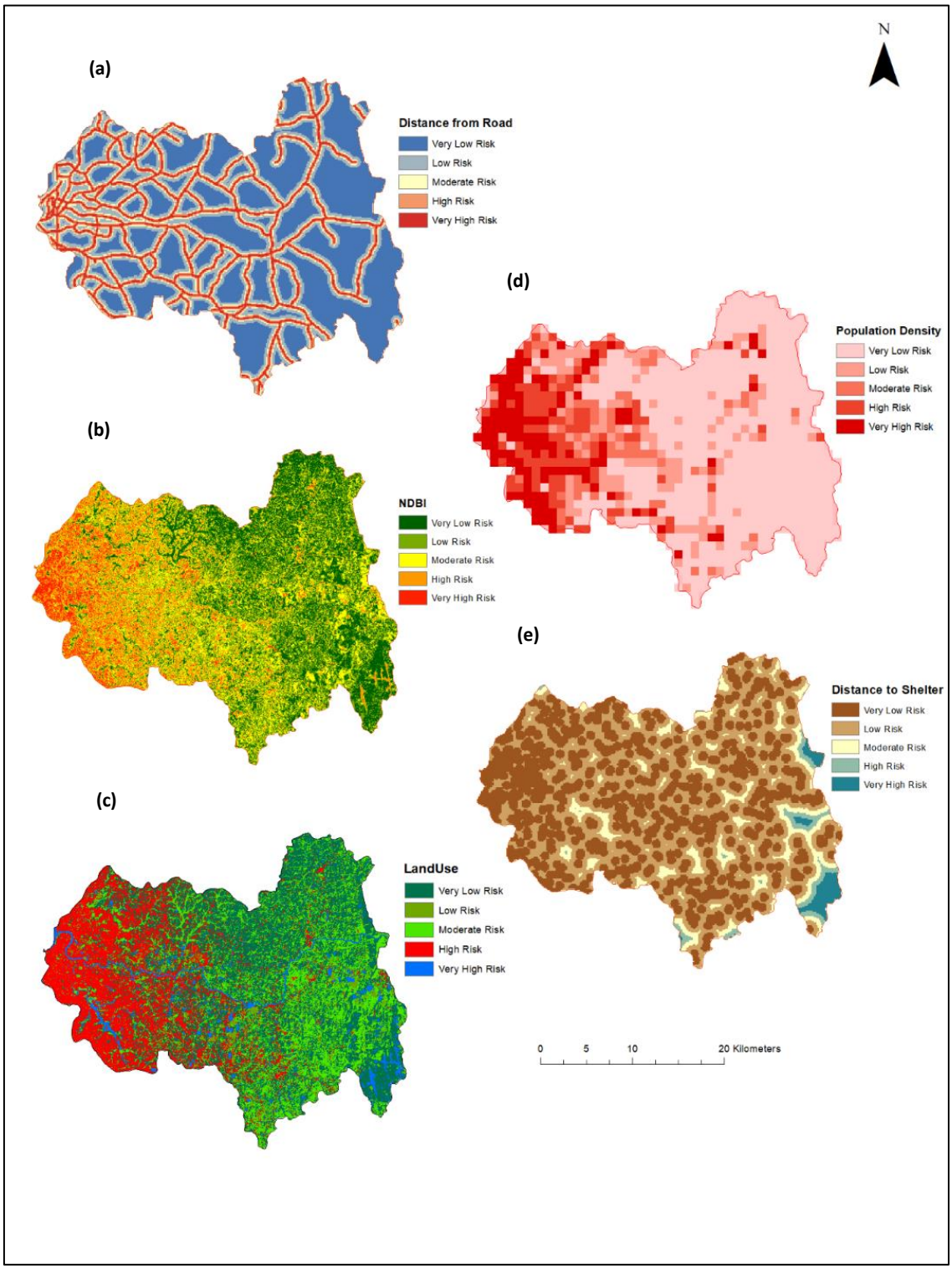

Figure 4.20 Thematic maps for social vulnerability of floods in the LKRB. Note: All maps were reclassified according to the flood risk level. The legends indicate very low risk to very high risk for flood hazards. (a) Distance from road, (b) NDBI, (c) Land use, (d) Population density, and (e) Distance to shelter

When considering the factor of distance from a road (Figure 4.20 (a)), a high proportion of (360.22 km^2) the LKRB has minimum vulnerability to flood risk, especially on the western side of the study area. Road density is concentrated on the western side of the LKRB, creating higher risks of flood. 9.83% of the area is at moderate risk category and 21.99% is belonged to high risk and very high risk of flood susceptibility categories. Building density and urbanisation process are at high levels there, so both NDBI and land use factors causing high and very high risk of flood susceptibility are visible on the western side of the LKRB (Figure 4.20 (b) & (c)). 377.92 km^2 of the area is at moderate to very high risk of flood due to building density. The area is closer to the built-up areas, which cover 454.45 km^2 of land and have a moderate to very high risk for flood. Figure 4.20 (d) illustrates the reclassified population density of the study area. Most of the area in the LKRB (57.51% land cover) has less population density (<1000). 97.4 km^2 of land area has a population density of >5000, specifically the western part, which is highly vulnerable to flood. Highly vulnerable and moderately vulnerable areas cover 17.02% of the total area of the LKRB. Distance to shelter (Figure 4.20 (e)) also shows an interesting pattern. The LKRB has many temples and government schools that the study considered as flood shelters. Only 30.62 km^2 (3.79%) of the LKRB, in the highly elevated eastern side, is at high risk of flood. In contrast, other areas are at moderate to very low risk of flood vulnerability. After the thematic reclassified maps were prepared, a weighted overlay was performed to prepare a social vulnerability map of flood hazard in the LKRB (Figure 4.21).

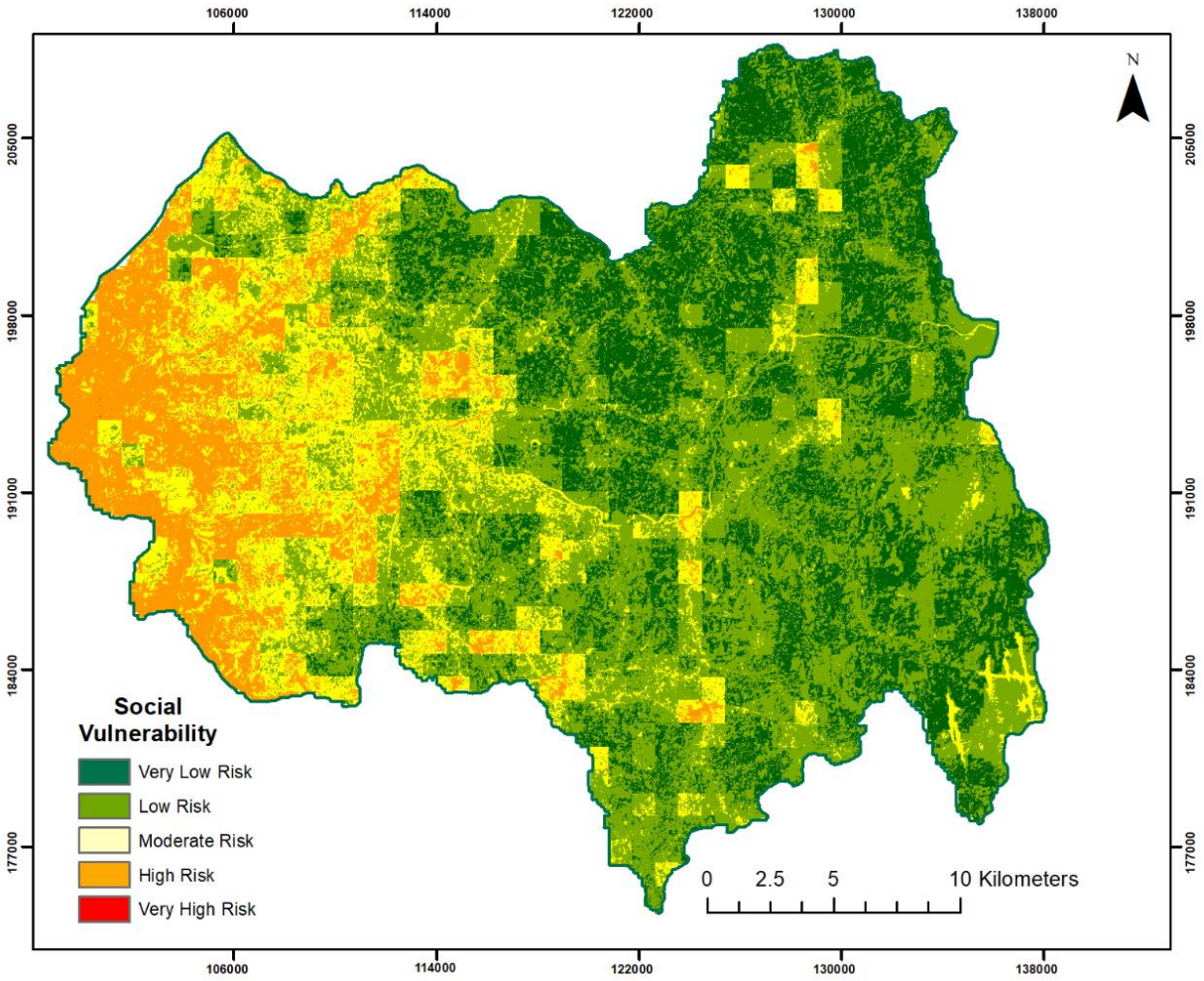

Figure 4.21 Social vulnerability for flood hazard in the LKRB

According to the social vulnerability map, most of the areas on the eastern side of the LKRB are at low and very low risk of flood. The total area belongs to those two categories is 562.81 km^2 (69.73%). Further, 18% of the total land area is at moderate risk of flood. High risk and very high risk areas are minimal compared to the other risk categories, and the total land area in the high and very high risk categories is only 98.04 km^2 (12.15 %) of the total study area. Most of the highly flood-vulnerable areas are situated on the western side, with high population and urbanisation visible.

4.3.1.3 Flood risk map for the LKRB

The final step for third objective was to prepare a flood risk map for the LKRB. The map was prepared (Figure 4.22) based on Equation 9 in the section 3.2.6.2, using a flood hazard map and flood vulnerability map.

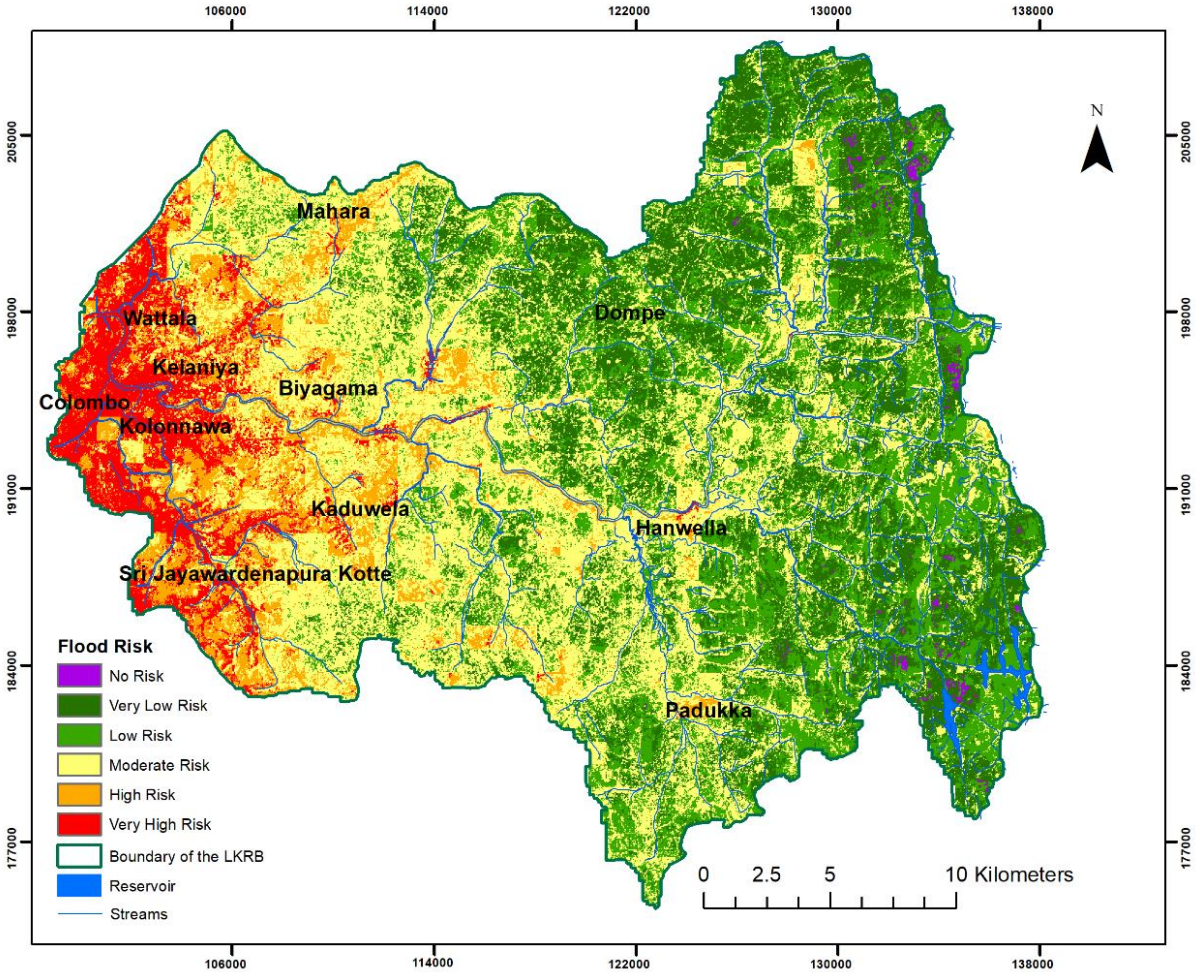

Figure 4.22 Flood risk distribution of the LKRB. Note: this map is a combination of physical and social vulnerability for flood hazard in the LKRB

As delineated in Figure 4.22, the areas at very high and high risk of floods are generally clustered at the western end of the LKRB, while some are scattered throughout the central area. An impressive area of approximately 3 km^2 on the higher eastern flank has been determined to be a 'no flood risk' zone. Very low and low susceptibility to flooding, particularly in the eastern sector, characterise a significant part of the total land area, accounting for 42.3% (367.56 km^2). A significant part of the area, distributed widely throughout the LKRB's central domain, is classified as moderate risk. Areas classified as very high risk account for 9.4% of the total area, mainly located on the

western side and there are been occasional pockets of moderate risk in the central and eastern sectors. A total area of 56.81 km^2 (7.04%), predominantly located on the western periphery, has been identified as very high risk, and additional areas have been identified close to the river in the middle area. The majority of these are classified in the moderate risk category, comprising 40.26% of the total land area of the LKRB.

4.3.2 Proposed integrated AFH method for flood risk assessment

As early mentioned, this proposed methodology only considers physical factors. As AHP physical vulnerability have been already discussed in section 4.3.1.2, this section presents results of FR, HAND and integrated AFH method.

4.3.2.1 FR based flood risk assessment

As mentioned in section 3.2.7, the FRF index and prediction rates values are presented in Appendix A. According to the prediction rates, drainage density appears with the highest value of 5.67, while NDVI records the lowest value at 1. Soil permeability comes second place, securing a prediction rate value of 3.24, with elevation ranking third at a prediction rate value of 2.95. Depending on prediction rate values of the each physical factor, FR based flood risk map has prepared in ArcGIS 10.8 environment (Figure 4.23).

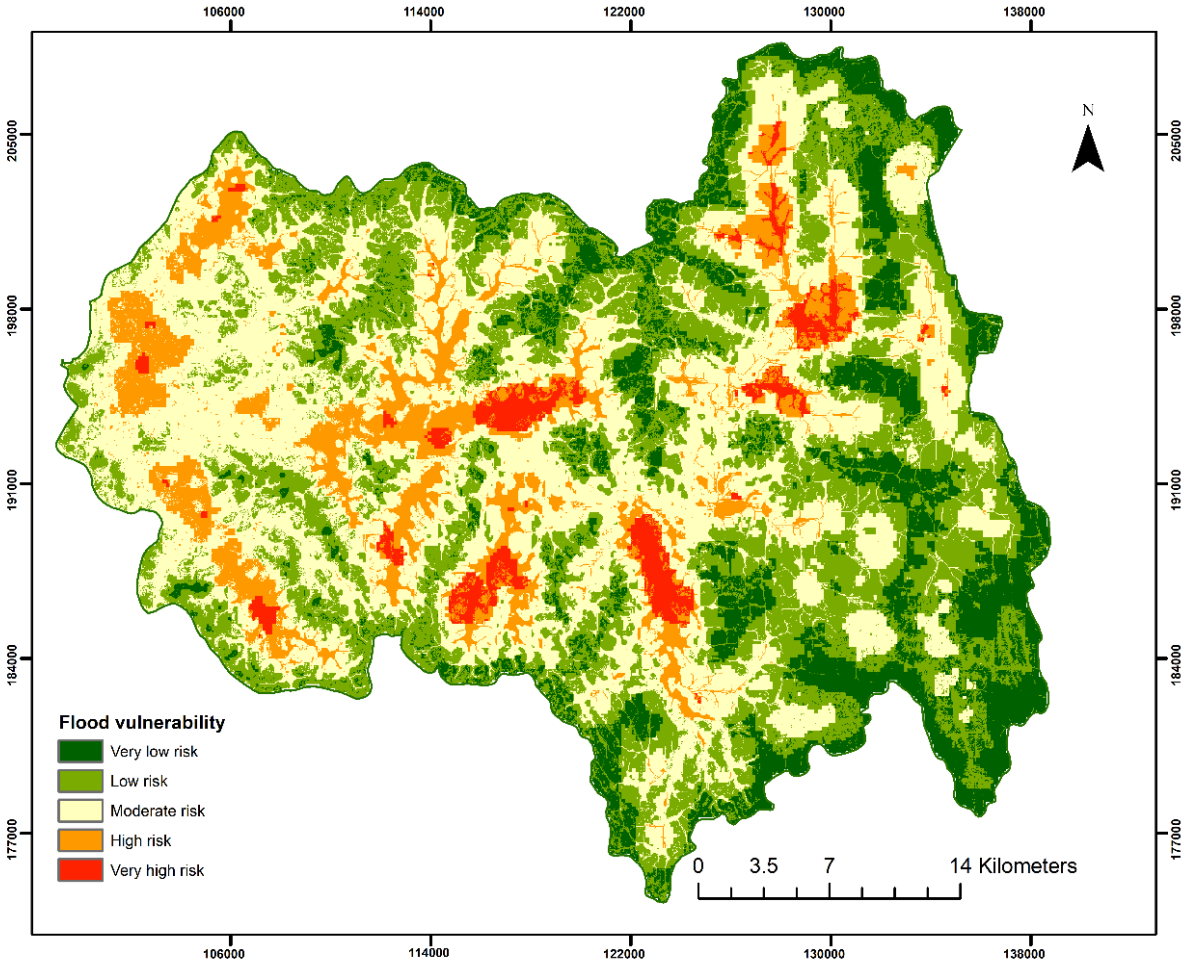

Figure 4.23 Flood susceptibility in the KRB based on FR model

As delineated in Figure 4.23, the areas at very high and high risk of floods are generally scattered throughout the central area. An impressive area of approximately 13.2 km^2 on the higher eastern flank and some patches in the eastern half of the LKRB have been determined to be 'no flood risk' zones. Zones of very low and low susceptibility to flooding are scattered throughout the study area, covering 51.6% of the land area (416.3 km^2). Areas classified as very high-risk account for 2.7% (22 km^2) of the total area, mainly at river merge areas and major river bend areas in the middle part of the LKRB. High risk areas and moderate risk areas are visible alongside the streams. The total areas of these zones are 8.8% (70.9 km^2) and 23.7% (191 km^2) of the study area, respectively.

To validate the FR flood susceptibility map, the AUC (Figure 4.24) was generated with the help of the ArcSDM tool. The AUC value for flood hazard using the FR method was 0.794, which indicates that this model is suitable for analysing flood susceptibility in the LKRB.

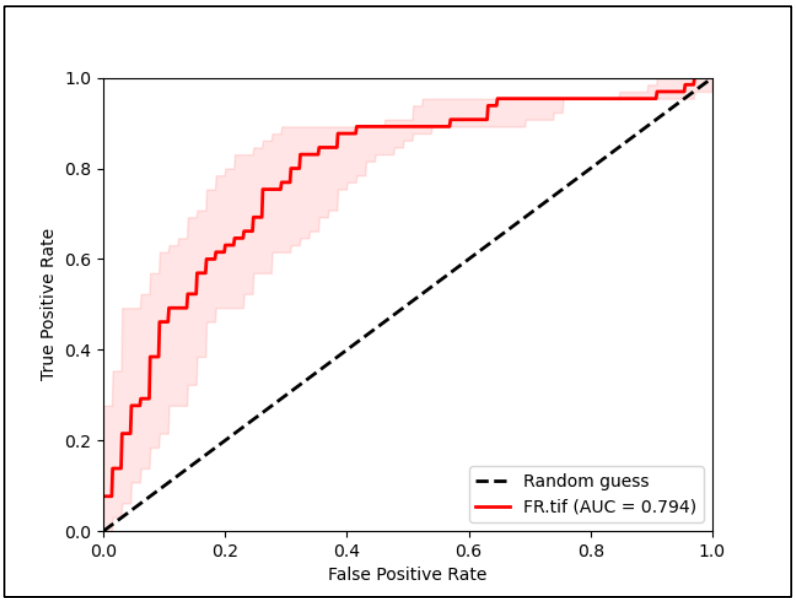

Figure 4.24 AUC for FR base flood susceptibility map.

Under this section, the study validated the AHP based physical vulnerability map and results indicate 0.739 value (Figure 4.25).

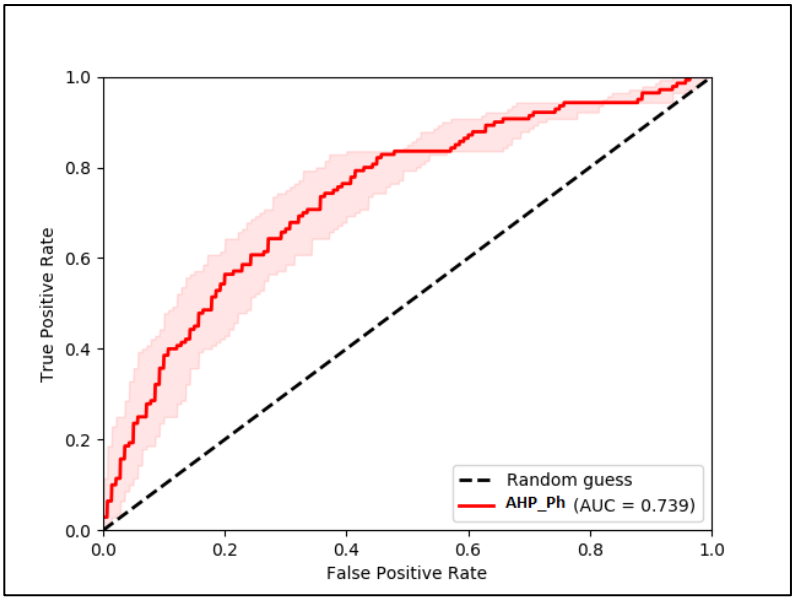

Figure 4.25 AUC for AHP base physical vulnerability map. Note: This map in presented in section 4.3.1.2

4.3.2.2 Flood inundation map based on HAND model

After preparing FR based flood susceptibility map, the study prepared the HAND model, whose results are presented below (Figure 4.26). According to the HAND model, the KRB has most area > 12 m, covering 39.7 % of the total land area of the LKRB. Land between 0 m and 1.5 m above the nearest drainage area covers 25.3% (204.3 km^2). In this model every minor stream was considered when calculating the HAND model, which is why there is a considerable area in the 0 – 1.5 m category. The Department of Irrigation says that when the water level of the main Kelani River is between 1.5 m and 2.1 m it considers it as a minor flood event in the basin. According to the HAND model, when there is such a minor flood hazard, an additional 38.9 km2 is inundated over and above the inundation of the 0 – 1.5 m height area. According to the HAND model, when the water level reaches between 2.1 m and 2.7 m, there is a major flood event in the LKRB and 34.5% of the total land area is inundated. Water levels between 2.7 m and 3.6 m constitute a dangerous flood event, which may inundate up to about 60% of the basin's total land area. However, due to some flood management projects implemented on the western side of the LKRB, riverine flood hazards in the Colombo city area are now minimal.

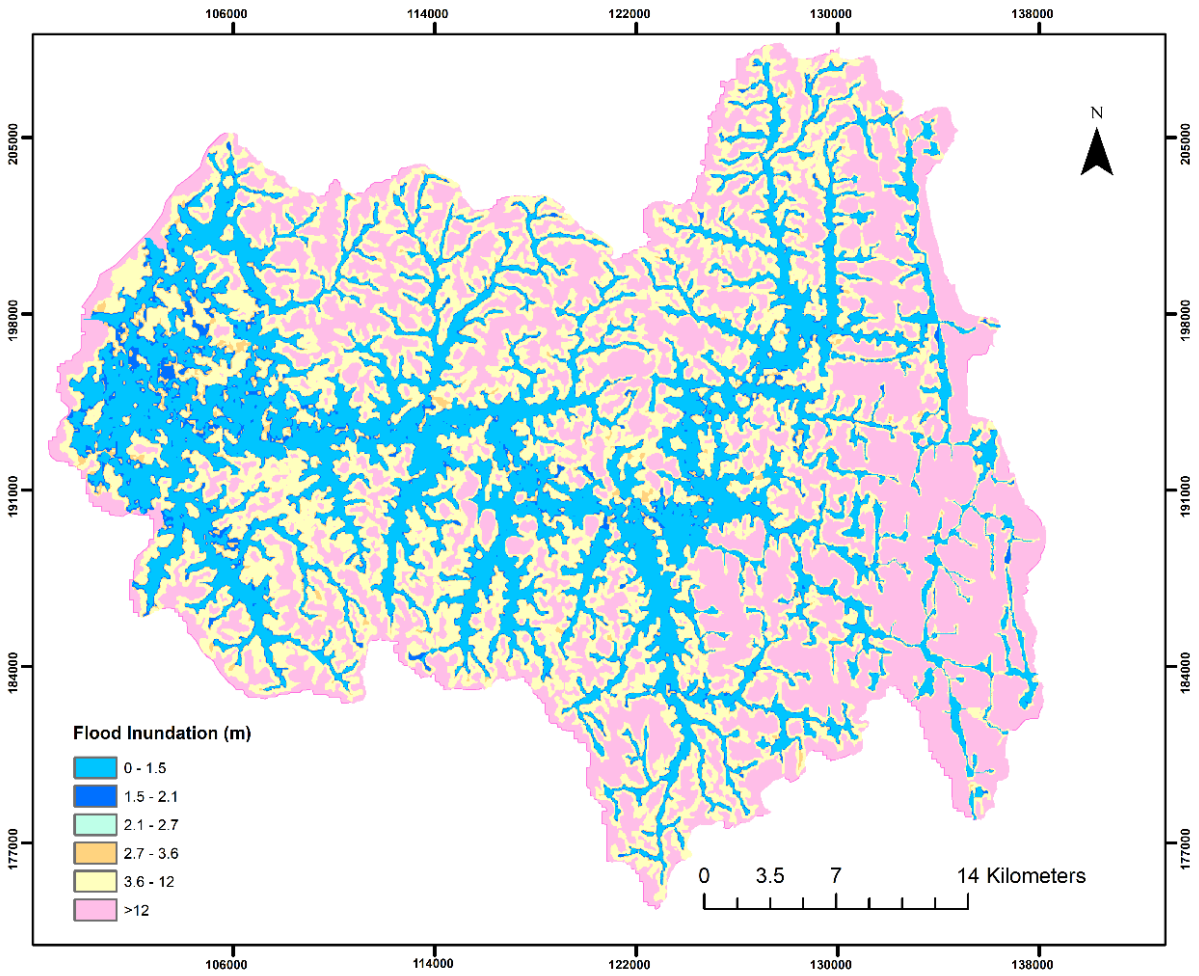

Figure 4.26 Flood inundation map based on the HAND model

4.3.2.3 Results of proposed integrated AFH method

The final goal of this objective is to integrate the AHP, FR, and HAND models and prepare a flood hazard map for the LKRB. The results of this new integrated model are shown in Figure 4.27. According to the integrated model map, most of the land area belongs to the low-risk and very-low-risk flood hazard categories. 46.8% (378.1 km^2) of the total land area falls into these two categories. 7.5% (60.7 km^2) of the land area is flood-free. Most of these flood-free areas are scattered throughout the far eastern hillsides of the LKRB. Moderate risk distribution areas can be seen close to the streams and 236.2 km^2 (29.3%) of the total land area falls into this category. High and very-high-risk flood hazard zones are mostly on the western side, central part, and north-eastern side of the LKRB. 16.4% (132 km^2) of the land area falls into these two risk categories.

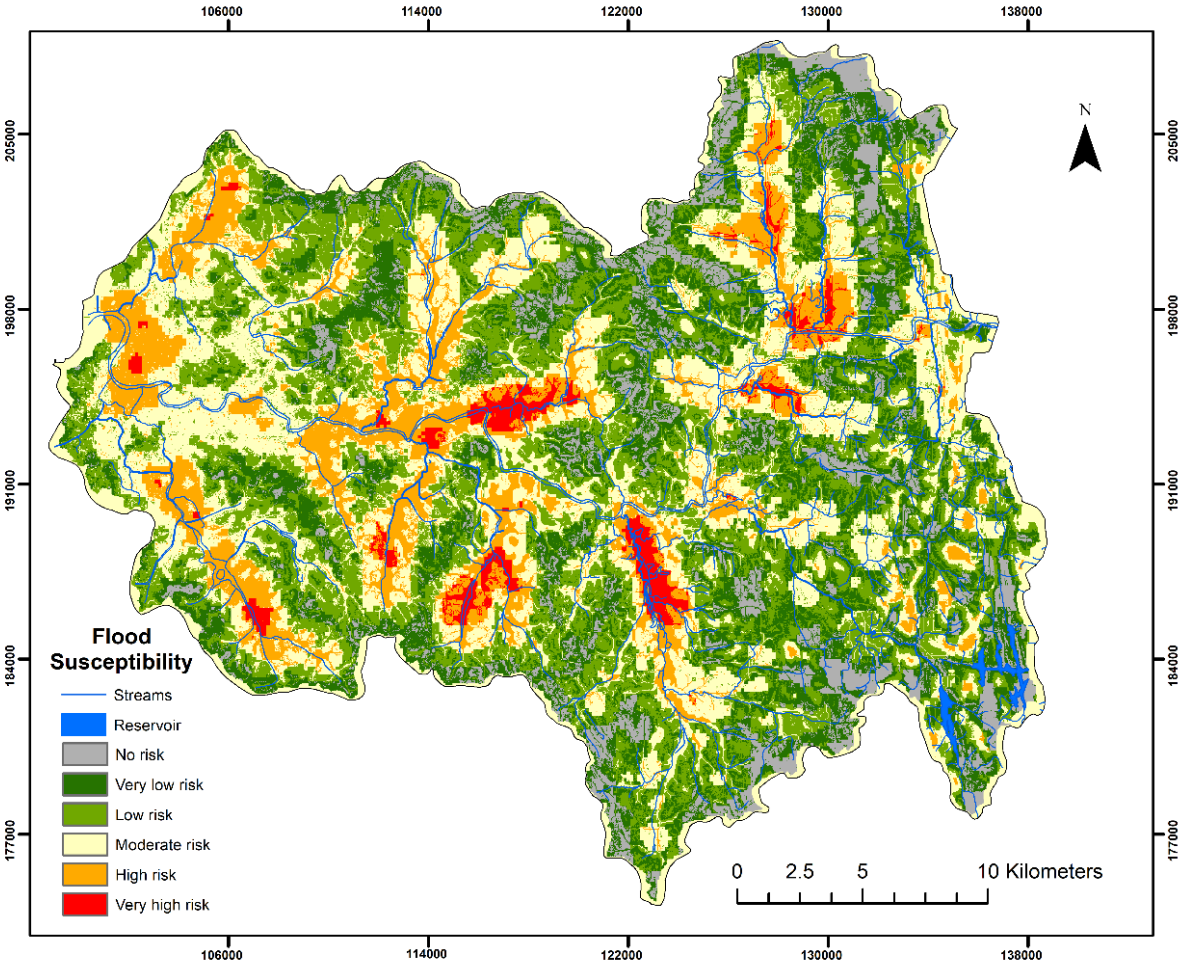

Figure 4.27 Flood risk distribution in the LKRB, based on AFH method

To validate this newly proposed AFH model, the AUC (Figure 4.28) was prepared, with a value of 0.807 (exclude water surface). According to the AUC classification, this novel AFH model belongs to the very good model category, which can be recommended for flood susceptibility mapping.

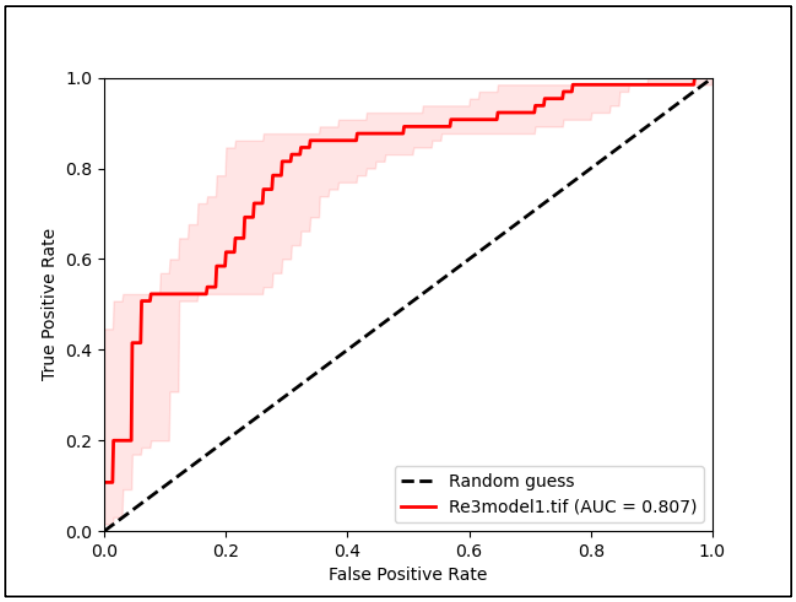

Figure 4.28 AUC for integrated AFH method base flood risk map

4.4 Chapter summary

This section provides a summary of the results in this study. The first part of this chapter presents outcomes that are in line with the primary objective and examines the spatial and temporal variations resulting from extreme rainfall across Sri Lanka. Nine relevant extreme rainfall indices – RX5day, RX1day, R99p, R95p, R20mm, R10mm, PRCPTOT, SDII, and CWD – have been used for this investigation. The spatial patterns of these indices (except SDII) show their highest accumulations in the Wet Zone during the study period. However, on the eastern coast of the Dry Zone, the SDII index shows its highest accumulations. In parallel, the values for PRCPTOT and CWD show less accumulation throughout this region, which indicates that the east coast receives low rainfall, but with high intensity. On a temporal basis, with the exception of CWD at the Kurgalaune station, the Intermediate Zone shows an increasing trend across all extreme indices. Similarly, the Dry Zone shows an overall positive trend for the extreme rainfall indices at most stations, although some stations show a decreasing trend for RX1day and R99p. On the other hand, only SDII and R95P indices – unlike other indices which have both rising and falling trends – have an increasing trend across all meteorological stations in the Wet Zone. Overall, results indicated that the Wet Zone is getting drier and the Intermediate Zone and Dry Zone were getting wetter

in the period considered. The ITA results also indicated that the Intermediate Zone had non-monotonic trends for most of the indices, unlike the other two climate zones. Nevertheless, there was no significant turning point for increasing or decreasing trends in the indices, according to the SqMK results.

This study investigated the correlation between precipitation patterns and water level within the KRB as part of its second research objective. The overall rainfall across the KRB shows a consistent and statistically significant increasing trend. In all four seasons, that trend has been observed consistently. In parallel, the Hanwella hydrology station shows a decreasing trend in water levels, as opposed to N'Street, where an apparent increasing trend has been observed. According to the MMK analysis, 60% of KRB weather stations showed increasing trends during the study period, with Colombo, Angoda, Chesterford, Labugama, and Maliboda stations recording significant increases. Notwithstanding this, only three and four stations appear to have increased during the SWM and IM2 seasons, which produce high rainfall in the KRB. Regarding the daily dynamics of rainfall and water levels, the Hanwella hydrology station showed a moderately positive correlation, whereas the N'Street station showed a weaker positive correlation. Moreover, the lag correlation analyses indicated that periods of increased rainfall are temporally associated with increases in water levels across the basin.

For its third objective, this research tried to assess flood risk due to extreme rainfall in the LKRB. Two methods were used to analyse the flood risk in the basin. The AHP method was used to identify the flood risk areas, based on physical vulnerability and social vulnerability. The area at high risk of floods is generally clustered at the west end of the LKRB. Most of the LKRB area is under the moderate risk category, comprising 40.26% of the total land area. Areas at very low risk of flooding, particularly in the eastern part of the LKRB, account for 42.3% of total land area. The integrated AFH method shows, high and very-high-risk flood hazard zones are mostly on the western side, central part, and north-eastern side of the LKRB. 16.4% (132 km^2) of the land area falls into these two risk categories. With 0.807 AUC model value, this model can be recommended for flood risk mapping in any river basin in the world with considered factors.

5. DISCUSSION

In recent times, Sri Lanka has seen an escalation in the occurrence of severe rainfall incidents, with projections indicating the likelihood of their continued increase. These information reveals that, the country is significantly impacted by extreme rainfall. While rainfall is a fundamental factor in Sri Lanka's economy, its extremes have contributed to consequential hazards like floods and landslides in recent times, significantly impairing the country's development.

Accordingly, this study examined spatial and temporal patterns of extreme rainfall over the island as the first objective. The spatial patterns of extreme rainfall in Sri Lanka are primarily influenced by orography and the monsoon effect. This pattern is consistent with the general rainfall pattern of the country, as observed in previous studies by Wickramagamage (2016) and Hapuarachchi and Premalal (2021). While the coherence of rainfall patterns across different regions is relatively low, a significant number of weather stations on the island have reported extreme rainfall increases in most indices, which agrees with the study by Naveendrakumar et al. (2018). During the study period, the spatial pattern of simple daily intensity (SDII) showed its highest accumulations on the country's east coastline (Dry Zone), while other indices had their highest values in the southwest part. Higher values for SDII on the east coastline could be due to the changes in the Northeast Monsoon (NEM), the primary rainfall source in the Dry Zone. Prakash et al. (2012) have confirmed a significant increasing trend in the NEM, and Wickramagamage (2016) found that the second phase of NEM is primarily positive, bringing rainfall to the island. Furthermore, the United Nations Office for Disaster Risk Reduction (UNDRR, 2022) revealed that, according to climate model projections, the intensity of extreme one-day rainfall has exhibited the most significant increase (58%) over South Asia. This could be one of the reasons behind the trend of increased intensity of extreme rainfall events observed in the eastern coastal area of the country.

The temporal patterns of extreme rainfall also provided valuable information. Most extreme precipitation measurements indicated an increase in mean values for South Asia, consistent with global observations (Sheikh et al., 2015). This study's results also found that most of the indices showed an increasing trend at most stations. The study by Xavier et al. (2018) identified that strengthening the monsoon low-level jet

stream brings heavy rainfall over the Indian subcontinent, which may be one of the reasons for the increasing trend of extreme rainfall over the island. In the study period, the frequency of extreme rainfall (R20 mm and R10 mm) has fallen in the Wet Zone. These findings are highly compatible with the studies by Basher et al. (2018) and Bhatti et al. (2020) of extreme rainfall over Bangladesh and Pakistan. The magnitude of extreme rainfall events (RX5day and RX1day indices) also declined in the Wet Zone. Along with that, the persistence of extreme rainfall (CWD) shows a similar pattern. However, a non-significant decreasing trend in SWM over Sri Lanka was observed by Shelton and Pushpawela (2022) between 1980 and 2013. Further, Swapna et al. (2022) revealed a weakening of SWM and an increasing frequency of extreme cyclones in the North Indian Ocean fuelled by global warming. This trend may sometimes reflect a decreasing trend in extreme rainfall events, as indicated by indices such as RX5day and R99p at stations like Ratmalana, Ratnapura, Katunayaka, Ktugastota, and Nuwara Eliya in the Wet Zone. Also, this may be the reason for a significant trend in extreme rainfall indices at stations like Anuradhapura, Pottuvil, Mannar, and Bandarawela in the Dry and Intermediate zones. Further, global warming especially has greatly influenced the island's SDII, R95p, and PRCPTOT increases. Thus, due to extreme rainfall events, many stations show an increasing trend in total precipitation (Jayawardena et al., 2018).

Bhatti et al. (2020) showed that extreme rainfall has an inverse relationship with altitude. The current study obtained data from four meteorological stations – Nuwara Eliya and Katugastota stations in the Wet Zone and Badulla and Bandarawela stations in the Intermediate Zone – at higher altitudes (>400 m). However, in the Sri Lankan context, the inverse relationship between extreme rainfall and elevation is only seen for the Wet Zone. The central highland areas of the country show decreasing trends of extreme rainfall events, as reported by Wickramagamage (2016) at Nuwara Eliya station, supporting the findings of this study.

In general, the temporal pattern, most of the Dry and Intermediate Zone stations showed an increasing trend of extreme rainfall events, whereas the Wet Zone showed both rising and falling trends for some extreme indices. This condition indicates that the Wet Zone became drier, and the Intermediate and Dry Zones became wetter which is resonate with the works of Bhatti et al. (2020), which delved into extreme rainfall pattern in Pakistan. By analysing extreme rainfall indices, they also found that core

monsoon rainfall and the westerly humid regions were drying in Pakistan. We observed that large-scale atmospheric and oceanic factors might be linked with extreme rainfall events over the area studied in similar studies in the South Asian Region (Basher et al., 2018; Sheikh et al., 2015). The results suggested that Sri Lanka is experiencing an increasing trend of extreme rainfall events, particularly in the Dry and Intermediate Zones, which could have serious implications for water resources, agriculture, and infrastructure planning and management. Further, the ITA results also presented that R99p and R95p indices in the Intermediate and Dry Zones have significant non-monotonic trends which will provide information for possible flood hazards in these regions. To get a better understanding, the general pattern of R95p index is presented in Figure 5.1. It is clearly visible that Intermediate and Dry zones have decreased pattern.

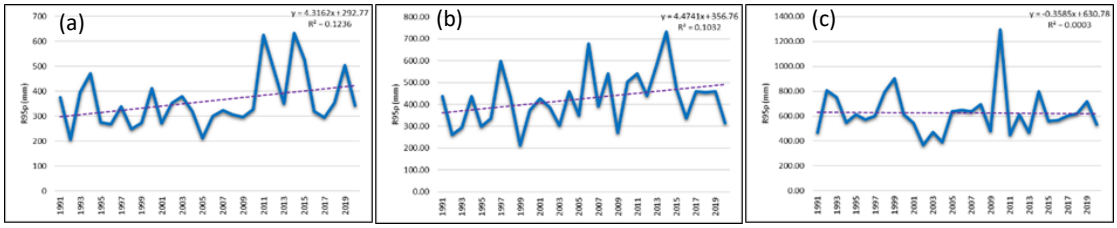

Figure 5.1 Linear regression for R99p index with 95% confidence level: (a) Dry Zone; (b) Intermediate Zone; (c) Wet Zone.

It is important to discuss extreme rainfall and its impact on the development of a country. As a South Asian country, Sri Lanka also faces severe extreme rainfall and its associated hazards. In 2016, when the SWM was activated, parts of the country were hit by the heaviest rainfall in over 18 years (Disaster Managment Center, 2016). The island faced similar extreme weather conditions again in 2017 and 2019, and most recently in 2021, with consequential hazards like flood which are barriers to the development of the country. As a developing country, this increase extreme rainfall is becoming a serious concern for the economic development of Sri Lanka. Furthermore, floods and landslides are not the only harmful effects of extreme rainfall. People's lives are also affected in areas not subject to such influences. Extreme rainfall events can impact social and economic activities like fishery, agriculture, and pottery. For instance, Alahacoon and Edirisinghe (2021) demonstrated that the increasing trend of rainfall on the island has led to a decrease in the production of salt in the Hambantota

District in the Dry Zone. Thus, climate change adaptation strategies should be devised to sustain communities in these climate zones. For instance, the findings of this work showed that the Anuradhapura meteorological station presents a significantly increasing trend of extreme rainfall events, indicating that people living in the Anuradhapura area should prepare for future adverse events caused by climate change. The area has intensive paddy cultivation, and an increase in extreme rainfall could severely impact paddy cultivation and negatively affect the farming community. Furthermore, the findings of this study will provide valuable insights for identifying changes associated with rainfall patterns over the island and in the Indian subcontinent. Additionally, these findings will serve as foundational information for the development of strategies, aimed at adapting to extreme rainfall events.

Further, increase in the frequency of extreme rainfall events across the country, underscoring the pivotal role in developing and implementing national adaptation strategies for climate change. Sri Lanka has already established a national adaptation plan for climate change (Climate Change Secretariat, 2016). The identification of gaps in climate information, which poses a significant obstacle to the development and implementation of adaptation measures by various stakeholders, is clearly emphasized within the scope of this plan. Furthermore, the increase in extreme rainfall events becomes imperative in strengthening resilience, which constitutes fundamental objectives underscored within the Paris Agreement. The Agreement stresses the enhancement of adaptive capacity and strengthening of resilience as integral components of comprehensive efforts to prepare for climate change. By facilitating the identification of current trends and spatial patterns, the findings on extreme rainfall patterns have the potential to address existing climate information gaps and identify areas for enhancing climate resilience.

However, evidence suggests that climate change has altered the spatiotemporal characteristics of rainfall, including total magnitude and seasonal dispersal (Feng et al., 2013). Also, the United Nations Office for Disaster Risk Reduction and World Meteorological Organizatio (2023) projects that extreme rainfall events will escalate threefold with a temperature increase of 2°C. In this scenario, Sri Lankan river basins would be highly vulnerable to floods, especially in the Wet Zone. Nevertheless, there

should be a detailed examination of the relationship between rainfall and water levels in river basins in Sri Lanka.

Rainfall acts as one of the critical factors influencing the increase of river water levels. The amount of rainfall directly influences the volume of water that flows across a river basin and causes flooding when extreme rainfall occurs. Accordingly, this study chose KRB to examine rainfall and water levels and the relationship between them. The findings indicate noteworthy outcomes, which are discussed in the following discussion.

Overall, the KRB has a significantly increasing trend in annual total rainfall, which do not in line with the study by Jayasekara et al. (2020) that shows a decreasing rainfall trend in the KRB from 1983 to 2013. Similarly, the study of Ampitiyawatta and Guo (2009) found the Kalu River basin in the Wet Zone, showed a decrease rainfall trend. These two studies discussed about rainfall pattern in river basins in the Wet Zone over a decade ago. However, as documented by Alahacoon and Edirisinghe (2021), rainfall pattern over Sri Lanka has significant increase in annual rainfall during 1989-2019 period due to climate change. This could be the reason showing significant increase trend in rainfall over the KRB in this study. Further, this increasing trend may be influenced by using mean based adjusted homogeneity daily rainfall data that, this study used. At the same time, all four seasons demonstrate an increasing trend in rainfall patterns, but the increasing trend in SWM and 2IM is incompatible with the results of the study of the KRB by Jayasekara et al. (2020).

Furthermore, the study of Chandimala and Zubair (2007) showed how the El Niño – Southern Oscillation (ENSO) and Indian Ocean Dipole (IOD) affect rainfall and streamflow in the KRB, especially during April – September. Therefore, rainfall over the basin significantly varies depending on these teleconnections (De Silva & Hornberger, 2019). During La Niña events, SWM rainfall increases, whereas during El Niño events it reduces. Zubair et al. (accessed 2016) explained that the flooding of May 2016 in the KRB was caused by the El Niño event. However, examining the influence of these dipolar ocean-atmosphere phenomena on rainfall distribution is beyond the scope of this study. In additional, this study found that, during 2017-2020 period, the KRB appeared to have more rainfall than typical and this may suggest that

there has recently been a shift in climatic conditions. However, a more thorough analysis would need to be undertaken before that can be confirmed.

The changes in the water levels of the KRB can be summarised as follows. Just like the overall water levels during the period, Hanwella station showed a decreasing trend. However, several factors have caused the reduction of water discharging into the river basin. Land use changes and river water management projects are prominent among them. In the KRB, reduced water volume is strongly connected to hydropower plants. The KRB has five major hydropower stations (JICA, 2004). To meet demand for electricity, the Ceylon Electricity Board has expanded hydropower projects in the major river basins of Sri Lanka in recent years. With decreasing rainfall and increasing electricity consumption, these hydropower stations must hold more dammed water to produce electricity, which may be a reason for decreasing water levels in this lower basin station.

Dissanayaka and Rajapakse (2019) also showed that the annual and SWM precipitation, and the IM2 streamflow at Hanwella hydrology stations will show negative trends in the 2020s. These results are in line with this study. Further, the reduction in streamflow largely affects urban water consumption of tap water by the metropolitan cities of Colombo and Gampha regions, mainly from the Kelani River Basin (Jayasekara et al., 2020). There are two major industrial areas in the river basin, at Seethawaka and Biyagama, as well as a significant number of industries that are not in the industrial zone along the river (Abeykoon & Nawarathna, 2011) but which also use water from the Kelani River.

Malede et al. (2022) found that rainfall alone does not affect water flows, but also changes in land cover and uses, as well as human interventions like extractions from groundwater. Decreasing water discharges at Hanwella Hydrology Station may influence future land use changes and human intervention. In addition, the decline in streamflow may have a negative impact on the aquatic biodiversity of the river and its ecosystem, the recharging capacity of the groundwater, and the natural degradability of KRB water (Jayasekara et al., 2020).

Water levels in the N'Steet showed an increasing trend during the study period. As this station is close to the Indian Ocean (only about 2 km away), increased water levels there may affect tidal and climate change. The study by Palamakumbure et al. (2020)

shows that, in the next 50 years, seasonally adjusted tidal gauge data in Colombo, Sri Lanka (rate of sea-level rising = 0.288 ± 0.118 mm/month) suggest an inundation height of approximately 0.1 to 0.2 m. It revealed that, increasing water levels will lead to inundations at heights up to about 3.5 – 15.0 m above today's sea level. Furthermore, the study by Samarasinghe et al. (2022) clearly explained how the tidal wave effects to backwash the Kelani River water closer to the N'Street station area. This tidal effect may result in an increasing trend at this hydrology station. Figure 5.2 depicts the increase in Indian Ocean tidal wave heights over recent years.

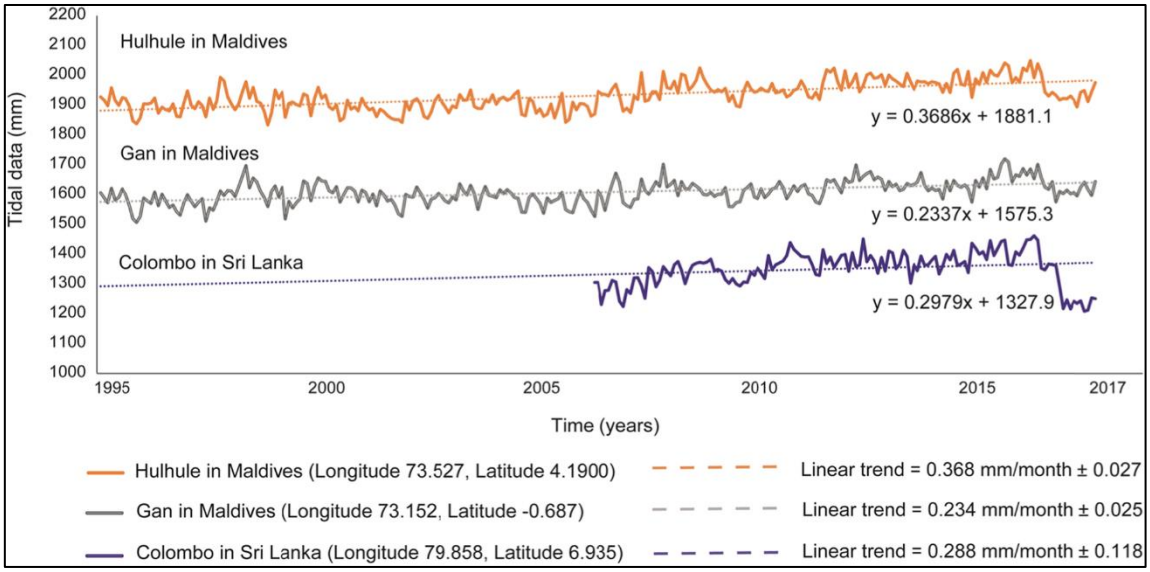

Figure 5.2 Seasonal pattern of tidal waves. Note: Seasonal component (solid lines) and linear trend line (dotted lines) for the Hulhule and Gan tidal stations in the Maldives and the Colombo tidal station in Sri Lanka (Source: Palamkumbure et al., 2020)

In this scenario, as this station is close to the sea, continual increases in water levels may be linked with increasing sea levels. The salt intrusion into the lower basin, which comes with rising sea levels, could pose another problem for users of KRB water. This phenomenon can be seen when salty water flows into Ambathale's treatment plant in the lower flow periods (Abeykoon & Nawarathna, 2011), but it needs more detailed research.

Jayasekara et al. (2020) specified that variations in streamflow are mainly attributed to the rainfall generated over the KRB catchment. However, this study found that the relation between rainfall and water level in the KRB shows a moderately positive correlation which is evidence of the implementation of water resources and flood management plans (Samarasinghe et al., 2022). Also, human interventions in land use/land cover are rapidly increasing in the KRB (Samarasinghe et al., 2022). Land use changes and human interventions may be the reasons for the moderately positive correlation between rainfall and water level observed during the study period. Nevertheless, monthly correlation shows positive correlations between rainfall and water level at the two stations. However, in the month of January N'Street Hydrology station had a slightly negative correlation. January is in the NEM period, where the KRB receives less rainfall.

The lower KRB is experiencing increased flood events with increased rainfall intensity (Wijeratne & Li, 2022). The lag correlation results for the basin clearly show how the rainfall sync with water level in the daily basis. This has provided a background to understand the extreme rainfall and its relation to flood hazard. Especially when upper KRB meteorological stations recorded total rainfall of more than 500 mm for more than two days, there is a chance that water levels in the basin will rise and cause a flood. The two recent major flood incidents in the KRB are shown below to visualise the relationship between extreme rainfall and the water level at two hydrology stations, which were not considered in this study.

In the month of May in both 2016 and 2018, during the SWM, the KRB faced flood hazards after extreme rainfall. Table 5.1 indicates the average rainfall received in the KRB over 10 days during these flood events.

Table 5.1 Average rainfall received in 10-day periods in the month of May for 2016 and 2018 (Source: Department of Meteorology of Sri Lanka)

2016 Day	Average Rainfall (mm)	2018 Day	Average Rainfall (mm)
13-May	37.45	17-May	9.83
14-May	29.15	18-May	14.58
15-May	182.90	19-May	42.24
16-May	73.42	20-May	116.54
17-May	72.69	21-May	55.59
18-May	10.69	22-May	14.78
19-May	68.47	23-May	50.57
20-May	12.52	24-May	50.29
21-May	17.30	25-May	37.05
22-May	11.12	26-May	22.57
23-May	18.09	27-May	26.75

It is visible on the graphs that, when average rainfall across the basin is over 100 mm, it tends to cause water level increases at the two stations on the following day (Figure 5.3).

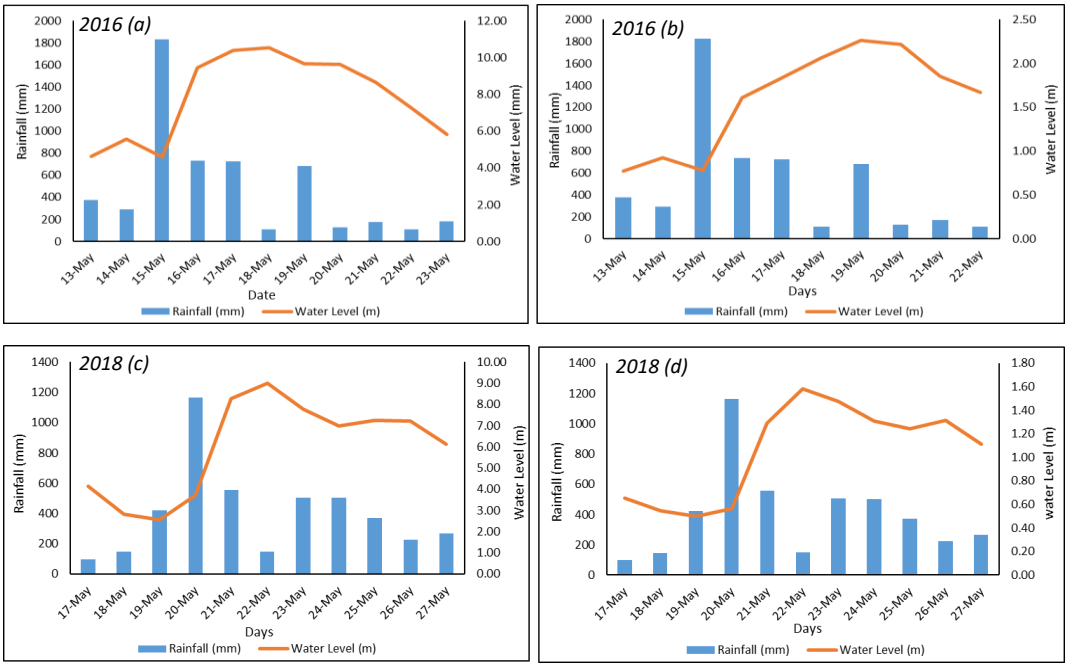

Figure 5.3 Rainfall and water levels during flood events in the lower KRB. Note: (a) & (c) Hanwella Station; (b) & (d) N'Street Station.

At Hanwella station the water level reached nearly 10 m, indicating a high flood event. During the 2016 flood event, from 15 – 17 May, the upper KRB meteorological stations received total rainfalls of 1083.5 mm, 695.4mm, and 662.0 mm, respectively. In 2018, the same stations received total rainfall of 901.0 mm and 533.3 mm on May 20th and 21st.

It is visible that, after the heavy rainfall over the basin, these two hydrology stations in the lower KRB recorded increases in water levels. Most probably, the water level reached its maximum the day after the extreme rainfall event, signalling a flood hazard in the LKRB. The maximum water level remained for a few days, severely damaging the people and environment of the river area. Samarasinghe et al. (2022) revealed that rapid land use changes and urbanisation in the KRB have significantly contributed to flooding and its severity in recent years.

Reports suggest that the KRB is flooding frequently. Approximately two-third of the KRB is hilly uplands, while the rest is in the lowlands and flat coastal areas (Abeykoon & Nawarathna, 2011). Due to heavy rainfall and rapid water discharge from upstream, the river may overflow its banks on the lower flats.

Floods have become some of the world's most severe and devastating disasters. Therefore, flood risk assessment plays a vital role in sustainable decision-making about flood management. Accordingly, assessing areas vulnerable to flood hazards and creating risk maps are main components of disaster mitigation (Ogato et al., 2020). Apart from riverine floods, the LKRB is undergoing rapid urbanisation and urban flood events can be seen which are caused by heavy rainfall. Disaster risk is a calculation combining hazard and vulnerability factors. Various factors related to hazard and vulnerability in a region provide a background to determining the risk level of a hazard in a region. The third objective of this study is assessment of the flood risk in the LKRB, so this study also used nine flood hazard factors and five flood vulnerability factors to identify flood risks in the LKRB.

The results of this study indicated that the western part of the LKRB is at high flood risk, while most of the eastern side is at low or very low risk of flood. As discussed earlier, high population density, low elevation, urbanisation, low vegetation, low slope angle, low drainage density, and exacerbated climatic hazards like extreme rainfall caused high flood risks on the western side of the LKRB. Further, flood severity depends greatly on population and its growth, and also on phenomena like frequent land cover changes or unauthorised landfilling in the study area.

To validate the AHP flood risk map, this study sent a final copy of its outcomes to the ten experts, from whom we got opinions for the AHP. Six were satisfied with the outcomes and four of them were moderately satisfied with the outcome. As the western side of the LKRB is highly urbanised, urban floods are frequently seen which are caused by inappropriate structures, land filling, and canal overflow in the LKRB (Figure 5.4).

Figure 5.4 Urban flooding in the Kolonnawa area of the LKRB (Source: Nishanthi and Dissanayaka, 2021)

Further, to validate the AHP flood risk map and AFH flood risk map, they were compared with the May, 2016 actual inundation map, prepared by the Survey Department of Sri Lanka and the Asian Disaster Preparedness Centre (ADCP, 2017) (Figure 5.5).

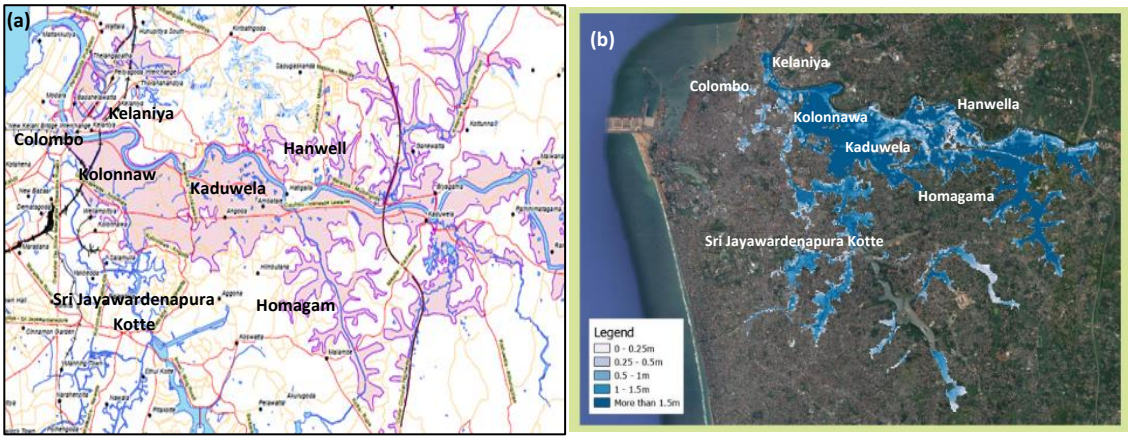

Figure 5.5 (a) Flood inundation map 2016 (Source: Survey Department of Sri Lanka) (b) Flood inundation depth (m) in May 2016 (Source: ADCP, 2017)

The flood inundation maps (Figure 5.5) show that Kelaniya, Kolonnawa, Kaduwela, and some parts of Colombo, Homagama, Hanwella, and Sri Jayawardenapura Kotte faced flood hazards. This study's risk maps also identifies those areas in the high-risk category. However, in the AHP risk map, some areas that are less affected by flood hazards arising from riverine flooding belong to the high-risk category for flood

susceptibility. This could be a reason that this study used rainfall as one of the factors for AHP method. However, AFH map was able to detect most of the flood susceptibility areas, which was proved by comparing with the actual inundation maps in the study area. As an example, the AFH map was compared to actual flood maps prepared by the Survey Department of Sri Lanka for the 2016 and 2018 disasters. The new map identified most of the areas affected by the 2016 and 2018 floods. Therefore, this novel method can be utilised for flood susceptibility mapping in any part of the world and could bring advantages for disaster management. Figure 5.6 shows inundation areas belongs to the 2016 and 2018 disasters.

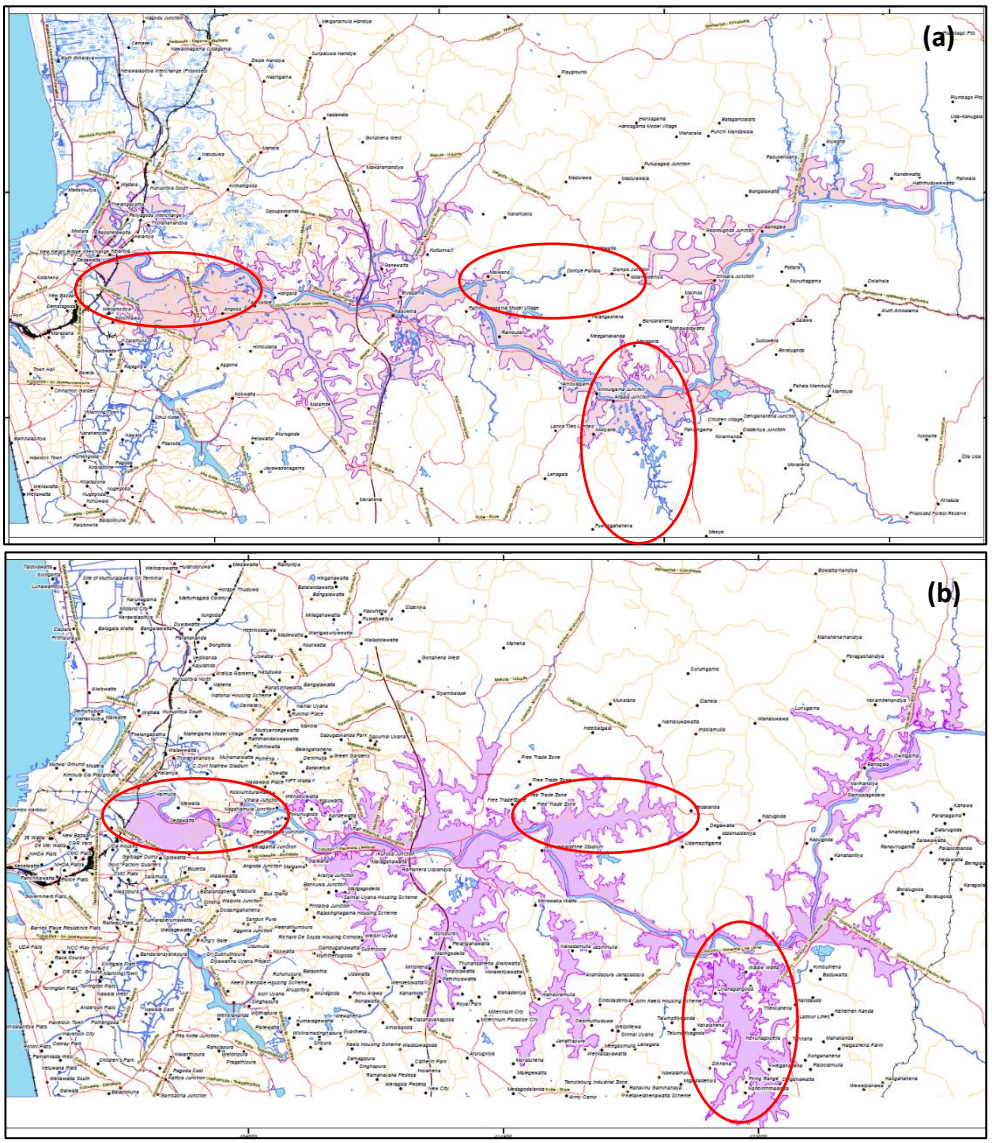

Figure 5.6 Inundation map for major flood events in LKRB. Note: (a) Inundation map for 2016 flood hazard and (b) inundation map for 2018 flood hazard. Area under the red ovals have compared with the integrated AFH map (Source: Survey Department of Sri Lanka, 2020)

The effects of urbanisation and the related human activities and population growth on flood hazards in the LKRB should also be discussed. To enhance accessibility to infrastructure and services, people in both the Colombo and Gampaha districts of the LKRB tend to live close to big cities (Manawadu & Wijeratne, 2021). Hence, the basin is rapidly urbanising. As the LKRB becomes an economic and residential centre, unplanned constructions are common sights in the study area and cause land use and land cover changes, when wetlands are exploited for development. The natural drainage system is obstructed by unauthorised settlement and industrial developments in wetlands, resulting in prolonged floodwater retention (Manawadu & Wijeratne, 2021). Also, because wetland areas retain floodwater, they are a natural flood-controlling factor, but wetland areas are gradually decreasing in the LKRB. For instance, Manawadu and Wijeratne (2021) showed that the Kolonnawa Divisional Secretariat in the LKRB showed a 42% decrease in marshy land between 2005 and 2017, which has created severe flood impacts in the study area. Samarasinghe et al. (2022) also explained that land use changes in the KRB have greatly impacted the severity of flooding in the basin. Wijeratne and Li (2022) also explained that flood events have increased due to the stress of urban sprawl in the LKRB. Further, during the last few years, some flooding events caused by extreme rainfall events have occurred where there was no time to evacuate (Wijeratne & Li, 2022), a tragic scenario for people and property. For example, in the 2016 flood event, 228,871 and 74,003 people were affected by floods in the Colombo and Gampaha districts along the Kelani River (CRIP, 2018). Paying attention to all these matters, Dissanayake et al. (2018) suggest several reasons for this unprecedented flooding in the KRB.

- The hydropower reservoirs located upstream at Laksapana, Castlereigh, and other points were full and were generating maximum power and discharging water into the Kelani River.
- The mouth of the Kelani River, where water discharges into the sea, was partially blocked during the dry months due to poor water outflow and the sea sand brought into the river mouth by littoral drift.
- The large amount of unauthorised housing in the vicinity of the riverbank.
- Unauthorised filling of marshes, canals, and drainage paths which drain or discharge rainwater remaining blocked and unable to discharge to their total capacity.

When considering these facts, it is evident that changes caused by human behaviour have increased flood severity and resulted in more significant damage to society and the environment. The Government of Sri Lanka has implemented several actions in the past to mitigate flood hazards. Accordingly, the Irrigation Department introduced the *Flood Protection Act No. 22 of 1955*. As this Act is outdated, a review with input from the Ministry of Disaster Management has been initiated (Dissanayake et al., 2018). Furthermore, the government collaborates with international institutions to implement flood management projects in the study area. The World Bank-funded "Strategic Environmental Assessment (SEA) for the Kelani River" is the most recent ongoing project aiming to propose flood and drought mitigation measures for the study area (CRIP, 2018).

Even though several flood mitigation steps have been implemented, the LKRB is still experiencing severe floods (e.g., the flood of June 2021), especially in its western part where urban sprawl and high population density prevail. Therefore, there should be more studies conducted on various aspects, as there is no single solution to mitigate flood hazards in the LKRB amidst extreme rainfall escalation. However, the final risk maps from this study will help overcome the lack of flood risk maps in the study area reported by Wijeratne and Li (2022) and Dissanayake et al. (2018) and can be used as a base map for flood management in the LKRB.

Further progress in flood risk assessment requires enhanced integration of scientific data and community knowledge into flood risk models, thereby improving their accuracy and applicability. This study contributes valuable insights into incorporating such data and knowledge into GIS-based flood risk models, offering guidance for future flood analysis. Moreover, the utilisation of methods such as AHP, FR, and AFH facilitates the incorporation of diverse factors into these models, thus enhancing their effectiveness. For instance, by employing weighted analysis within these models, priority areas for wetland restoration and afforestation, which serve as nature-based solutions for flood risk mitigation, can be identified. Consequently, the findings of this study hold significance for both current and future flood risk management strategies in the island, aiding in the identification of critical areas vulnerable to flooding. Additionally, the adaptable nature of the proposed AFH method enables its application

in flood risk assessment in any part of the world, accommodating various criteria tailored to specific contexts.

In addition, for national climate change adaptation strategies and disaster risk reduction initiatives, the results of this research could be very useful. Sri Lanka's commitment to reducing risks stemming from natural hazards is illustrated by its alignment with the Sendai Framework for disaster risk reduction. In line with the Sendai Framework for disaster risk reduction, the proposed AFH method can be used as a strategic approach for the identification of flood risk zones, and its suitability can be reinforced by its alignment with initiatives undertaken by the Disaster Management Centre of Sri Lanka.

Further, incorporating climate change projections into flood risk assessments is crucial for anticipating future flood scenarios and developing adaptive strategies. Collaborative efforts between government agencies, academia, NGOs, and local communities are essential for holistic flood risk management. This will help for capacity building among local authorities and communities. Finally, leveraging emerging technologies such as GIS, RS, artificial intelligence, and crowd-sourced data can revolutionize flood risk assessment and response mechanisms for Sri Lanka.

6. CONCLUSIONS AND RECOMMENDATIONS

Over the last few years, extreme rainfall events have increased and they are expected to increase even further in the near future. The frequency and intensity of rainfall extremes are linked with risks of riverine and flash floods in susceptible regions across the globe. Sri Lanka is an island state, which is particularly vulnerable to extreme rainfall events and consequential hazards. The variations in rainfall caused by the two monsoons bring unique flows of water throughout the island. The complex rainfall patterns of the island contribute to its high agricultural productivity, rich biodiversity, and remarkable beauty. However, the island has faced extreme rainfall events in recent years due to climate change and atmospheric teleconnections. Extreme rainfall-related consequential hazards like floods and landslides have caused massive damage to the country's people, economy, and environment. However, there has been no detailed examination of the spatial and temporal patterns of extreme rainfall events in the Sri Lankan context. The Kelani River Basin on the island is highly vulnerable to annual flooding due to extreme rainfall. The Kelani River flows through the country's main cities and most densely populated areas. Moreover, floods are common in the river basin, highlighting the need to regularly monitor rainfall patterns, water levels, and water capacity throughout the region. There should also be comprehensive research on rainfall and water levels in the KRB for better water resource management. Moreover, Sri Lanka still needs proper flood-risk assessment, especially a flood-risk map, of hazards associated with extreme rainfall. Considering all these facts, the following conclusions can be drawn based on the main findings of this study.

As the first step, the study examined spatial and temporal variations of extreme rainfall over Sri Lanka. For this task, daily rainfall data from 19 meteorological stations were used to derive nine extreme rainfall indices (RX5day, RX1day, SDII, R99p, R95p, PRCPTOT, R20mm, R10mm, and CWD) during 1991–2020. Orography and the monsoon effect influence the spatial patterns of extreme rainfall in Sri Lanka. In particular, the R95p and SDII indices demonstrated a noticeable increase at all the meteorological stations, indicating a significant rise in heavy precipitation and extreme rainfall intensity over recent years.

These trends are reflected in the increased frequency of flood and landslide hazard events throughout the country. The east coast region exhibited high rainfall intensity,

with the highest SDII values. However, the persistence (CWD) and total precipitation (PRCPTOT) remained low within the same area (Batticaloa, Trincomalee, and surrounding areas). The study revealed that this area experienced less rainfall but with higher intensity. The study also found that the Dry and Intermediate Zones showed increasing trends in extreme rainfall events, while the Wet Zone showed both rising and falling trends. Further, the magnitude of extreme rainfall events is declining in the Wet Zone. These findings were based on *in situ* rainfall data and did not consider the direct influence of atmospheric teleconnections.

The findings could help policymakers take necessary measures to minimise the impacts of extreme rainfall events in Sri Lanka. Further research should be conducted to assess the relationship between global warming and extreme rainfall events in the country. Also, the risks, exposure indices, and remedies associated with extreme precipitation in the island should be addressed in future studies.

Under the second objective, this study examined rainfall and water levels and their relationship during the 1991–2020 period. Using MK and MMK tests, trends were detected in all variables. The study used Pearson's correlation coefficient and lag correlation to identify the relationship between rainfall and variability of river flows. The study's conclusions can be summarised in the following way:

- The annual total rainfall over the KRB has shown a significant increase from 1991 to 2020.
- On an annual basis, 50% of the meteorological stations studied had a significant increasing trend (Colombo, Angoda, Chesterford, Labugama Tank, and Maliboda). 40% of the meteorological stations showed a decreasing trend in rainfall during the study period.
- Water levels at Hanwella hydrology station showed a significant decreasing trend, while N'Street had a significant increasing trend in the study period.
- Considering seasonal rainfall patterns, there was a decreasing trend at 70% of meteorological stations in SWM, 50% in IM2, 30% in NEM, and 50% in IM1.
- All the stations in the LKRB had an increasing trend in rainfall, except the Hanwell Group meteorological station. In contrast, a decreasing trend was seen at the UKRB stations, except for Maliboda with a significantly increasing trend.

- Intensity of extreme rainfall is decreasing, while duration and amount of extreme rainfall is increasing in the KRB.
- The relationship between daily rainfall and water levels was moderately positively correlated from 1991 to 2020.
- Lag correlation revealed that daily rainfall affects water levels and increases vulnerability to flood hazards.
- The months of May, June, July, September, and November show the highest correlations between rainfall and water levels in the KRB.

Although rainfall plays a crucial role in driving changes in the KRB, the impact of human activities has consistently been recognised as harsh and as a contributor to exacerbating the complexity of the natural environment's reactions. The Sri Lankan government has adopted sustainable water management plans for the catchment area because the Kelani River flows through densely populated urban areas which are frequently subject to flooding. In particular, the government aims to prevent harmful effects on individuals and the environment in the basin caused by extreme rainfall-related floods. In order to plan new water projects for the KRB, it will thus be helpful to consider the findings of this study to understand climatic variability across the basin.

Identifying flood hazard zones in the LKRB was the key objective of this study. Flood risk assessment in the LKRB has done in two ways. As the first part of this objective, the AHP-based MCDM method was used to analyse 13 factors under two criteria, flood physical and social vulnerability. A literature review, personal observations, and experts' opinions used to identify the risk factors for flooding. Flood risk is a combination of flood hazard and flood vulnerability. Accordingly, the study created a flood hazard map showing physical vulnerabilities prior to flood hazard occurrence. The results of this flood hazard map indicate that 0.27% (2.2 km^2), 12.85% (103.68 km^2), 47.34% (382.11 km^2), 39.11% (315.7 km^2), and 0.43% (3.43 km^2) of the LKRB is at very high, high, moderate, low, and very low risk of flooding, respectively. These values indicate that moderate hazard areas are proportionally high in the watershed (47.34%). Further, most high and very high-risk areas are on the western side of the LKRB. Considering flood vulnerability in the study area, 0.002 % (0.012 km^2), 12.44 % (98.02 km^2), 18.12% (146.29 km^2), 44.83% (361.85 km^2), and 24.9% (200.95 km^2) of the LKRB is at very high, high, moderate, low, and very low risk of flood, respectively. Most of the area (69.73%) has low or very low flood vulnerability. The

remaining area (30.27%) falls into the moderate to very high category. The flood-risk map in the watershed illustrates that 7.03% (56.81 km^2), 9.4% (75.86 km^2), 40.26% (325.02 km^2), 23.92% (193.09 km^2), 19.01% (153.47 km^2), and 0.36% (2.94 km^2) of the LKRB is at very high, high, moderate, low, very low, and no risk for flooding, respectively. These values indicate that the most areas belong to the LKRB has a moderate risk of flood susceptibility. However, the western part is at high or very high risk of flooding.

The map generated through the integrated AFH method for physical vulnerability (flood hazard) has provided a more detailed assessment of flood risk in the LKRB. The AFH flood-risk map in the watershed illustrates that 46.8% (378.1 km^2) belongs to the low-risk and very low-risk categories, which constitute the highest proportion in the LKRB area. 7.5% (60.7 km^2) of the land area is flood-free. Moderate-risk areas include 236.2 km^2 (29.3%), while 16.4% (132 km^2) belong to the high and very high-risk categories. These areas lie mostly in the western, central, and northeastern parts of the LKRB. This model has an AUC value of 0.807, denoting its accuracy for flood susceptibility assessment in the basin. This new method can be applied in any river basin, taking into account relevant factors.

The results of this study will be beneficial for the flood mitigation processes of the LKRB. As this study shows flood-risk areas in the LKRB, it is easy to identify which zones should be prioritised for flood hazard management. Suggestions for measures to combat flood risk include restricting human interventions on marshy lands and riverbanks, regulated construction on high and very high-risk areas, accurate flood alarming and monitoring systems, community awareness programs, sustainable drainage systems in urban areas, and enhanced environmental education in civil society. However, if the principles of good government are not applied, no approach will be effective. Finally, the findings of this study can be helpful in identifying factors that improve resilience and should be included in subsequent flood-risk management and planning decisions. Such a study could be carried out at district or basin level, making it possible to develop more comprehensive risk maps and provide better assessments of risks associated with riverine flooding.

Furthermore, a detailed flood-risk map needs to be made which comprehensively identifies relevant mitigation measures to minimise flood risks throughout the

designated study area. These invaluable tools (AHP and proposed integrated AFH method) have the potential to provide policymakers and the responsible authorities with valuable insight and guidance and enable them to make informed decisions. At the same time, the flood risk map will also benefit local people by providing them with essential information to enable them to spot and manage possible dangers in their vicinity. In addition, the lack of flood-risk maps makes identifying vulnerable areas difficult and prevents effective flood mitigation strategies from being developed. Such essential cartographic resources will ensure the ability to carry out accurate risk assessments in future. Further, it is critical to continue to improve the quality and amount of data utilised in flood risk mapping. Hence, integrating numerous datasets can be used to improve the accuracy and reliability of flood risk assessment. The advancement of technologies such as Geographic Information Systems (GIS), is paved the path for utilize the advanced modelling approaches, not just for flood risk assessment, but also for other risk assessment like landslides.

REFERENCES

Abbas, A., Amjath-Babu, T., Kächele, H., Usman, M., & Müller, K. (2016). An overview of flood mitigation strategy and research support in South Asia: implications for sustainable flood risk management. *International Journal of Sustainable Development & World Ecology, 23*(1), 98-111.

Abeykoon, A. M. H. K., & Nawarathna, N. M. A. L. B. (2011, 25–29 September). *Enhancing water quality by salinity barriers and its impact on environment* XIVth IWRA World Water Congress, Pernambuco, Brazil.

Abeysekera, A. B., Punyawardena, B. V. R., & Premalal, K. H. M. S. (2015). Recent trends of extreme positive rainfall anomalies in the dry zone of Sri Lanka. *Tropical Agriculturist, VOL. 163, 2015*.

ACIAR. [A. C. o. I. A. Research]. (2023). *Climate chage*. https://www.aciar.gov.au/program/climate-change

ADCP. (2017). *Protecting Colombo against Future Floods*. https://www.adpc.net/igo/category/ID1167/doc/2017-e30Ldp-ADPC-Handout_for_PublicEvent_page__set3.pdf

Adler, R. F., Sapiano, M. R., Huffman, G. J., Wang, J.-J., Gu, G., Bolvin, D., Chiu, L., Schneider, U., Becker, A., & Nelkin, E. (2018). The Global Precipitation Climatology Project (GPCP) monthly analysis (new version 2.3) and a review of 2017 global precipitation. *Atmosphere, 9*(4), 138.

Ahmad, D., & Afzal, M. (2020). Flood hazards and factors influencing household flood perception and mitigation strategies in Pakistan. *Environmental Science and Pollution Research, 27*(13), 15375-15387.

Al-Abadi, A. M. (2017). Modeling of groundwater productivity in northeastern Wasit Governorate, Iraq using frequency ratio and Shannon's entropy models. *Applied Water Science, 7*(2), 699-716. https://doi.org/10.1007/s13201-015-0283-1

Alahacoon, N., & Edirisinghe, M. (2021). Spatial Variability of Rainfall Trends in Sri Lanka from 1989 to 2019 as an Indication of Climate Change. *ISPRS International Journal of Geo-Information, 10*(2). https://doi.org/10.3390/ijgi10020084

Alahacoon, N., Matheswaran, K., Pani, P., & Amarnath, G. (2018). A Decadal Historical Satellite Data and Rainfall Trend Analysis (2001–2016) for Flood Hazard Mapping in Sri Lanka. *Remote Sensing, 10*(3), 448. https://www.mdpi.com/2072-4292/10/3/448

Alexander, L. V., Zhang, X., Peterson, T. C., Caesar, J., Gleason, B., Klein Tank, A. M. G., Haylock, M., Collins, D., Trewin, B., Rahimzadeh, F., Tagipour, A., Rupa Kumar, K., Revadekar, J., Griffiths, G., Vincent, L., Stephenson, D. B., Burn, J., Aguilar, E., Brunet, M., Taylor, M., New, M., Zhai, P., Rusticucci, M., & Vazquez-Aguirre, J. L. (2006). Global observed changes in daily climate extremes of temperature and precipitation. *Journal of Geophysical Research: Atmospheres, 111*(D5). https://doi.org/https://doi.org/10.1029/2005JD006290

Ali, S. A., Khatun, R., Ahmad, A., & Ahmad, S. N. (2019). Application of GIS-based analytic hierarchy process and frequency ratio model to flood vulnerable mapping and risk area estimation at Sundarban region, India. *Modeling Earth Systems and Environment, 5*(3), 1083-1102. https://doi.org/10.1007/s40808-019-00593-z

Amarasinghe, A. G. (2016). *Progress in Controlling Efforts of Inland Water Pollution in Sri Lanka: The Case of Lower Kelani River Basin in Sri Lanka*. http://repository.kln.ac.lk/handle/123456789/14795?show=full

Amarasinghe, A. G. (2020). Analysis of Long-Term Rainfall Trends in Sri Lanka Using CHRIPS Estimates. *American Journal of Multidisciplinary Research & Development (AJMRD) Volume 2, Issue 11 (November- 2020), PP 34-44*.

Ammarapala, V., Chinda, T., Pongsayaporn, P., Ratanachot, W., Punthutaecha, K., & Janmonta, K. (2018). Cross-border shipment route selection utilizing analytic hierarchy process (AHP) method. *Songklanakarin J. Sci. Technol., 40 (1)*, 31-37.

Ampitiyawatta, A. D., & Guo, S. (2009). PRECIPITATION TRENDS IN THE KALU GANGA BASIN IN SRI LANKA. *The Journal of Agricultural Science, vol.4, no.1*.

Aristizabal, F., Salas, F., Petrochenkov, G., Grout, T., Avant, B., Bates, B., Spies, R., Chadwick, N., Wills, Z., & Judge, J. (2023). Extending Height Above Nearest Drainage to Model Multiple Fluvial Sources in Flood Inundation Mapping Applications for the U.S. National Water Model. *Water Resources Research, 59*(5), e2022WR032039. https://doi.org/https://doi.org/10.1029/2022WR032039

Arnell, N. W., & Gosling, S. N. (2013). The impacts of climate change on river flow regimes at the global scale. *Journal of Hydrology, 486*, 351-364. https://doi.org/https://doi.org/10.1016/j.jhydrol.2013.02.010

Aryal, Y. N., Villarini, G., Zhang, W., & Vecchi, G. A. (2018). Long term changes in flooding and heavy rainfall associated with North Atlantic tropical cyclones: Roles of the North Atlantic Oscillation and El Niño-Southern Oscillation. *Journal of Hydrology, 559*, 698-710.

Asadieh, B., & Krakauer, N. Y. (2015). Global trends in extreme precipitation: climate models versus observations. *Hydrol. Earth Syst. Sci., 19*(2), 877-891. https://doi.org/10.5194/hess-19-877-2015

Ashfaq, M., Shi, Y., Tung, W. w., Trapp, R. J., Gao, X., Pal, J. S., & Diffenbaugh, N. S. (2009). Suppression of south Asian summer monsoon precipitation in the 21st century. *Geophysical Research Letters, 36*(1).

Ashok, K., Guan, Z., & Yamagata, T. (2001). Impact of the Indian Ocean dipole on the relationship between the Indian monsoon rainfall and ENSO. *Geophysical Research Letters, 28*(23), 4499-4502. https://doi.org/https://doi.org/10.1029/2001GL013294

Ávila, A., Justino, F., Wilson, A., Bromwich, D., & Amorim, M. (2016). Recent precipitation trends, flash floods and landslides in southern Brazil. *Environmental Research Letters, 11*(11), 114029. https://doi.org/10.1088/1748-9326/11/11/114029

Ayantika, D., Krishnan, R., Singh, M., Swapna, P., Sandeep, N., Prajeesh, A., & Vellore, R. (2021). Understanding the combined effects of global warming and anthropogenic aerosol forcing on the South Asian monsoon. *Climate Dynamics, 56*, 1643-1662.

Azari, M., Moradi, H. R., Saghafian, B., & Faramarzi, M. (2016). Climate change impacts on streamflow and sediment yield in the North of Iran. *Hydrological Sciences Journal, 61*(1), 123-133. https://doi.org/10.1080/02626667.2014.967695

Azman, A. H., Nurul Nadrah Aqilah, T., & Malek, M. A. (2021). Comparison of Missing Rainfall Data Treatment Analysis at Kenyir Lake. *IOP Conference Series. Materials Science and Engineering, 1144*(1). https://doi.org/https://doi.org/10.1088/1757-899X/1144/1/012046

Basher, M. A., Stiller-Reeve, M. A., Saiful Islam, A. K. M., & Bremer, S. (2018). Assessing climatic trends of extreme rainfall indices over northeast Bangladesh. *Theoretical and Applied Climatology, 134*(1), 441-452. https://doi.org/10.1007/s00704-017-2285-4

Basnayake, S., Punyawardena, B., Jayasinghe, S., Gupta, N., Shrestha, M., & Premalal, K. (2019). *Climate Smart Disaster Risk Reduction Interventions inAgriculture Sector – Flood hazard – A Practitioner's Handbook*. Asian Disaster Preparedness Center. https://www.researchgate.net/publication/340931543_CLIMATE_SMART_DISASTER_RISK_REDUCTION_INTERVENTIONS_IN_AGRICULTURE_SECTOR_-_FLOOD_HAZARD

Bell, V. A., Kay, A. L., Davies, H. N., & Jones, R. G. (2016). An assessmentof the possible impacts of climate change on snow and peak river flowsacross Britain. *Clim. Change, 136 (3): 539–553*. https://doi.org/https://doi.org/10.1007/s10584-016-1637-x

Beven, K. J., & Kirkby, M. J. (1979). A physically based, variable contributing area model of basin hydrology / Un modèle à base physique de zone d'appel variable de l'hydrologie du bassin versant. *Hydrological Sciences Bulletin, 24*(1), 43-69. https://doi.org/10.1080/02626667909491834

Bhatti, A. S., Wang, G., Ullah, W., Ullah, S., Fiifi Tawia Hagan, D., Kwesi Nooni, I., Lou, D., & Ullah, I. (2020). Trend in Extreme Precipitation Indices Based on Long Term In Situ Precipitation Records over Pakistan. *Water, 12*(3). https://doi.org/10.3390/w12030797

Birkholz, S., Muro, M., Jeffrey, P., & Smith, H. M. (2014). Rethinking the relationship between flood risk perception and flood management. *Science of the total environment, 478*, 12-20.

Biswas, B., Rahaman, A., & Barman, J. (2023). Comparative Assessment of FR and AHP Models for Landslide Susceptibility Mapping for Sikkim, India and Preparation of Suitable Mitigation Techniques. *Journal of the Geological Society of India, 99*(6), 791-801. https://doi.org/10.1007/s12594-023-2386-x

Bonham-Carter, G. (1994). *Geographic information systems for geoscientists: modelling with GIS*. Elsevier.

Brouwer, R., Akter, S., Brander, L., & Haque, E. (2007). Socioeconomic Vulnerability and Adaptation to Environmental Risk: A Case Study of Climate Change and Flooding in Bangladesh. *Risk Analysis, 27*(2), 313-326. https://doi.org/https://doi.org/10.1111/j.1539-6924.2007.00884.x

Brown, P. J., Bradley, R. S., & Keimig, F. T. (2010). Changes in Extreme Climate Indices for the Northeastern United States, 1870–2005. *Journal of Climate, 23*(24), 6555-6572. https://doi.org/https://doi.org/10.1175/2010JCLI3363.1

Bui, Q.-T., Nguyen, Q.-H., Nguyen, X. L., Pham, V. D., Nguyen, H. D., & Pham, V.-M. (2020). Verification of novel integrations of swarm intelligence algorithms into deep learning neural network for flood susceptibility mapping. *Journal of Hydrology, 581*, 124379. https://doi.org/https://doi.org/10.1016/j.jhydrol.2019.124379

Burt, T. P., & Weerasinghe, K. D. N. (2014). Rainfall Distributions in Sri Lanka in Time and Space: An Analysis Based on Daily Rainfall Data. *Climate 2014, 2*, 242-263. https://doi.org/DOI:10.3390/cli2040242

Cai, S., Fan, J., & Yang, W. (2021). Flooding Risk Assessment and Analysis Based on GIS and the TFN-AHP Method: A Case Study of Chongqing, China. *Atmosphere, 12*(5). https://doi.org/10.3390/atmos12050623

Chandimala, J., & Zubair, L. (2007). Predictability of stream flow and rainfall based on ENSO for water resources management in Sri Lanka. *Journal of Hydrology, 335*(3), 303-312. https://doi.org/https://doi.org/10.1016/j.jhydrol.2006.11.024

Chandio, I. A., Matori, A. N. B., WanYusof, K. B., Talpur, M. A. H., Balogun, A.-L., & Lawal, D. U. (2013). GIS-based analytic hierarchy process as a multicriteria decision analysis

instrument: a review. *Arabian Journal of Geosciences, 6*(8), 3059-3066. https://doi.org/10.1007/s12517-012-0568-8

Chaudhuri, C., Gray, A., & Robertson, C. (2021). InundatEd-v1.0: a height above nearest drainage (HAND)-based flood risk modeling system using a discrete global grid system. *Geosci. Model Dev., 14*(6), 3295-3315. https://doi.org/10.5194/gmd-14-3295-2021

Chauluka, F., Singh, S., & Kumar, R. (2021). Rainfall and streamflow trends of Thuchila River, Southern Malawi. *Materials Today: Proceedings, 34*, 846-855. https://doi.org/https://doi.org/10.1016/j.matpr.2020.06.228

Chowdhuri, I., Pal, S. C., & Chakrabortty, R. (2020). Flood susceptibility mapping by ensemble evidential belief function and binomial logistic regression model on river basin of eastern India. *Advances in Space Research, 65*(5), 1466-1489. https://doi.org/https://doi.org/10.1016/j.asr.2019.12.003

Climate Change Secretariat, M. o. M. D. a. E. (2016). *National Adaptation Plan for Climate Change Impacts in Sri Lanka*. https://www4.unfccc.int/sites/NAPC/Documents%20NAP/National%20Reports/National%20Adaptation%20Plan%20of%20Sri%20Lanka.pdf

Coburn, A. W., Spence, R. J. S., & Pomonis, A. (1994). Training manual: vulnerability and risk assessment (2nd edition). *UNDP Disaster Management Training Programme*.

Costa, A. C., & Soares, A. (2009). Homogenization of Climate Data: Review and New Perspectives Using Geostatistics. *Mathematical Geosciences, 41*(3), 291-305. https://doi.org/10.1007/s11004-008-9203-3

Costache, R., Pham, Q. B., Sharifi, E., Linh, N. T. T., Abba, S. I., Vojtek, M., Vojteková, J., Nhi, P. T. T., & Khoi, D. N. (2019). Flash-Flood Susceptibility Assessment Using Multi-Criteria Decision Making and Machine Learning Supported by Remote Sensing and GIS Techniques. *Remote Sensing, 12*(1). https://doi.org/10.3390/rs12010106

Couasnon, A., Eilander, D., Muis, S., Veldkamp, T. I., Haigh, I. D., Wahl, T., Winsemius, H. C., & Ward, P. J. (2020). Measuring compound flood potential from river discharge and storm surge extremes at the global scale. *Natural Hazards and Earth System Sciences, 20*(2), 489-504.

CRIP. (2018). *Strategic Environmental Assessment of Development of River Basin Level Flood 399 and Drought Mitigation Investment Plans (DBIP)*. http://crip.lk/wp-content/uploads/2019/01/Kelani-River-SEA-Study-Final-Report.pdf.

Danumah, J. H., Odai, S. N., Saley, B. M., Szarzynski, J., Thiel, M., Kwaku, A., Kouame, F. K., & Akpa, L. Y. (2016). Flood risk assessment and mapping in Abidjan district using multi-

criteria analysis (AHP) model and geoinformation techniques, (cote d'ivoire). *Geoenvironmental Disasters, 3*(1). https://doi.org/10.1186/s40677-016-0044-y

de Santana, R. O., Delgado, R. C., & Schiavetti, A. (2021). Modeling susceptibility to forest fires in the Central Corridor of the Atlantic Forest using the frequency ratio method. *Journal of Environmental Management, 296*, 113343. https://doi.org/https://doi.org/10.1016/j.jenvman.2021.113343

De Silva, M., Ratnyake, U., Mahanama, S., Herath, S., & Weerakoon, S. (2012). Flood inundation mapping along the lower reach of Kelani river basin under the impact of climatic change.

De Silva M, T., & Hornberger, G. M. (2019). Identifying El Niño–Southern Oscillation influences on rainfall with classification models: implications for water resource management of Sri Lanka. *Hydrology and Earth System Sciences, 23*(4), 1905-1929. https://doi.org/10.5194/hess-23-1905-2019

De Silva, M. T., & Hornberger, G. M. (2019). Identifying El Niño–Southern Oscillation influences on rainfall with classification models: implications for water resource management of Sri Lanka. *Hydrology and Earth System Sciences, 23*(4), 1905-1929. https://doi.org/10.5194/hess-23-1905-2019

de Brito, M. M., & Evers, M. (2016). Multi-criteria decision-making for flood risk management: a survey of the current state of the art. *Nat. Hazards Earth Syst. Sci., 16*(4), 1019-1033. https://doi.org/10.5194/nhess-16-1019-2016

Demiray, B. Z., Sit, M., & Demir, I. (2021). D-SRGAN: DEM super-resolution with generative adversarial networks. *SN Computer Science, 2*, 1-11.

Department of Meteorology, S. L. (2019). *Climate of Sri Lanka*. Department of Mereorology, Sri Lanka. http://www.meteo.gov.lk/index.php?option=com_content&view=article&id=94&Itemid=310&lang=en

Desertification Indicator System for Mediterranean Europe. (2004). *SOIL PERMEABILITY*. https://esdac.jrc.ec.europa.eu/public_path/shared_folder/projects/DIS4ME/indicator_descriptions/soil_permeability.htm

Dewan, A. M., & Yamaguchi, Y. (2009). Land use and land cover change in Greater Dhaka, Bangladesh: Using remote sensing to promote sustainable urbanization. *Applied Geography, 29*(3), 390-401. https://doi.org/https://doi.org/10.1016/j.apgeog.2008.12.005

Disaster Information Management System in Sri Lanka. (2017). *Latest disaster incident in Sri lanka*. Retrieved 12/03/2020, from

https://www.desinventar.lk/#:~:text=Around%20717%2C622%20People%20were%20affected,around%2012%2C529%20houses%20partially%20damage.

Disaster Managment Center, S. L. (2016). *Annual Report - 2016*. https://www.dmc.gov.lk/images/pdfs/AnnualReports/2016_compressed.pdf

Disaster Managment Center, S. L. (2018). *Annual Report- 2017*.

Dissanayaka, K., & Rajapakse, R. (2018). Climate extremes and precipitation trends in Kelani river basin, Sri Lanka and impacts on streamflow variability under climate change.The Proceedings of The International Conference on Climate Change,

Dissanayaka, K., & Rajapakse, R. (2019). Long-term precipitation trends and climate extremes in the Kelani River basin, Sri Lanka, and their impact on streamflow variability under climate change. *Paddy and Water Environment, 17*, 281-289.

Dissanayake, D., Morimoto, T., Murayama, Y., Ranagalage, M., & Perera, E. N. C. (2020). Analysis of Life Quality in a Tropical Mountain City Using a Multi-Criteria Geospatial Technique: A Case Study of Kandy City, Sri Lanka. *Sustainability, 12*(7). https://doi.org/10.3390/su12072918

Dissanayake, P., Hettiarachchi, S., & Siriwardana, C. (2018). Increase in Disaster Risk due to inefficient Environmental Management, Land use policies and Relocation Policies. Case studies from Sri Lanka. *Procedia Engineering, 212*, 1326-1333. https://doi.org/https://doi.org/10.1016/j.proeng.2018.01.171

Döll, P., & Schmied, H. M. (2012). How is the impact of climate change on river flow regimes related to the impact on mean annual runoff? A global-scale analysis. *Environmental Research Letters, 7*(1). https://doi.org/10.1088/1748-9326/7/1/014037

Domroes, M. (1998). Variability of the temporal and spatial organization of rainfall in Sri Lanka.

Douglas, I. (2009). Climate change, flooding and food security in south Asia. *Food Security, 1*, 127-136.

Dushyantha, C., & Ptuhina, I. (2020). Flood risk assessment of river "Kelani Ganga" exceeding its threshold water level. *E3S Web Conf., 157*, 02006. https://doi.org/10.1051/e3sconf/202015702006

EM-DAT. (2023). *2022 Disasters in numbers; climate in action*. https://www.cred.be/sites/default/files/2022_EMDAT_report.pdf

Fang, L., Zhang, Z., & Huang, J. (2023). Rapid flood modelling using HAND-FFA-SRC coupled approach and social media-based geodata in a coastal Chinese watershed. *Environmental Modelling & Software, 170*, 105862. https://doi.org/https://doi.org/10.1016/j.envsoft.2023.105862

Fatah, K. K., Mustafa, Y. T., & Hassan, I. O. (2022). Flood Susceptibility Mapping Using an Analytic Hierarchy Process Model Based on Remote Sensing and GIS Approaches in Akre District, Kurdistan Region, Iraq. *Iraqi Geological Journal, 55*(2C), 121-149. https://doi.org/10.46717/igj.55.2C.10ms-2022-08-23

Feng, X., Porporato, A., & Rodriguez-Iturbe, I. (2013). Changes in rainfall seasonality in the tropics. *Nature Climate Change, 3*(9), 811-815.

Flood-List. (2020). *India – 24 Dead and 11,000 Rescued After Floods in Madhya Pradesh*. https://floodlist.com/asia/india-floods-madhya-pradesh-late-august-2020

Flood-List. (2021). *China – Over 350,000 Evacuated, 33 Dead, 8 Missing After Zhengzhou and Henan Floods*. https://floodlist.com/asia/china-henan-zhengzhou-floods-update-july-2021

Floodsite. (2006). Guidelines for socio-economic flood damage evaluation. FLOODsite project Report number T9-06-01.

Folland, C., Karl, T., Christy, J., Clarke, R., Gruza, G., Jouzel, J., Mann, M., Oerlemans, J., Salinger, M., & Wang, S. (2001). Observed climate variability and change. *Climate change, 2001*, 99.

Frans, C., Istanbulluoglu, E., Mishra, V., Munoz-Arriola, F., & Lettenmaier, D. P. (2013). Are climatic or land cover changes the dominant cause of runoff trends in the Upper Mississippi River Basin? *Geophysical Research Letters, 40*(6), 1104-1110. https://doi.org/https://doi.org/10.1002/grl.50262

Fu, G., Yu, J., Yu, X., Ouyang, R., Zhang, Y., Wang, P., Liu, W., & Min, L. (2013). Temporal variation of extreme rainfall events in China, 1961–2009. *Journal of Hydrology, 487*, 48-59. https://doi.org/10.1016/j.jhydrol.2013.02.021

Gacu, J. G., Monjardin, C. E. F., Senoro, D. B., & Tan, F. J. (2022). Flood Risk Assessment Using GIS-Based Analytical Hierarchy Process in the Municipality of Odiongan, Romblon, Philippines. *Applied Sciences, 12*(19). https://doi.org/10.3390/app12199456

Ganguli, P., Paprotny, D., Hasan, M., Güntner, A., & Merz, B. (2020). Projected changes in compound flood hazard from riverine and coastal floods in northwestern Europe. *Earth's Future, 8*(11), e2020EF001752.

Ghosh, A., & Kar, S. K. (2018). Application of analytical hierarchy process (AHP) for flood risk assessment: a case study in Malda district of West Bengal, India. *Natural Hazards, 94*(1), 349-368. https://doi.org/10.1007/s11069-018-3392-y

Godbout, L., Zheng, J. Y., Dey, S., Eyelade, D., Maidment, D., & Passalacqua, P. (2019). Error assessment for height above the nearest drainage inundation mapping. *JAWRA Journal of the American Water Resources Association, 55*(4), 952-963.

Good data. (2023). *Time Series Analysis - Lagged Correlation and R-Squared*. Retrieved 30/10/2023, from https://community.gooddata.com/metrics-and-maql-kb-articles-43/time-series-analysis-lagged-correlation-and-r-squared-233

Goonatilake, S. d. A., N. Perera, G.D. Silva, Weerakoon, D., & Mallawatantri, A. (2016). *Natural Resource Profile of the Kelani River Basin.* https://www.unicef.org/srilanka/media/301/file/Natural%20Resource%20Profile%20of%20the%20kelani%20river%20Basin.pdf

Gordon Tami, A., & Moses, O. (2015). Flood Vulnerability Assessment of Niger Delta States Relative to 2012 Flood Disaster in Nigeria. *American Journal of Environmental Protection, 3*(3), 76-83. http://pubs.sciepub.com/

Gornitz, V. M., Daniels, R. C., White, T. W., & Birdwell, K. R. (1994). Thedevelopment of a coastal risk assessment database: Vulnerability to sea-level rise in the US Southeast. *J. Coast. Res, 12 (1): 327–338*.

Goswami, P., & Ramesh, K. V. (2008). Extreme Rainfall Events: Vulnerability Analysis forDisaster Management and Observation System Design. *Current Science, Vol. 94, No. 8*. https://www.jstor.org/stable/24100799?seq=1#metadata_info_tab_contents

Guagliardi, I., Buttafuoco, G., Caloiero, P., Caloiero, T., Frustaci, F., & Ricca, N. (2016). Annual and seasonal rainfall trend analysis in Europe and in the Mediterranean area. *Soc Geol It, 40*(1), 382.

Gujree, I., Ahmad, I., Zhang, F., & Arshad, A. (2022). Innovative Trend Analysis of High-Altitude Climatology of Kashmir Valley, North-West Himalayas. *Atmosphere, 13*(5), 764. https://www.mdpi.com/2073-4433/13/5/764

Hagos, Y. G., Andualem, T. G., Yibeltal, M., & Mengie, M. A. (2022). Flood hazard assessment and mapping using GIS integrated with multi-criteria decision analysis in upper Awash River basin, Ethiopia. *Applied Water Science, 12*(7). https://doi.org/10.1007/s13201-022-01674-8

Haimes, Y. Y. (2009). Risk modelling, assessment, and management. *New Jersey (Wiley)*.

Halpert, M. S., & Ropelewski, C. F. (1992). Surface temperature patterns associated with the Southern Oscillation. *Journal of Climate, Vol. 5, No. 6*, 577–593. https://doi.org/https://doi.org/10.1175/1520-0442(1992)005<0577:STPAWT>2.0.CO;2

Hamed, K. H., & Rao, A. R. (1998). A modified Mann-Kendall trend test for autocorrelated data. *Journal of Hydrology, 204*(1), 182-196. https://doi.org/https://doi.org/10.1016/S0022-1694(97)00125-X

Hapuarachchi, H. A. P., Wang, Q. J., & Pagano, T. C. (2011). A review of advances in flash flood forecasting. *Hydrological Processes, 25*(18), 2771-2784. https://doi.org/10.1002/hyp.8040

Hapuarachchi, H. A. S. U., & Premalal, S. (2021). Identification of Extreme Rainfall Events for the Period 1970–2019 in Sri Lanka Using Percentile-Based Analysis and Its Projections for 2100 for the Emission Scenarios of RCP 4.5 and 8.5..pdf. *Multi-Hazard Early Warning and Disaster Risks*. https://doi.org/https://doi.org/10.1007/978-3-030-73003-1_28

Hariadi, M. H., van der Schrier, G., Steeneveld, G. J., Sutanto, S., Sutanudjaja, E., Ratri, D. N., Sopaheluwakan, A., & Klein Tank, A. (2023). A high-resolution perspective of extreme rainfall and river flow under extreme climate change in Southeast Asia. *Hydrol. Earth Syst. Sci. Discuss., 2023*, 1-29. https://doi.org/10.5194/hess-2023-14

Held, I., & Soden, B. (2006). Robust Responses of the Hydrological Cycle to Global Warming. *Journal of Climate, Volume 19*, 5686 - 5699.

Hettiarachchi, P. (2016). Hydrological report on the Kelani River flood in May 2016. *Hydrological annual, irrigation department*.

Hu, S., Cheng, X., Zhou, D., & Zhang, H. (2017). GIS-based flood risk assessment in suburban areas: a case study of the Fangshan District, Beijing. *Natural Hazards, 87*(3), 1525-1543. https://doi.org/10.1007/s11069-017-2828-0

Hwang, C. L., & Yoon, K. (1981). Multiple Attribute Decision Making: Methods and Applications—A State-of-the-Art Survey. *Springer: New York, NY, USA, Volume 186*.

Imbulana, N., Gunawardana, S., Shrestha, S., & Datta, A. (2018). Projections of extreme precipitation events under climate change scenarios in Mahaweli River Basin of Sri Lanka. *Current Science, 114*(7), 1495-1509. http://www.jstor.org/stable/26495505

International Federation of Red Cross and Red Crescent Societies. (2020). *Sri Lanka - Floods and Landslides - Final Report*

IPCC. (2007). *Climate Change 2007: The Physical Science Basis* (Contribution of Working Group I to the Fourth Assessment

Report of the Intergovernmental Panel on Climate Change, Issue. United Kingdom and New York, NY, USA, 996 pp.

IPCC. (2012). *Managing the Risks of Extreme Events and Disasters to Advance Climate Change Adaptation. A Special Report of Working Groups I and II of the Intergovernmental Panel on Climate Change*.

IPCC. (2021). *Climate Change 2021: The Physical Science Basis.* (Contribution of Working Group I to the Sixth Assessment Report of the Intergovernmental Panel on Climate Change, Issue. https://public.wmo.int/en/resources/bulletin/regional-trends-extreme-events-ipcc-2021-report

Jain, C. K., & Singh, S. (2018). Impact of climate change on the hydrological dynamics of River Ganga, India. *Journal of Water and Climate Change, 11*(1), 274-290. https://doi.org/10.2166/wcc.2018.029

Jarvis, C. S. (1936). *Floods in the United States: Magnitude and frequency* (Vol. 771). US Government Printing Office.

Jayasekara, S. M., Abeysingha, N. S., & Meegastenna, T. J. (2020). Streamflow trends of Kelani river basin in Sri Lanka (1983-2013). *Journal of the National Science Foundation of Sri Lanka, 48*(4). https://doi.org/10.4038/jnsfsr.v48i4.9440

Jayawardena, I. M. S. P., Darshika, D. W. T. T., & C. Herath, H. M. R. (2018). Recent Trends in Climate Extreme Indices over Sri Lanka. *American Journal of Climate Change, 07*(04), 586-599. https://doi.org/10.4236/ajcc.2018.74036

Jayawardena, I. M. S. P., Sumathipala, W. L., & Basnayake, B. R. S. B. (2017). Impact of Madden Julian oscillation (MJO) and other meteorological phenomena on the heavy rainfall event from 19th− 28th December, 2014 over Sri Lanka. *Journal of the National Science Foundation of Sri Lanka, 45(2)*.

Jiang, R., Wang, Y., Xie, J., Zhao, Y., Li, F., & Wang, X. (2019). Assessment of extreme precipitation events and their teleconnections to El Niño Southern Oscillation, a case study in the Wei River Basin of China. *Atmospheric Research, 218*, 372-384. https://doi.org/10.1016/j.atmosres.2018.12.015

JICA, J. I. C. A. (2004). *Study of hydropower optimization in Sri Lanka* (Final Report, Issue.

Jones, C., Waliser, D. E., Lau, K. M., & Stern, W. (2004). Global Occurrences of Extreme Precipitation and the Madden–Julian Oscillation: Observations and Predictability. *J. Climate, 17*, 4575–4589. https://doi.org/https://doi.org/10.1175/3238.1

Kelly, M., & Kuleshov, Y. (2022). Flood Hazard Assessment and Mapping: A Case Study from Australia's Hawkesbury-Nepean Catchment. *Sensors (Basel), 22*(16). https://doi.org/10.3390/s22166251

Kelman, I., & Spence, R. (2004). An overview of flood actions on buildings. *Engineering Geology, 73*(3-4), 297-309. https://doi.org/10.1016/j.enggeo.2004.01.010

Kendall, M. G. (1962). Rank correlation methods. *J. Am. Stat. Assoc., , 63(324)*, 1379 – 1389. https://doi.org/doi:10.1080/01621459.1968.10480934.

Khadgarai, S., Kumar, V., & Pradhan, P. K. (2021). The Connection between Extreme Precipitation Variability over Monsoon Asia and Large-Scale Circulation Patterns. *Atmosphere, 12*(11), 1492. https://www.mdpi.com/2073-4433/12/11/1492

Khajehei, S., Ahmadalipour, A., Shao, W., & Moradkhani, H. (2020). A Place-based Assessment of Flash Flood Hazard and Vulnerability in the Contiguous United States. *Scientific Reports, 10*(1), 448. https://doi.org/10.1038/s41598-019-57349-z

Khan, H., Shafique, M., Khan, M. A., Bacha, M. A., Shah, S. U., & Calligaris, C. (2019). Landslide susceptibility assessment using Frequency Ratio, a case study of northern Pakistan. *The Egyptian Journal of Remote Sensing and Space Science, 22*(1), 11-24. https://doi.org/https://doi.org/10.1016/j.ejrs.2018.03.004

Khaniya, B., Jayanayaka, I., Jayasanka, P., & Rathnayake, U. (2019). Rainfall Trend Analysis in Uma Oya Basin, Sri Lanka, and Future Water Scarcity Problems in Perspective of Climate Variability. *Advances in Meteorology, 2019*, 3636158. https://doi.org/10.1155/2019/3636158

Komolafe, A. A., Awe, B. S., Olorunfemi, I. E., & Oguntunde, P. G. (2020). Modelling flood-prone area and vulnerability using integration of multi-criteria analysis and HAND model in the Ogun River Basin, Nigeria. *Hydrological Sciences Journal, 65*(10), 1766-1783. https://doi.org/10.1080/02626667.2020.1764960

Koriche, S. A., & Rientjes, T. H. M. (2016). Application of satellite products and hydrological modelling for flood early warning. *Physics and Chemistry of the Earth, Parts A/B/C, 93*, 12-23. https://doi.org/https://doi.org/10.1016/j.pce.2016.03.007

Krishnan, R., Sabin, T., Madhura, R., Vellore, R., Mujumdar, M., Sanjay, J., Nayak, S., & Rajeevan, M. (2019). Non-monsoonal precipitation response over the Western Himalayas to climate change. *Climate Dynamics, 52*, 4091-4109.

Kumar, V., Jain, S. K., & Singh, Y. (2010). Analysis of long-term rainfall trends in India. *Hydrological Sciences Journal–Journal des Sciences Hydrologiques, 55*(4), 484-496.

Kundzewicz, Z. W., Kanae, S., Seneviratne, S. I., Handmer, J., Nicholls, N., Peduzzi, P., Mechler, R., Bouwer, L. M., Arnell, N., Mach, K., Muir-Wood, R., Brakenridge, G. R., Kron, W., Benito, G., Honda, Y., Takahashi, K., & Sherstyukov, B. (2014). Flood risk and climate change: global and regional perspectives. *Hydrological Sciences Journal, 59*(1), 1-28. https://doi.org/10.1080/02626667.2013.857411

Lang, T. J., & Barros, A. P. (2004). Winter Storms in the Central Himalayas. *Journal of the Meteorological Society of Japan. Ser. II, 82*(3), 829-844. https://doi.org/10.2151/jmsj.2004.829

Laura, J. S., & Deswal, M. (2018). GIS based modeling using Analytic Hierarchy Process (AHP) for optimization of landfill site selection of Rohtak city, Haryana (India). *Journal of Applied and Natural Science, 10*(2), 633-642. https://doi.org/10.31018/jans.v10i2.1753

Li, L., & Revesz, P. (2004). Interpolation methods for spatio-temporal geographic data. *Computers, Environment and Urban Systems, 28*(3), 201-227. https://doi.org/https://doi.org/10.1016/S0198-9715(03)00018-8

Li, X., Yan, D., Wang, K., Weng, B., Qin, T., & Liu, S. (2019). Flood Risk Assessment of Global Watersheds Based on Multiple Machine Learning Models. *Water, 11*(8). https://doi.org/10.3390/w11081654

Li, Z., Duque, F. Q., Grout, T., Bates, B., & Demir, I. (2023). Comparative analysis of performance and mechanisms of flood inundation map generation using Height Above Nearest Drainage. *Environmental Modelling & Software, 159*, 105565. https://doi.org/https://doi.org/10.1016/j.envsoft.2022.105565

Liyanage, L. C., Weerakoon, O. S., Palliyaguru, S. T., & Wimalaratne, G. D. S. P. (2019, November 12-14, 2019). *Towards Prediction of Landslide Susceptibility using Random Forest for Kalutara District Sri Lanka* 2019 IEEE Region 10 Humanitarian Technology Conference, https://ieeexplore.ieee.org/stamp/stamp.jsp?tp=&arnumber=9042450

Madduma Bandara, C. M., & Wickramagamage, P. (2004). Climate change and its impact on upper watershed of the hill country of Sri Lanka. *Proceedings of the International Conference on Sustainable Water Resources Management in the Changing Environment of the Monsoon Region* 17 - 19. (Colombo, Sri Lanka)

Mahagamage, M. G. Y. L., & Manage, P. M. (2018). SOCIO-ECONOMIC BACKGROUND OF THE HEAD ANDTRANSITIONAL REGIONS OF THE KELANI RIVER BASIN,SRI LANKA. *Asian Jr. of Microbiol. Biotech. Env. Sc. , ol. 20, No. (3) : 2018 : 744-756*.

Malczewski, J. (1999). GIS and multicriteria decision analysis. *New York (Wiley)*.

Malede, D. A., Agumassie, T. A., Kosgei, J. R., Linh, N. T. T., & Andualem, T. G. (2022). Analysis of rainfall and streamflow trend and variability over Birr River watershed, Abbay basin, Ethiopia. *Environmental Challenges, 7*, 100528. https://doi.org/https://doi.org/10.1016/j.envc.2022.100528

Malmgren, B. A., Hullugalla, R., Lindeberg, G., Inoue, Y., Hayashi, Y., & Mikami, T. (2006). Oscillatory behavior of monsoon rainfall over Sri Lanka during the late 19th and 20th centuries and its relationships to SSTs in the Indian Ocean and ENSO. *Theoretical and Applied Climatology, 89*(1-2), 115-125. https://doi.org/10.1007/s00704-006-0225-9

Malmgren, B. A., Hulugalla, R., Hayashi, Y., & Mikami, T. (2003). Precipitation trends in Sri Lanka since the 1870s and relationships to El Niño-southern oscillation. *International Journal of Climatology, 23*(10), 1235-1252. https://doi.org/10.1002/joc.921

Manawadu, L., & Wijeratne, V. (2021). Anthropogenic drivers and impacts of urban flooding-A case study in Lower Kelani River Basin, Colombo Sri Lanka. *International Journal of Disaster Risk Reduction, 57*, 102076.

Mann, H. B. (1945). Nonparametric Tests Against Trend. *Econometrica, , 13(3)*, 245–259.

Mård, J., Di Baldassarre, G., & Mazzoleni, M. (2018). Nighttime light data reveal how flood protection shapes human proximity to rivers. *Sci Adv, 4*(8), eaar5779. https://doi.org/10.1126/sciadv.aar5779

Martins, J. A., Brand, V. S., Capucim, M. N., Machado, C. B., Piccilli, D. G. A., & Martins, L. D. (2016). The Impact of Rainfall and Land Cover Changes on the Flow of a Medium-sized River in the South of Brazil. *Energy Procedia, 95*, 272-278. https://doi.org/10.1016/j.egypro.2016.09.068

Megahed, H. A., Abdo, A. M., AbdelRahman, M. A. E., Scopa, A., & Hegazy, M. N. (2023). Frequency Ratio Model as Tools for Flood Susceptibility Mapping in Urbanized Areas: A Case Study from Egypt. *Applied Sciences, 13*(16), 9445. https://www.mdpi.com/2076-3417/13/16/9445

Mehravar, S., Razavi-Termeh, S. V., Moghimi, A., Ranjgar, B., Foroughnia, F., & Amani, M. (2023). Flood susceptibility mapping using multi-temporal SAR imagery and novel integration of nature-inspired algorithms into support vector regression. *Journal of Hydrology, 617*. https://doi.org/10.1016/j.jhydrol.2023.129100

Merz, B., Elmer, F., & Thieken, A. H. (2009). Significance of “high probability/low damage” versus “low probability/high damage” flood events. *Natural Hazards Earth System Sciences, 9*, 1033-1046.

Ministry of National Policies and Economic Affairs and Ministry of Disaster Management. (2017). *Sri Lanka rapid post disaster needs assessment: floods and landslides: May 2017*. https://lk.one.un.org/wp-content/uploads/2017/11/PDNA-Sri-lanka-2017.pdf

Ministry of National Policies and Economic Affairs, M. o. D. M. (2016). *Sri Lanka Post-Disaster Needs Assessment*. http://documents.worldbank.org/curated/en/872611496221419957/pdf/115335-WP-PUBLIC-pda-2016-srilanka.pdf

Mirza, M. M. Q. (2011). Climate change, flooding in South Asia and implications. *Regional Environmental Change, 11*(1), 95-107. https://doi.org/10.1007/s10113-010-0184-7

Mishra, A., Mukherjee, S., Merz, B., Singh, V. P., Wright, D. B., Villarini, G., Paul, S., Kumar, D. N., Khedun, C. P., Niyogi, D., Schumann, G., & Stedinger, J. R. (2022). An Overview of Flood Concepts, Challenges, and Future Directions. *Journal of Hydrologic Engineering, 27*(6), 03122001. https://doi.org/doi:10.1061/(ASCE)HE.1943-5584.0002164

Mishra, V., Aaadhar, S., Shah, H., Kumar, R., Pattanaik, D., & Tiwari, A. (2018). The Kerala flood of 2018: combined impact of extreme rainfall and reservoir storage. *Hydrol Earth Syst Sci Discuss pp 1–13*.

Mojaddadi, H., Pradhan, B., Nampak, H., Ahmad, N., & Ghazali, A. H. b. (2017). Ensemble machine-learning-based geospatial approach for flood risk assessment using multi-sensor remote-sensing data and GIS. *Geomatics, Natural Hazards and Risk, 8*(2), 1080-1102. https://doi.org/10.1080/19475705.2017.1294113

Mukaka, M. M. (2012). Statistics corner: A guide to appropriate use of correlation coefficient in medical research. *Malawi Med J, 24*(3), 69-71.

Mukherjee, S., & Mishra, A. K. (2021). Cascading effect of meteorological forcing on extreme precipitation events: Role of atmospheric rivers in southeastern US. *Journal of Hydrology, 601*, 126641.

Nanditha, J. S., Kushwaha, A. P., Singh, R., Malik, I., Solanki, H., Chuphal, D. S., Dangar, S., Mahto, S. S., Vegad, U., & Mishra, V. (2023). The Pakistan Flood of August 2022: Causes and Implications. *Earth's Future, 11*(3), e2022EF003230. https://doi.org/https://doi.org/10.1029/2022EF003230

NASA. (1999). Tropical Rainfall Measuring Mission: Importance to Global Change and Human Welfare. URL: https://earthobservatory.nasa.gov/features/TRMM/trmm2.php. Accessed on 13 March 2020

Nasiri, H., Mohd Yusof, M. J., & Mohammad Ali, T. A. (2016). An overview to flood vulnerability assessment methods. *Sustainable Water Resources Management, 2*(3), 331-336. https://doi.org/10.1007/s40899-016-0051-x

Naveendrakumar, G., Vithanage, M., Kwon, H.-H., Iqbal, M. C. M., Pathmarajah, S., & Obeysekera, J. (2018). Five Decadal Trends in Averages and Extremes of Rainfall and

Temperature in Sri Lanka. *Advances in Meteorology, 2018*, 4217917. https://doi.org/10.1155/2018/4217917

Nisansala, W., Abeysingha, N., Islam, A., & Bandara, A. (2020). Recent rainfall trend over Sri Lanka (1987–2017). *International Journal of Climatology, 40*(7), 3417-3435.

Nisansala, W. D. S., Abeysingha, N. S., Islam, A., & Bandara, A. M. K. R. (2019). Recent rainfall trend over Sri Lanka (1987–2017). *International Journal of Climatology, 40*(7), 3417-3435. https://doi.org/10.1002/joc.6405

Nishanthi, K., & Dissanayaka, D. M. N. P. (2021). SWOT Analysis of Urban Development on Kolonnawa Urban Council, Sri Lanka. *World News of Natural Sciences 39 (2021)* 46-60. file:///C:/Users/19613358/Downloads/SWOT_Analysis_of_Urban_Development_.pdf

Nobre, A. D., Cuartas, L. A., Hodnett, M., Rennó, C. D., Rodrigues, G., Silveira, A., & Saleska, S. (2011). Height Above the Nearest Drainage–a hydrologically relevant new terrain model. *Journal of Hydrology, 404*(1-2), 13-29.

Nobre, C. A., Young, A. F., Saldiva, P., Marengo, J., Nobre, A. D., Alves Jr, S., Silva, G. d., & Lombardo, M. (2010). Vulnerabilidades das megacidades brasileiras às mudanças climáticas: Região Metropolitana de São Paulo. *Embaixada Reino Unido, Rede Clima e Programa FAPESP em Mudanças Climáticas*.

Nouaceur, Z., & Murărescu, O. (2016). Rainfall variability and trend analysis of annual rainfall in North Africa. *International Journal of Atmospheric Sciences, 2016*.

OCHA. (2023). *PAKISTAN: 2022 Monsoon Floods* (Situation Report No. 16, Issue. file:///C:/Users/19613358/Downloads/Pakistan%20Floods%20Response%20SitRep%20No.16.pdf

OECD. (2016). *Financial Managment of Flood Risk*.

Ogato, G. S., Bantider, A., Abebe, K., & Geneletti, D. (2020). Geographic information system (GIS)-Based multicriteria analysis of flooding hazard and risk in Ambo Town and its watershed, West shoa zone, oromia regional State, Ethiopia. *Journal of Hydrology: Regional Studies, 27*. https://doi.org/10.1016/j.ejrh.2019.100659

Oh, H.-J., Lee, S., & Hong, S.-M. (2017). Landslide Susceptibility Assessment Using Frequency Ratio Technique with Iterative Random Sampling. *Journal of Sensors, 2017*, 3730913. https://doi.org/10.1155/2017/3730913

Organization, W. M. (2013). *The Global Climate 2001-2010: a decade of climate extremes* (WMO- No. 1103, Issue. https://library.wmo.int/doc_num.php?explnum_id=7802

Oti, J. O., Kabo-Bah, A. T., & Ofosu, E. (2020). Hydrologic response to climate change in the Densu River Basin in Ghana. *Heliyon, 6*(8), e04722. https://doi.org/10.1016/j.heliyon.2020.e04722

Ouma, Y. O., & Tateishi, R. (2014). Urban Flood Vulnerability and Risk Mapping Using Integrated Multi-Parametric AHP and GIS: Methodological Overview and Case Study Assessment. *Water, 6*(6), 1515-1545. https://www.mdpi.com/2073-4441/6/6/1515

Ozturk, U., Wendi, D., Crisologo, I., Riemer, A., Agarwal, A., Vogel, K., López-Tarazón, J. A., & Korup, O. (2018). Rare flash floods and debris flows in southern Germany. *Science of The Total Environment, 626*, 941-952. https://doi.org/https://doi.org/10.1016/j.scitotenv.2018.01.172

Pachauri, R. K., Allen, M. R., Barros, V. R., Broome, J., Cramer, W., Christ, R., Church, J. A., Clarke, L., Dahe, Q., & Dasgupta, P. (2014). *Climate change 2014: synthesis report. Contribution of Working Groups I, II and III to the fifth assessment report of the Intergovernmental Panel on Climate Change*. Ipcc.

Padrón, R. S., Gudmundsson, L., Decharme, B., Ducharne, A., Lawrence, D. M., Mao, J., Peano, D., Krinner, G., Kim, H., & Seneviratne, S. I. (2020). Observed changes in dry-season water availability attributed to human-induced climate change. *Nature Geoscience, 13*(7), 477-481. https://doi.org/10.1038/s41561-020-0594-1

Palamakumbure, L., Ratnayake, A. S., Premasiri, H. M. R., Ratnayake, N. P., Katupotha, J., Dushyantha, N., Weththasinghe, S., & Weerakoon, W. A. P. (2020). Sea-level inundation and risk assessment along the south and southwest coasts of Sri Lanka. *Geoenvironmental Disasters, 7*(1), 17. https://doi.org/10.1186/s40677-020-00154-y

Palmer, M. A., Reidy Liermann, C. A., Nilsson, C., Flörke, M., Alcamo, J., Lake, P. S., & Bond, N. (2008). Climate change and the world's river basins: anticipating management options. *Frontiers in Ecology and the Environment, 6*(2), 81-89. https://doi.org/10.1890/060148

Panditharathne, R., Gunathilake, M. B., Chathuranika, I. M., Rathnayake, U., Babel, M. S., & Jha, M. K. (2022). Trends and Variabilities in Rainfall and Streamflow: A Case Study of the Nilwala River Basin in Sri Lanka. *Hydrology, 10*(1). https://doi.org/10.3390/hydrology10010008

Perera, H., Gunathilake, M. B., Panditharathne, R., Al-mahbashi, N., & Rathnayake, U. (2022). Statistical Evaluation and Trend Analysis of ANN Based Satellite Products (PERSIANN) for the Kelani River Basin, Sri Lanka. *Applied Computational Intelligence and Soft Computing, 2022*.

Perera, K. (2021). FLOOD HAZARD ASSESSMENT USING GIS-BASED MULTICRITERIA ANALYSIS: A CASE STUDY FROM DOWNSTREAM OF KELANI RIVER BASIN, SRI LANKA. *KJMS 2021 VOL.3 (1): 50-68*.

Peries, T. S. G. (2004). Coconut production: Issues, approaches and challenges. *In Proceedings of the International Conference at the 75th Anniversary of the Coconut Research Institute. , Peiris T.S.G., Ranasinghe C.S. (eds). Coconut Research Institute: Lunuwila*.

Pinault, J.-L. (2012). Global warming and rainfall oscillation in the 5–10 yr band in Western Europe and Eastern North America. *Climatic change, 114*(3-4), 621-650.

Polka, E. [P. h. post]. (2018). *Global Flood Risk under Climate Change*. https://www.publichealthpost.org/databyte/global-flood-risk-under-climate-change/

Prakash, S., C, M., Sathiyamoorthy, V., & Gairola, R. M. (2012). Increasing trend of northeast monsoon rainfall over the equatorial Indian Ocean and peninsular India. *Theoretical and Applied Climatology, 112*(1-2), 185-191. https://doi.org/10.1007/s00704-012-0719-6

Qi, W., Ma, C., Xu, H., Chen, Z., Zhao, K., & Han, H. (2021). A review on applications of urban flood models in flood mitigation strategies. *Natural Hazards, 108*, 31-62.

R-Core-Team. [V. Foundation for Statistical Computing, Austra]. (2013). *R: A language and environment for statistical computing.* http://wwww.Rproject.org.

Radwan, F., Alazba, A. A., & Mossad, A. (2018). Flood risk assessment and mapping using AHP in arid and semiarid regions. *Acta Geophysica, 67*(1), 215-229. https://doi.org/10.1007/s11600-018-0233-z

Rahman, M., Ningsheng, C., Mahmud, G. I., Islam, M. M., Pourghasemi, H. R., Ahmad, H., Habumugisha, J. M., Washakh, R. M. A., Alam, M., Liu, E., Han, Z., Ni, H., Shufeng, T., & Dewan, A. (2021). Flooding and its relationship with land cover change, population growth, and road density. *Geoscience Frontiers, 12*(6). https://doi.org/10.1016/j.gsf.2021.101224

Rahmati, O., Zeinivand, H., & Besharat, M. (2016). Flood hazard zoning in Yasooj region, Iran, using GIS and multi-criteria decision analysis. *Geomatics, Natural Hazards and Risk, 7*(3), 1000-1017. https://doi.org/10.1080/19475705.2015.1045043

Rameshwaran, P., Bell, V. A., Davies, H. N., & Kay, A. L. (2021). How might climate change affect river flows across West Africa? *Climatic Change, 169*(3), 21. https://doi.org/10.1007/s10584-021-03256-0

Randil, C., Siriwardana, C., & Sandaruwan Rathnayaka, B. (2022). A statistical method for pre-estimating impacts from a disaster: A case study of floods in Kaduwela, Sri Lanka. *International Journal of Disaster Risk Reduction, 76*, 103010. https://doi.org/https://doi.org/10.1016/j.ijdrr.2022.103010

Razandi, Y., Pourghasemi, H. R., Neisani, N. S., & Rahmati, O. (2015). Application of analytical hierarchy process, frequency ratio, and certainty factor models for groundwater potential mapping using GIS. *Earth Science Informatics, 8*(4), 867-883. https://doi.org/10.1007/s12145-015-0220-8

Rebolho, C., Andréassian, V., & Le Moine, N. (2018). Inundation mapping based on reach-scale effective geometry. *Hydrol. Earth Syst. Sci., 22*(11), 5967-5985. https://doi.org/10.5194/hess-22-5967-2018

Rehman, A., Song, J., Haq, F., Mahmood, S., Ahamad, M. I., Basharat, M., Sajid, M., & Mehmood, M. S. (2022). Multi-Hazard Susceptibility Assessment Using the Analytical Hierarchy Process and Frequency Ratio Techniques in the Northwest Himalayas, Pakistan. *Remote Sensing, 14*(3), 554. https://www.mdpi.com/2072-4292/14/3/554

Rennó, C. D., Nobre, A. D., Cuartas, L. A., Soares, J. V., Hodnett, M. G., Tomasella, J., & Waterloo, M. J. (2008). HAND, a new terrain descriptor using SRTM-DEM: Mapping terra-firme rainforest environments in Amazonia. *Remote Sensing of Environment, 112*(9), 3469-3481. https://doi.org/https://doi.org/10.1016/j.rse.2008.03.018

Rose, A. (2004). Defining and measuring economic resilience to disasters. *Disaster Prevention and Management, 13*, 307-314.

Saaty, T. L. (1977). A scaling method for priorities in hierarchical structures. *Journal of Mathematical Psychology, 15*(3), 234-281. https://doi.org/https://doi.org/10.1016/0022-2496(77)90033-5

Saaty, T. L. (1980). The Analytic Hierarchy Process. (McGraw-Hill, New York)

Saha, A., Pal, S. C., Arabameri, A., Blaschke, T., Panahi, S., Chowdhuri, I., Chakrabortty, R., Costache, R., & Arora, A. (2021). Flood Susceptibility Assessment Using Novel Ensemble of Hyperpipes and Support Vector Regression Algorithms. *Water, 13*(2), 241. https://www.mdpi.com/2073-4441/13/2/241

Saji, N. H., Goswami, B. N., Vinayachandran, P. N., & Yamagata, T. (1999). A dipole mode in the tropical Indian Ocean. *Nature, 401*(6751), 360-363. https://doi.org/10.1038/43854

Samantaray, P., & Gouda, K. C. (2023). A review on the extreme rainfall studies in India. *Natural Hazards Research*. https://doi.org/https://doi.org/10.1016/j.nhres.2023.08.005

Samarasinghe, J. T., Makumbura, R. K., Wickramarachchi, C., Sirisena, J., Gunathilake, M. B., Muttil, N., Teo, F. Y., & Rathnayake, U. (2022). The Assessment of Climate Change Impacts and Land-use Changes on Flood Characteristics: The Case Study of the Kelani River Basin, Sri Lanka. *Hydrology, 9*(10), 177.

Samarasinghe, S. M. J. S., Nandalal, H. K., Weliwitiya, D. P., Hazarika, M. K., & Samarakoon, L. (2010). APPLICATION OF REMOTE SENSING AND GIS FOR FLOOD RISK ANALYSIS: A CASE STUDY AT KALU- GANGA RIVER, SRI LANKA.

Santini, M., & di Paola, A. (2015). Changes in the world rivers' discharge projected from an updated high resolution dataset of current and future climate zones. *Journal of Hydrology, 531*, 768-780. https://doi.org/https://doi.org/10.1016/j.jhydrol.2015.10.050

Sarkar, D., & Mondal, P. (2019). Flood vulnerability mapping using frequency ratio (FR) model: a case study on Kulik river basin, Indo-Bangladesh Barind region. *Applied Water Science, 10*(1). https://doi.org/10.1007/s13201-019-1102-x

Seejata, K., Yodying, A., Wongthadam, T., Mahavik, N., & Tantanee, S. (2018). Assessment of flood hazard areas using Analytical Hierarchy Process over the Lower Yom Basin, Sukhothai Province. *Procedia Engineering, 212*, 340-347. https://doi.org/https://doi.org/10.1016/j.proeng.2018.01.044

Sen, P. K. (1968). Estimates of the Regression Coefficient Based on Kendall's Tau. *Journal of the American Statistical Association, 63(324)*. https://doi.org/https://doi.org/10.2307/2285891

Şen, Z. (2012). Innovative trend analysis methodology. *Journal of Hydrologic Engineering, 17*(9), 1042-1046.

Senanayake, S., Pradhan, B., Huete, A., & Brennan, J. (2020). Assessing Soil Erosion Hazards Using Land-Use Change and Landslide Frequency Ratio Method: A Case Study of Sabaragamuwa Province, Sri Lanka. *Remote Sensing, 12*(9). https://doi.org/10.3390/rs12091483

Shafapour, M., Kumar, L., Neamah Jebur, M., & Shabani, F. (2019). Evaluating the application of the statistical index method in flood susceptibility mapping and its comparison with frequency ratio and logistic regression methods. *Geomatics, Natural Hazards and Risk, 10*(1), 79-101. https://doi.org/10.1080/19475705.2018.1506509

Shahid, S. (2011). Trends in extreme rainfall events of Bangladesh. *Theoretical and Applied Climatology, 104*(3), 489-499. https://doi.org/10.1007/s00704-010-0363-y

Sheikh, M. M., Manzoor, N., Ashraf, J., Adnan, M., Collins, D., Hameed, S., Manton, M. J., Ahmed, A. U., Baidya, S. K., Borgaonkar, H. P., Islam, N., Jayasinghearachchi, D., Kothawale, D. R., Premalal, K. H. M. S., Revadekar, J. V., & Shrestha, M. L. (2015). Trends in extreme daily rainfall and temperature indices over South Asia. *International Journal of Climatology, 35*(7), 1625-1637. https://doi.org/10.1002/joc.4081

Shelton, S., & Pushpawela, B. (2022). Observed southwest monsoon rainfall changes in Sri Lanka and possible mechanisms. *Modeling Earth Systems and Environment, 8*(3), 4165-4175. https://doi.org/10.1007/s40808-021-01346-7

Silalahi, F. E. S., Pamela, Arifianti, Y., & Hidayat, F. (2019). Landslide susceptibility assessment using frequency ratio model in Bogor, West Java, Indonesia. *Geoscience Letters, 6*(1), 10. https://doi.org/10.1186/s40562-019-0140-4

Sirinanda, K. U. (1983). Rainfall variability patterns and agriculture production in Sri Lanka. *Climatological Notes, 33: 83-110*.

Sivakumar, M. V. K., & Stefanski, R. (2011). Climate Change in South Asia. In R. Lal, M. V. K. Sivakumar, S. M. A. Faiz, A. H. M. Mustafizur Rahman, & K. R. Islam (Eds.), *Climate Change and Food Security in South Asia* (pp. 13-30). Springer Netherlands. https://doi.org/10.1007/978-90-481-9516-9_2

Sivakumar, S. (2015). Flood Mitigation Strategies Adopted in Sri LankaA Review. *International Journal of Scientific & Engineering Research, Volume 6*(Issue 2).

Smith, J. A., Baeck, M. L., Zhang, Y., & Doswell, C. A. (2001). Extreme Rainfall and Flooding from Supercell Thunderstorms. *Journal of Hydrometeorology, 2*(5), 469-489. https://doi.org/https://doi.org/10.1175/1525-7541(2001)002<0469:ERAFFS>2.0.CO;2

Sneyers, R. (1990). On the Statistical Analysis of Series of Observations. *Technical Note No. 143, WMO No. 415, World Meteorological Organization, Geneva,*.

Solin, L., & Skubincan, P. (2013). Flood risk assessment and management: review of concepts, definitions and methods. *Geogr. J, 65*, 23-44.

Sørensen, R., Zinko, U., & Seibert, J. (2006). On the calculation of the topographic wetness index: evaluation of different methods based on field observations. *Hydrol. Earth Syst. Sci., 10*(1), 101-112. https://doi.org/10.5194/hess-10-101-2006

Speckhann, G. A., Borges Chaffe, P. L., Fabris Goerl, R., Abreu, J. J. d., & Altamirano Flores, J. A. (2018). Flood hazard mapping in Southern Brazil: a combination of flow frequency analysis and the HAND model. *Hydrological Sciences Journal, 63*(1), 87-100. https://doi.org/10.1080/02626667.2017.1409896

Stolbova, V., Martin, P., Bookhagen, B., Marwan, N., & Kurths, J. (2014). Topology and seasonal evolution of the network of extreme precipitation over the Indian subcontinent and Sri Lanka. *Nonlin. Processes Geophys., 21*(4), 901-917. https://doi.org/10.5194/npg-21-901-2014

Sun, Q., Miao, C., & Duan, Q. (2017). Changes in the Spatial Heterogeneity and Annual Distribution of Observed Precipitation across China. *Journal of Climate, 30*(23), 9399-9416. https://doi.org/https://doi.org/10.1175/JCLI-D-17-0045.1

Sun, Q., Miao, C., Duan, Q., Ashouri, H., Sorooshian, S., & Hsu, K. L. (2018). A review of global precipitation data sets: Data sources, estimation, and intercomparisons. *Reviews of Geophysics, 56*(1), 79-107.

Sun, R., Gong, Z., Gao, G., & Shah, A. A. (2020). Comparative analysis of Multi-Criteria Decision-Making methods for flood disaster risk in the Yangtze River Delta. *International Journal of Disaster Risk Reduction, 51*, 101768. https://doi.org/https://doi.org/10.1016/j.ijdrr.2020.101768

Suppiah, R. (1996). Spatial and temporal variations in the relationships between the southern oscillation phenomenon and the rainfall of Sri Lanka. *International Journal of Climatology, vol. 16,1391-1407 (1996)*.

Suppiah, R., & Yoshino, M. M. (1984). Rainfall Variations of Sri Lanka, Part 2: regional fluctuations. *Arch. Met. Geoph. Biocl., Ser. B 35,*. https://doi.org/https://doi.org/10.1007/BF02269411

Survey Department, S. L. (2019). *Mapping Mannual*. https://www.survey.gov.lk/sdweb/pdf/download/publications/Mapping_Manual.pdf

Swapna, P., Sreeraj, P., Sandeep, N., Jyoti, J., Krishnan, R., Prajeesh, A. G., Ayantika, D. C., & Manmeet, S. (2022). Increasing Frequency of Extremely Severe Cyclonic Storms in the North Indian Ocean by Anthropogenic Warming and Southwest Monsoon Weakening. *Geophysical Research Letters, 49*(3), e2021GL094650. https://doi.org/https://doi.org/10.1029/2021GL094650

Tabari, H. (2020). Climate change impact on flood and extreme precipitation increases with water availability. *Sci Rep, 10*(1), 13768. https://doi.org/10.1038/s41598-020-70816-2

Tabari, H., Hosseinzadehtalaei, P., AghaKouchak, A., & Willems, P. (2019). Latitudinal heterogeneity and hotspots of uncertainty in projected extreme precipitation. *Environmental Research Letters, 14*(12). https://doi.org/https://doi.org/10.1088/1748-9326/ab55fd

Taherdoost, H., & Madanchian, M. (2023). Multi-Criteria Decision Making (MCDM) Methods and Concepts. *Encyclopedia, 3*(1), 77-87. https://doi.org/10.3390/encyclopedia3010006

Tamagnone, P., Comino, E., & Rosso, M. (2020). Rainwater harvesting techniques as an adaptation strategy for flood mitigation. *Journal of hydrology, 586*, 124880.

Tang, X., Li, J., Liu, M., Liu, W., & Hong, H. (2020). Flood susceptibility assessment based on a novel random Naïve Bayes method: A comparison between different factor discretization methods. *CATENA, 190*, 104536. https://doi.org/https://doi.org/10.1016/j.catena.2020.104536

Tao, B., Tian, H., Ren, W., Yang, J., Yang, Q., He, R., Cai, W., & Lohrenz, S. (2014). Increasing Mississippi river discharge throughout the 21st century influenced by changes in climate, land use, and atmospheric CO2. *Geophysical Research Letters, 41*(14), 4978-4986.

Tariq, A., Yan, J., Ghaffar, B., Qin, S., Mousa, B., Sharifi, A., Huq, M. E., & Aslam, M. (2022). Flash flood susceptibility assessment and zonation by integrating analytic hierarchy process and frequency ratio model with diverse spatial data. *Water, 14*(19), 3069.

Tewari, A., Kshemkalyani, V., Kukreja, H., Menon, P., & Thomas, R. (2021, 6-8 May 2021). Application of LSTMs and HAND in Rapid Flood Inundation Mapping.2021 5th International Conference on Intelligent Computing and Control Systems (ICICCS),

Thambyahpillay, G. (1965). Dry zone climatology. *J. Nat Agric. Soc. (Ceylon), 2,143.*

The Guardian. (2019, Wed 14 Aug 2019).

This article is more than 4 years old India issues new flood alert as monsoon death toll reaches 244. https://www.theguardian.com/world/2019/aug/14/india-flood-alert-monsoon-kerala

Thevakaran, A., Suppiah, R., & Sonnadara, U. (2019). Trends in extreme rainfall events in Sri Lanka, 1961 - 2010. *Journal of the National Science Foundation of Sri Lanka, 47*(3). https://doi.org/10.4038/jnsfsr.v47i3.9280

Tiwari, A., Shoab, M., & Dixit, A. (2021). GIS-based forest fire susceptibility modeling in Pauri Garhwal, India: a comparative assessment of frequency ratio, analytic hierarchy process and fuzzy modeling techniques. *Natural Hazards, 105*(2), 1189-1230. https://doi.org/10.1007/s11069-020-04351-8

Tiwari, H., & Pandey, B. K. (2019). Non-parametric characterization of long-term rainfall time series. *Meteorology and Atmospheric Physics, 131*, 627-637. https://doi.org/10.1007/s00703-018-0592-7

Trenberth, K. E. (2005). The Impact of Climate Change and Variability on Heavy Precipitation, Floods, and Droughts. In *Encyclopedia of Hydrological Sciences*. https://doi.org/https://doi.org/10.1002/0470848944.hsa211

Tucker, C. J. (1979). Red and photographic infrared linear combinations for monitoring vegetation. *Remote Sensing of Environment, 8*(2), 127-150. https://doi.org/https://doi.org/10.1016/0034-4257(79)90013-0

Turkes, M. (1996). Spatial and temporal analysis of annual rainfall variation in Turkey. *International journal of climatology, vol.16: 1057-1076*.

Ullah, K., & Zhang, J. (2020). GIS-based flood hazard mapping using relative frequency ratio method: A case study of Panjkora River Basin, eastern Hindu Kush, Pakistan. *PLoS One, 15*(3), e0229153. https://doi.org/10.1371/journal.pone.0229153

UN, U. N. (1992). Internationally agreed glossary of basic terms related to disaster management. *Geneva (United Nations Department of Humanitarian Affairs)*.

UNDP. (2004). Reducing disaster risk: a challenge for development, a global report. New York. *(United Nations Development Programme, Bureau for Crisis Prevention and Recovery*.

UNDP. (2009). *ASSESSMENT OF DEVELOPMENT RESULTS: SRI LANKA*.

UNDP. (2011). *Practitioners' Guidebook on the Best Agricultural Practices for Drought and Floods in Sri Lanka*. UNDP: Sri Lanka.

UNDRR. (2019). *Disaster Risk Reduction in Sri Lanka - Status Report 2019*.

United Nations Office for Disaster Risk Reduction. (2024). *Sendai Framework*. Retrieved 22/04, from

United Nations Office for Disaster Risk Reduction and World Meteorological Organizatio. (2023). *Global Status of Multi-Hazard Early Warning Systems*. https://www.undrr.org/media/91954/download?startDownload=true

Vilasan, R. T., & Kapse, V. S. (2022). Evaluation of the prediction capability of AHP and F-AHP methods in flood susceptibility mapping of Ernakulam district (India). *Natural Hazards, 112*(2), 1767-1793. https://doi.org/10.1007/s11069-022-05248-4

Wang, X. L., Chen, H., Wu, Y., Feng, Y., & Pu, Q. (2010). New Techniques for the Detection and Adjustment of Shifts in Daily Precipitation Data Series. *Journal of Applied Meteorology and Climatology, 49*(12), 2416-2436. https://doi.org/https://doi.org/10.1175/2010JAMC2376.1

Wang, Y., Xu, Y., Tabari, H., Wang, J., Wang, Q., Song, S., & Hu, Z. (2020). Innovative trend analysis of annual and seasonal rainfall in the Yangtze River Delta, eastern China.

Atmospheric Research, 231, 104673. https://doi.org/https://doi.org/10.1016/j.atmosres.2019.104673

Waqas, H., Lu, L., Tariq, A., Li, Q., Baqa, M. F., Xing, J., & Sajjad, A. (2021). Flash flood susceptibility assessment and zonation using an integrating analytic hierarchy process and frequency ratio model for the Chitral District, Khyber Pakhtunkhwa, Pakistan. *Water, 13*(12), 1650.

Weerasinghe, K. M., Gehrels, H., Arambepola, N. M. S. I., Vajja, H. P., Herath, J. M. K., & Atapattu, K. B. (2018). Qualitative Flood Risk assessment for the Western Province of Sri Lanka. *Procedia Engineering, 212*, 503-510. https://doi.org/https://doi.org/10.1016/j.proeng.2018.01.065

Wickramagamage, P. (2016). Spatial and temporal variation of rainfall trends of Sri Lanka. *Theoretical and Applied Climatology, 125*(3), 427-438. https://doi.org/10.1007/s00704-015-1492-0

Wijeratne, V., & Li, G. (2022). Urban sprawl and its stress on the risk of extreme hydrological events (EHEs) in the Kelani River basin, Sri Lanka. *International Journal of Disaster Risk Reduction, 68*, 102715.

Wijesinghe, W. M. D. C., Mishra, P. K., Tripathi, S., Abdelrahman, K., Tiwari, A., & Fnais, M. S. (2023). Integrated Flood Hazard Vulnerability Modeling of Neluwa (Sri Lanka) Using Analytical Hierarchy Process and Geospatial Techniques. *Water, 15*(6), 1212. https://www.mdpi.com/2073-4441/15/6/1212

Wijetunge, J., & Neluwala, N. (2023). Compound flood hazard assessment and analysis due to tropical cyclone-induced storm surges, waves and precipitation: a case study for coastal lowlands of Kelani river basin in Sri Lanka. *Natural Hazards, 116*(3), 3979-4007.

WMO. (2018). *Guide to climatological practices*.

WMO, W. M. O. (2020). *Climate change detection and indices*. World Meteorological Organization (WMO). Retrieved 22 October 2022, from https://community.wmo.int/climate-change-detection-and-indices

Worldometer. (2023). *South Asia Population*. Retrieved 14/12/2023, from https://www.worldometers.info/world-population/southern-asia-population/

Wubalem, A., Tesfaw, G., Dawit, Z., Getahun, B., Mekuria, T., & Jothimani, M. (2020). Comparison of statistical and analytical hierarchy process methods on flood susceptibility mapping: in a case study of Tana sub-basin in northwestern Ethiopia. *Natural Hazard and Earth System Sciences*. https://doi.org/10.5194/nhess-2020-332

Xavier, A., Kottayil, A., Mohanakumar, K., & Xavier, P. K. (2018). The role of monsoon low-level jet in modulating heavy rainfall events. *International Journal of Climatology, 38*, e569-e576. https://doi.org/10.1002/joc.5390

Xu, F., Zhao, L., Niu, C., & Qiu, Y. (2022). Effect of Climate Change and Anthropogenic Activities on Streamflow Indicators in a Tropical River Basin in Southern China. *Water, 14*(3). https://doi.org/10.3390/w14030304

Yadav, M. (2022). South Asian monsoon extremes and climate change. In *Extremes in Atmospheric Processes and Phenomenon: Assessment, Impacts and Mitigation* (pp. 59-86). Springer.

Yang, S.-Y., Chang, C.-H., Hsu, C.-T., & Wu, S.-J. (2022). Variation of uncertainty of drainage density in flood hazard mapping assessment with coupled 1D–2D hydrodynamics model. *Natural Hazards, 111*(3), 2297-2315. https://doi.org/10.1007/s11069-021-05138-1

Yang, X. Z. a. F. (2004). *RClimDex (1.0): User Manual*. Climate Research Branch, Environment Canada. https://acmad.net/rcc/procedure/RClimDexUserManual.pdf

Yilmaz, O. S. (2022). Flood hazard susceptibility areas mapping using Analytical Hierarchical Process (AHP), Frequency Ratio (FR) and AHP-FR ensemble based on Geographic Information Systems (GIS): a case study for Kastamonu, Türkiye. *Acta Geophysica, 70*(6), 2747-2769.

Zainudini, M. A., & Sardarzaei, A. (2022). Flood causes, consequences, protection, measures and management in Kaserkand, Sarbaz and Dashtyari Districts, Makoran, Iran. *Glob. J. Eng. Technol. Adv., 10, 94–102*.

Zarenistanak, M., Dhorde, A., & Kripalani, R. (2023). Trend analysis and change point detection of annual and seasonal precipitation and temperature series over southwest Iran. *J. Earth Syst. Sci., 123, No. 2,*.

Zha, Y., Gao, J., & Ni, S. (2003). Use of normalized difference built-up index in automatically mapping urban areas from TM imagery. *International journal of remote sensing, 24*(3), 583-594.

Zhou, W., & Zhang, D. (1999). Progressive switching median filter for the removal of impulse noise from highly corrupted images. *IEEE Transactions on Circuits and Systems II: Analog and Digital Signal Processing, 46*(1), 78-80. https://doi.org/10.1109/82.749102

Zubair, L., Rao, S. A., & Yamagata, T. (2003). Modulation of Sri Lankan Maha rainfall by the Indian Ocean Dipole. *Geophysical Research Letters, 30*(2). https://doi.org/https://doi.org/10.1029/2002GL015639

Zubair, L., Siriwardhana, M., Chandimala, J., & Yahiya, Z. (2007). Predictability of Sri Lankan rainfall based on ENSO. *International Journal of Climatology, 28*(1), 91-101. https://doi.org/10.1002/joc.1514

APPENDIX A – Flood relative frequency index with prediction rate

No	Factors	Factor class	Classes area	% of classes area	No of point	% of point counts	FR	RF	Prediction rate
1	Elevation	1	482598	54.12	32400	25.71	0.48	0.06	2.92
		2	211309	23.70	33300	26.43	1.12	0.14	
		3	95662	10.73	27000	21.43	2.00	0.24	
		4	56068	6.29	19800	15.71	2.50	0.31	
		5	46082	5.17	13500	10.71	2.07	0.25	
2	Drainage Density	1	41187	4.62	24300	19.29	4.18	0.59	5.67
		2	230241	25.82	51300	40.71	1.58	0.22	
		3	384710	43.14	42300	33.57	0.78	0.11	
		4	199400	22.36	6300	5.00	0.22	0.03	
		5	36181	4.06	1800	1.43	0.35	0.05	
3	Soil	1	1255	0.14	900	0.71	5.08	0.49	3.24
		2	9327	1.05	1800	1.43	1.37	0.13	
		3	218421	24.49	17100	13.57	0.55	0.05	
		4	518022	58.09	50400	40.00	0.69	0.07	
		5	144694	16.23	55800	44.29	2.73	0.26	
4	Proximity to river	1	280175	31.42	9900	7.86	0.25	0.04	1.8
		2	177184	19.87	29700	23.57	1.19	0.21	
		3	117213	13.14	23400	18.57	1.41	0.25	
		4	141814	15.90	29700	23.57	1.48	0.26	
		5	175333	19.66	33300	26.43	1.34	0.24	
5	TWI	1	305687	34.28	29700	23.57	0.69	0.10	1.97
		2	331469	37.17	41400	32.86	0.88	0.13	
		3	168593	18.91	30600	24.29	1.28	0.19	
		4	70270	7.88	19800	15.71	1.99	0.29	
		5	15700	1.76	4500	3.57	2.03	0.29	
6	Slope	1	57350	6.43	4500	3.57	0.56	0.13	1.05
		2	38469	4.31	2700	2.14	0.50	0.12	
		3	60831	6.82	9900	7.86	1.15	0.28	
		4	255806	28.69	27000	21.43	0.75	0.18	
		5	479265	53.75	81900	65.00	1.21	0.29	
7	Rain	1	98438	11.04	900	0.71	0.06	0.01	2.15
		2	267834	30.04	37800	30.00	1.00	0.22	
		3	229792	25.77	39600	31.43	1.22	0.26	
		4	132352	14.84	28800	22.86	1.54	0.33	
		5	163303	18.31	18900	15.00	0.82	0.18	

8	NDVI	1	265599	29.79	36000	28.57	0.96	0.19	1
		2	299415	33.58	37800	30.00	0.89	0.18	
		3	176169	19.76	27900	22.14	1.12	0.23	
		4	115239	12.92	20700	16.43	1.27	0.26	
		5	35297	3.96	3600	2.86	0.72	0.15	
9	Land Use	1	370913	41.60	50400	40.00	0.96	0.15	1.99
		2	19574	2.20	6300	5.00	2.28	0.36	
		3	233985	26.24	36900	29.29	1.12	0.18	
		4	227932	25.56	26100	20.71	0.81	0.13	
		5	39315	4.41	6300	5.00	1.13	0.18	

Appendix B: MK and Sen's slope values for extreme rainfall indices

No	Station Name	R99p			R95p			R10 mm			R20 mm			PRCPTOT			SDII		
		Z Value	p value (two-tailed)	Sen's slope	Z Value	p value (two-tailed)	Sen's slope	Z Value	p value (two-tailed)	Sen's slope	Z Value	p value (two-tailed)	Sen's slope	Z Value	p value (two-tailed)	Sen's slope	Z Value	p value (two-tailed)	Sen's slope
1	Anuradhapura	2.623	0.009	2.583	2.248	0.025	9.417	1.023	0.306	0.188	1.737	0.082	0.286	1.82	0.069	13.69	2.517	0.012	0.125
2	Batticaloa	1.759	0.078	0	1.838	0.066	13.623	0.358	0.72	0.038	0.769	0.442	0.125	1.249	0.212	10.6	1.357	0.175	0.135
3	Hambantota	0	1	0	0.607	0.544	1.867	0.592	0.554	0.071	0.304	0.761	0	0.285	0.775	2.435	0.232	0.816	0.01
4	Maha Illuppallama	-0.224	0.823	0	0.821	0.412	2.924	0.771	0.441	0.111	0.572	0.567	0.095	1.106	0.269	6.5	0.536	0.592	0.025
5	Pottuvil	0.096	0.924	0	1.678	0.093	7.505	1.61	0.107	0.458	1.54	0.124	0.333	1.767	0.077	19.46	-0.393	0.694	-0.043
6	Puttalam	-0.466	0.641	0	-0.232	0.817	-0.475	0.573	0.567	0.077	0.448	0.654	0.05	-0.321	0.748	-1.75	0.393	0.694	0.021
7	Trincomalee	-0.019	0.985	0	0.036	0.972	0.661	1.108	0.268	0.2	1.076	0.282	0.143	0.928	0.354	5.371	0.286	0.775	0.022
8	Vavuniya	0.877	0.381	0	1.874	0.061	8.506	1.76	0.078	0.308	1.059	0.29	0.125	1.731	0.083	10.95	1.696	0.09	0.111
9	Mannar	0.465	0.642	0	3.287	0.001	10.486	1.145	0.25	0.2	0.701	0.483	0.087	1.589	0.112	7.556	2.393	0.017	0.214
10	Badulla	0.649	0.516	0.45	1.356	0.175	4.768	1.143	0.253	0.286	0.967	0.334	0.143	1.106	0.269	8.667	1.197	0.231	0.048
11	Bandarawela	1.129	0.259	1.119	1.534	0.125	6.674	1.145	0.252	0.222	1.612	0.107	0.25	1.891	0.058	10	1.591	0.112	0.043
12	Kurunegala	0.503	0.615	0.073	0.999	0.318	3.83	0.197	0.844	0	0.287	0.774	0	0.464	0.643	1.617	1.18	0.238	0.054
13	Colombo	0.616	0.538	0	-0.071	0.943	-0.165	-0.09	0.929	0	0.215	0.83	0	0.143	0.886	2.564	0.143	0.886	0.015
14	Galle	-0.197	0.844	0	0.856	0.392	6.814	-0.161	0.872	-0.048	0.645	0.519	0.125	0.856	0.392	5.883	0.965	0.335	0.045
15	Nuwara-Eliya	0.326	0.74	0	-0.428	0.669	-2.026	-1.215	0.224	-0.276	-0.537	0.592	-0.111	-1.32	0.187	-8.208	0.286	0.775	0.012
16	Katugastota	0.216	0.829	0	0.178	0.858	0.78	-0.697	0.486	-0.158	0.376	0.707	0.048	0.571	0.568	2.92	0.536	0.592	0.025
17	Katunayaka	0.252	0.801	0	0.607	0.544	4.462	-0.197	0.844	-0.048	-0.143	0.886	0	0.357	0.721	2.688	0	1	0
18	Ratmalana	-1.01	0.313	-4.362	-0.892	0.372	-4.94	0.572	0.567	0.143	0.537	0.591	0.083	-0.285	0.775	-1.377	0.161	0.872	0
19	Rathnapura	0.394	0.694	0.555	-0.856	0.392	-7	0.018	0.986	0	-0.161	0.872	0	-0.607	0.544	-5.953	-0.822	0.411	-0.025

Appendix C: MMK test results according to the annual and seasonal level

Table 1 Annual MMK results

Station Name	Z-value	P-value	Sen's Slope	Tau
Colombo	2.164	0.030	0.000	0.014
Angoda				
Hanwella	1.911	0.056	0.000	0.028
Awissawella	-0.081	0.935	0.000	-0.001
Chesterford	-1.019	0.308	0.000	-0.014
Undugoda	1.954	0.051	0.000	0.058
Maliboda	-0.016	0.987	0.000	0.000
Laxapana	2.055	0.040	0.000	0.166
Maussakelle	-1.220	0.223	0.000	-0.012
Labugama	-1.385	0.166	0.000	-0.020
Average	1.871	0.061	0.000	0.019

Table 4 IM2 MMK results

Station Name	Z-value	P-value	Tau	Sen's Slope
Colombo	0.3925	0.6947	0.0529	2.0857
Angoda	0.0768	0.9388	0.0115	1.0364
Hanwella	-0.0571	0.9545	-0.0069	0.3907
Awissawella	-1.0171	0.3091	-0.1333	-6.8011
Chesterford	0.2141	0.8305	0.0299	1.2522
Undugoda	-0.3568	0.7212	-0.0483	-1.7183
Maliboda	5.2453	0.0000	0.6782	55.8367
Laxapana	-1.3202	0.1868	-0.1724	-10.7545
Maussakelle	-2.0696	0.0385	-0.2690	-7.5889
Labugama	0.0000	1.0000	0.0023	0.0034
Average	0.5383	0.5904	0.0759	3.1125

Table 5 NEM MMK results

Station Name	Z-value	P-value	Tau	Sen's Slope
Colombo	2.0696	0.0385	0.2690	6.5000
Angoda	0.4639	0.6427	0.0621	1.1004
Hanwella	-0.0357	0.9715	-0.0069	-0.3552
Awissawella	-1.3322	0.1828	-0.2138	-5.8782
Chesterford	0.8207	0.4118	0.1080	3.7125
Undugoda	-0.7136	0.4754	-0.0943	-2.3428
Maliboda	5.4237	0.0000	0.7011	22.4030
Laxapana	0.3568	0.7212	0.0483	1.2091
Maussakelle	1.2132	0.2251	0.1586	2.3727
Labugama	0.0357	0.9715	0.0069	0.2500
Average	1.1061	0.2687	0.1448	2.4536

Table 2 IM1 MMK results

Station Name	Z-value	P-value	Sen's Slope	Tau
Colombo	0.9634	0.3353	3.7619	0.1264
Angoda	0.3568	0.7212	0.9814	0.0482
Hanwella	0.4282	0.6685	1.8992	0.0575
Awissawella	-0.9990	0.3177	-0.1310	-4.3857
Chesterford	1.5700	0.1164	8.5588	0.2046
Undugoda	-0.3917	0.6953	-1.6838	-0.0437
Maliboda	8.1086	0.0000	34.3572	0.7931
Laxapana	-1.3811	0.1672	-0.1586	-6.2960
Maussakelle	-1.2489	0.2117	-4.2400	-0.1632
Labugama	-0.0357	0.9715	-0.2773	-0.0069
Average	1.2846	0.1989	0.1678	3.7536

Table 3 SWM MMK results

Station Name	Z-value	P-value	Tau	Sen's Slope
Colombo	-0.6423	0.5207	0.5207	-0.0851
Angoda	0.0714	0.9431	0.0115	0.3144
Hanwella	-0.7493	0.4537	-0.0989	-6.5695
Awissawella	-2.2123	0.0269	-0.2874	-20.7958
Chesterford	2.9259	0.0034	0.3793	22.5909
Undugoda	-0.2855	0.7753	-0.0391	-4.2108
Maliboda	5.4527	0.0000	0.8207	155.3184
Laxapana	-1.2489	0.2117	-0.1632	-16.1667
Maussakelle	-2.1766	0.0295	-0.2828	-22.1600
Labugama	-0.4282	0.6685	-0.0575	-3.2000
Average	1.8555	0.0635	0.2414	12.5774

Appendix D: Monthly correlation coefficient of rainfall and water level in two Hydrology st ations (with 95% confidence level)

Month	Hanwella station	N'Street station
January	0.486474	-0.02805
February	0.317721	0.4293
March	0.316389	0.529025
April	0.567867	0.626604
May	0.825415	0.89896
June	0.62556	0.712226
July	0.755624	0.7555
August	0.301845	0.761322
September	0.752237	0.870345
October	0.555205	0.72496
November	0.640162	0.810837
December	0.627676	0.712474
Yearly	-0.01751	0.756372